Pelagiaria (Teleostei: Acanthomorpha) as a non-analogue adaptive radiation.

Hermione T. Beckett

A thesis submitted for the degree of Doctor of Philosophy

Department of Earth Sciences

St Hugh's College, University of Oxford



Supervisors: Prof. Matt Friedman, Dr Sam Giles,

and Dr Zerina Johanson

Trinity Term 2018

Declaration

I confirm that the contents of this thesis are my own work and that all contributions from others have been fully and accurately acknowledged.

Signed:

Date:

Abstract

Pelagiaria is an anatomically disparate clade of open-ocean fishes identified through molecular studies, comprising 16 families not previously united on the basis of morphology. It has been postulated that ecologically distinct lineages of Pelagiaria diverged rapidly early in the Paleogene. This differs from 'model' adaptive radiations like cichlid fishes and *Anolis* lizards in age and geographic scale, but corresponds closely to patterns in Cenozoic mammals, the group where the concept was first defined. Well-preserved material from the UK, Angola and other sites provides an opportunity to investigate the evolutionary history of Pelagiaria and test these hypotheses of adaptive radiation. I use micro computed tomography (μCT) to investigate key three-dimensionally preserved fossils belonging to groups now assigned to Pelagiaria, focussing on scombrids (tunas, mackerels) and trichiuroids (snake mackerels). I develop character sets for trichiuroids and scombrids, allowing placement of key fossils associated with these groups. I also use μCT to collect three-dimensional cranial landmark data from 68 extant species of Pelagiaria, representing 15/16 extant families and a quarter of living species. These phenotypic data are studied in combination with a time-calibrated molecular phylogeny, which I apply using multiple comparative approaches. Results indicate that Pelagiaria showed an initial, diffusive phase of phenotypic evolution in the early Paleogene, followed by constrained patterns of cranial change from the Eocene onward. This adds quantitative support to previous hypotheses of adaptive radiation in the group, and suggest Pelagiaria might represent a useful a new study system for investigating this key macroevolutionary concept.

Extended Abstract

Percomorphs (the largest subset of Acanthomorpha, the spiny-rayed fishes) comprise more than 14,450 species in around 250 families, numbering nearly a third of living vertebrates. Diversifying rapidly in the aftermath of the Cretaceous-Paleogene (K-Pg) extinction, percomorphs have received increasing molecular attention in recent years as the focus of large-scale genomic studies. Despite this, the relationships between families within the radiation remain uncertain, and morphological studies of the group are often historical, before the advent of formal phylogenetic analyses. Pelagiaria, one of the earliest diverging orders of percomorphs, provide a study system for the evolutionary dynamics of this aquatic radiation. Named for their uniting factor of a pelagic environment, their diversity of bodyplans appears to have evolved over 5-10 million years during the early Paleogene in the aftermath the K-Pg extinction. Although a key interval in their evolution, the early Paleogene also corresponds to a period in their history where fossils are scarce. Despite this gap, the fossil record of Pelagiaria is relatively good, particularly for the Scombridae (tunas and mackerels). Using palaeontological and extant data, this thesis aims to investigate relationships within Pelagiaria and the details of their rapid radiation in the early Cenozoic.

Scombridae have received study in the palaeontological literature for well over a century, although many of these fossils have not been revisited in reference to extant species for over a decade. Other specimens have been the subject of superficial study, but have not been described in detail. In Chapter 2, I describe the monotypic scombrid fish †*Micrornatus*, represented by a single skull

from the early Eocene (Ypresian) London Clay Formation of southeastern England. Although Arthur Smith Woodward, one of the greats of fish palaeontology, substantially increased the diversity of scombrids and scombrid-like taxa known from this deposit, but he seems not to have studied the fossil that would later be recognized as †*Micrornatus*. I re-examine this specimen using micro-computed tomography (μCT), with two principal aims: first, a revised anatomical account with an emphasis on internal features; and, second, 'proof-of-concept' for the tomographic study of fish crania from the London Clay. Scans reveal new details of the braincase, suspensorium and ventral hyoid arch. I compare the cranial anatomy of †*Micrornatus* with other members of †Eocoelopomini, a group aligned with Scombridae also containing the genera †*Eocoelopoma*, †*Palaeothunnus* and possibly †*Landanichthys*. Clarification of the taxonomy and phylogeny of early fossil scombrids is needed, and I suggest that micro computed tomography (μCT) will be a useful tool for revealing the anatomical evidence needed to accomplish this goal.

Utilising μCT on London Clay specimens, Chapter 3 investigates the superfamily Trichiuroidea, which has historically been associated with scombrids. Trichiuroidea, composed of 'gempylids' (snake mackerels) and trichiurids (cutlassfishes) are pelagic fishes characterized by slender to eel-like bodies, deep-sea predatory ecologies, and large fang-like teeth. Several hypotheses of relationships between these groups have been proposed, but a consensus remains elusive. Fossils attributed to 'gempylids' and trichiurids consist almost exclusively of highly compressed body fossils and isolated teeth and otoliths. I use μCT to redescribe two three-dimensional crania, historically assigned to †*Eutrichiurides winkleri* and †*Progempylus edwardsii*, as well as an isolated braincase (NHMUK PV OR 41318).

All from the London Clay Formation (Eocene, Ypresian), these specimens represent some of the oldest fossils identified as trichiuroids. I find that †*Eutrichiurides winkleri* does not show diagnostic characters of †*Eutrichiurides*, and it is assigned to a new genus. To investigate the placement of these fossils relative to extant lineages, I combine existing morphological character sets for 'gempylids' and trichiurids along with published mitogenomic data. The analyses recover a monophyletic Trichiuridae nested within a paraphyletic 'Gempylidae'. The taxon formerly attributed to †*Eutrichiurides winkleri* is considered Trichiuroidea *incertae sedis*, while †*Progempylus edwardsii* and NHMUK PV OR 41318 are recovered within the 'gempylid' grade. Using previously published descriptions and character optimizations from the phylogenetic analyses possible placements for laterally compressed body fossils historically associated with Trichiuroidea (†*Argestichthys*, †*Abadzekhia*, †*Chelifichthys*, †*Anenchelum*, †*Eutrichiurides*, †*Musculopedunculus*) are suggested.

As molecular evidence grows for a rapid radiation in many groups after the K-Pg boundary, chapters 4 and 5 investigate the evolutionary dynamics of Pelagiaria during this time period. Chapter 4 presents the oldest known specimen of Scombridae, and the first fossil percomorph to be assigned to an extant family level group, with implications for evolutionary patterns in Pelagiaria. Relatively little is known of the fossil record of marine fishes between the latest Cretaceous and the Paleocene-Eocene boundary, despite it being an important interval in the diversification of many modern groups. The scombrid †*Landanichthys* is a three-dimensionally preserved Selandian fossil from Angola, which unusually for the Paleocene fossil record has been historically interpreted as highly nested within a crown percomorph family. Here we perform μCT on †*Landanichthys* in order to

place it in a formal phylogenetic analysis for the first time. The results show that †*Landanichthys* is nested within the scombrid crown group most likely as a deeply diverging member of the Scomberomorini. The placement of †*Landanichthys* as a highly nested member of a percomorph family has implications for the rapid diversification of Scombridae in the aftermath of the K-Pg extinction, suggesting that by the Paleocene-Eocene boundary modern phenotypes have been established, supporting growing evidence for a postulated adaptive radiation in Pelagiaria.

With †*Landanichthys* providing tighter constraints on the origin of morphological disparity in the group, Chapter 5 investigates evolutionary patterns in the history of the group Pelagiaria using molecular and morphological data. Using comparative methods in evolutionary biology I use Pelagiaria as a case study to investigate the dynamics of adaptive radiation. Here I use μCT to assemble a three-dimensional cranial dataset of extant and extinct Pelagiaria. Using a time calibrated ultra-conserved element molecular tree as a backbone, I sample 68 pelagiaran fishes, belonging to Pelagiaria, representing 53 of the 74 genera and approximately one-third of all species. Four fossil taxa are added to create a second, combined, dataset. I apply disparity through time and model fitting approaches to investigate the evolutionary patterns in the group, specifically if they show evolutionary patterns associated with adaptive radiation. I find that Pelagiaria show deviations from a null model of Brownian motion evolution, and that a model of changing mode from Brownian motion to an Ornstein-Uhlenbeck process, here called the SHIFT model, best fits the data. The age at which this shift occurs is optimised for the first time as part of a model fitting approach, and is recovered as mid-Ypresian ($\sim$51Ma) in both analyses. The addition of fossil taxa to the analysis does not significantly alter the results. Pelagiaria show a change in

evolutionary mode that would be consistent with definitions of adaptive radiation, however this differs to the observed patterns in mammals and it is therefore unclear if the evolutionary dynamics of postulated adaptive radiations are the same.

Pelagiaria appear to have diversified rapidly in the aftermath of the Cretaceous-Paleogene extinction before becoming constrained in ecological niches in the early Eocene, adding quantitative support to previous hypotheses of adaptive radiation in the group. Pelagiaria provide a non-analogue study system for adaptive radiation, globally distributed and yet tractable in their species richness, and a basis for future synthetic studies of evolutionary dynamics in radiations.

Acknowledgements

Science is a collaborative discipline and nothing here would have been possible without the help and support of others, for which I thank them. First and foremost I would like to thank Matt Friedman without whom this work would not have happened, nor I suspect would I have become a palaeontologist! Since being interviewed by him for Oxford 9 years ago, he has put up with my terrible grammar and inability to spell through an undergraduate degree, a masters thesis and four years working on my PhD. I am sure he wished that emails didn't exist at times, but I feel so fortunate to have been his student, and without him I would not have made it through! An extra special thanks for putting me up when I came across the Ocean to visit, and to Elizabeth too.

Secondly I would like to thank Sam Giles for stepping into the breach when Matt moved out to America. If Matt taught me grammar rules, Sam taught me about paragraph structure! Sam, thank you for your willingness to read things even at the 11th hour, for teaching me Mimics and Blender, and for the honest conversations. Finally among my supervisors, Zerina Johnson thank you for being unfailingly steady. Thank you for reading my work so fast, for giving me access to the collections at the Natural History Museum, for teaching me to radiograph and CT specimens, and for sharing your expertise.

As with any palaeontology PhD my work wouldn't have been possible without collections managers and curators who have given me access to specimens. Emma Bernard, James MacLaine, Oliver Crimmen, Dan Sykes, Farah Ahmed, Rebecca Summerfield, and Patrick Campbell at the Natural History Museum London; Caleb McMahan at the Field Museum of Natural History; Christine Thacker, Rick

Feeney and Javier Gago at the Los Angeles County Museum of Natural History; and Doug Nelson at the University of Michigan Museum of Zoology.

Thank yous must also go to the many, many friends who have helped and supported over the last four years. Harrie Drage, thanks for being my stand in supervisor on multiple occasions, for getting me into cycling and riding with me, but most importantly for being a great friend to me. Oxford hasn't been the same without you this last year. To Palaeoclub and office 40.18 (sometimes one and the same) thank you for your inputs on presentations, helpful discussions, reading, coding help, and everything else over the years. Gemma Benevento, Serjoscha Evers and Dave Ford, sometimes being the palaeo office is a route to insanity, but I will miss our coffee and chats, and being able to turn around and ask you questions, thanks for a great 4 years.

Life outside of academia has kept me sane, in the first few years rowing with St Hugh's Boat Club and the lovely ladies there, but more recently by my constant cycling buddies. There are too many wonderful people at the Cowley Road Condors, and I can't name you all, but thank you and you are awesome! Also to those I have met through OUCC, I am sad it took me so long to find uni sport, but we had a great year, thank you! Special cycling shoutouts go to Cyndi Goh and Becca Kearney, thank you for putting up with my moaning on our rides, for always being my training partners, for racing with me, and Eleanor Law for the same thing a year ago! Ines Rahtz for our early morning rides and Eleanor McKay for being all around lovely (and my jelly baby supplier). Cycling has been my escape and my sanity.

Finally, and most importantly I want to thank my wonderful, patient, kind husband Jono, who not only married me and keeps me sane but has input as much

of his time as he can into helping me complete this PhD. He has put up with constant coding requests, monopolising computing power on the Dept. of Maths computers so my analyses could run (don't tell Maths!). He also spent a week in France on "holiday" helping me debug and tidy my code, and rewrite functions to deal with my terrible fossil data. What I write here can never convey how much he supports me or how lucky I am to have him, so thank you.

Contents

Abstract iii

Extended Abstract ix

Acknowledgements xiii

List of Abbreviations xxiii

1 Introduction **1**

1.1 Fossil record 4

1.2 Adaptive radiation 10

1.3 Aims and Objectives 13

2 Cranial anatomy of †*Micrornatus* (Acanthomorpha: Scombridae) revealed using computed microtomography **15**

2.1 Introduction 16

2.2 Materials and methods 22

2.2.1 Materials examined 22

2.2.2 Specimen preparation: computed tomography 23

2.3 Systematic palaeontology 25

2.4 Description 26

2.4.1 Neurocranium and associated bones 26

2.4.2 Infraorbital bones and sclerotic ossicles 32
2.4.3 Jaws 32
2.4.4 Suspensorium 34
2.4.5 Ventral hyoid arch 37
2.4.6 Opercular series 39
2.5 Discussion 41
2.5.1 The challenges of interpreting fossil scombroids 41
2.5.2 The placement of †*Microrhynchus* 42
2.5.3 The taxonomy of London Clay scombrids and related taxa . 44
2.6 Acknowledgements 49

3 Morphology and phylogenetic relationships of fossil snake mackerels and cutlassfishes (Trichiuroidea) from the Eocene (Ypresian) London Clay formation 51

3.1 Introduction 53
3.2 Material and Methods 57
3.2.1 Institutional abbreviations 57
3.2.2 Specimens examined 57
3.2.3 X-ray computed tomography 61
3.2.4 Radiography 61
3.2.5 Dataset assembly 62
3.2.6 Phylogenetic analysis 63
3.3 Systematic palaeontology 64
3.3.1 Description 66
3.3.2 Description 77

3.3.3 Remarks 82
3.3.4 Description 84
3.4 Phylogenetic Results 88
3.4.1 Parsimony 88
3.4.2 Bayesian morphology 89
3.4.3 Bayesian combined analysis 93
3.5 Discussion 95
3.5.1 Relationships within Trichiuroidea 95
3.5.2 Placement of London Clay fossils within Trichiuroidea 98
3.5.3 An overview of the fossil record of Trichiuroidea, with comments on the placement of key fossil taxa 101
3.6 Conclusions 107
3.7 Acknowledgements 108

4 The oldest fossil mackerel and the Paleocene origin of modern percomorph families 111

4.1 Introduction 112
4.2 Methods 114
4.2.1 Micro-computed tomography 114
4.2.2 Phylogenetic dataset assembly and analysis 115
4.3 Systematic Palaeontology 116
4.3.1 Material 117
4.3.2 Locality and horizon 117
4.3.3 Diagnosis 117
4.3.4 Remarks 118

4.3.5 Description 121
4.4 Phylogenetic results 126
4.5 Discussion 128
4.5.1 Morphological framework for Scombridae 128
4.5.2 Fossil evidence for rapid diversification in Pelagiaria 129
4.6 Conclusion 132
4.7 Acknowledgements 132

5 Patterns of phenotypic evolution in Pelagiaria 135
5.1 Introduction 136
5.2 Material and Methods 142
5.2.1 Institutional Abbreviations 142
5.2.2 Landmark dataset assembly 142
5.2.3 Tree assembly 147
5.2.4 Disparity through time analysis 149
5.2.5 Model-fitting analyses 152
5.2.6 Parametric bootstrapping 155
5.3 Results 157
5.3.1 Morphospace 157
5.3.2 Disparity through time analysis 159
5.3.3 Model-fitting analyses 159
5.3.4 Parametric bootstrapping 164
5.4 Discussion 165
5.4.1 Deviations from a Brownian motion model of evolution . . . 166
5.4.2 *Lagerstätten* effects 168

5.4.3 Implications for models of radiation 172
5.5 Conclusion 177

6 Conclusions and Further Work **179**

6.1 Morphological understanding in Pelagiaria and its implications for evolutionary analyses 179
6.2 Evolutionary patterns in Pelagiaria 184
6.3 Inclusion of fossils in evolutionary analyses 187
6.4 Evolution in percomorphs 189
6.5 Summary 190

7 Bibliography **191**

Appendix A Supplementary Information associated with Chapter 3 'Morphology and phylogenetic relationships of fossil snake mackerels and cutlassfishes (Trichiuroidea) from the Eocene (Ypresian) London Clay formation' **227**

A.1 Scan Parameters 228
A.1.1 Radiography 228
A.1.2 Computed Tomography 228
A.2 Character List 230
A.3 Character Matrix 249
A.4 Character Optimisations 260
A.5 Extant Mr Bayes tree 262

Appendix B Supplementary Information associated with Chapter 4 'The oldest fossil mackerel and the Paleocene origin of modern percomorph families' 263

B.1 Specimens studied using μCT 263

B.2 Comparisons with Eocoelopomini 264

B.2.1 Original description of †*Landanichthys* 264

B.2.2 Comparisons with London Clay Eocoelopomines 265

B.2.3 Comparisons to †*Eocoelopoma portentosum* 269

B.3 Percomorpha *incertae sedis* RG 9.165 270

B.3.1 Brief Description 271

B.4 Scombrid character list 274

B.5 Removed characters 295

B.6 Character Matrix 295

B.7 Phylogenetic Analysis 298

B.8 Optimisation Tree 302

Appendix C Supplementary Information associated with Chapter 5 'Patterns of phenotypic evolution in Pelagiaria' - Scan Parameters for extant specimens used in this study 305

Appendix D Supplementary Information associated with Chapter 5 'Patterns of phenotypic evolution in Pelagiaria' 311

D.1 Landmarks 311

D.1.1 Midline 311

D.1.2 Left and Right 312

D.2 Additional fossil specimens 313

D.3 Fossil placement argumentation 314
D.4 A sample UCE Tree from Friedman et al. (Submitted) 316

Appendix E Supplementary Information associated with Chapter 5 - Parameters obtained in mvMORPH models **319**

Appendix F Supplementary Information associated with Chapter 5 - Code for Evolutionary Analysis **323**

Appendix G Applying the SHIFT model to the 'classical' mammal radiation **393**

List of Abbreviations

Anatomical

a.c	anterior ceratohyal
ang	angular
art	articular
bas	basisphenoid
bb	basibranchial
bh	basihyal
boc	basioccipital
bs	basisphenoid
hb	hypobranchial
cb	ceratobranchial
cl	cleithrum
cor	coracoid
den	dentary
d.h	dorsal hypohyal
eb	epibranchial
ecp	ectopterygoid
enp	endopterygoid
epo	epiotic
exo	exoccipital
fr	frontals
f.ic	foramen for internal carotid
f.nII	foramen for optic nerve (II)
f.nIII	foramen for ocular motor nerve (III)
f.nX	foramen for the vagus nerve (X)
g.a	gill arches
hb	hypobranchial
hyo	hyomandibular
hyo.fac	hyomandibular facet

Anatomical

int	intercalar
iop	interoperculum
lac	lacrimal
lat.com	lateral commissure
l.et	lateral ethmoid
mes	mesethmoid
m.et	median ethmoid
mpt	metapterygoid
mx	maxilla
na	nasal
op	operculum
pal	palatine
par	parietal
pb	pharyngobranchial
pmx	premaxilla
pop	preoperculum
p.pm	posterior opening of the posterior myodome
pro	pterotic
psp	parasphenoid
pt	post-temporal
pts	pterosphenoid
pto	pterotic
q	quadrate
s.c.p	supraorbital canal pores
soc	supraoccipital
soc.c	supraoccipital crest
sop	suboperculum
spo	sphenotic
sym	symplectic
tfc	trigeminal facial chamber
up	unicinate process
tp	toothplate
u	urohyal
v.h	ventral hypohyal
vo	vomer

Institutional

BMNH	Life Sciences collections, Natural History Museum, London, UK
CAMSM	Sedgwick Museum, University of Cambridge, Cambridge, UK
FMNH	Division of Fishes, Field Museum, Chicago, USA
IRSNB	Institut Royal des Sciences Naturelles de Belgique, Brussels, Belgium
LACM	Natural History Museum of Los Angeles County, Los Angeles, USA
NHMUK	Earth Sciences collections, Natural History Museum, London, UK
RGM	Naturalis Biodiversity Centre, the Netherlands
UMMZ	Division of Fishes, University of Michigan Museum of Zoology, Ann Arbor, USA

Other

†	Denotes extinct taxa following Patterson and Rosen (1977)

Chapter 1

Introduction

Percomorphs, a major clade within Acanthomorpha (spiny-rayed fishes), comprise more than 14,540 species in around 250 families, making up a quarter of living vertebrates. Diversifying rapidly in the aftermath of the Cretaceous-Paleogene (K-Pg) extinction, percomorphs have received increasing attention in recent years as the focus of large-scale genomic studies (Near et al., 2012, 2013; Betancur-R et al., 2013; Harrington et al., 2016; Betancur-R et al., 2017; Alfaro et al., 2018). Pelagiaria, comprising 16 families of open-ocean marine fishes united by a pelagic ecology is a group within Percomorpha (Miya et al., 2013; Campbell et al., 2018). Pelagiaria is distributed worldwide and encompasses over 220 species (Miya et al., 2013; Campbell et al., 2018) split into the families Pomatomidae (bluefish), Bramidae (pomfrets), Arripidae (australian salmons), Caristiidae (manefishes), Chiasmodontidae (swallowers), Icosteidae (ragfishes), Scombrolabracidae (longfin escolar), Centrolophidae (medusafishes), Nomeidae (driftfishes), Stromateidae (butterfishes), Amarsipidae (bagless glassfishes), Ariommatidae (ariommatids), Tetragonuridae (squaretails), Gempylidae (snake mackerels), Trichiuridae

(cutlassfishes) and Scombridae (tunas and mackerels) (Fig. 1.1). These extant families are likely joined by the extinct †Euzaphlegidae, a likely polyphyletic assemblage (Patterson, 1993*b*; Monsch and Bannikov, 2012). Historically attributed to the 'gempylid' stem (Monsch and Bannikov, 2012) owing to the presence of large premaxillary fangs, it is clear that some putative members of the group share characters with scombrolabracids e.g †*Palimphyes* (see below). A thorough review of †Euzaphlegidae is required to further clarify this aspect of taxonomy. Characterised by their open-marine ecology (Miya et al., 2013; Near et al., 2013; Betancur-R et al., 2013), Pelagiaria also show some remarkable specialisations, ranging from bioluminescence and distensible stomachs in chiasmodontids (Melo, 2009*b*, 2010), to endothermy independently acquired in multiple lineages of scombrids (Block et al., 1993), pharyngeal sacs in stromateoids (Haedrich, 1967), enlarged dorsal and anal fins in caristiids and bramids (Miya et al., 2013), and elongated body forms in trichiuroids (Russo, 1983; Gago, 1998). Coupled with molecular evidence showing very short branch lengths early in the history of the group (Miya et al., 2013), this morphological diversity has been suggested as evidence of an ancient adaptive radiation in Pelagiaria (Miya et al., 2013; Campbell et al., 2018).

Identified through large-scale molecular studies (Miya et al., 2013; Near et al., 2013; Betancur-R et al., 2013; Alfaro et al., 2018), Pelagiaria have never been united in their entirety based on their morphology. The monophyly of many of their subclades is strongly supported by anatomical evidence (e.g. Scombroidei Johnson, 1986; Collette et al., 1984; Stromateoidei, Doiuchi et al., 2004). Additionally, morphological studies of individual families are often manually constructed, from before the advent of formal phylogenetic analyses. Character sets exist in

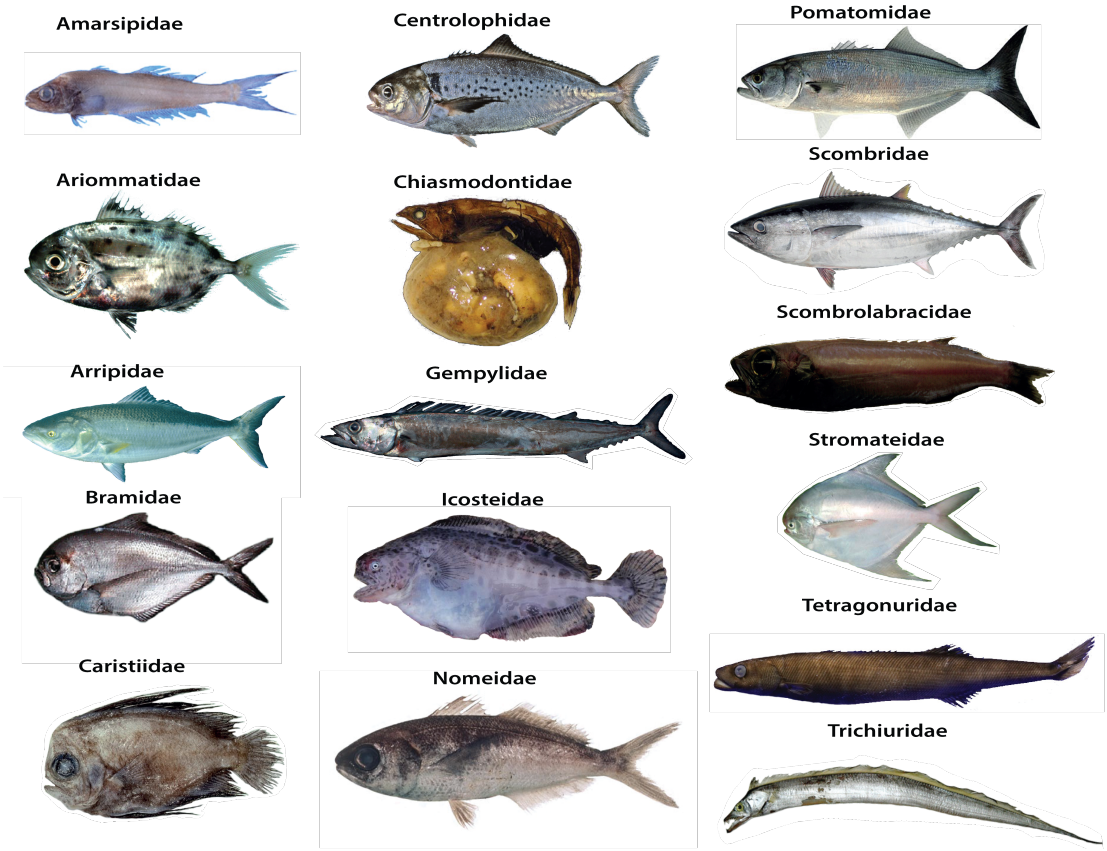


Figure 1.1: The phenotypic diversity represented in the 16 families of Pelagiaria.

isolation for gempylids (Russo, 1983), trichiurids (Gago, 1997, 1998), chiasmodontids (Melo, 2009*b*,*a*, 2010), and the stromateoid families (Ariommatidae, Amarsipidae, Centrolophidae, Nomeidae, Stromateidae and Tetragonuridae) (Haedrich, 1967; Doiuchi et al., 2004; Jawad and Jig, 2017). There is also detailed verbal argumentation for the relationships of Scombroidei (including billfishes, no longer associated with the group) put forward in a series of papers (Johnson, 1986; Collette and Russo, 1984; Collette et al., 1984; Collette and Gillis, 1992; Collette, 1999; Collette et al., 2001). Descriptions of caristiids (Trunov et al., 2006; Kukuev et al., 2012, 2013; Stevenson and Kenaley, 2011, 2013), bramids (Mead, 1972; Last

and Moteki, 2001) and tetragonurids (Smith, 1953; Grey, 1955; Haedrich, 1967) are available but no formal analyses including character matrices exist. There are also descriptions available for the monotypic families Icosteidae (Komori, 1993), Pomatomidae (Leapley, 1952) and Scombrolabracidae (Grey, 1960), the latter of which has been included in discussions of trichiuroid systematics (Russo, 1983; Gago, 1998). Initial development of character sets for families within the group, initially for the better known families previously indentified as Scombroidei (with the exclusion of xipihoids), will allow further development of a character set for the whole of Pelagiaria.

1.1 Fossil record

A major source of ambiguity for investigating putative patterns of adaptive radiation in Pelagiaria is the poorly understood relationship between fossil taxa and their extant relatives. This lack of clarity is somewhat surprising given that the fossil record of Pelagiaria is relatively good, although some families are better represented and understood than others. In addition to their wide geographical range in the modern, the fossil record of Pelagiaria is widely distributed with specimens found in North America, Europe (Leriche, 1910; Casier, 1966), Africa (Dartevelle and Casier, 1943, 1949, 1959; Arambourg and Signeux, 1952), Russia (Monsch and Bannikov, 2012), the Middle East (Arambourg, 1967; Monsch, 2005) and Australasia (Monsch, 2005). A number of these sites preserve complete and articulated flattened specimens, useful for discerning body form and postcranial characters. However, uncrushed three-dimensional material is also known, notably from the London Clay (Ypresian, 52-49 Ma) of the UK, the Boom Clay (Rupelian,

33-28 Ma) of Belgium and the Landana Formation (Selandian, ∼61 Ma) of Angola. Three-dimensional fossil examples provide an opportunity to obtain details of skeletal morphology not visible in flattened fossils, including details of internal surfaces of bones and articulations with other ossifications, that are comparable to osteologial observations for extant material. This enables direct comparison with an extant morphological framework for skeletal characters, and it is these three-dimensional fossil examples which are the focus of this thesis.

The fossil record of Pelagiaria is unevenly distributed across the families (Fig. 1.2). The stratigraphically oldest material previously associated with Pelagiaria was isolated 'gempylid' otoliths from the early Campanian, but recent work has highlighted that these belong to an aulopiform (Schwartzhans et al., 2018). Therefore the oldest material assigned to Pelagiaria is either isolated teeth of †*Eutrichiurides*from the latest Danian/earliest Selandian of Morocco (Arambourg and Signeux, 1952), or an articulated scombrid, †*Landanichthys*, and isolated teeth of †*Eutrichiurides*, associated with Trichiuridae, both from the early Selandian (∼61 Ma) Landana Formation, Angola (Dartevelle and Casier, 1949, 1959; Miya et al., 2013; Solé et al., 2018). The oldest articulated Trichiuridae, however, are from the London Clay Formation, UK, which is Ypresian in age (56-53 Ma) (Monsch, 2005; Miya et al., 2013). The oldest unequivocal 'gempylid' material is the body fossil †*Argestichthys* from the Danatinsk Suite, Turkmenistan (Prokofiev, 2002). Previously the oldest known caristiid fossil was thought to be †*Exellia* (Blot, 1969; Patterson, 1993*c*), also with an oldest occurance from the Danatinsk Suite, Turkmenistan, however elevated vertebral counts have led to the rejection of this association (Bannikov and Tyler, 2004). The oldest, and only, known caristiids *Absalomichthys* and *Chalcidichthys* are Miocene in age (David, 1943; Fierstine

et al., 2012). Similarly the fossil record of bramids has previously been thought to extend back to †*Bramoides* in the Ypresian London Clay (Casier, 1966), however Patterson (1993*b*) questioned the affinity of †*Bramoides* and personal observations of the fossils associated with the genus show that it is a gasterochismatine (Scombridae). The oldest representative of Bramidae is therefore †*Paucaichthys elamensis* (Přikryl and Bannikov, 2014) from the Eocene. Stromateoids are known from body fossils from around the Paleocene-Eocene boundary of Denmark (Bonde et al., 2008). The Centrolophidae are tentatively known from three extinct monotypic genera, the oldest of which is †*Zorzinia* from Bolca, Italy (Ypresian: 49.11 Ma) (Bannikov, 2000*c*; Baciu and Bannikov, 2003; Bannikov, 2012), some uncertainty is associated with the placement of these taxa, because of their generalised percoid body plan and the difficulties of seeing pharyngeal dentition in fossil taxa (Bannikov, 2018). †*Carangopsis* has putatively been assigned to the Pomatomidae, which would give the family a fossil record extending back to the Ypresian (Bolca: 49.11 Ma) (Blot, 1969). However the fossil record of the pomatomids remains relatively poorly constrained (Bannikov and Fedotov, 1989; Purdy et al., 2001), and if this interpretation of †*Carangopsis* is incorrect the earliest representative of Pomatomidae would be †*Lednevia* from the Miocene of the Caucasus (Bannikov, 1996). The Stromateidae, to which †*Pinichthys* is tentatively assigned, is from the Rupelian of coeval deposits from Poland and North Caucasus (31.35 Ma). The Ariommatidae also have a fossil record stretching back to the Rupelian, with †*Isurichthys* known from the lower Oligocene of the Northern Caucasus (Bannikov, 2012; Miya et al., 2013). †*Palimphyes* bears strong similarities to Scombrolabracidae, with large premaxillary fangs and enlarged pectoral fins, characters that have led it to be previously associated with Gempylidae (Monsch

and Bannikov, 2012). Association between Scombrolabracidae and 'gempylids' is also supported by Friedman et al. (Submitted). However if this association between †*Palimphyes* and Scombrolabracidae is not confirmed the oldest known fossils associated wih the family are from the Morozaki Group of Japan (11.62 Ma; Ohe, 1993). The remaining families in Pelagiaria have relatively shallow and poorly constrained fossil records: Tetragonuridae: 2.588 Ma (Landini and Sorbini, 1992); and Chiasmodontidae: 11.62 Ma; (Carnevale, 2007), while the Arripidae, Amarsipidae and Icosteidae have no known fossil record.

A literal reading of this fossil record suggests that the group must have diversified in the immediate aftermath of the Cretaceous-Paleogene (K-Pg) boundary. The K-Pg boundary shows patterns of high turnover in fish and other marine groups (Alfaro et al., 2009; Friedman, 2010). Teleosts in particular show clear patterns of ecomorphological selectivity across the K-Pg boundary, with those occupying higher tropic levels tending to be most affected by the mass extinction event (Cavin, 2002; Friedman, 2009). Notably, many teleosts that went extinct at the K-Pg exhibit phenotypes that are very similar to a subset of extant Pelagiaria (e.g. predatory form, fusiform body, open water free swimming) and may represent the extinct ecological analogues of this group (Friedman, 2010). This pattern of replacement observed in Pelagiaria is also seen in other groups across the K-Pg boundary, for example predatory chondrichthyans (Kriwet and Benton, 2004). Ecological replacement is postulated as a driver of adaptive radiation (Schluter, 2000), with the extinction of previously diverse groups providing opportunities to surviving lineages by emptying of niches, and this pattern of replacement can be seen throughout the fossil record (Erwin, 2001; Glor, 2010). Other well-known examples include the replacement of non-avian dinosaurs by placental mammals after

the K-Pg boundary (O'Leary et al., 2013) and the replacement of crurotarsan archosaurs by dinosaurs across the Triassic-Jurrasic boundary (Brusatte et al., 2008, 2010).

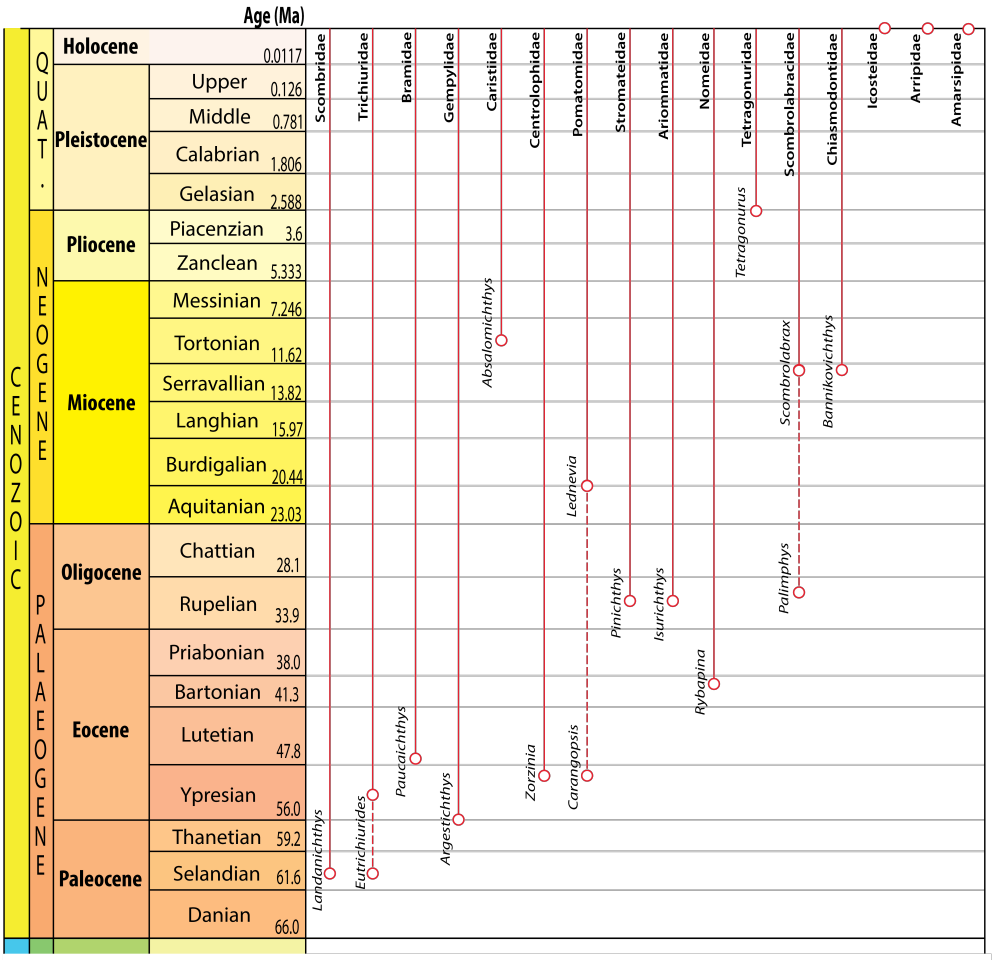


Figure 1.2: The known fossil record for the families comprising Pelagiaria, added to and adapted from Miya et al. (2013). Dotted lines indicate uncertainties in assignment of older fossils.

The fossil record of Pelagiaria is of particular significance when set against the percomorph record more generally. Many of the earliest known percomorph fossils, found in the latest Cretaceous, are either 'perciformes' *sensu lato* or belong to deeply diverging percomorph lineages (Ophidiiformes: Carnevale and Johnson,

2015; Batrachoidiformes: Bannikov and Sorbini, 2000; Syngnathiformes Sorbini, 1981). During the critical Paleocene interval when many percomorph groups are assumed to have diversified, the fossil record is similarly sparse (Patterson, 1993*c*), and only a few articulated or associated percomorph fossils are known from this interval, and most are *incertae sedis* (Davis, 1890; Adolfssen et al., 2017; Arratia et al., 2004; Alaniz-Galvan, 2011; Cantalice and Alvarado-Ortega, 2017). There are however four exceptions: a sygnathiform, †*Eekaulostomus cuevasae* assigned to an extinct monotypic family (Cantalice and Alvarado-Ortega, 2016); †*Mene purdyi* assigned to the menids (Friedman and Johnson, 2005); a putative serranid, †*Paleoserranus lakamhae* (Alaniz-Galvan, 2011; Alvarado-Ortega et al., 2015; Cantalice et al., 2018); and a scombrid, †*Landanichthys* (Dartevelle and Casier, 1949, 1959). By the Paleocene-Eocene boundary percomorphs are common in the fossil record, aided by a substantially better record for fossil fishes as a whole (Friedman and Carnevale, 2018). Sites like Bolca and the London Clay yield diverse fish assemblages (Bannikov, 2000*b*; Prokofiev, 2002; Friedman et al., 2016; Friedman and Carnevale, 2018), with abundant fossil members of living percomorph families, reminiscent of modern diversity (Patterson, 1993*c*).

This good fossil record combined with the excellent three-dimensional preservation of many specimens makes Pelagiaria an ideal group for integrating palaeontological, anatomical, and molecular data in order to test hypotheses about evolutionary diversification. Micro computed tomography (μCT), now a commonly used tool in paleontological research, provides an opportunity to obtain details of internal anatomy in both fossil and extant specimens in three-dimensions without destructive sampling. The benefits of this for studying Pelagiaria are two-fold.

Firstly, it enables recovery of skeletal character information for historically prepared fossil specimens, particularly those that are three-dimensionally preserved. Two sites in particular provide articulated three-dimensional pelagiarian skulls, the Eocene London Clay and the Selandian Landana Formation, and these two sites provide fossils for the focus of this thesis. Secondly, in combination with equivalent data for extant specimens, it is possible to build a three-dimensional geometric morphometric dataset, with which to examine evolutionary patterns.

1.2 Adaptive radiation

Adaptive radiation was first proposed by Osborn in a series of papers at the beginning of the 20th century to explain the radiation of mammals in the Cenozoic (Osborn, 1902). Simpson brought it to the fore in the 1950s and it has since been widely adopted as a term in both biology and palaeobiology. Studies of adaptive radiation overwhelmingly target modern microcosms, which are used as model systems for macroevolutionary processes, for example cichlids in African rift valley lakes (Kocher, 2004; Seehausen, 2006). Despite the use of the term in recent literature for small-scale radiations of forms, the original definition of an adaptive radiation was much broader, both temporally and spatially (Osborn, 1902). Examination of the fossil record highlights patterns of widespread and apparently rapid origination of disparate lineages on multiple occasions, often in association with the time period immediately after a mass extinction event (Schluter, 2000; Erwin, 2001; Kriwet and Benton, 2004; Alfaro and Santini, 2010). It is unclear whether modern radiations are analogous to these postulated radiations in the fossil record. Many of the classic modern examples have poor fossil records (Schluter,

2000) making them difficult to study in such a framework, but larger-scale examples like the radiation of placental mammals, despite having better fossil records, are challenging to study in their own right as they represent overwhelmingly large study systems of several thousand modern and extinct species.

An adaptive radiation can be characterised as the rapid divergence of a lineage from a single ancestor into numerous lines specialised for a particular niche, or adaptive zone (Simpson, 1953; Schluter, 2000). This rapid cladogenesis is associated with morphological and ecological divergence between lineages, and in the case of adaptive radiation is followed by a period of relatively low cladogenesis in association with persistent and conserved morphologies or ecologies (Foote, 1997; Jackson and Cheetham, 1999; Schluter, 2000; Harmon et al., 2003; Hansen and Houle, 2004; Estes and Arnold, 2007; Simões et al., 2016).

Modern thinking on adaptive radiation can be traced back to the work of Simpson (1944) in *Tempo and Mode in Evolution*. Here, as the title suggests, he presents a model of adaptive radiation based on the interplay of two factors, rate (tempo) and mode. Simpson presents this model visually (see Simpson, 1944: fig. 35), but describes an early "explosive" phase of evolution followed by a period of "normal" evolution. This model has been broadly built on and interpreted in recent literature as a model where rates of evolution change across the tree, in the case of adaptive radiation with high rates early in the history of the group. This is most commonly now implemented in evolutionary analyses as the "Early Burst" model (Harmon et al., 2010), with a variety of other models also describing similar process (e.g. Pagel's δ; Pagel, 1998). Surprisingly, it has been found that relatively few groups show this pattern of adaptive radiation (Harmon et al., 2010).

Furthermore, much of the research into models of adaptive radiation focus on

rate and not the other facet of evolutionary processes, mode, to the point that 'fast rates of evolution' have become synonymous with discussions of adaptive radiation. Changes in mode are poorly understood and poorly constrained in evolutionary processes, with only a couple of studies implementing models of shifting mode (Slater, 2013; Vidal-García and Keogh, 2017). This is despite constraint being implicit in ideas of adaptive peaks and adaptive zones (Simpson, 1944). Mode of evolution can change as a result of intrinsic or extrinsic factors which influence a clade, but does not require a change in the rate of evolution. In the example of the mammal radiation, some period of constraint when they competed with non-avian dinosaurs was followed by a period of unconstrained evolution (Slater, 2013), an example of a change in mode where no change in rate is required to observe this evolutionary pattern.

Pelagiaria present an opportunity to test our understanding of the term adaptive radiation, the processes of rate and mode, and to investigate the evolutionary dynamics of such a radiation on broad temporal and spatial scales. They have a well-established molecular phylogenetic framework (Miya et al., 2013; Campbell et al., 2018; Alfaro et al., 2018; Friedman et al., Submitted), a good fossil record (see Fig. 1.2) and are a group that is phenotypically diverse (see Fig. 1.1) while containing a tractable number of species. Even with the remaining uncertainty in the relationships between families in the early history of the group (Miya et al., 2013; Alfaro et al., 2018; Campbell et al., 2018), the pattern of diversification in Pelagiaria currently recovered by molecular datasets seems to be characteristic of an adaptive radiation, with rapid early divergences leading to morphologically and ecologically distinct family groups. The fossil record provides a second strand of

evidence for this, with a literal reading suggesting that recognisably modern phenotypes were established by the Paleocene-Eocene boundary as indicated by the first appearances of many extant family-level lineages (see Fig. 1.2).

1.3 Aims and Objectives

This thesis aims to take a synthetic approach to the group Pelagiaria. I investigated the fossil record in the context of the extant diversity of the group in order to use it as a study system for the concept of adaptive radiation. The thesis can be split into three broad strands:

1. I use micro computed tomography (μCT) scanning to visualise anatomical details in extant and fossil taxa within the group Pelagiaria. Many fossil taxa have not been studied in detail in the last few decades, with existing accounts made prior to the widespread use of technologies capable of visualising internal skeletal elements. Consequently the relationships of fossils to extant taxa are largely uncertain, with identity limited to a broad family level assignments. The Ypresian London Clay (Friedman et al., 2015) preserves many of these specimens, which are relatively unique in their three-dimensional articulated preservation. This makes these specimens ideal for study in an extant framework. Chapters 2-4 investigate these three-dimensional pelagiarian taxa, revealing new details about their anatomy.

2. Using a combination of: literature searches; observation of specimens, both wet and dry; radiography and μCT, I create a morphological framework for the three most speciose families within Pelagiaria, the 'gempylids' and

trichiurids (Chapter 3) and the scombrids (Chapter 4). Key fossil taxa are then placed in this framework for the first time.

3. Using the resulting morphological framework, in addition to molecular information, I assess if evolutionary patterns within Pelagiaria show changes in mode or rate (Chapter 5), indicating adaptive radiation-like dynamics, and compare this to other adaptive radiations discussed in the literature.

Chapter 2

Cranial anatomy of †*Micrornatus* (Acanthomorpha: Scombridae) revealed using computed microtomography

This paper was published as:

Beckett, H. T. and Friedman, M. 2016. The one that got away from Smith Woodward: cranial anatomy of †*Micrornatus* (Acanthomorpha: Scombridae) revealed using computed microtomography. *In*: Johanson, Z., Barrett, P. M., Richter, M. & Smith, M. (eds) Arthur Smith Woodward: His Life and Influence on Modern Vertebrate Palaeontology. *Geological Society, London, Special Publications*, **430**. First published online November 5th, 2015, http://doi:10.1144/SP430.16.

MF scanned the material. HB generated the CT renderings. HB, with input and comments from MF, interpreted the specimen, wrote the manuscript, produced the figures and supplementary data.

Abstract

The monotypic scombrid fish †*Micrornatus* is represented by a single skull from the early Eocene (Ypresian) London Clay Formation of southeastern England. Although Arthur Smith Woodward substantially increased the diversity of scombrids and scombrid-like taxa known from this deposit, he seems not to have studied the fossil that would later be recognized as †*Micrornatus*. Here we re-examine this specimen using computed microtomography, with two principal aims: first, a revised anatomical account with an emphasis on concealed features; and, second, 'proof-of-concept' for the tomographic study of fish crania from the London Clay. Scans reveal new details of the braincase, suspensorium and ventral hyoid arch. We compare the cranial anatomy of †*Micrornatus* with other members of Eocoelopomini, a group also containing the genera †*Eocoelopoma*, †*Palaeothunnus* and possibly †*Landanichthys*. Clarification of the taxonomy and phylogeny of early fossil scombrids is needed, and we suggest that computed tomography will be a useful tool for revealing the anatomical evidence needed to accomplish this goal.

2.1 Introduction

In his *Catalogue of Fossil Fishes in the British Museum (Natural History)*, Arthur Smith Woodward described numerous specimens from the early Eocene (Ypresian) London Clay Formation (see Friedman et al., 2015). Among these materials was a diversity of forms currently aligned with scombroids (Monsch, 2005), a group that has undergone considerable taxonomic restructuring over the past century (e.g. Regan, 1909; Gosline, 1968; Collette et al., 1984; Johnson, 1986; Carpenter et al.,

1995; Collette et al., 2001; Orrell et al., 2006; Yagishita et al., 2009; Betancur-R et al., 2013; Miya et al., 2013; Near et al., 2013) but includes a core membership of three percomorph families: Scombridae (tunas and mackerels), Gempylidae (snake mackerels) and Trichiuridae (cutlassfishes).

Smith Woodward's classification included a Scombriformes containing a variety of lineages now recognized as constituting a polyphyletic assemblage. Apart from a Scombridae equivalent in composition to the 'core' Scombroidei of current usage (Scombridae + Gempylidae + Trichiuridae), Smith Woodward's Scombriformes included carangids, menids, stromateoids and xiphioids, as well as taxa now recognized as pleuronectiforms (Friedman, 2008), polymixiids (Patterson, 1964) and lampridiforms (Davesne et al., 2014). Smith Woodward's Catalogue represented a substantial increase in the diversity of mackerel-like taxa known from the London Clay, adding four new genera to Agassiz's †*Sphyraenodus*: †*Eothynnus* (now interpreted as a carangid; Bannikov 1979), †*Scombrinus*, †*Eocoelopoma* and †*Scombramphodon*. These accounts drew on numerous specimens of each of these new taxa (†*Eothynnus*, 13 specimens; †*Scombrinus*, 35 specimens; †*Eocoelopoma*, 33 specimens).

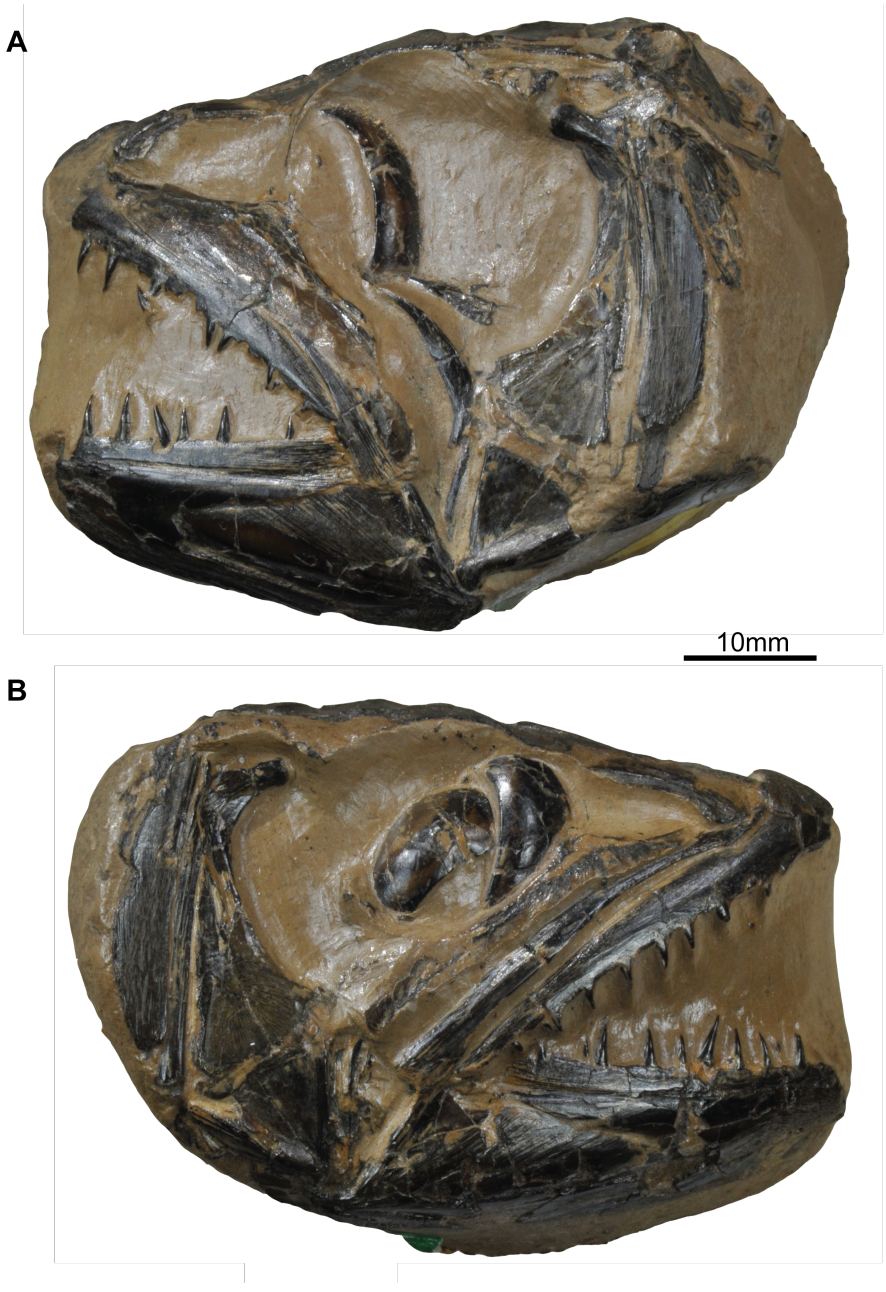


Figure 2.1: Photos of the fossil †NHMUK PV OR 36136 †*Micrornatus hopwoodi*in A, left lateral view and B, right lateral view.

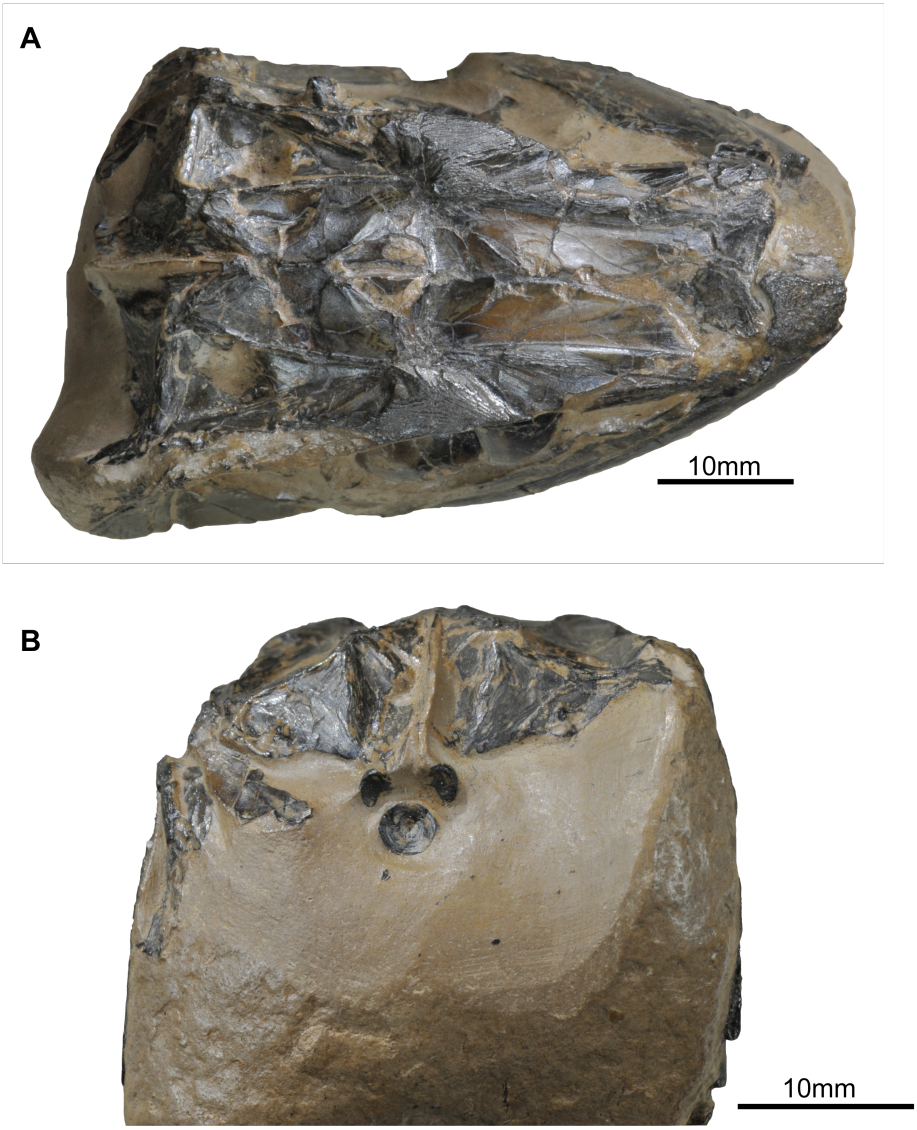


Figure 2.2: Photos of the fossil †NHMUK PV OR 36136 †*Micrornatus hopwoodi*in A, dorsal view and B, posterior view.

Given Smith Woodward's care in reviewing these and other materials from the London Clay, it is surprising that he made no mention of specimen NHMUK PV OR 36136, a well-preserved and uncrushed skull from the Isle of Sheppey, acquired by the British Museum (Natural History) in 1851, several decades before he began work on the Catalogue. This fossil was first described by Casier (1966) in his monumental overview of the London Clay fish fauna, where he placed it as a new species in Smith Woodward's †*Eocoelopoma*: †*Eocoelopoma hopwoodi*. On the basis of differences related to cranial ornament, dental morphology and patterns of skull roofing bones, Monsch (2005) recognized this individual as distinct from other species of †*Eocoelopoma*, and erected the genus †*Micrornatus* to accommodate it. At present, NHMUK PV OR 36136 represents the type and only example of †*Micrornatus*.

We have re-examined this fossil with two goals in mind. First, we seek to provide a revised account of the anatomy of †*Micrornatus*, the 'one that got away' from Smith Woodward. Although descriptions of this specimen are available (a full account is given in Casier (1966, pp. 284-286), with minor amendments given in Monsch (2005, p. 476)), these are based exclusively on external structure and many aspects of internal morphology remain unclear. Specifically, we have applied computed microtomography (μCT) in order to visualize concealed structure in this unique specimen. This reflects our second goal: to provide proof-of-concept of this approach for studying fishes from the London Clay (as done successfully in birds from this deposit; Milner and Walsh, 2009; Walsh and Milner, 2011), as well as three-dimensionally preserved fossil teleosts more generally (Friedman et al., 2015).

New insights on the anatomy of extinct scombroids are particularly topical,

given an emerging picture from molecular data placing tunas and their immediate relatives in a previously unrecognized clade characterized by pelagic ecologies (Betancur-R et al., 2013; Miya et al., 2013; Near et al., 2013). Evolutionary timescales for diversification in this group, variously called Pelagia, Pelagiaria or Scombriformes, vary by tens of millions of years (Betancur-R et al., 2013; Miya et al., 2013; Near et al., 2013; Santini, 2013). Part of this ambiguity stems from difficulties in applying fossil-based calibrations in molecular clock studies of scombroids and their immediate relatives, as no extinct member of these groups has ever been placed in a formal, published cladistic analysis (informal or adapted trees are found in Bannikov (1985) and Monsch and Bannikov (2012); a formal, but unpublished, cladistic analysis is presented by Monsch (2000)). A re-evaluation of the relationships of scombroids both fossil and modern is desperately needed, but well beyond the scope of this contribution. Instead, we aim to demonstrate the utility of μCT as a non-destructive tool for surveying the anatomy of three-dimensionally preserved teleost crania and, by extension, providing raw character data that might feed into future phylogenetic analyses.

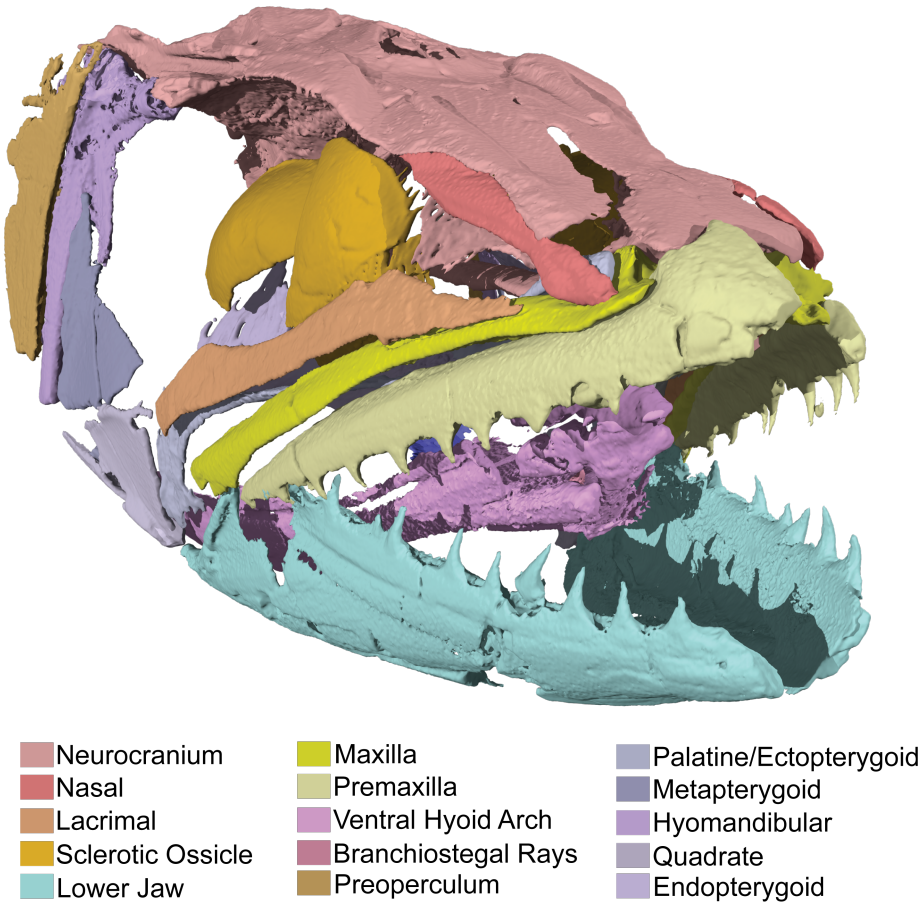


Figure 2.3: Three-dimensional rendering of the skull of NHMUK PV OR 36136 †*Micrornatus hopwoodi*.

2.2 Materials and methods

2.2.1 Materials examined

All fossil specimens listed below and examined in the course of this study are from the London Clay Formation (Ypresian) of SE England. Provenance data are poor for many of these specimens, but all probably derive from the Isle of Sheppey. For a review of geological context, see Friedman et al. (2015). †*Eocoelopoma*

colei (Woodward, 1901). NHMUK PV P 26702 (specimen referred to species by Monsch, 2005), three-dimensionally preserved neurocranium and sclerotic ossicle. †*Eocoelopoma curvatum* (Owen, 1854). NHMUK PV OR 44877 (neotype specimen), three-dimensionally preserved skull; NHMUK PV OR 24613, (specimen referred to species by Monsch, 2005, three-dimensionally preserved neurocranium; NHMUK PV P 9455 (specimen referred to species by Monsch, 2005), three-dimensionally preserved skull. †*Eocoelopoma gigas* Casier, 1966. NHMUK PV OR 39221, three-dimensionally preserved skull. †*Micrornatus hopwoodi* Casier, 1966. NHMUK PV OR 36136 (holotype and only specimen), three-dimensionally preserved skull (Figs 2.1,2.2).

2.2.2 Specimen preparation: computed tomography

Historical preparation of the type and only specimen of †*Micrornatus* (NHMUK PV OR 36136) revealed bones on the surface of the specimen, including the external faces of the neurocranium, jaws, preoperculum and part of the suspensorium. We applied μCT in order to visualize anatomical components that remain buried in the clay matrix, without risking damage to this unique specimen through additional mechanical preparation.

Sample scanning.

The specimen was scanned with a Metris X-Tek HMX ST μCT scanner in the Imaging and Analysis Centre of the Natural History Museum, London. It was scanned using a 2.5 mm copper filter, with the following settings: 205 kV, 198 mA and 3128 projections.

Segmentation of tomographic data.

We segmented the reconstructed series of tomographs using the software package Mimics Research Version 17.0 x64 (http://biomedical.materialise.com/mimics). Segmentation within Mimics can be achieved in a number of ways depending on bone and matrix contrast and other aspects of preservation. These factors greatly influence the quality of the model produced. Pyritization in particular can affect whether the margins and sutures of bones are clearly visible, as the mineral is often apparent as a sheath surrounding individual ossifications or sets of adjacent bones in material from the London Clay (Beckett & Friedman *pers. obs.* of additional scans). This can make it difficult to use a general thresholding technique. In NHMUK PV OR 36136, there is considerable internal pyrite growth, particularly in the anterior portion of the skull. Initially the model (Fig. 2.3) was built up from a global threshold that selected the majority of the bone. This was then split into individual masks for each ossification, using a combination of the region-growing tool (which populates a new mask with interconnected voxels of the specified grey values) and the 3D edit tool (where sections of bone can be deleted or separated).

These separate masks for each bone were then edited manually, by segmenting the parts of these bones that could not be added to the mask using general thresholding techniques. This approach is particularly useful in cases where there is a very low contrast between the bone and the matrix (e.g. in the middle or on the edge of the specimen), or where there is a high degree of pyritization. The manual technique involves selecting an area of bone visible in cross-section in every nth slice and interpolating between these slices. Where possible this is done using a threshold value, so that only voxels within the area highlighted that fall within a

specific range of user-specified grey values are selected. However, in some sections of the fossil bones are so poorly mineralized, or so heavily pyritized, that they must be added manually without specifying grey values. There are particularly high levels of pyritization in the anterior portion of the skull, around the anterior of the parasphenoid, vomer and hyoid arch.

Rendering of 3D models.

High-resolution models produced in Mimics were exported as surface (.ply) files. These surface files were then imported into Blender (blender.org) and rendered into two-dimensional high-resolution images.

2.3 Systematic palaeontology

Teleostei Müller, 1845

Percomorpha Rosen, 1973 *sensu* Johnson and Patterson, 1993

Pelagia Miya & Friedman, 2013 in Miya et al., 2013

Scombroidei Regan, 1909 sensu Miya et al., 2013

Scombridae Rafinesque-Schmaltz, 1815

Eocoeolopomini Monsch and Bannikov, 2012

†*Micrornatus* Monsch, 2005

†*Micrornatus hopwoodi* Casier, 1966

1966 †*Eocoelopoma hopwoodi* Casier, p. 284, text fig. 65, pl. 44, fig. 3.

2005 †*Micrornatus hopwoodi*(Casier) Monsch, p. 476, fig. 31.

2.4 Description

2.4.1 Neurocranium and associated bones

Casier (1966, fig. 65) provided a drawing of the dorsal surface of the neurocranium indicating the position of sutures. With the exception of the division between the frontals, we had great difficulty in tracing sutures on exposed surfaces of this specimen. Pyritization, combined with the resolution of our tomographs, does not permit the identification of sutures between most ossifications of the neurocranium. Our references to individual bones below are based on positional comparisons with other scombrids (Starks, 1910; Collette and Chao, 1975; Collette et al., 1984) rather than explicit delimitation of ossifications based on visible sutures.

In dorsal view the neurocranium is broad and relatively square, and narrows slightly anteriorly (Figs 2.4A & 2.5A). The paired frontals are broad and meet in a suture that is approximately straight, with some minor deviations from the midline. A shallow concavity on the lateral margin of the frontal anterior to the orbit marks the articulation with the elongate nasal (Fig. 2.3). Fine ornament radiates anterolaterally from the middle of the frontal, immediately above the orbit (Fig. 2.2A). The frontals surround an opening along the dorsal midline near the rear of the orbit. This opening is subtriangular and narrows posteriorly, and has been interpreted previously as a pineal foramen (Monsch 2005). However, remnants of thin bony laminae are apparent within it, both through visual inspection and in tomographs. We cannot exclude the possibility that the pineal region was completely covered with a thin surface of bone. The median ethmoid sits anterior to the frontals and articulates ventrally with the dorsal margin of the vomer (Figs

2.4B & 2.5B). The median ethmoid has a concave anterior margin, conferring a saddle shape in dorsal view that is apparent both externally and from models derived from μCT (Figs 2.2A, 2.4A & 2.5A).

In dorsal view, the posterior half of the braincase bears a series of shallow fossae bounded by ridges (Figs 2.4A & 2.5A). Thickenings extending along the posterior and lateral margins of the skull define the outer margins of the more lateral fossa; the pterotic and frontals contribute to the equivalent of the lateral ridge in modern scombrids. These ridges join at the pointed posterolateral corner of the braincase. The lateral and posterior ridges are joined by a pair of low crests that extend anteroposteriorly, subparallel to the midline. Based on comparison with other scombrids, we conclude that the parietals and epiotics contribute to these more medially placed ridges, although we cannot clearly identify the sutures delimiting these bones. Bone appears to be absent from the centre of the lateral fossa defined by these ridges, consistent with the cartilage-filled fontanelle between ossifications that contribute to the equivalent cranial depression in some modern scombrids (e.g. Allis 1903, pl. 4, fig. 5). The midline of the skull posterior to the frontals bears a supraoccipital crest, although this is clearly broken dorsally and posteriorly. In combination with the parietal–epiotic crest and the raised posterior region of the frontals, the supraoccipital defines an additional fossa on the dorsal surface of the skull roof. This is shallower than its more lateral counterpart.

In posterior view, the neurocranium is substantially wider than deep. The foramen magnum is triangular in shape. It is continuous with a keyhole-shaped gap that extends dorsally along the midline, terminating at the posterior margin of the supraocciptial and separating bones of the right and left half of the skull. Similar gaps between the exoccopitals are apparent in some modern scombrids

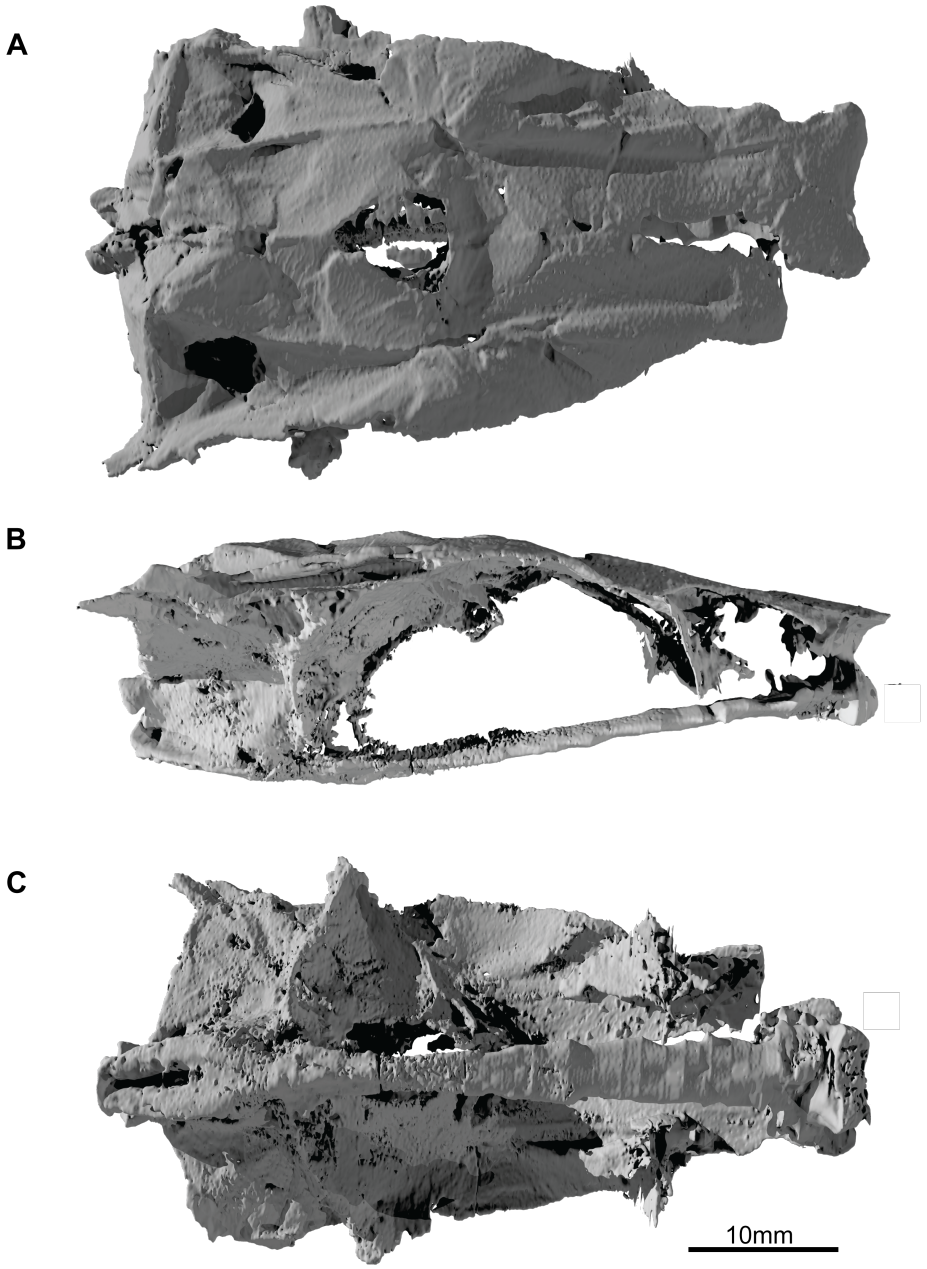


Figure 2.4: Three-dimensional renderings of the neurocranium of NHMUK PV OR 36136 †*Micrornatus hopwoodi*in A, dorsal view, B, right lateral view and C, ventral view.

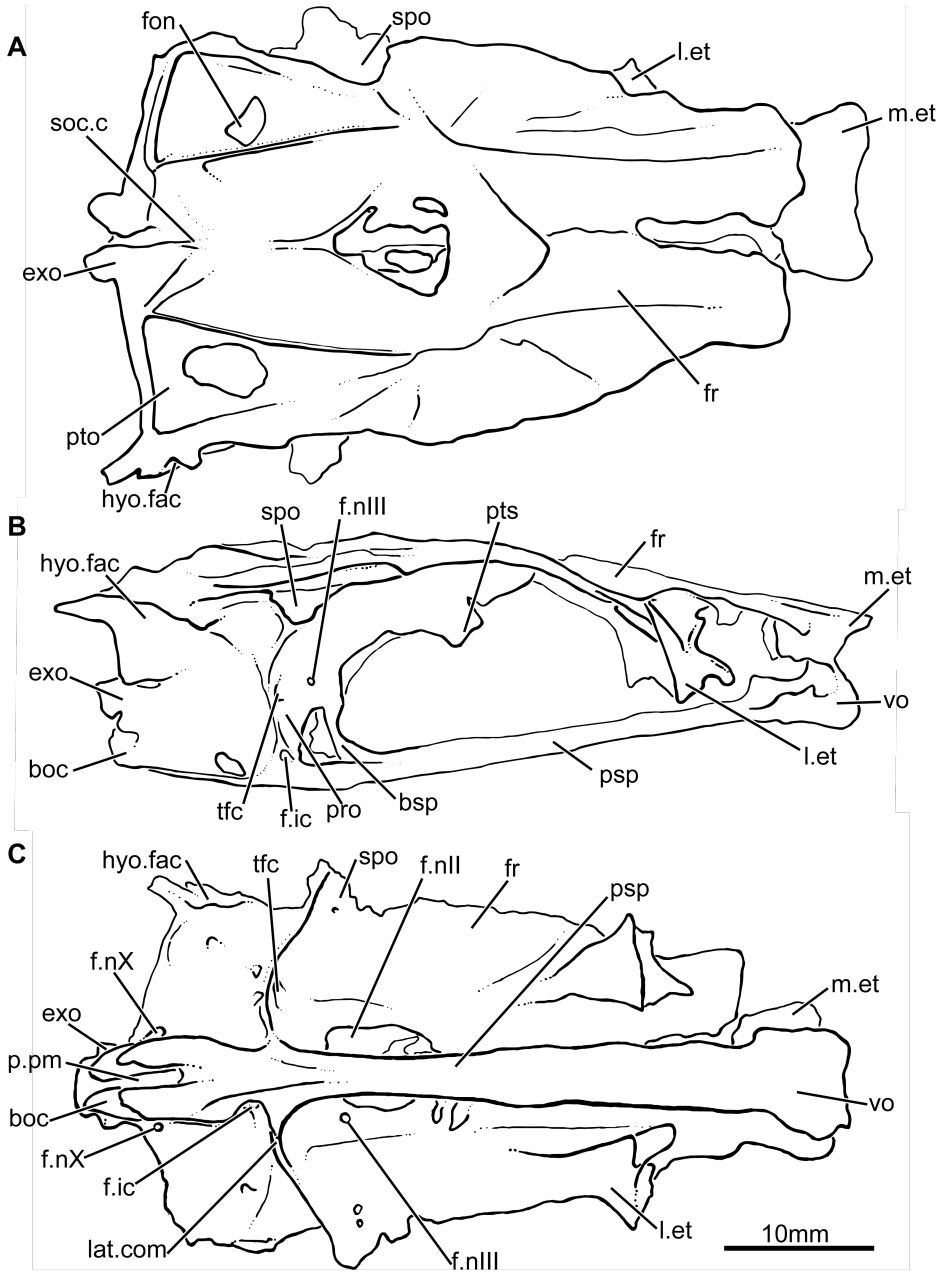


Figure 2.5: Interpretive drawings of the neurocranium of NHMUK PV OR 36136 †*Micrornatus hopwoodi*in A, dorsal view, B, right lateral view and C, ventral view. boc, basioccipital; bsp, basisphenoid; exo, exoccipital; fr, frontals; f.ic, foramen for internal carotid; f.nII, foramen for optic nerve (II); f.nIII, foramen for ocular motor nerve (III); f.nX, foramen for the vagus nerve (X); hyo.fac, hyomandibular facet; lat.com, lateral commissure; l.et, lateral ethmoid; m.et, median ethmoid; p.pm, posterior opening of the posterior myodome; pro, prootic; psp, parasphenoid; pto, pterotic; pts, pterosphenoid; soc.c supraoccipital crest, spo, sphenotic; tfc, trigemino facial chamber; vo, vomer.

(Collette and Chao, 1975, fig. 26). The tripartite occipital condyle comprises a pair of dorsal facets borne by the exoccipitals and a large circular facet on the posterior surface of the basioccipital (Fig. 2.6). The exocciptial facets are kidney shaped, and only narrowly separated along the midline. Foramina for the vagus nerve (X) are visible in ventral view lateral to these facets, and are assumed to lie within the bodies of the exoccipitals. The facet on the basioccipital is gently concave. In ventral view, the basioccipital bears a deep sulcus along its ventral midline that opens into the posterior myodome (2.4C & 2.5C). The intercalar is assumed to form the posteroventral margin of the neurocranium. Some sutures can be delimited in this region based on external observation (rather than tomographs), but the complete outline of the bone remains obscure.

Divisions between bones making up the ventral and lateral walls of the neurocranium are unclear. A strong lateral projection from the side of neurocranium, posterodorsal to the orbit, represents the sphenotic, and thin sheets of bone applied to the ventral surface of the frontals and defining the dorsomesial roof of the orbital chamber represent the pterosphenoids. However the limits of these and other bones that contribute to the ventrolateral walls of the braincase (e.g. prootic) are unclear. However, several features are visible on the ventrolateral wall of the neurocranium posterior to the orbit. Most obvious is the strut-like lateral commissure, which defines the outer wall of the trigemino-facialis chamber (Figs 2.4B, C, 2.5B, C & 2.6). The foramen for the internal carotid artery lies ventral to the lateral commissure, along the dorsolateral margin of the parasphenoid (Figs 2.4C, 2.5C & 2.6C, D). An unossified area is apparent on both sides of the braincase, immediately posterior to the foramen for the internal carotid. A similar cartilaginous region is apparent in the same position of *Scomber*, where

it is visible in an interior view of the cranial endocavity and marks the division between the prootic and basioccipital (Allis 1903, pl. 4, fig. 8). We suggest that this unossified area also delimits the extent of these ossifications in †*Micrornatus*. The hyoid facet is developed as a shallow, ventrally directed depression (Figs 2.4 & 2.5). It is anteroposteriorly elongated, and extends to the lateral margin of the neurocranium.

Additional features are visible on the anterior surface of the postorbital wall (Fig. 2.6C, D). There is a large midline fenestration for the optic nerve (II). This opening is separated from the more ventrally located aperture of the posterior myodome by the basisphenoid (Figs 2.4C, 2.5C & 2.6C, D), which bears a slender ventral limb that contacts the dorsal surface of the parasphenoid. A small foramen immediately lateral to the transverse bar separating the opening for the optic nerve and the aperture for the myodome is interpreted as accommodating the oculomotor nerve (III) (cf. Allis 1903, pl. 4, fig. 9). Other apparent perforations in the postorbital wall cannot be identified with confidence.

In ventral view, the most conspicuous feature is the parasphenoid (Figs 2.4C & 2.5C). It is splint-shaped in ventral view, and only expands modestly in width approaching its anterior and posterior limits. The parasphenoid bears a short, triangular ascending process at the level of the lateral commissure (Figs 2.4B & 2.5B). The posterior margin of the parasphenoid is notched, with short flanges extending along the lateral margins of the rear opening of the posterior myodome. Anteriorly, pyrite growth obscures the suture between the parasphenoid and vomer, as well as the morphology of the vomer more generally. The lateral ethmoids (Figs 2.4B & 2.5B) extend from the level of the parasphenoid to the ventral surface of the frontals, and define the anterior margin of the orbital region. They are

topologically complex bones: concave posteriorly with two lateral protrusions and an anterior protrusion, resulting in an hourglass shape.

2.4.2 Infraorbital bones and sclerotic ossicles

Sclerotic ossicles are preserved on both sides of the skull (Fig. 2.3). They comprise anterior and posterior ossifications. The lacrimal (Fig. 2.7A, B) is a thin, plate-like ossification preserved on both sides of the skull. It extends from the lateral ethmoid to near the posterior margin of the maxilla, and overlaps the dorsal margin of that bone.

2.4.3 Jaws

The maxilla is a long, narrow bone that extends the length of the ethmoid and otic regions of the neurocranium (Figs 2.1, 2.3, & 2.7). In dorsal view, the anterior portion of the maxilla widens laterally to form an articular head. In anterior view, this bears a wide notch marking the point of articulation with the premaxilla. Posterior to the articular head, the body of the maxilla is roughly circular in cross-section. At its posterior tip, the maxilla becomes mediolaterally flattened such that it is plate-like. It is unclear whether a supramaxilla is present. There is a bone on the left side of the specimen that could be interpreted as a supramaxilla (Fig. 2.7A, B), but comparisons with the right-hand side of the skull suggest that it represents the broken posterior limb of the lacrimal. On the right-hand side of the specimen the region expected to bear the supramaxilla has been deeply excavated by historical preparation, possibly destroying this bone were it present.

The premaxilla extends most of the length of the maxilla, is robust anteriorly and tapers to a point posteriorly (Fig. 2.7C, D). The anterior portion of the premaxilla forms a beak-like tip. The ascending process is broken, but appears to have been short. It is accommodated by the concave anterodorsal surface of the median ethmoid. The premaxilla bears a single row of widely spaced, slender teeth. These decrease in length towards the posterior end of the jaw. The right premaxilla bears nine teeth, while the left bone has seven. The maxilla and premaxilla lie parallel to one another.

The lower jaw extends approximately two-thirds the length of the neurocranium. The dentary forms all of the oral border and the anterior two-thirds of the ventral border of the lower jaw. Neither the left nor right dentary is complete anteriorly. The oral border bears nine teeth on the right-hand side and six on the left; these teeth are relatively similar in size and evenly spaced along the oral margin of the bone. The angular forms the posterior portion of the lower jaw, and articulates with the dentary in an elongated 'v'-shaped contact. A small hook-like extension at the posteroventral corner of the jaw marks the position of the articulation with the quadrate.

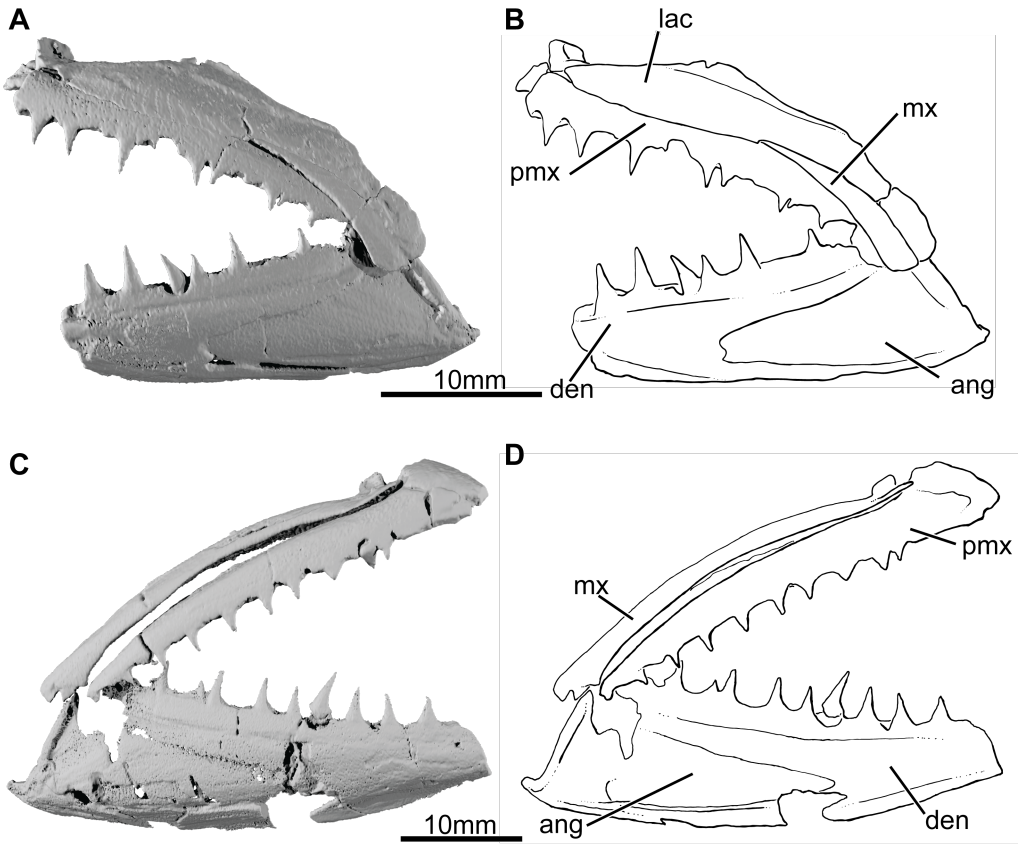


Figure 2.7: Lateral views of the jaws of NHMUK PV OR 36136 †*Micrornatus hopwoodi*: A, three-dimensional rendering of jaws and lacrimal in left lateral view; B, interpretive drawing of jaws and lacrimal in left lateral view; C, three-dimensional rendering of jaw in right lateral view; and D, interpretive drawing of jaws in right lateral view. ang, angular; den, dentary; lac, lacrimal; mx, maxilla; pmx, premaxilla.

2.4.4 Suspensorium

Much of the suspensorium is intact. The palatine, metapterygoid, quadrate and hyomandibular are well preserved; the endopterygoid and ectopterygoid are present but heavily pyritized (Fig. 2.8). The palatine is short, and extends the length of the ethmoid region of the neurocranium (Figs 2.3 & 2.8). The body of the palatine consists of a thick rod that bears a thin trapezoidal plate ventrally. The flattened

maxillary process of the palatine is long and extends anterolaterally to embrace the anterior head of the maxilla. The palatine is enveloped in sheets of pyrite, making it difficult to determine whether it bore small teeth. Large teeth or tooth sockets, however, are absent. On the left-hand side of the specimen, a suture between the palatine and the ectopterygoid is not distinguishable, but on the right-hand side these two elements have separated taphonomically and are offset from one another. The long, thin ectopterygoid articulates with the posterodorsal margin of the palatine. The posterior half of the ectopterygoid curves ventrally and extends along the anterior margin of the quadrate.

A groove extends along the dorsal surface of the anterior arm of the ectopterygoid, giving it a gutter-like cross-section.

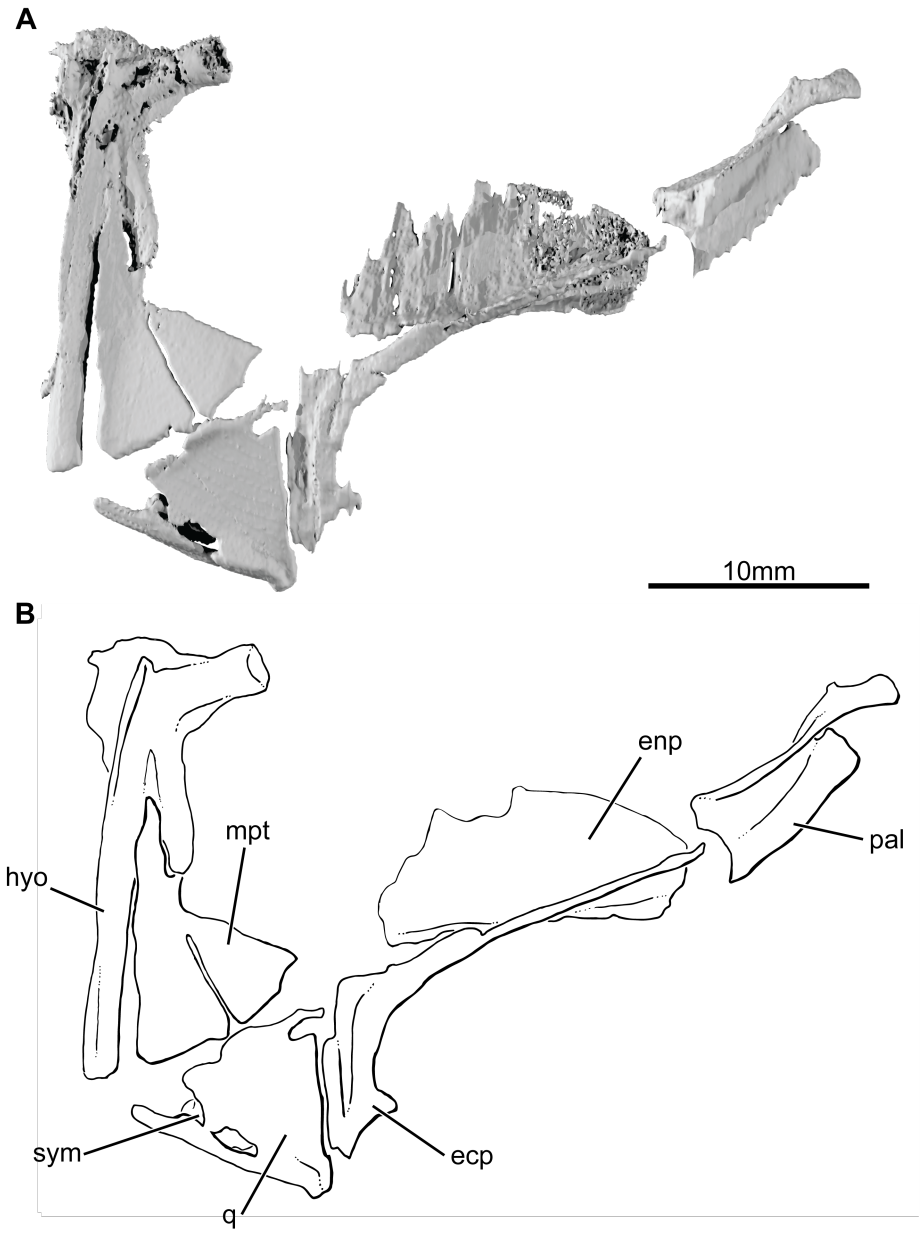


Figure 2.8: Right lateral view of the suspensorium of NHMUK PV OR 36136 †*Micrornatus hopwoodi*: A, three-dimensional rendering of suspensorium and B, interpretive drawing of suspensorium. ecp, ectopterygoid; enp, endopterygoid; hyo, hyomandibular; mpt, metapterygoid; pal, palatine; q, quadrate; sym, symplectic.

The endopterygoid is a broad, flat plate. It sits medial to the ectopterygoid,

with a concave lateral face. The posterolateral margin of the left endopterygoid curves ventrally to form a plate-like extension. The metapterygoid is fan-shaped, widest ventrally with a large posteriodorsal extension marking its articulation with the hyomandibular.

The quadrate is fan-shaped and bears a short posterodorsal process (Figs 2.1, 2.3 & 2.8). The antero-ventral condyle articulates with the glenoid of the lower jaw. The symplectic is housed in an elongated notch parallel to the posterior margin of the quadrate. The symplectic is preserved in situ on the right-hand side of the specimen. It is a small, narrow bone approximately half the height of the quadrate, with a small posterior projection.

The dorsal end of the hyomandibular is expanded as a small head, bearing two facets for articulation with the neurocranium. The anterior facet is circular in cross-section, while the top of the hyomandibular head is broadened to form the posterior articular facet of the head. On the posterior margin of the hyomandibular head is a broad flat surface that articulates with the anterior facet of the operculum. The ventral shaft of the hyomandibular is long and slender, and articulates with the posterior margin of the metapterygoid. An anteriorly directed lamina of bone extends from the head of the hyomandibular to a point dorsal to the midpoint of the shaft. This extension is overlapped by the posterodorsal process of the metapterygoid.

2.4.5 Ventral hyoid arch

The ceratohyals are preserved on both sides of the specimen (Fig. 2.3), but the anterior ceratohyal on the left hand side is broken in half and displaced from life

position. The anterior ceratohyal is narrow in dorsal view and hourglass-shaped in lateral view, with a pronounced constriction in the middle of the bone (Fig. 2.9). The anterior ceratohyal has a complex anterior articular facet, with a long process that extends under the ventral hypohyal. Only visible on the right-hand side of the specimen, the ventral hypohyal articulates anterodorsally with the dorsal hypohyal. Both the dorsal and ventral hypohyals are elongated cylinders; the ventral hypohyal expands ventrally to articulate with anterior extension of the anterior ceratohyal. A shallow groove extends along the dorsal half the lateral surface of both the anterior and posterior ceratohyal. On the anterior ceratohyal this is developed as a slit-like ceratohyal window. The posterior ceratohyal is approximately the same height as the anterior ceratohyal anteriorly, but narrows posteriorly to give the bone a triangular shape. Branchiostegal rays are present, but incomplete. They are narrow and circular in cross-section, but their pattern of articulation with the hyoid bar is unclear.

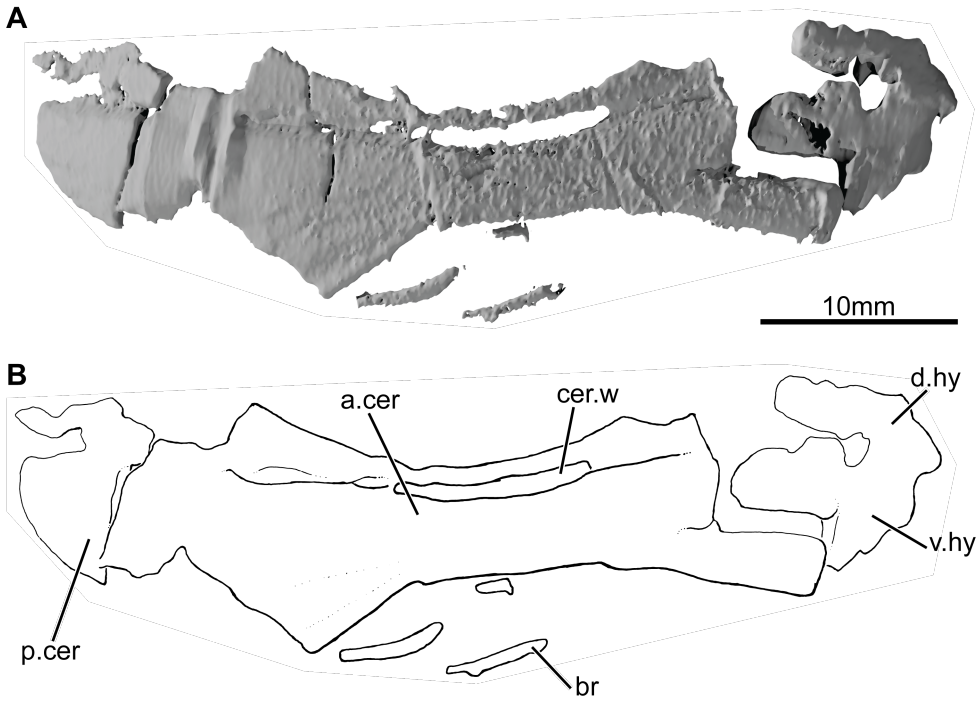


Figure 2.9: Right lateral view of the ventral hyoid arch of NHMUK PV OR 36136 †*Micrornatus hopwoodi*: A, three-dimensional rendering of hyoid arch and B, interpretive drawing of hyoid arch. a.cer, anterior ceratohyal; br, branchiostegal rays; cer.w, ceratohyal window; d.hy, dorsal hypohyal; p.cer, posterior ceratohyal; v.hy, ventral hypohyal.

2.4.6 Opercular series

The opercular series is not preserved in its entirety (Fig. 2.3). The preoperculum is present on both sides of the specimen, and the operculum is preserved on the left-hand side. The preoperculum is an upright semi-ellipse, with a small ventral protrusion where the preoperculum articulates with the hyomandibular. The preoperculum is approximately the same height as the hyomandibular. The operculum is fragmentary, preserving only the articular facet for the hyomandibular and a plate-like extension dorsally.

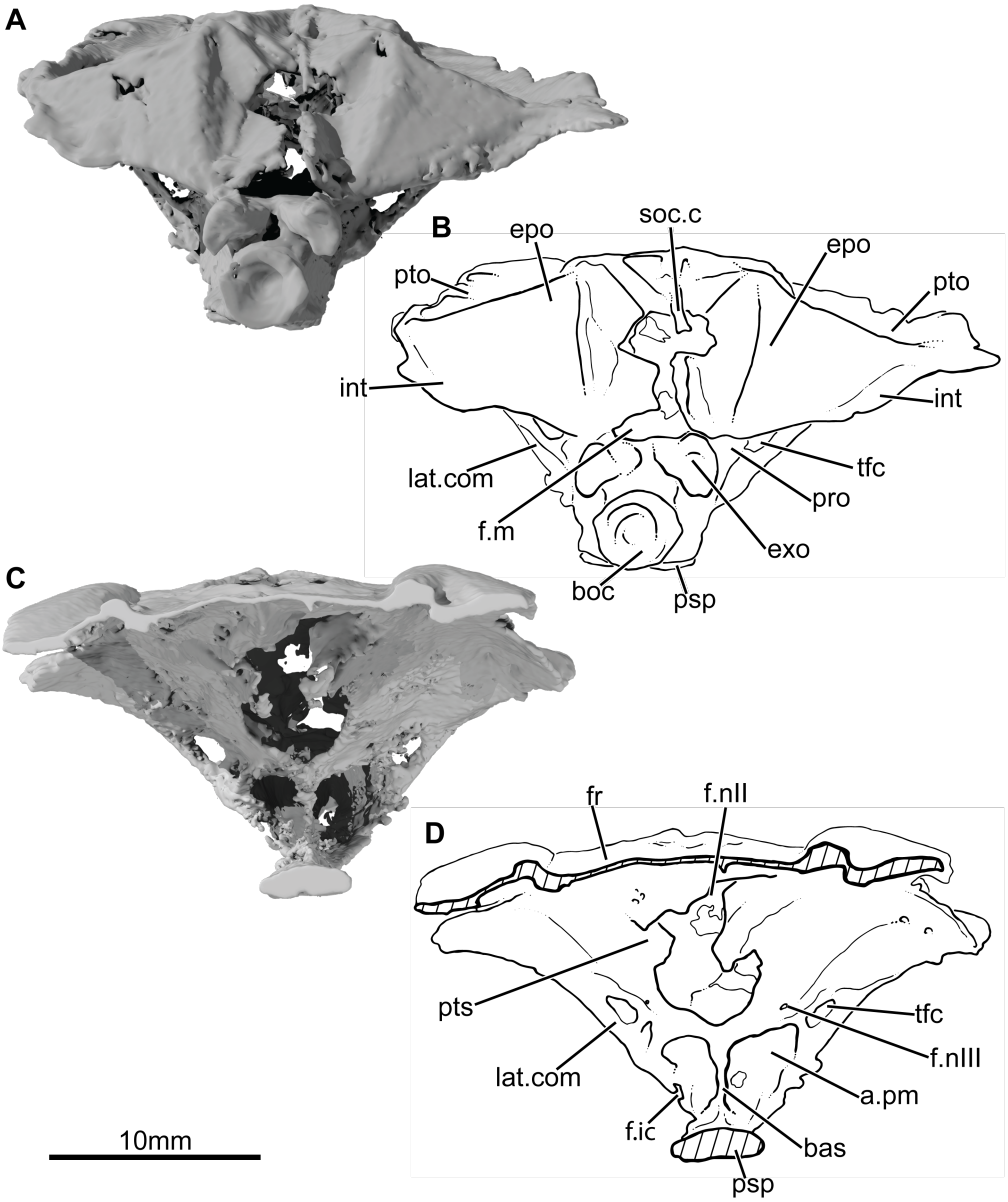


Figure 2.6: Reconstruction of the neurocranium of NHMUK PV OR 36136 †*Micrornatus hopwoodi*: A, three-dimensional rendering of neurocranium in posterior view; B, interpretive drawing of neurocranium in posterior view; C, three-dimensional rendering of an anterior view of a cut-through of the neurocranium; and D, interpretive drawing of an anterior view of a cut-through of the neurocranium. a.pm, anterior opening of the posterior myodome; bas, basisphenoid; boc, basioccipital; exo, exoccipital; epo, epiotic; f.ic, foramen for internal carotid; f.m, foramen magnum; f.nII, foramen for optic nerve (II); f.nIII, foramen for ocular motor nerve (III); fon, fontanelle; fr, frontals; int, intercalar; lat.com, lateral commissure; pro, prootic; psp, parasphenoid; pto, pterotic; pts, pterosphenoid; soc.c, supraoccipital crest; tfc, trigemino facial chamber.

2.5 Discussion

2.5.1 The challenges of interpreting fossil scombroids

The modern era of scombroid systematics began when Regan (1909) removed a series of families (Coryphaenidae, Rachycentridae, Carangidae, Bramidae, Menidae) present in older classifications (including Woodward 1901), and restricted the group to four 'divisions': his Trichiuriformes (Trichiuridae and Gempylidae), Scombriformes (Scombridae), Luvariformes (Luvaridae) and Xiphiiformes (Xiphiidae, Istiophoridae, and a series of extinct families). With the exception of the removal of *Luvarus* to Acanthuroidei (Tyler et al., 1989), a Scombroidei containing these lineages has been a feature of most morphological classifications ever since. Existing cladistic analyses based on anatomy all conform to the hypothesized monophyly of these lineages (Collette et al., 1984; Johnson, 1986; Carpenter et al., 1995; Monsch, 2000), but this agreement is not universal: some non-cladistic treatments argued that billfishes evolved independently of other scombroids, and that their shared characteristics represented common adaptations to high-speed swimming (Gosline, 1968; Potthoff et al., 1980; Nakamura, 1983; the latter also rejected billfish monophyly). Molecular evidence strongly supports a polyphyletic origin of the 'classical' Scombroidei, which is divided into two independent clades: one including the billfishes, and another containing scombrids, gempylids, and trichiurids, among others (Finnerty and Block, 1995; Orrell et al., 2006; Smith and Wheeler, 2006; Yagishita et al., 2009; Betancur-R et al., 2013; Miya et al., 2013; Near et al., 2013). Here we accept that Regan's Scombroidei minus *Luvarus* is not a natural group, consistent with the overwhelming signal from multiple molecular markers.

Because existing morphological synapomorphy schemes are predicated on the monophyly of the classical Scombroidei, the placement of fossils in association with any of its past members is problematic. Compounding matters, cladistic classifications of scombroids vary substantially from one another, particularly with respect to the intra- and inter-relationships of Scombridae: Johnson (1986) regarded this as a paraphyletic assemblage with respect to billfishes, while Collette et al. (1984) indicate that it is the monophyletic sister group of billfishes. Although a monophyletic Scombridae is resolved in many molecular analyses (e.g. Miya et al., 2013), this is not universal (e.g. Near et al., 2013), and patterns of intrarelationships vary considerably between analyses (compare Miya et al., 2013 and Santini, 2013).

2.5.2 The placement of †*Micrornatus*

Discord with respect to the relationships of Scombridae is particularly relevant to interpreting the phylogenetic affinities of †*Micrornatus* because it has consistently been identified as a scombrid for the past century (Woodward, 1901; Casier, 1966; Bannikov, 1985; Monsch and Bannikov, 2012; but see Monsch, 2005). We review the evidence for the phylogenetic placement of †*Micrornatus* here, with the obvious caveats that must accompany such an exercise given the uncertainty surrounding the relationships of scombroids *sensu lato*.

Many characters that feature prominently in classic cladistic treatments of scombroids (Collette et al., 1984; Johnson, 1986; Carpenter et al., 1995) pertain to the gill skeleton or postcranium. Unfortunately, neither is preserved in

†*Micrornatus*, although complete gill skeletons are present in other putative scombroids from the London Clay that we have scanned using μCT (Beckett & Friedman, *pers. obs.*). †*Micrornatus* has non-prostrusible jaws (Collette et al. 1984, character 19; Johnson 1986, character 9; Carpenter et al. 1995, character 9), a feature previously interpreted as a synapomorphy of scombroids inclusive of billfishes (and, in the case of Johnson 1986, sphyraenids), but which must now be considered convergent between the two lineages. †*Micrornatus* also lacks an inner row of fang-like premaxillary teeth (Collette et al. 1984, character 18; Johnson 1986, character 32), which has been interpreted as a synapomorphy of scombrids and billfishes. However, the absence of such dentition is certainly a plesiomorphic feature among percomorphs (Johnson 1986, p. 5), so derived status in this case depends on the placement of fang-bearing taxa (e.g. trichiurids, gemplyids, Scombrolabrax) as proximate outgroups.

At present, the most compelling evidence for the scombrid affinities of †*Micrornatus* derives from hypothesized links with coeval taxa known from more complete material: †*Eocoelopoma* and †*Palaeothunnus*. Monsch and Bannikov (2012) recognize these three genera as a clade they call Eocoelopomini, united by two cranial features present in all putative members: postero-superior fossae extending to mid-orbit combined with thickenings of the frontals located anterior to these fossae and ornamented with radiating ridges (such features are also common to †*Landanichthys* from Angola; Dartevelle and Casier, 1949, fig. 69). Specimens of †*Eocoelopoma* from the London Clay are largely cranial, but postcranial material attributed to this genus and †*Palaeothunnus* is known from slightly older deposits in Turkmenistan (Bannikov, 1985). Both taxa show the presence of two epurals (one in the case of †*Palaeothunnus*; Collette et al. 1984, character 7; Johnson 1986,

character 36; the latter interpreted this feature as a character of Scombridae inclusive of billfishes, with a reversal in billfishes) and caudal hypurostegy (Collette et al. 1984, character 14; Johnson 1986, character 33; this feature is also shared with billfishes and many other fast-swimming fish groups, and is probably convergent). †*Eocoelopoma* has fused of upper and lower hypural plates (Collette et al. 1984, character 34; Johnson 1986, character 39; †*Palaeothunnus* retains separate dorsal and ventral plates), which has been interpreted as either a synapomorphy of a subset of Scombridae (Collette et al., 1984) or of some scombrids plus billfishes (Johnson, 1986). Additional features of the caudal skeleton of †*Eocoelopoma* that support this placement include preural centra 2 – 4 shortened, and a bony caudal keel (Bannikov, 1985; Monsch and Bannikov, 2012). On these grounds, Monsch & Bannikov (2012, p. 278) tentatively propose that Eocoelopomini is the extinct sister lineage of Sardini + Thunnini. More precise statements about the placement of †*Micrornatus* await better documentation of anatomy in fossil scombrids and a consistent, more stable hypothesis among modern species that receives support from both morphological and molecular datasets.

2.5.3 The taxonomy of London Clay scombrids and related taxa

As part of the reassessment of this fossil we revisited the collections of †*Eocoelopoma* from the London Clay at the Natural History Museum, London. This deposit yields three species of †*Eocoelopoma*: the type species †*E. colei* and the attributed species †*E. curvatum* and †*E. gigas*. In distinguishing

†*Micrornatus* from †*Eocoelopoma*, Monsch (2005) indicated the following differences: the presence of pineal foramen in †*Micrornatus* v. absence in †*Eocoelopoma*; fine ornament ridges of frontals in †*Micrornatus* v. coarse ridges in †*Eocoelopoma*; concave anterior margin of the median ethmoid in †*Micrornatus* v. convex margin in †*Eocoelopoma*; and slender teeth in †*Micrornatus* v. stouter ones †*Eocoelopoma*. Based on our visual and tomographic re-examination of †*Micrornatus*, we are not convinced that the putative pineal foramen in this taxon is a genuine biological feature rather than a taphonomic one (see above). We do, however, agree that the three other features cited by Monsch (2005) distinguish †*Micrornatus* from the type species of †*Eocoelopoma*, †*E. colei*. To these differences we add two others that relate to the geometry of the skull roof. First, the lateral margins of the frontals in †*Micrornatus* are convex posteriorly but are straight to slightly concave anteriorly, in contrast with conspicuous convexity along the same margin in †*E. colei* (Fig. 2.10). Second, the dorsal surface of the frontals is convex along the midline in †*Micrornatus*, whereas this area is marked by a concave pit in †*E. colei*.

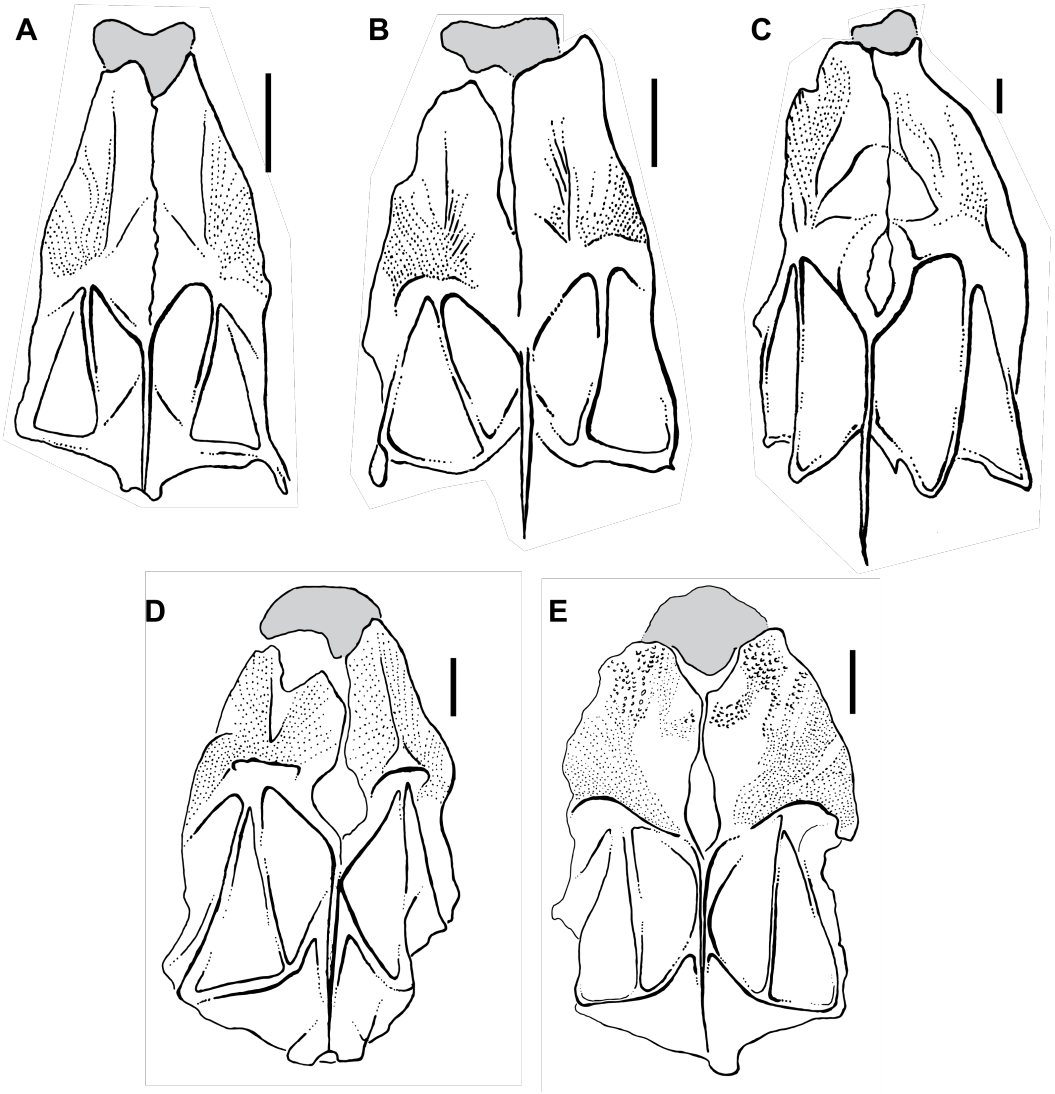


Figure 2.10: Dorsal view of the neurocranium and median ethmoid (shaded grey) of the holotypes and referred specimens of †*Micrornatus* and †*Eocoelopoma*. All material is from the Eocene (Ypresian) London Clay. Scale bar indicates 10 mm. A †*Micrornatus hopwoodi*, NHMUK PV OR 36136 (holotype); B †*Eocoelopoma curvatum*, NHMUK PV OR 44877 (neotype); C †*Eocoelopoma gigas*, NHMUK PV OR 39221, (holotype); D †*Eocoelopoma colei*, NHMUK PV P 26702 (referred specimen; Monsch 2005); and E †*Eocoelopoma curvatum*, NHMUK PV P 9455 (referred specimen; Monsch 2005).

These observations might have some bearing on the taxonomy of eocoelopomines from both the London Clay and other deposits. First, we found

that the neotype specimen of †*E. curvatum* (NHMUK PV OR 44877) shares features with †*Micrornatus* not apparent in †*E. colei*: fine ornament of the frontals (Fig. 2.10B); straight or concave antero-lateral margins of the frontals; convex dorsal surface of the frontals; slender teeth. We also note that the holotype of †*E. gigas* shares with †*Micrornatus* and †*E. curvatum* a median ethmoid with a concave anterior margin in dorsal view and a convex dorsal surface of the frontals. Referred material of †*E. gigas* shows very slender teeth on the premaxilla (Monsch 2005, fig. 28), resembling those of †*Micrornatus*.

Type specimens of †*Micrornatus* and †*E. curvatum* are of comparable size, but are both substantially smaller than material of †*E. gigas*. We are uncertain at present if differences between these smaller specimens and †*E. gigas* are taxonomically relevant or instead represent ontogenetic variation.

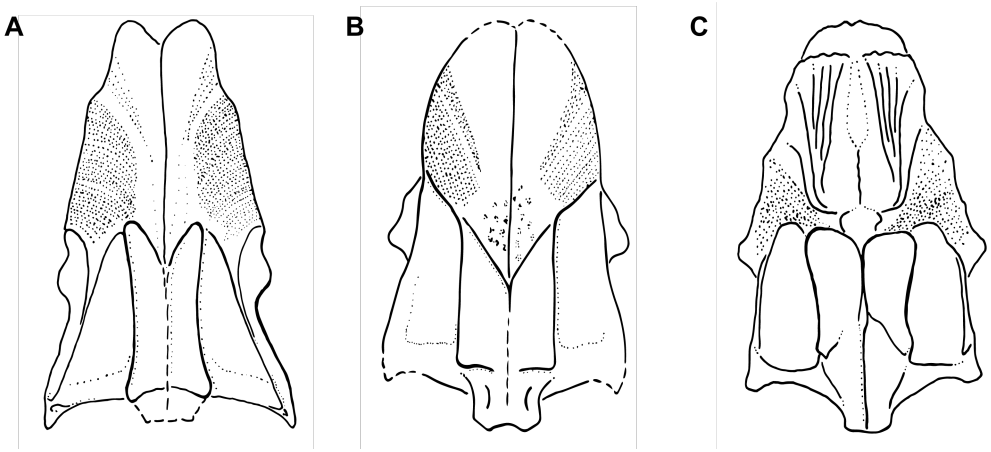


Figure 2.11: Dorsal views of neurocrania of probable Eocoelopomini from deposits other than the London Clay. A †*Eocoelopoma portentosa*, Palaeontological Institute of the Russian Academy of Sciences, Moscow, PIN 1762-85 (redrawn from Bannikov 1985), from the earliest Eocene Danatinsk Formation, Turkmenistan. B †*Palaeothunnus parvidentatus*, PIN 3363-22, from the earliest Eocene Danatisnk Formation, Turkmenistan. C †*Landanichthys moutai*, from the late Paleocene of Angola (redrawn from Darteville & Casier 1949).

In any case, it seems prudent to delay any formal taxonomic evaluations until more data, including that derived from μCT, are available for relevant specimens. However, in light of our preliminary observations, we suggest that subsequent analysis might require reassignment of some London Clay specimens of †*Eocoelopoma* to †*Micrornatus*.

More broadly, it is possible to extend this contrast between †'*Eocoelopoma*-like' and '†*Micrornatus*-like' eocoelopomines to consider examples from other deposits (Fig. 2.11). Bannikov (1985) described two new species of large scombrid from the earliest Eocene Danatinsk Formation of Turkmenistan: †*Eocoelopoma portentosa* and †*Palaeothunnus parvidentatus*. In terms of overall geometry of the frontals, †*E. portentosa* is more similar to †*Micrornatus* than †*E. colei*. In contrast, the strongly convex lateral margins of the frontals of †*Palaeothunnus* closely resemble those in the type species of ††*Eocoelopoma*. A further taxon that can be considered here is †*Landanichthys*. From the Paleocene of Angola, this genus is potentially the oldest fossil scombrid. Some material described and figured by Darteville & Casier (1949, fig. 69, pl. 21) shows diagnostic features of Eocoelopomini (Monsch & Bannikov 2012). The frontals as reconstructed by these authors are more similar to those of †*Micrornatus* than †*Eocoelopoma*, and appear to be concave anterior to the pineal region (Darteville & Casier 1949, fig. 69). The teeth in †*Landanichthys* also appear to be relatively slender, as in †*Micrornatus*. Darteville & Casier (1949, fig. 69) show a median ethmoid with a convex anterior margin as in †*Eocoelopoma*, but this is not apparent in their plates. However, we note that the material assigned to †*Landanichthys* is morphologically highly variable (see Darteville & Casier 1959, pl. 38), and might in fact belong to multiple genera. As with the taxonomy of London Clay eocoelopomines, we do not advocate any taxonomic changes before

the anatomy of these species is better understood and the polarity of the characters in question is better constrained. Instead, we outline these observations here to provide a road-map for future investigation.

2.6 Acknowledgements

We would like to thank Emma Bernard (NHMUK) and Zerina Johanson (NHMUK), for access to specimens or information on material in their care, and Dan Sykes (NHMUK), Farah Ahmed (NHMUK) and Rebecca Summerfield (NHMUK) for assistance with CT scanning. We would also like to thank Roger Close (Oxford University) and the reviewers for constructive comments on this manuscript. This research was supported by NERC studentship to HB on the DTP Environmental Research (NE/L002 1612/1), and a Leverhulme Research Project Grant (RPG-2012-658) and Leverhulme Prize (PLP- 2012-130), both to MF.

Chapter 3

Morphology and phylogenetic relationships of fossil snake mackerels and cutlassfishes (Trichiuroidea) from the Eocene (Ypresian) London Clay formation

This paper was published as:

Beckett, H.T., Giles, S., Johanson, Z. and Friedman, M., Morphology and phylogenetic relationships of fossil snake mackerels and cutlassfishes (Trichiuroidea) from the Eocene (Ypresian) London Clay Formation. *Papers in Palaeontology.*

https://doi.org/10.1002/spp2.1221.

HB, MF and ZJ scanned material. HB generated CT renderings and figures. HB coded characters, with some discussions with MF and SG, and performed the phylogenetic analyses. HB wrote the text with input and comments from all authors.

Abstract

'Gempylids' (snake mackerels) and trichiurids (cutlassfishes) are pelagic fishes characterized by slender to eel-like bodies, deep-sea predatory ecologies, and large fang-like teeth. Several hypotheses of relationships between these groups have been proposed, but a consensus remains elusive. Fossils attributed to 'gempylids' and trichiurids consist almost exclusively of highly compressed body fossils and isolated teeth and otoliths. We use micro-computed tomography to redescribe two three-dimensional crania, historically assigned to †*Eutrichiurides winkleri* and †*Progempylus edwardsii*, as well as an isolated braincase (NHMUK PV OR 41318). All from the London Clay Formation (Eocene, Ypresian), these specimens represent some of the oldest fossils identified as trichiuroids. We find that †*Eutrichiurides winkleri* does not show diagnostic characters of †*Eutrichiurides*, and it is assigned to a new genus. To investigate the placement of these fossils relative to extant lineages, we combine existing morphological character sets for 'gempylids' and trichiurids along with published mitogenomic data. Our analyses recover a monophyletic Trichiuridae nested within a paraphyletic 'Gempylidae'. The taxon formerly known as †*Eutrichiurides winkleri* is considered Trichiuroidea *incertae sedis*, while †*Progempylus edwardsii* and NHMUK PV OR 41318 are recovered within the 'gempylid' grade. Using previously published descriptions and character optimizations from our phylogenetic analyses we suggest possible placements for laterally compressed body fossils assigned to Trichiuroidea (†*Argestichthys*, †*Abadzekhia*, †*Chelifichthys*, †*Anenchelum*, †*Eutrichiurides*, †*Musculopedunculus*).

3.1 Introduction

'Gempylids' (snake mackerels) and trichiurids (cutlassfishes) are two closely related families of pelagic percomorph fishes. Typically, they have slender to eel-like bodies, deep-sea predatory ecologies and large fang-like teeth. These nominal families are only modestly diverse; 'gempylids' include 23 species in 16 genera, and trichiurids 32 species in 9 genera (Nakamura and Parin, 1993). For the past century, 'Gempylidae' and Trichiuridae have been closely associated with Scombridae (tunas and mackerels) and, less consistently, with Xiphoidei (billfishes). Regan (1909) recognized the divisions Trichiuriformes and Scombriformes (in addition to Luvariformes and Xiphiiformes, which are now associated with other groups) in a suborder Scombroidei. While a close affinity between 'gempylids' and trichiurids has long been recognized (here referred to as Trichiuroidea *sensu* Nakamura and Parin (1993)), the exact relationship between the families remains equivocal in light of both anatomical and molecular evidence. Some morphological (Johnson, 1986; Patterson and Rosen, 1986; Carpenter et al., 1995) and molecular analyses support trichiuroid monophyly, with trichiurids nested within 'gempylids' (Orrell et al., 2006) or with reciprocally monophyletic trichiurids and gempylids (Betancur-R et al., 2013; Alfaro et al., 2018). However, others indicate trichiuroids are paraphyletic to (morphological: Collette et al. 1984; molecular: Miya et al. 2013) or polyphyletic within (Near et al., 2013; Betancur-R et al., 2017) a group with variable composition but which always contains scombrids. Despite these differences, two patterns consistently emerge in addition to the close association of trichiurids and 'gempylids'. First, trichiurids always form a clade. Second,

'gempylids' are typically interpreted as paraphyletic, either with respect to trichiurids (Johnson, 1986; Patterson and Rosen, 1986; Carpenter et al., 1995; Orrell et al., 2006) or other groups (Collette et al. 1984; Miya et al. 2013; Near et al. 2013; but see Betancur et al. 2013, 2017). Unfortunately, many of these molecular studies are limited in their sampling of taxa (Near et al. 2013: two 'gempylids' and two trichiurids; Betancur-R et al. 2013: four 'gempylids' and six trichiurids; Betancur-R et al. 2017: six 'gempylids' and six trichiurids) or sequence data (e.g. mitochondrial genes only; Miya et al. 2013. Additionally, the most comprehensive morphological analyses of relationships have focused on either 'gempylids' (Russo, 1983) or trichiurids (Gago, 1998) or, when combined, have employed limited character sampling (ontogenetic characters only; Gago 1997).

Fossils identified as 'gempylids' and trichiurids consist almost exclusively of isolated teeth, otoliths, and highly compressed, effectively two-dimensional body fossils (Miya et al. 2013, SI text S2). The earliest putative remains assigned to each group are problematic. Nolf and Stringer (1996) interpreted Late Cretaceous (Campanian) otoliths as belonging to 'gempylids', but similar in situ examples show that they derive from aulopiforms (Stringer et al., 2016; Schwartzhans et al., 2018). Isolated teeth from the early Paleocene (Danian) of Angola (Dartevelle and Casier, 1959) are attributed to the trichiurid †*Eutrichiurides*, but their affinities are also subject to question (see below). More secure evidence for the early history of trichiuroids derives from the body fossil record. The oldest articulated fossils interpreted as 'gempylids' are from early Eocene (early Ypresian) deposits, and include undescribed material from the Fur Formation of Denmark (Bonde, 2008). Younger Eocene specimens include a three-dimensionally preserved

skull of †*Progempylus* and an unnamed braincase from the London Clay Formation of the UK (Casier, 1966; Monsch, 2005), undescribed material of two taxa from Monte Solane, Italy (Gempylidae gen. indet., Gempylidae gen. indet. cf. *Thyrsitoides*; Zorzin et al. 2011, figs 8-9; Giusberti et al. 2014, figs 5C, 6A-B) and Iranian material assigned to *Epinnula* and *Thyrsitoides* (Arambourg 1967; originally interpreted as Oligocene, but see Afsari et al. (2014) for a reassessment of age). Post-Eocene 'gempylids' are represented by †*Abadzekhia* (Oligocene (Rupelian-Chattian) of the Caucasus and Germany; Bannikov 1985, 2005, 2000*a*), †*Chelifichthys* (Miocene (Messinian) of Algeria; Carnevale 2006) and *Hemithyrsites* (Miocene (Messinian) of Italy and Miocene (Burdigalian) of the Caucasus; Sauvage 1873; Daniltshenko 1960). Excluding isolated teeth, the oldest articulated skeletal remains placed in Trichiuridae are an incomplete skull assigned to †*Eutrichiurides* (Casier, 1966) from the early Eocene (Ypresian) London Clay Formation of the UK, a fragmentary skull also assigned to †*Eutrichiurides* (Bonde, 2008) from the Lilleblt Clay of Denmark, and an as-yet undescribed specimen similar to †*Anenchelum* from roughly contemporaneous deposits of Monte Solane, Italy (Zorzin et al., 2011). Most other trichiurid body fossils are assigned to either †*Anenchelum* (Blainville, 1818) or the extant *Lepidopus* (Blainville 1818) and are middle Eocene-Pliocene in age, but some distinctive fossil taxa have been recognized, most notably †*Musculopedunculus micklichi* (Oligocene (Rupelian) of Germany; Parin and Astakhov 2007.

Uncertainty surrounding the relationships of fossil 'gempylids' and trichiurids stems from a number of factors. First, fossil taxa, including those discussed above, have not been included in a formal, published phylogenetic analysis (but see a formal cladogram in an unpublished PhD by Monsch (2000) and informal placement,

based on verbal argumentation, in Monsch and Bannikov (2012, fig. 2). Second, morphological datasets for 'Gempylidae' and Trichiuridae rely heavily on soft-tissue and cranial characters (c. 80%: Russo 1983; c. 50%: Gago 1998). The former are almost impossible to obtain from fossils, and the latter challenging due to the prevalence of two-dimensional fossils in which postcranial structure is clear but crania are often badly crushed. Third, available character lists target either 'gempylids' (Russo, 1983) or trichiurids (Gago, 1998) and the intrarelationships of those individual families, rather than sampling both extensively to explore their mutual relationships. This is particularly problematic given uncertainties in the relationships between these groups, which is amplified in the case of fossils that putatively exhibit unusual mosaics of 'gempylid' and trichiurid-like characters (e.g. †*Argestichthys*; Prokofiev 2002). In this study, we combine existing morphological character sets for 'gempylids' and trichiurids along with published molecular sequence data and additional observations of extant taxa in order to infer phylogenetic placements for some of the earliest fossil trichiuroids. Specifically, we investigate a series of fossils from the Eocene (Ypresian) London Clay Formation of the UK: †*Eutrichiurides winkleri*, †*Progempylus edwardsii*, and an isolated braincase previously identified as a 'gempylid' (Fig. 3.1). These specimens represent nearly all three-dimensionally preserved examples of trichiuroids (Casier, 1966; Monsch, 2005) with the potential to preserve many of the cranial features that feature prominently in anatomical analyses of living species. We present new descriptions of these specimens, based on a combination of external examination and micro-computed tomography (μCT) scanning. In addition to analytically inferred placements for these three-dimensionally preserved London Clay specimens based on a morphological character matrix for Trichiuroidea, we provide possible

placements of other fossil taxa associated with the group.

3.2 Material and Methods

3.2.1 Institutional abbreviations

BMNH, Life Sciences collections, Natural History Museum, London, UK; FMNH, Division of Fishes, Field Museum, Chicago, USA; IRSNB, Institut Royal des Sciences Naturelles de Belgique, Brussels, Belgium; LACM, Natural History Museum of Los Angeles County, Los Angeles, USA; NHMUK, Earth Sciences collections, Natural History Museum, London, UK; UMMZ, Division of Fishes, University of Michigan Museum of Zoology, Ann Arbor, USA.

3.2.2 Specimens examined

Below we list the specimens used in the course of this study. Both wet and dry specimens were studied for extant taxa, indicated with [W] and [D] respectively. Wet specimens were studied using radiography and μCT, indicated by [R] and [C] respectively.

Trichiuroidea

Additional observations were made of extant Trichiuroidea based on descriptions by Nakamura (1983), Russo (1983), Fujita (1990), Nakamura and Parin (1993), and Gago (1998).

'Gempylidae'

NHMUK PV OR 41318 (Fig. 3.1B) an isolated braincase from the Eocene (Ypresian, 52-49 Ma) London Clay Formation, UK (Friedman et al., 2016); *Gempylus serpens* BMNH 44.670[D], FMNH 71423[W,C]; *Hemithyrsites prometheus* BMNH 44.650[D], BMNH 1906.9.8.149[W,R], UMMZ 250143[W,C]; *Lepidocybium flavobrunneum* LACM 36320-1[W,C]; *Nealotus tripes* BMNH 2016.4.14.59[W,R]; *Neoepinnula orientalis* BMNH 1986.9.8.164.5[W,R]; *Nesiarchus nasutus* BMNH 1998.8.9.127.37-38[W,R], FMNH 71422[W,C]; *Paradiplospinus gracilis* BMNH 2009.5.18.74-75[W,R], BMNH 2009.5.18.143[W,C]; †*Progempylus edwardsii* NHMUK PV OR 32388[C] (Fig. 3.1A) a cranium from the Eocene (Ypresian, 52-49 Ma) London Clay Formation, UK (Friedman et al., 2016); *Rexea prometheoides* FMNH 120779[W,C]; *Ruvettus pretiosus* BMNH 44.620[D], BMNH 1997.5.21.40[W,R], BMNH 1938.6.23[W,C]; *Thyrsites prometheus* BMNH 99.1.16.4[W,R]; *Thyrsitoides marleyi* BMNH 1986.9.8.147[W,R,C].

Trichiuridae

NHMUK PV P 26904[C] (Fig. 3.1C) a cranium from the Eocene (Ypresian, 52-49 Ma) London Clay Formation, UK (Friedman et al., 2016); *Aphanopus carbo* BMNH 1899.1.16.5 [D], BMNH 1961.6.20.1[W,R], BMNH 2006.6.27.1[W,C]; *Benthodesmus simonyi* BMNH 1972.1.10.64[W,R,C]; *Eupleurogrammus glossodon* BMNH 1955.5.13.3[W,R]; *Lepidopus caudatus* BMNH 44.820[D], BMNH 1864.10.5.7[W,R], BMNH 1903.6.27.22[W,C]; *Lepturacanthus savala* BMNH 51.19.27.14.3[W,R], UMMZ 219522[W,C]; *Tentoriceps cristatus* BMNH 1974.3.5.1-3[W,R], BMNH 1987.1.23-28[W,C]; *Trichiurus lepturus* BMNH 44.850[D], BMNH

1897.12.1.343[W,R], UMMZ 219710[W,C].

Pomatomidae

Pomatomus saltatrix studied from the literature (Leapley, 1952) and UMMZ 111069[W,C].

Scombridae

Gasterochisma melampus studied from the literature (Kohno, 1984) and specimen photographs of AMNH 098426SD[D].

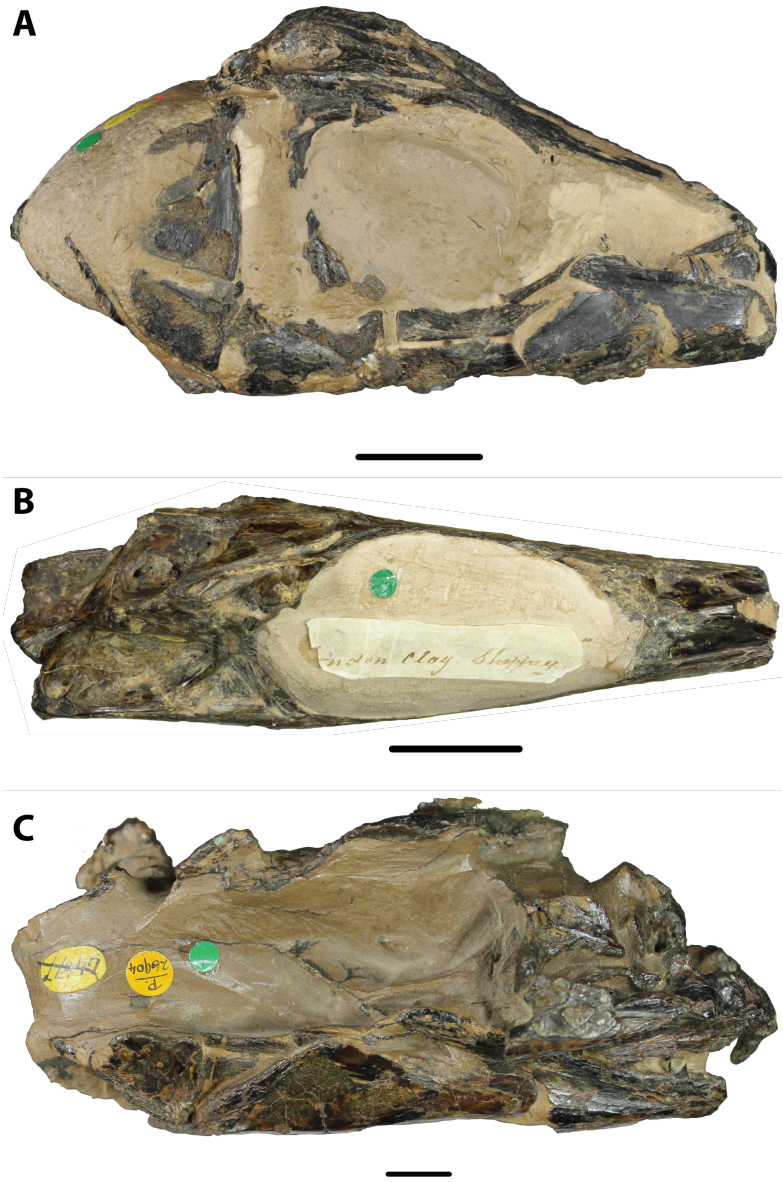


Figure 3.1: Photographs of the fossil specimens. A, †*Progempylus edwardsii* (NHMUK PV OR 32388). B, NHMUK PV OR 41318. C, NHMUK PV P26904. All scale bars represent 10 mm.

3.2.3 X-ray computed tomography

Fossil specimens

†*Eutrichiurides winkleri* and †*Progempylus edwardsii* were studied using μCT scanning. These had previously been mechanically prepared to expose external bones, and μCT presents an effective method of obtaining additional information on the internal anatomy of London Clay material (Beckett and Friedman, 2016). Extant taxa were scanned to obtain details of internal osteological anatomy not available from radiography or the literature.

Fossil specimens and Recent BMNH specimens were scanned using the Metris X-Tek HMX ST μCT scanner in the Imaging and Analysis Centre of the Natural History Museum, London. FMNH and UMMZ specimens were scanned using the Metris X-Tek XT H 225ST μCT scanner at the CTEES facility in the Department of Earth and Environmental Sciences, University of Michigan. Scan settings are provided in Appendix A.1. Tomogram stacks were segmented using Mimics Materialise v.16.0-19.0 9 64 (http://biomedical.materialise.com/mimics). High-resolution models produced in Mimics were exported as .ply files, then imported into Blender (https://blender.org) and rendered as two-dimensional images.

3.2.4 Radiography

Radiography of extant specimens from the Life Sciences collections of the Natural History Museum, London was undertaken in the Radiography Suite using the Solus Schall X-ray setup. All specimens were imaged at 3 μA with a working distance of 75 cm. Voltages and exposure times are given in Appendix A.1.

3.2.5 Dataset assembly

Morphology

We combined datasets for 'gempylids' (Russo, 1983) and trichiurids (Gago 1997, 1998) to create a single morphological character matrix. Russo (1983) provided a character list, but no character-by-taxon matrix is presented in his thesis. However, we were able to reconstruct his character matrix based on his most parsimonious cladogram (Russo 1983, fig. 47). Characters duplicated in source matrices were amalgamated, and indicated as such in the character list Beckett et al. (2018) (Appendix A.2). We also excluded characters that we could not interpret in comparative material due to ambiguity in the original character definitions (Gago 1998, ch. 4, 36, 60; Russo 1983, ch. 2, 7, 10, 27, 30, 32, 37, 55, 62, 69, 71, 72, 77, 78). We used published descriptions by Nakamura (1983), Russo (1983), Fujita (1990) and Gago (1998) to code characters for taxa from Russo (1983) not included in Gago (1998) and vice versa. Additional character states for extant taxa were obtained by studying dry specimens, radiographs and μCT data.

We also added five taxa to this combined dataset. In addition to the three fossil specimens described below (†*Eutrichiurides winkleri*, †*Progempylus edwardsii* and NHMUK PV OR 41318), we increased our sampling of outgroup lineages by including the pomatomid (bluefish) *Pomatomus saltatrix* (Leapley, 1952) and early diverging scombrid *Gasterochisma melampus* (Kohno, 1984) in addition to the scombrolabracid (longfin escolar) *Scombrolabrax heterolepis*, used in previous systematic studies. The resulting character matrix has 32 taxa coded for 144 characters (Appendix A.3). Of these, 103 relate to the skeleton (73 cranial, 38 postcranial), 3 refer to otoliths, 7 concern soft tissues, and 23 are developmental

characters.

Individual ossifications are sometimes difficult to identify in fossils, particularly when they are closely sutured (as is often the case in the neurocranium). References to individual ossifications in our descriptions are based on visible sutures and positional comparisons with other taxa (both from the literature and first-hand observation).

Molecular data

From our morphological dataset, 17 taxa were matched with mitochondrial sequences from Miya et al. (2013; 12n3rRTn dataset, comprising 13 596 base pairs). This molecular dataset represents whole mitogenomic sequences with the ND6 gene removed.

3.2.6 Phylogenetic analysis

Parsimony

We analysed the morphology only dataset using maximum parsimony as an optimality criterion in PAUP v.4.0a150 for Mac (Swofford and Sullivan, 2003). We performed an heuristic search (addseq = random, hold = 5, nreps = 500) with unweighted and unordered characters and the tree bisection and reconstruction strategy enabled. Nodal support was measured in PAUP by manual calculation of Bremer decay indices and by bootstrap analysis (nreps = 100, hold = 5, search = heuristic, addseq = random) retaining those clades with a frequency greater than 50%. We rooted our networks on *Pomatomus*.

Bayesian

Both the morphology only and the combined morphological and molecular dataset were analysed in MrBayes v.3.2.6 (Huelsenbeck and Ronquist, 2001). A gamma distribution was specified for the morphologicalonly dataset. Molecular data were divided into five partitions, with a GTR substitution model specified for each with gamma-distributed rates (following Miya et al. 2013). The Mkv model was used for morphological data, with gamma-distributed rate variation among characters. Networks were rooted on *Pomatomus saltatrix* based on topologies presented in past studies (Orrell et al., 2006; Betancur-R et al., 2013, 2017). Monophyly of the trichiuroid ingroup was enforced. Each analysis ran for two independent runs of four chains, sampling every 500 generations for 15 million generations, and the first quarter of each run was discarded as burn-in. Convergence was indicated by average standard deviation of split frequencies < 0.01, effective sample sizes $>$ 200 and visual inspection of the marginal probability distribution and trace of the analyses in Tracer v.1.6 (Drummond and Rambaut, 2007).

3.3 Systematic palaeontology

Teleostei Mller, 1845

Percomorpha Rosen, 1973 *sensu* Johnson and Patterson, 1993

Pelagiaria Miya & Friedman, 2013 in Miya et al., 2013

Trichiuroidea *sensu* Nakamura and Parin, 1993

'Gempylidae' Gill, 1862

Genus †*Progempylus* Casier, 1966

Type species

†*Progempylus edwardsii*.

Diagnosis

As for type and only species.

†*Progempylus edwardsii* (Casier, 1966)

1901 Percidae? cf. *Planesox vorax* Woodward, p. 519.

1966 *Progempylus edwardsi* Casier, p. 250, pl. 40 fig. 2.

2005 *Progempylus edwardsi* Casier; Monsch, p. 449, fig. 4.

Holotype

NHMUK PV OR 32388, an articulated skull preserved in three dimensions.

Diagnosis

'Gempylid' fish distinguished by the following combination of characters: braincase narrows above orbit and widens again anteriorly, lower jaw short with point of articulation with quadrate beneath the orbit, two pairs of vomerine teeth and lateral process on vomer.

Material

Type and only specimen, NHMUK PV OR 32388, an historically prepared fossil that visibly preserves an articulated braincase, jaws, supsensoria and opercular series.

Occurrence

London Clay Formation, Isle of Sheppey, UK. Specimens from this locality are Ypresian in age and dated at 52-49 Ma (Friedman et al. 2016). The depositional setting is outlined in greater detail in Friedman et al. (2016).

Remarks

After being figured and described by Casier (1966), this specimen was revisited by Monsch (2005) who described the specimen briefly and associated it with 'gempylids'.

3.3.1 Description

†*Progempylus edwardsii* (NHMUK PV OR 32388) preserves the skull including the braincase, lower jaw, suspensorium, hyoid arch, gill-arch skeleton and opercular series.

Braincase

In dorsal view the neurocranium is narrow and long, approximately half as wide anteriorly as posteriorly. The paired frontals (Figs 3.2A, 3.3A) form the majority of the anterior portion of the skull roof. They are constricted above the orbit, but broken anteromedially such that it is not possible to discern the medial suture of the frontals with the mesethmoid. Narrow ridges ornament the frontals, and radiate from a point above the orbit. The supraorbital sensory canal extends through the frontal in an enclosed tube, branching twice and exiting the frontals via three branches. The first branch is directed medially in the posterior portion

of the frontals and is visible as a large pore in the pineal region. The second offshoot exits the bone in a pore close to the medial suture of the frontals above the orbit. The main line continues anteriorly and exits the frontals in a small pore anterior to the orbit that is aligned with a groove that extends to the anterior margin of the frontal (Fig. 3.2A). The frontals are bordered posteriorly by the supraoccipital, parietals, pterotics and sphenotics. An elongate supraoccipital is bordered by the epiotics posteromedially and the parietals anteromedially. The supraoccipital ridge bifurcates, extending anteriorly to the level of the orbit. The parietals suture with the frontals anteriorly, and form part of the epiotic ridge, suturing with the pterotic laterally. The pterotic is elongate with a large ridge. The suture between the parietals and the pterotic can be traced posteriorly to the mid-point of the pterotic shelf. Laterally the pterotic sutures with the sphenotic, which forms the posterior margin of the orbit. The epiotic meets the posteromedial margin of the parietals and the lateral margin of the supraoccipital. A clear suture is visible posteriorly between the epiotic and the exoccipitals. The small intercalar is visible dorsally. It has a curved anterior margin that meets the exoccipitals anteromedially and the posterior margin of the pterotic anterolaterally.

In lateral view (Figs 3.2B, 3.3B) the neurocranium is deepest posteriorly, the parasphenoid curves dorsally to suture with the posterior margin of the vomer. The vomer is widest anteriorly where it meets the mesethmoid. Wings on either side of the vomer extend dorsolaterally from behind the vomerine teeth to the point of articulation with the parasphenoid. The vomer bears two pairs of teeth, which are small and posteriorly recurved. The anterior tooth is smaller than the posterior. Posteriorly the parasphenoid overlaps and sutures to the basioccipital. At the posterior margin of the orbit, the strut-like lateral commissure defines the

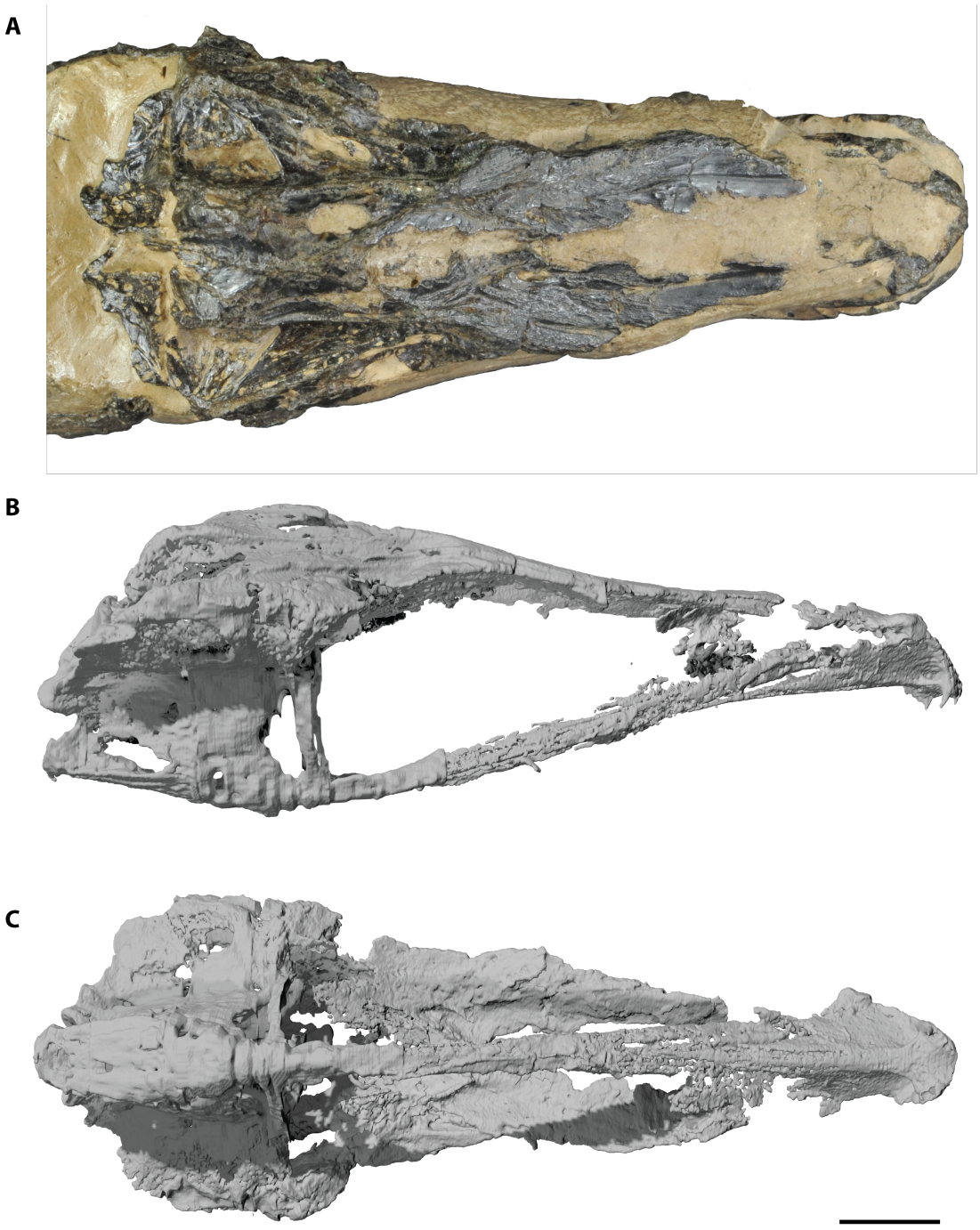


Figure 3.2: The braincase of †*Progempylus edwardsii* (NHMUK PV OR 32388). A, specimen photograph, dorsal view. B-C, rendering in: B, lateral; C, ventral view. Scale bar represents 10 mm.

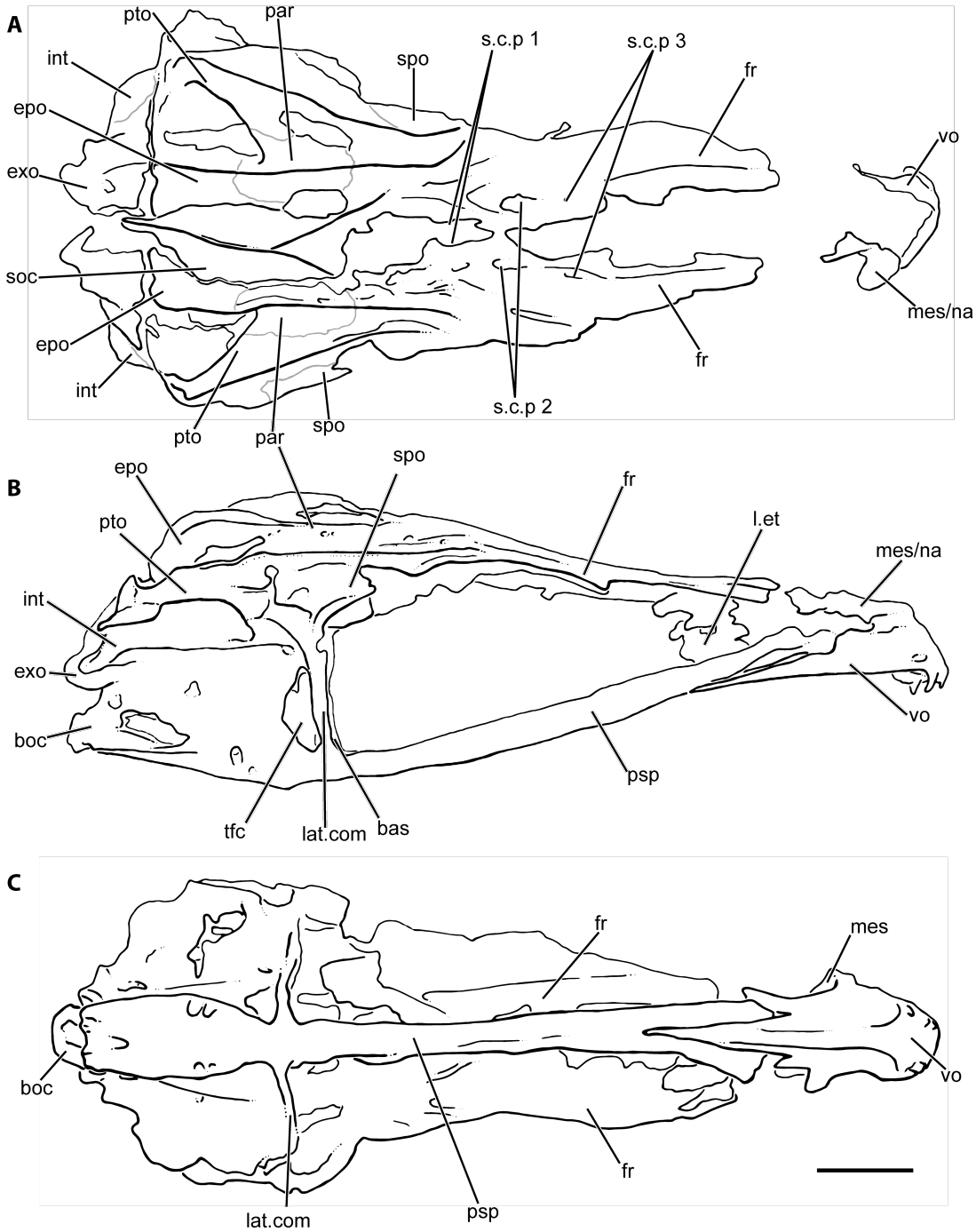


Figure 3.3: The braincase of †*Progempylus edwardsii* (NHMUK PV OR 32388), drawings in: A, dorsal; B, lateral; C, ventral view. Abbreviations: bas, basisphenoid; boc, basioccipital; epo, epiotic; exo, exoccipitals; fr, frontal; int, intercalar; lat.com, lateral commissure; l.et, lateral ethmoid; mes, mesethmoid; na, nasal; par, parietal; psp, parasphenoid; pto, pterotic; s.c.p.1-3, supraorbital canal pores 1-3; soc, supraoccipital; spo, sphenotic; tfc, trigeminal facial chamber; vo, vomer. Scale bar represents 10 mm.

margin of a large trigeminal facial chamber (Fig. 3.3B).

Jaws

The lower jaw is short and deep, even accounting for missing bone at the anterior and posterior margins (Fig. 3.4A, B). The dentary exclusively forms the dorsal margin and contributes to the ventral margin of the jaw, with the anguloarticular inserted into the notch-like excavation in the posterior margin of the dentary. A series of small teeth are borne on the dorsal margin of the mandible, with three preserved on the right dentary and the base of three or four on the left. These teeth are relatively similar in size and evenly spaced along the jaw. The ventral-posterior margin of the lower jaw and its articulation with the quadrate appear to be missing, as the metapterygoid and fragmentary quadrate are preserved posterior to the preserved portion of the lower jaw. No components of the dermal upper jaw are preserved.

Suspensorium

The suspensorium comprises the palatine, ectopterygoid, endopterygoid, metapterygoid, quadrate, hyomandibula and symplectic (Fig. 3.4C, D). In lateral view the palatine consists of an elongate dorsal ridge and a ventral plate-like expansion. The lower margin of the ventral ridge is jagged but no obvious teeth are visible. The anterior process of the dorsal ridge is hooked and expanded medially, articulating posteriorly with the anterior margin of the endopterygoid, which is oval in shape, pointed anteriorly and concave dorsally. The ectopterygoid is poorly preserved and highly pyritized. On the left side of the specimen, a thin lamina of bone on the internal surface of the quadrate may also represent a fragment of

ectopterygoid. A broad, flat metapterygoid with a posterodorsal extension sits anterior to the hyomandibular shaft, although the nature of the contact between the two bones is obscured by pyrite. The ventral margin of the metapterygoid articulates with the dorsal margin of the quadrate. The hyomandibula is fragmentary on the right side of the specimen, with only the anterodorsal head and a small ventral extension that articulates with the metapterygoid preserved. More complete on the left side, the hyomandibula has a flat dorsal head and long, slender ventral shaft. The dorsal head has two articular areas: an anterior projection that articulates with the sphenotic, and a posterior expansion articulating with the lateral margin of the braincase beneath the pterotic. The opercular process extends directly perpendicular to the ventral shaft of the hyomandibula. The quadrate is preserved as a fragment on both sides and its shape cannot be discerned. The symplectic is small and elongate.

Hyoid arch

The dorsal and ventral hypohyals are tightly bound. Each hypohyal is rectangular individually, but the dorsal and ventral components are tightly bound to form a square (Fig. 3.4E, F). The anterior ceratohyal is approximately three times the length of the hypohyals, and bears a narrow, longitudinal groove on its lateral surface. There is no ceratohyal window. The posterior ceratohyal is as deep as the anterior ceratohyal, but shorter in length. It tapers to a posterior point, forming a triangular shape. The anterior and posterior ceratohyals join in an interdigitated suture. Two narrow branchiostegals articulate with the posterior ceratohyal. Additional elements of the branchiostegal series are not apparent.

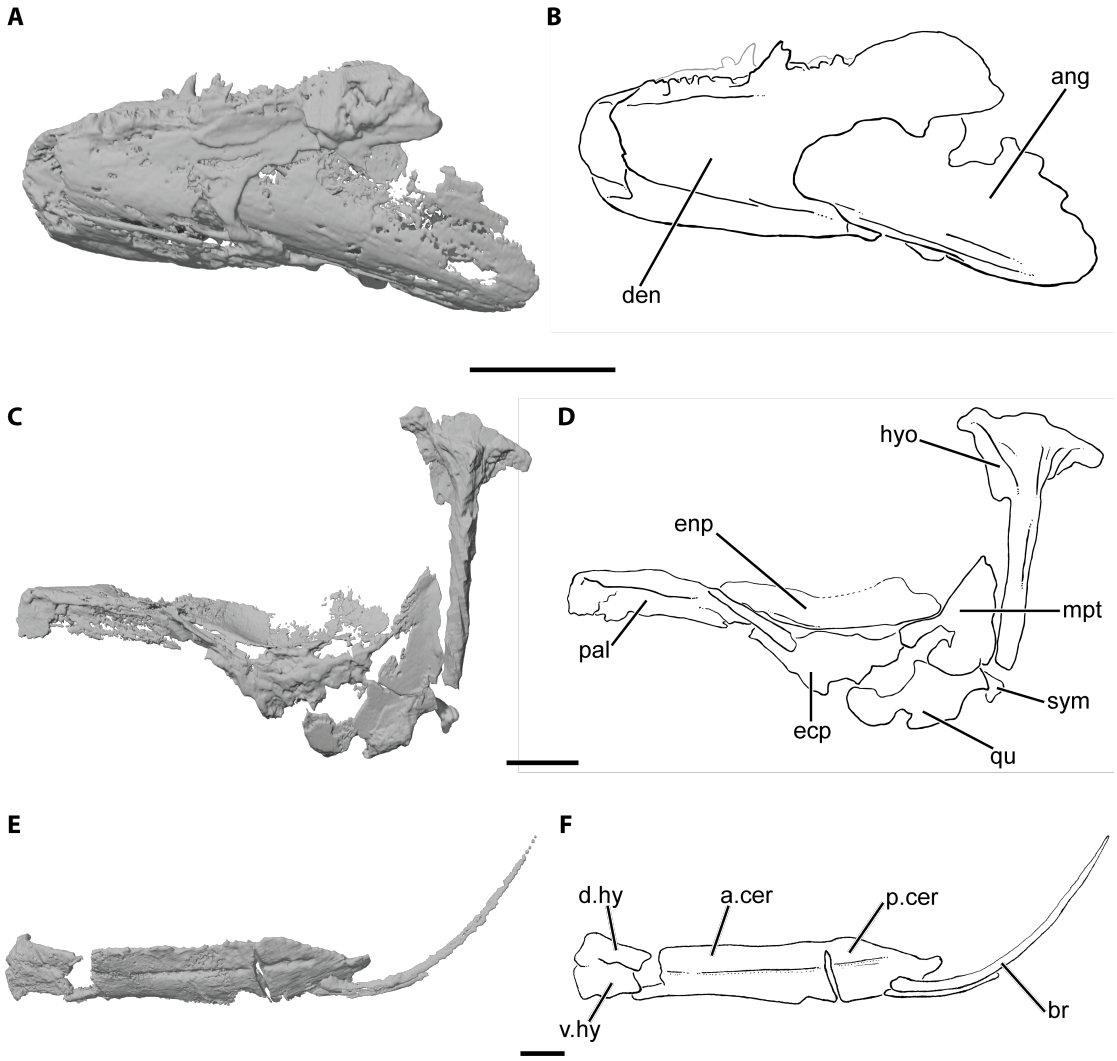


Figure 3.4: †*Progempylus edwardsii* (NHMUK PV OR 32388). A-B, lower jaws in left lateral view; A, rendering; B, drawing (components of right mandible shown lighter). C-D, suspensorium in left lateral view; C, rendering; D, drawing. E-F, hyoid arch in left lateral view; E, rendering; F, drawing. Abbreviations: a.cer, anterior ceratohyal; ang, anguloarticular; br, branchiostegal; den, dentary; d.hy, dorsal hypohyal; ecp, ectopterygoid; enp, endopterygoid; hyo, hyomandibula; mpt, metapterygoid; pal, palatine; p.cer, posterior ceratohyal; sym, symplectic; qu, quadrate; v.hy, ventral hypohyal. Scale bars represent 10 mm.

Gill skeleton

The gill skeleton is well preserved and largely in articulation, particularly posteriorly (Fig. 3.5). It preserves the urohyal, hypobranchials 1-3, ceratobranchials 1-5, epibranchials 1-4 and pharyngobranchial 3. Pharyngobranchial 1 is preserved only on the left side.

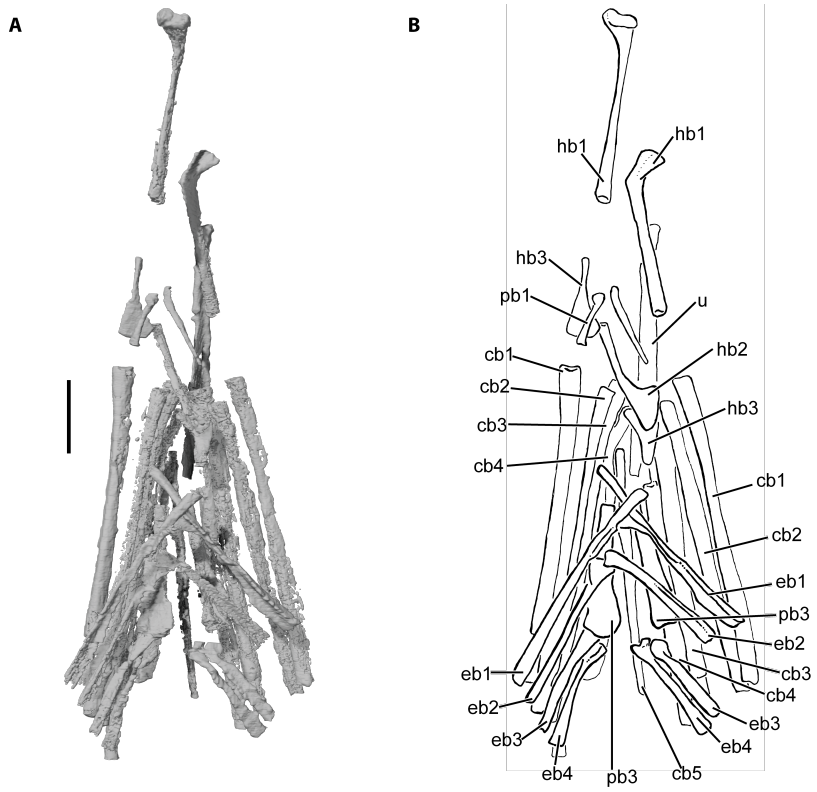


Figure 3.5: Dorsal view of the gill arches of †*Progempylus edwardsii* (NHMUK PV OR 32388). A, rendering. B, drawing. Abbreviations: cb, ceratobranchial; eb, epibranchial; hb, hypobranchial; pb, pharyngobranchial; u, urohyal. Scale bar represents 10 mm.

Hypobranchial 1 is preserved on both sides of the specimen, although both elements have been rotated out of life position. It is elongate with a large laterally-directed anterior head. Hypobranchial 2 is preserved most completely on the left side and has been rotated posteriorly. It is long and straight with an anteriorly

expanded head of a similar size to hypobranchial 1. A fragment of bone on the right side occupies the expected position of hypobranchial 2. Hypobranchial 3 is well preserved on the left side, with a broad posterior expansion that is triangular in shape and extends anteriorly. The right hypobranchial 3 has been rotated posteriorly and is missing the elongate anterior expansion.

Ceratobranchials 1-5 are elongate and straight with a groove extending the length of the ventral surface. Ceratobranchials 1-4 are of approximately equal length but ceratobranchial 5 is only two-thirds the length of the other ceratobranchials and meets its antimere anteriorly. Ceratobranchial 5 is also slightly wider than ceratobranchials 1-4, expanding ventrally so the groove faces medially. No teeth are visible on the ceratobranchials.

Epibranchials 1-4 are elongate, curve medially and become progressively smaller from epibranchial 1 to epibranchial 4. Each epibranchial bears a groove on its dorsal surface. Epibranchial 1 widens into a dorsolateral process one-third of the way along its length from the anterior margin. Epibranchial 2 lacks a process but is expanded anteriorly to form a flat triangular shaped head, and epibranchials 3 and 4 are also expanded slightly anteriorly. Epibranchial 3 has no associated processes, while the left epibranchial 4 shows a dorsal process.

Pharyngobranchial 1 is small and rod like with a small anterior head. It is preserved only on the left side, shifted anteriorly from its presumed life position. Pharyngobranchial 3 is equal in length to hypobranchial 2 but wider posteriorly, forming a shallow concavity in dorsal view. The ventral surface of the right pharyngobranchial 3 is rough, suggesting the possible presence of a sutured toothplate, although this is not clearly preserved. The urohyal is plate-like, triangular in lateral view, and anteriorly tapers to a trapezoidal head. The ventral margin of the

urohyal has a small lateral expansion about the midline.

Opercular series

The opercular series consists of the preoperculum, operculum and suboperculum (Fig. 3.6). The preoperculum curves anteroventrally and is widest at the angle of the bone, with a weakly convex posterodorsal margin. The operculum and suboperculum are approximately triangular in shape, with the suboperculum smaller and positioned medio-ventrally to the operculum. A circular facet for articulation with the hyomandibula is preserved on the medial surface of the right operculum, and completely covered by a plate-like lateral process in lateral view. The operculum has a large notch on its posterodorsal margin. The ventral posterior margin of the notch forms a point at the posterodorsal corner of the operculum.

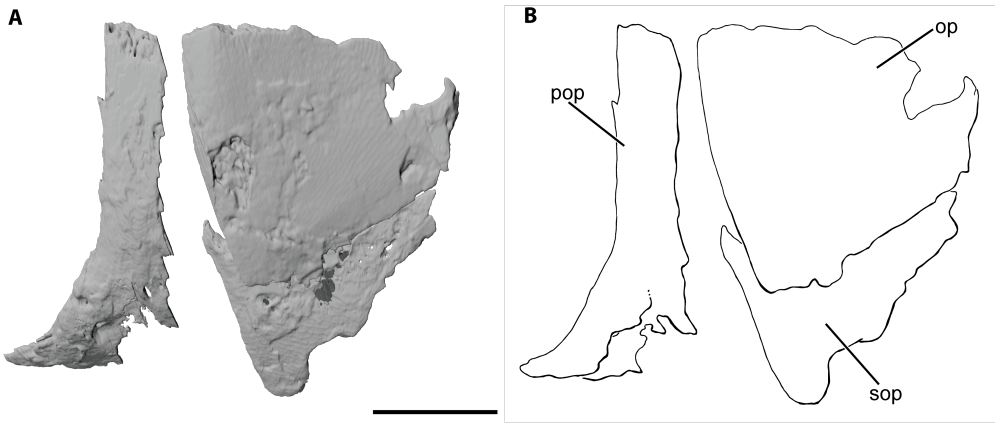


Figure 3.6: Left lateral view of the opercular series of †*Progempylus edwardsii* (NHMUK PV OR 32388). A, rendering. B, drawing. Abbreviations: op, operculum; pop, preoperculum; sop, suboperculum. Scale bar represents 10 mm.

‘Gempylidae’ *incertae sedis*

1966 cf. Eutrichiurides Casier, p. 249, text fig. 56, pl. 24 fig. 3.

2005 Gempylinae? *incertae sedis* Monsch, p. 449, fig. 5.

Material

NHMUK PV OR 41318, three-dimensionally preserved braincase.

Occurrence

London Clay Formation, Isle of Sheppey, UK. Specimens from this locality are Ypresian in age and dated at 52-49 Ma. The depositional setting is outlined in greater detail in Friedman et al. (2016).

Remarks

An historically prepared braincase referred to †*Eutrichiurides* by Casier (1966) and then to 'Gempylidae' by Monsch (2005), this specimen is incomplete anteriorly but is otherwise well-preserved. The specimen is characterized by an elongate braincase with frontals that narrow appreciably above the orbits, prominent parietal and epiotic ridges, a supraoccipital ridge that bifurcates on the supraoccipital, and exoccipitals that extend posteriorly. Comparisons with NHMUK PV P26904 are limited by the small amount of overlap in the regions of the braincase preserved in the specimens. Characters differentiating NHMUK PV OR 41318 from NHMUK PV P26904 are: vomer does not extend markedly posterior to the lateral ethmoids (vomer in NHMUK PV P26904 extends over half the length of the neurocranium to the midpoint of the orbit); strong ornament not apparent on frontal (compared to the ornament on the right fragmentary frontal in NHMUK PV P26904). NHMUK PV OR 41318 also shows clear differences from †*Progempylus edwardsii*: parasphenoid and vomer are approximately parallel to the frontals in NHMUK PV OR

41318 (the parasphenoid and vomer curve dorsally in lateral view in †*Progempylus edwardsii*); basioccipital and exoccipitals extend far posterior to the rear margin of the intercalar and pterotic (in †*Progempylus edwardsii* the basioccipital and exoccipitals do not exhibit such a marked posterior projection relative to the intercalar and pterotic).

3.3.2 Description

Braincase

In dorsal view the paired frontals are elongate, narrowing medially above the orbit (Figs 3.7A, 3.8A). In the pineal region of the frontals the pores for the medial branch of the supraorbital canal are visible. The frontals suture anteriorly with the mesethmoid which narrows anteriorly and is broken laterally. In lateral view the mesethmoid extends to meet the dorsal surface of the vomer (Figs 3.7B, 3.8B). The lateral ethmoids extend laterally beyond the mesethmoid and the frontals in dorsal view, and meet the posterior margin of the vomer and mesethmoid in lateral view. The posterior margin of the frontals sutures to the supraoccipital, which bears the supraoccipital crest (Figs 3.7A, 3.8A). Dorsally the supraoccipital crest is broken but is well developed and extends posteriorly over the exoccipitals. The parietals lie lateral to the supraoccipital. Posteromedially, the frontals are bordered by the sphenotic. The sphenotic forms the posterior margin of the orbit and sutures with the pterotic posteriorly. The parietals suture to the pterotic laterally and the epiotic posteriorly. The pterotic has a pronounced shelf and a well-developed pterotic ridge, almost the same height as the epiotic ridge in lateral view. In dorsal view the epiotics are approximately round and suture with the intercalar and exoccipitals

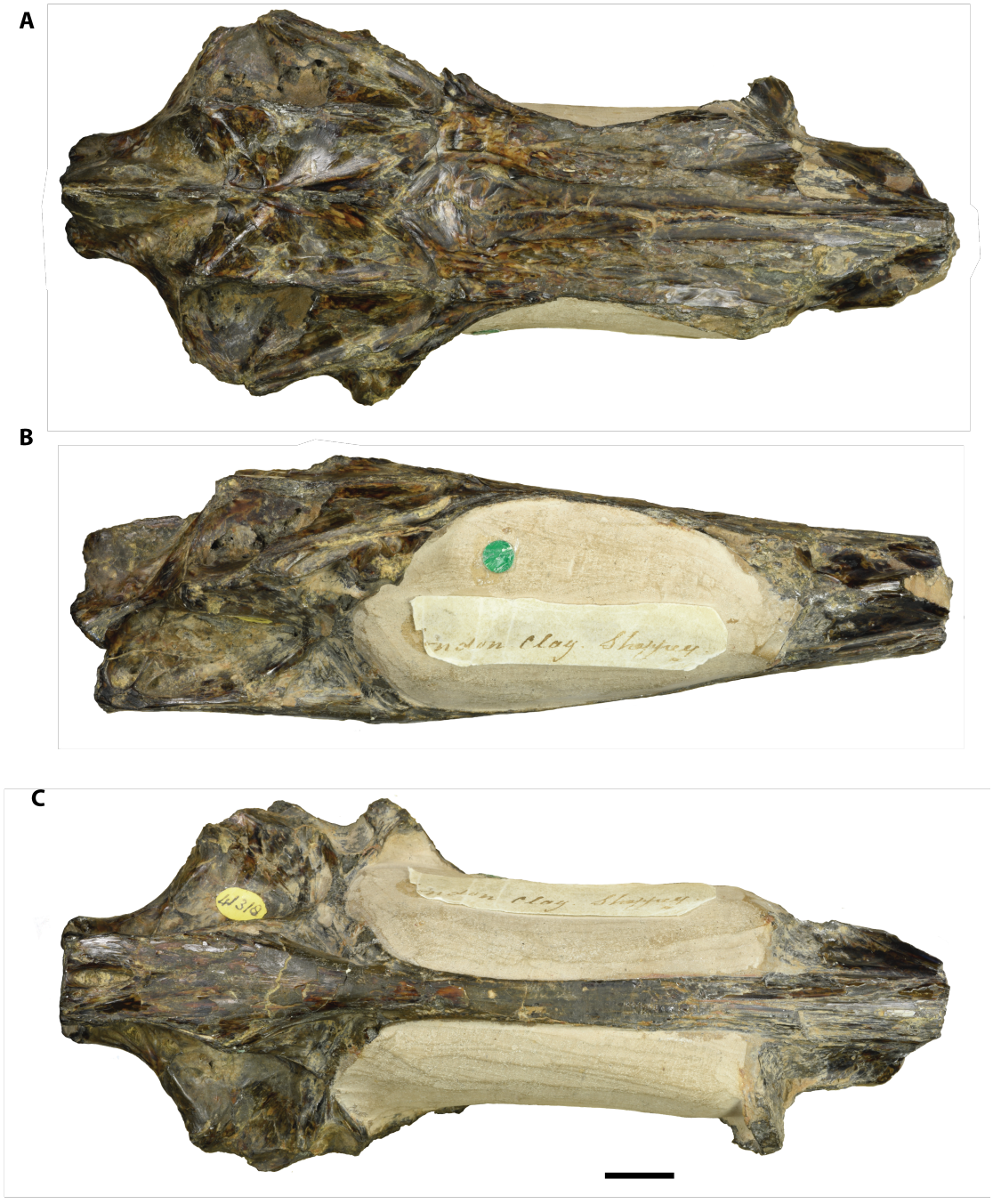


Figure 3.7: The braincase of NHMUK PV OR 41318 ('Gempylidae' *incertae sedis*); photographs in: A, dorsal; B, lateral; C, ventral view. Scale bar represents 10 mm.

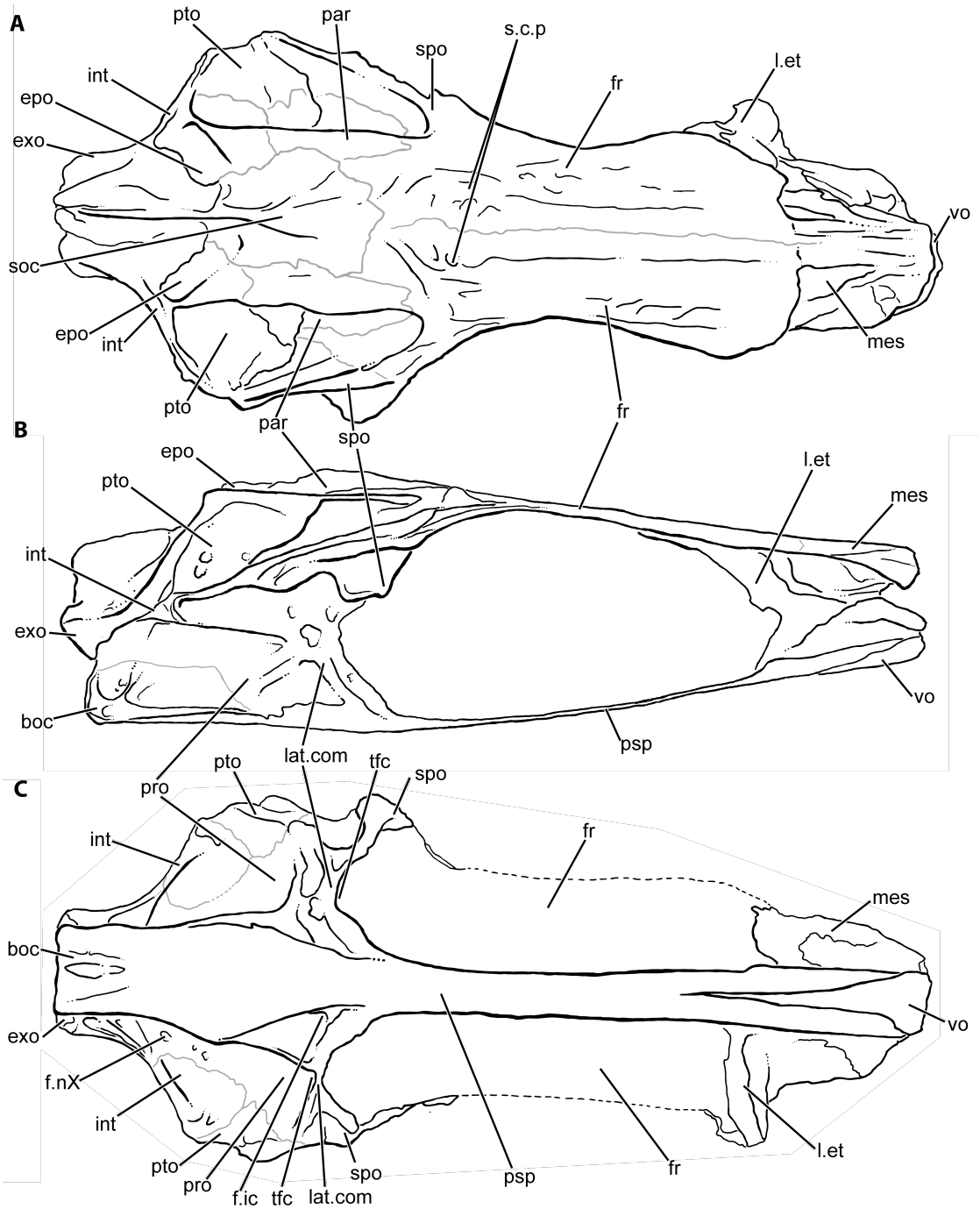


Figure 3.8: The braincase of NHMUK PV OR 41318 ('Gempylidae' *incertae sedis*); drawings in: A, dorsal; B, lateral; C, ventral view. Abbreviations: boc, basioccipital; epo, epiotic; exo, exoccipitals; f.ic, foramen for internal carotid; f.nX, foramen for the vagus nerve (X); fr, frontal; int, intercalar; lat.com, lateral commissure; l.et, lateral ethmoid; mes, mesethmoid; par, parietal; pro, prootic; psp, parasphenoid; pto, pterotic; s.c.p, supraorbital canal pore; soc, supraoccipital; spo, sphenotic; tfc, trigeminal facial chamber; vo, vomer. Scale bar represents 10 mm.

posteriorly. The intercalar is visible on the dorsal surface but is small, being larger on the ventral surface of the neurocranium, suturing with the sphenotics laterally and the basioccipital medially. The exoccipitals are kidney-shaped in lateral view. The basioccipital sutures to the underside of the exoccipitals and is concave in posterior view. In lateral view the basioccipital sutures to the dorsal side of the parasphenoid anteroventrally and the posterior side of the prootic anteriorly (Figs 3.7B, 3.8B). A ventrally placed foramen marks the exit of the vagus nerve from the exoccipital. In both lateral and ventral view the prootic is visible and connects the parasphenoid to the medial margin of the sphenotics. The lateral margin of the trigeminal facial chamber is defined by the strut-like lateral commissure, which forms the anterior margin of the prootic. At the junction of the parasphenoid and the prootic is the foramen for the internal carotid. The parasphenoid, which meets the basisphenoid posteriorly, extends anteriorly to the posterior margin of the vomer and meets this along a 'v'-shaped contact at the posterior point of the lateral ethmoids (Figs 3.7C, 3.8C). The anterior tip of the vomer is missing and it is not possible to determine if teeth were present.

Trichiuroidea *incertae sedis*

Genus †*Macroynis* nov. LSID.

urn:lsid:zoobank.org:act:28EAA039-9656-40B7-8EE90098BBA9FD0E

Derivation of name

Macro, long, large; *ynis*, vomer; meaning long vomer in Greek.

Type species

†*Macroynis casieri* sp. nov. Diagnosis. As for type and only species.

†*Macroynis casieri* sp. nov.

1966 *Eutrichiurides winkleri* Casier; Casier, p. 244, textfigs 55-56, pl. 23 figs 2-5.

2005 *Eutrichiurides winkleri* Casier; Monsch, p. 447, fig. 3.

LSID. urn:lsid:zoobank.org:act:FD07E026-37DF-4A68-ACE7-EB07EB19EF82

Derivation of name

Specific name honours Edgard Casier, who first described the specimen.

Holotype and only specimen

NHMUK PV P26904 (Fig. 3.9) is a historically prepared, incomplete isolated skull from the London Clay of Sheppey, UK (for a review of depositional setting and age see Friedman et al. 2016). The braincase of this specimen is highly fragmented, particularly the dorsal surface.

Diagnosis

Trichiuroid fish distinguished by the following combination of characters: elongate vomer extending markedly behind the lateral ethmoid, single large premaxillary fang, anterior tooth on dentary in line with other teeth, anteroposteriorly abbreviated hypohyals located greatly anterior to the anterior ceratohyal, presence of a ceratohyal window in anterior ceratohyal, palatine triangular and ventrally extended in lateral view.

Occurrence

London Clay from the Isle of Sheppey, UK. Specimens from this locality are Ypresian in age and dated at 52-49 Ma. The depositional setting is outlined in greater detail in Friedman et al. (2016).

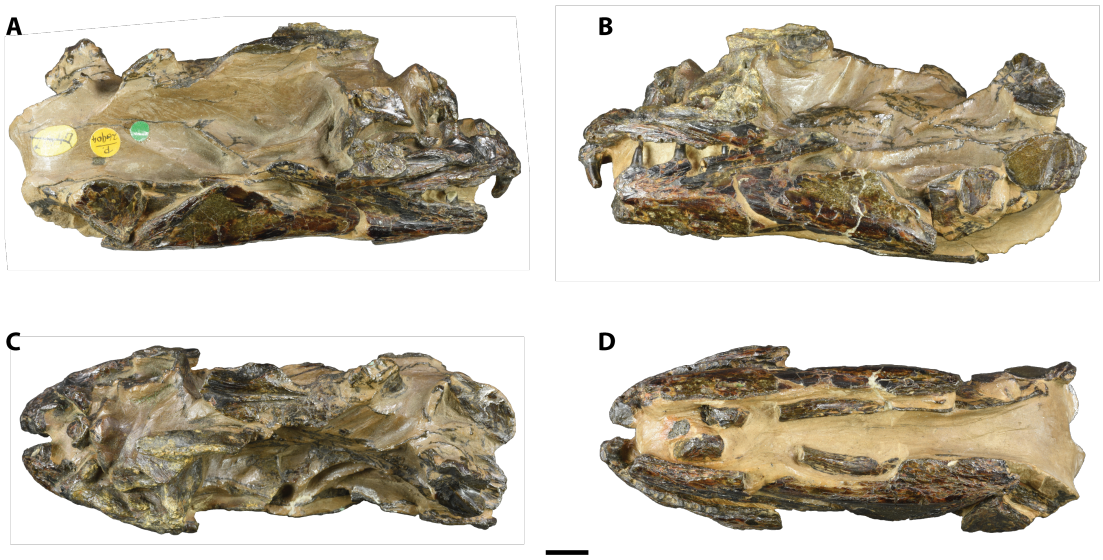


Figure 3.9: Photographs of the skull of †*Macroynis casieri* (NHMUK PV P26904) in: A, right lateral; B, left lateral; C, dorsal; D, ventral view. Scale bar represents 10 mm.

3.3.3 Remarks

The holotype of †*Eutrichiurides delheidi*, the type species of †*Eutrichiurides* (Casier, 1944), comprises a dentary, premaxilla and series of teeth belonging to a single individual (Leriche 1908; pl. 25 figs 1-2) from the Oligocene (Rupelian) Boom Clay of Belgium. Casier (1944, 1946, 1966) subsequently attributed isolated teeth removed from †*Trichiurides* to †*Eutrichiurides*. He reinterpreted teeth retained within the former genus as belonging to a gadiform. These isolated dentitions have a tortuous taxonomic history, featuring

associations with lepisosteids (Woodward, 1891) and lophiids (Leriche, 1905) in addition to the trichiurid interpretation advocated by Casier and others (Winkler, 1876; White, 1931). It is from some of these isolated dentitions that Casier (1946) erected †*Eutrichiurides winkleri* (type series: IRSNB P 00320, 00324-00329) from the Eocene (Ypresian) of Forest-lez-Bruxelles, Schaerbeeck, Belgium (Casier 1946, pl. 6 fig. 19a-b). In his review of the London Clay fish fauna, Casier (1966) attributed NHMUK PV P26904 to †*Eutrichiurides winkleri* as the only skeletal (rather than exclusively dental) material of the species.

We question this attribution of NHMUK PV P26904. There are no obvious features shared uniquely between NHMUK PV P26904 and the type material of †*Eutrichiurides winkleri*, and we find no clear evidence that they are conspecific beyond similarity in age. Indeed, the type material of †*Eutrichiurides winkleri* is sufficiently non-diagnostic that we regard identification of these remains at the species level dubious. With respect to generic assignment, more detailed comparisons are possible with the substantially younger type species of the genus, †*Eutrichiurides delheidi*. Similarities with NHMUK PV P26904 are present (e.g. enlarged premaxillary fangs), but these are general features of trichiuroids that provide no evidence for relationships within the group. Pertinently, †*Eutrichiurides delheidi* bears an anteroventral projection at the tip of the dentary, a feature with limited distribution among trichiurids (e.g. *Assurger*, *Evoxymetopon*) but which appears not to be present in NHMUK PV P26904 despite damage to the anterior region of the mandibles. We have no confidence that NHMUK PV P26904 and †*Eutrichiurides delheidi* form a monophyletic group relative to other trichiuroids, and therefore erect the new taxon †*Macroynis casieri* to accommodate the London Clay specimen.

3.3.4 Description

Braincase

The braincase is highly fragmented, presumably due to damage during preservation (Fig. 3.10). The parasphenoid extends the whole length of the neurocranium but is broken midway along its length, and the posterior part of the parasphenoid and braincase is rotated and displaced laterally. The posteriorly convex basisphenoid that bears a gutter along its midline overlays the posterior margin of the parasphenoid (see .vol files in Beckett et al. 2018). A lateral wing of the parasphenoid contacts the prootic dorsally. Anteriorly, the parasphenoid extends dorsal to the vomer, and the suture between the parasphenoid and vomer is visible in cross section (see .vol files in Beckett et al. 2018). The edentulous vomer is fully half the length of the braincase, tapering to a point well posterior to the lateral ethmoids. Anterolaterally, the vomer widens into broad processes. Hourglass-shaped lateral ethmoids are present on either side of the vomer, with their anterior margins level with the widest part of that bone. Posteriorly, the lateral ethmoids are formed of three struts, one of which contacts the frontal.

Jaws

The upper and lower jaws are preserved on both sides of the specimen (Fig. 3.11A, B). The upper jaws comprise the maxilla and premaxilla; a supramaxilla is not apparent. The maxilla extends along the length of the ethmoid region of the neurocranium and widens anteriorly to form the premaxillary articular head. At least seven small teeth, of which only the bases are preserved, are borne on the premaxilla. In addition, a single large fang, preserved only on the right side, sits

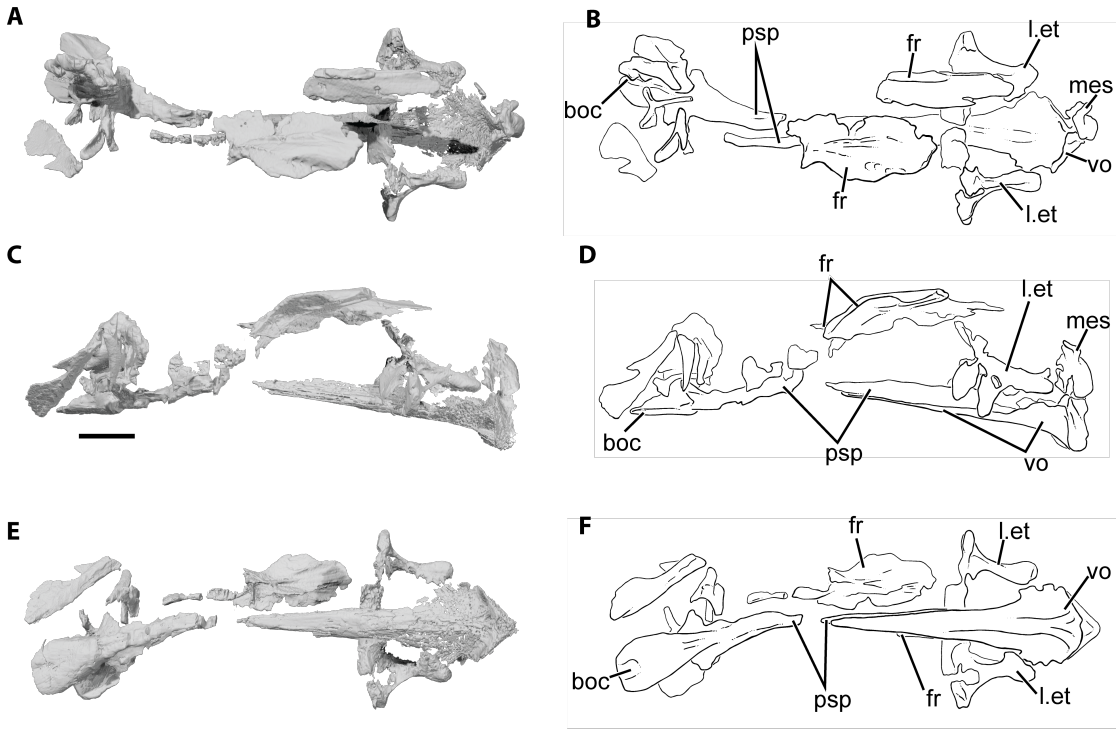


Figure 3.10: The braincase of †*Macroynis casieri* (NHMUK PV P26904). A-B, dorsal view; A, rendering; B, drawing. C-D, lateral view; C, rendering; D, drawing. E-F, ventral view; E, rendering; F, drawing. Abbreviations: boc, basioccipital; fr, frontal; l.et, lateral ethmoid; mes, mesethmoid; psp, parasphenoid; vo, vomer. Scale bar represents 10 mm.

anterior to the smaller teeth. The lower jaw is roughly twice as long as the upper jaw and extends the full length of the neurocranium. The dentary bears a single row of teeth, which decrease in height posteriorly. Up to four smooth, gently recurved teeth are preserved on each dentary, and smaller cusps at the base of some of these may represent extraosseous replacement teeth (Trapani 2001; see .vol files in Beckett et al. 2018). The posterior portion of the lower jaw is formed by the anguloarticular, which contacts the dentary along a v-shaped margin. A projection of the posterior margin of the anguloarticular forms the articulation point with the head of the quadrate.

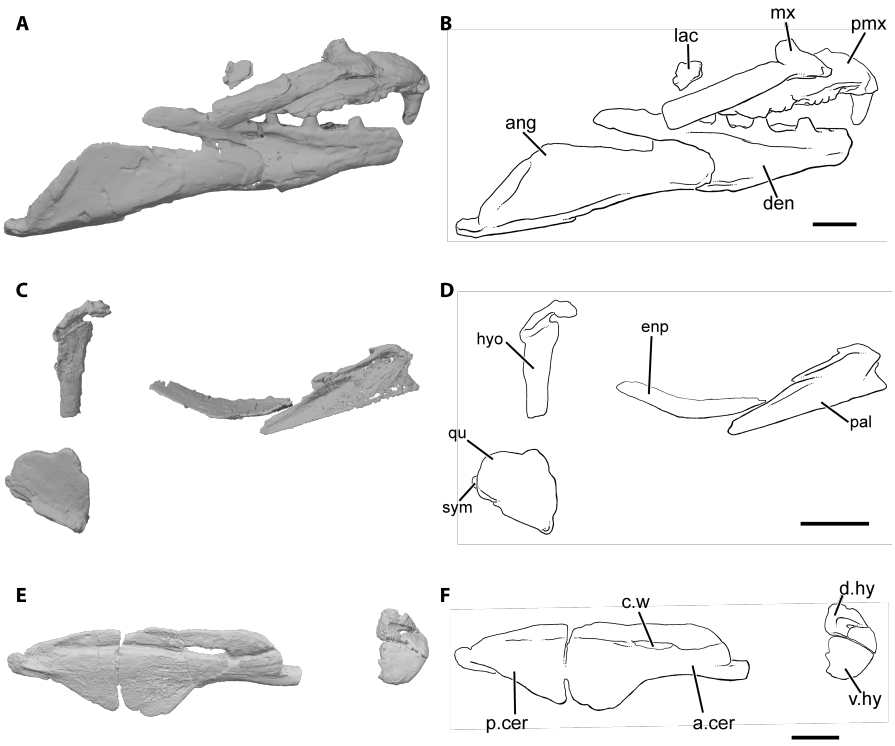


Figure 3.11: †*Macroynis casieri* (NHMUK PV P26904). A-B, jaws in right lateral view; A, rendering; B, drawing. C-D, suspensorium in right lateral view; C, rendering; D, drawing. E-F, hyoid arch in right lateral view; E, rendering; F, drawing. Abbreviations: a.cer, anterior ceratohyal; ang, anguloarticular; c.w, ceratohyal window; den, dentary; d.hy, dorsal hypohyal; enp, endopterygoid; hyo, hyomandibula; lac, lacrimal; mx, maxilla; pal, palatine; p.cer, posterior ceratohyal; pmx, premaxilla; sym, symplectic; qu, quadrate; v.hy, ventral hypohyal. Scale bars represent 10 mm.

Suspensorium

Well-preserved components of the suspensorium include the palatine, endopterygoid, quadrate and symplectic (Fig. 3.11C, D). In lateral view the palatine consists of an elongate rod dorsally, with a ventral plate-like extension. The ventral expansion is triangular in shape and bears a single row of very small teeth on its lower margin. The anterior margin is concave and articulates with the posterior margin of the maxillary head. In dorsal view, a median palatine shelf extends

approximately half the length of the palatine, narrowing anteriorly and widening posteriorly. The shallow, concave endopterygoid is extensively pyritized; no ectopterygoid or metapterygoid is preserved. The preservation of this bone is compromised by extensive pyritization. A fan-shaped quadrate bears a ventral articular condyle. The symplectic is thin and rod-like, the length of which is approximately two-thirds the height of the quadrate. It is housed in a groove on the medial surface of the quadrate. A fragment of bone on the right side of the fossil probably represents the ventral extension of the hyomandibula, with a small anterior extension forming an articular head.

Hyoid arch

The anterior and posterior ceratohyals and dorsal and ventral hypohyals are preserved on both sides of the skull (Fig. 3.11E, F). They are largely intact, with minor preparation damage to the ventral margin of the right anterior ceratohyal. The triangular posterior ceratohyal is sutured to the anterior ceratohyal via interleaved bone on its medial surface. The anterior ceratohyal is approximately twice the length of the posterior ceratohyal and is constricted at midlength. The lateral surface is grooved for the afferent hyoidean artery. A perforation (the ceratohyal window) is present at the narrowest point of the anterior ceratohyal and anteriorly there is a robust tubular extension. The dorsal and ventral components of the trapezoidal hypohyals contact each other at their widest point. The hypohyals are positioned far forward relative to the ceratohyals. The shape of the anterior ceratohyal and position of the hypohyals is mirrored on each side of the specimen, suggesting that the anteriormost portion of the anterior ceratohyal was cartilaginous.

3.4 Phylogenetic Results

3.4.1 Parsimony

A maximum parsimony analysis of morphological data yields 40 most parsimonious trees with a length of 434 steps (consistency index (CI): 0.4097; retention index (RI): 0.7267; rescaled consistency index (RCI): 0.2977; Fig. 3.12). Trichiuroidea (Fig. 3.12, node A) is supported by five characters, two of which have a CI of 1: ch. 18[1], short ascending process of the premaxilla; ch. 86[1], elongate dorsal articular process of cleithrum. The parsimony analysis recovers 'gempylids' as a grade with respect to monophyletic trichiurids, and clades within the 'gempylid' grade are largely supported by homoplastic characters. *Diplospinus* + *Paradiplospinus*is resolved as the immediate sister clade to trichiurids, but with very low nodal support (bootstrap support: 0.56, Bremer decay index: 1). (*Diplospinus* + *Paradiplospinus*) + Trichiuridae (Fig. 3.12, node C) is supported by 13 characters, 3 of which have a CI of 1: ch. 4[1], concave posterodorsal margin of the preopercle; ch. 91[1], scale-like external spinous elements of pelvic fin; ch. 113[1], small hypural notch. Trichiurids are recovered as monophyletic, supported by 33 characters, 12 of which have a CI of 1 (Fig. 3.12, node D; Appendix A.4, Fig. A.1). Many of the clades within Trichiuridae are also supported by non-homoplastic characters. †*Progempylus* is resolved as the sister taxon of *Ruvettus*. Eight characters are optimized as supporting this node, but only two of these can be assessed in †*Progempylus*: ch. 10 [1], rounded anterior process of subopercle; ch. 68[1], bifurcation of supraoccipital ridge on the supraoccipital. Together †*Progempylus* and *Ruvettus* form the sister clade to all other 'gempylid' and trichiurid taxa, with the

exception of *Lepidocybium*. Monophyly of trichiuroids minus *Lepidocybium* (Fig. 3.12 node B) is supported by four characters, one of which has a CI of 1 and can be coded for †*Progempylus*: ch. 53[1], two pairs of teeth on the vomer (also seen in *Ruvettus*, *Thyrsites* and *Neoepinnula*). NHMUK PV OR 41318 is recovered as the sister taxon of *Rexea*. This placement is supported by a single character: ch. 61[1], narrowing of the frontals above the orbit before they widen again above the lateral ethmoids. This is a homoplastic character also present in †*Progempylus*. Of the characters supporting trichiurids, NHMUK PV OR 41318 can be coded for one: ch. 67[0], pterotic ending before the posterior margin of the neurocranium, a primitive feature excluding it from Trichiuridae. In a strict consensus, †*Macroynis casieri* is the sister taxon to *Evoxymetopon*, within Trichiuridae. This placement is supported by two characters, both reversals occurring elsewhere in the tree but only co-occurring in these two genera: ch. 23[0], anterior tooth in line with the remaining dentary teeth; ch. 33[0], presence of a ceratohyal window. All characters coded for †*Macroynis casieri* show homoplasy.

3.4.2 Bayesian morphology

As in the parsimony analysis, 'gempylids' are recovered as a grade with respect to a monopyletic Trichiuridae (Fig. 3.12). In the maximum clade credibility tree (Fig. 3.12A), nodes within the 'gempylid' grade are poorly supported, with all relationships of 'gempylids' deeper in the tree than *Nesiarchus* collapsing to 'gempylid' polytomy in the majority-rule tree (Fig. 3.12B). In the maximum clade credibility tree, †*Progempylus edwardsii* and NHMUK PV OR 41318 are recovered as sister taxa in a clade with *Neoepinnula*+ *Epinnula* and †*Macroynis casieri* is recovered

as sister taxon to the grade that includes *Thyrsitoides*, *Gempylus*, *Nesiarchus*, *Diplospinus* + *Paradiplospinus* and Trichiuridae (Fig. 3.12A). However, in the majority-rule tree all fossil taxa lie within the 'gempylid' polytomy. *Diplospinus* + *Paradiplospinus* represent the immediate 'gempylid' sister group to the monophyletic trichiurids with a support value of 0.70. The trichiurid clade has a posterior probability of 0.88.

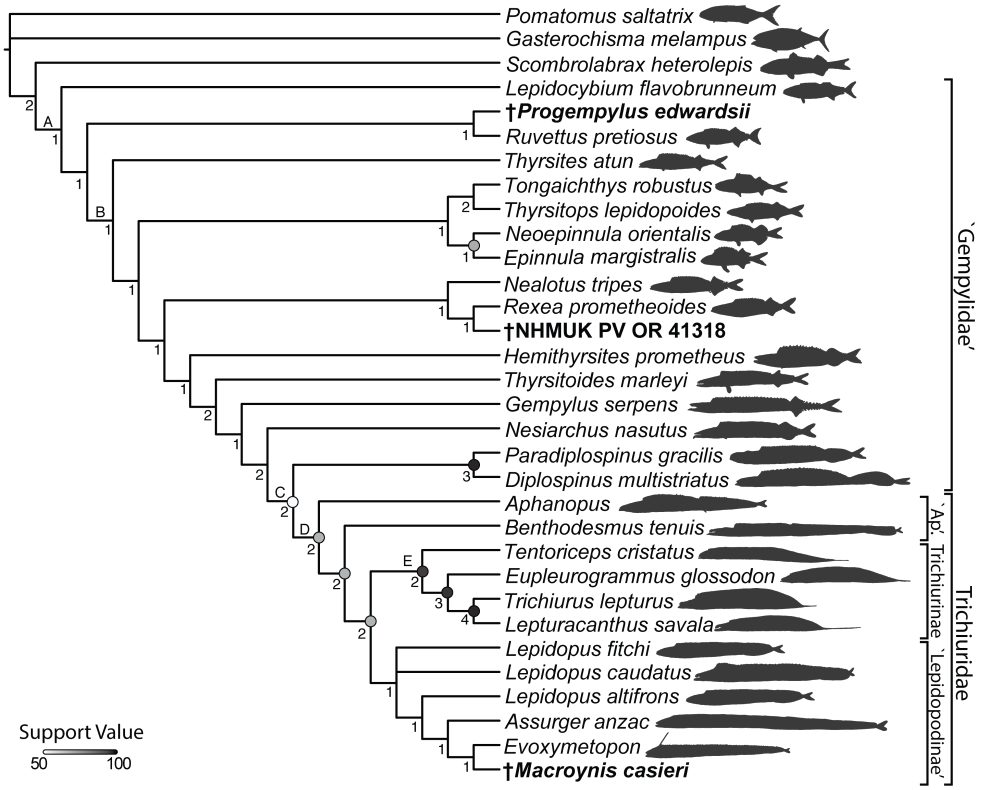


Figure 3.12: Relationships of Trichiuroidea based on parsimony analysis of morphological data. Strict consensus of three most parsimonious trees with tree length = 434 steps. Numbers below nodes represent Bremer decay indices. Circles at nodes indicate bootstrap support values. Fossil taxa in bold. 'Ap.', 'Aphanopodinae'. Trichiurinae as indicated here follows Gago (1998), with the addition of *Tentoriceps* and *Eupleurogrammus*, which are always recovered in this clade. Letters at nodes indicate selected character changes with a CI of 1, for remaining characters see Appendix A.4: A, 18[1], short ascending process of the premaxilla; 86[1], elongate dorsal articular process of cleithrum; B, 53[1], two pairs of teeth on the vomer; C, 4[1], concave posterodorsal margin of the preopercle; 91 [1], scale-like external spinous elements of pelvic fin; 113[1], small hypural notch; D, 1[1] posterior margin of opercular series strongly splintered or fimbriate; 58[1] lateral bony tubular extension of supraorbital lateral-line canal to orbital rim; 67[1] pterotic ends well past the posterior margin of the neurocranium; 83[1] posteroventral plate on coracoid present; 96[1], first neural spine distally bifurcate; 101[1], proximal, middle and distal radials in soft dorsal-fin pterygiophores; 117[1], median caudal cartilage present; E, 30[1], anterodorsal corner of ceratohyal pointed; 36[2], articular head of first basibranchial knob-like and bearing dorsolateral processes; 78 [2], anteroventral process of posttemporal separate from poteroventral process; 103[1], foramen at anterioventral corner between the proximal and distal portions of the dorsal-fin proximal radials present; 106[1], anal-fin pterygiophores fused to form a single unit; 108 [1], ultimate centrum not flexed.

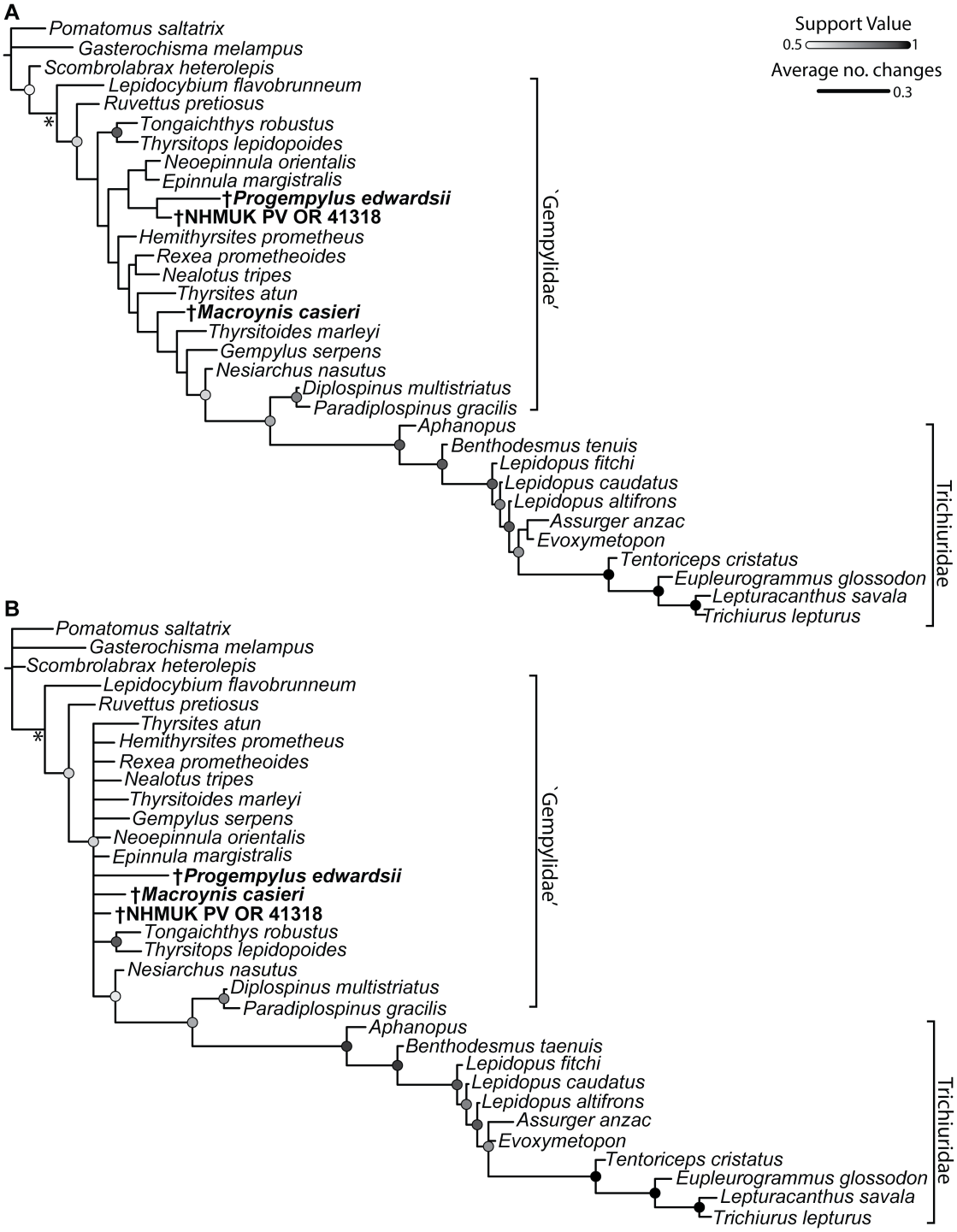


Figure 3.13: Relationships of Trichiuroidea based on Bayesian analysis of the morphological dataset: A, the maximum clade credibility tree; B, the majority-rule consensus tree. Circles at nodes indicate Bayesian posterior probabilities above 0.5. Starred nodes are enforced. Fossil taxa in **bold**.

3.4.3 Bayesian combined analysis

In agreement with the parsimony and Bayesian morphology only analyses, 'gempylids' are recovered as a grade with respect to trichiurids in the maximum clade credibility tree, albeit with very poor support (Fig. 3.13A). Trichiurids are resolved as a clade with a posterior probability of 0.87. In the majority-rule consensus tree (Fig. 3.14B), 'gempylids' form a polytomy at the base of the tree and Trichiuridae are monophyletic, the latter supported by a Bayesian posterior probability of 0.87. Three pairs of 'gempylid'-grade taxa form clades with variable support: *Thyrsitoides* + *Gempylus* (0.73), *Neoepinnula* + *Epinnula* (0.56), and *Tongaichthys* + *Thyrsitops* (0.89). *Diplospinus* and *Paradiplospinus* form a clade with *Nesiarchus* as its sister taxon; the monophyly of this group is supported with a posterior probability of 0.82. In the maximum clade credibility tree †*Progempylus edwardsii* and †*Macroynis casieri* form a clade, with NHMUK PV OR 41318 falling as the sister taxon of *Rexea* + (*Hemithyrsites* + *Nealotus*). However, all of the fossil taxa are placed within the basal polytomy in the majority-rule consensus tree. Removing fossils from the analysis recovers a tree (Appendix A.5) with three principal clades, all of which have posterior probabilities above 0.8. Two of these clades contain 'gempylids', and branch as two successively more remote outgroups to a monophyletic Trichiuridae, the latter supported by a posterior probability of 1. The most deeply diverging clade contains *Lepidocybium*, *Ruvettus*, *Neoepinnula*, *Epinnula*, *Tongaichthys* and *Thyrsitops*. The remaining 'gempylids' form a clade that falls as sister to the trichiurids, and this sister relationship has a posterior probability of 1. Trichiurid monophyly is also strongly supported, with a posterior probability of 1.

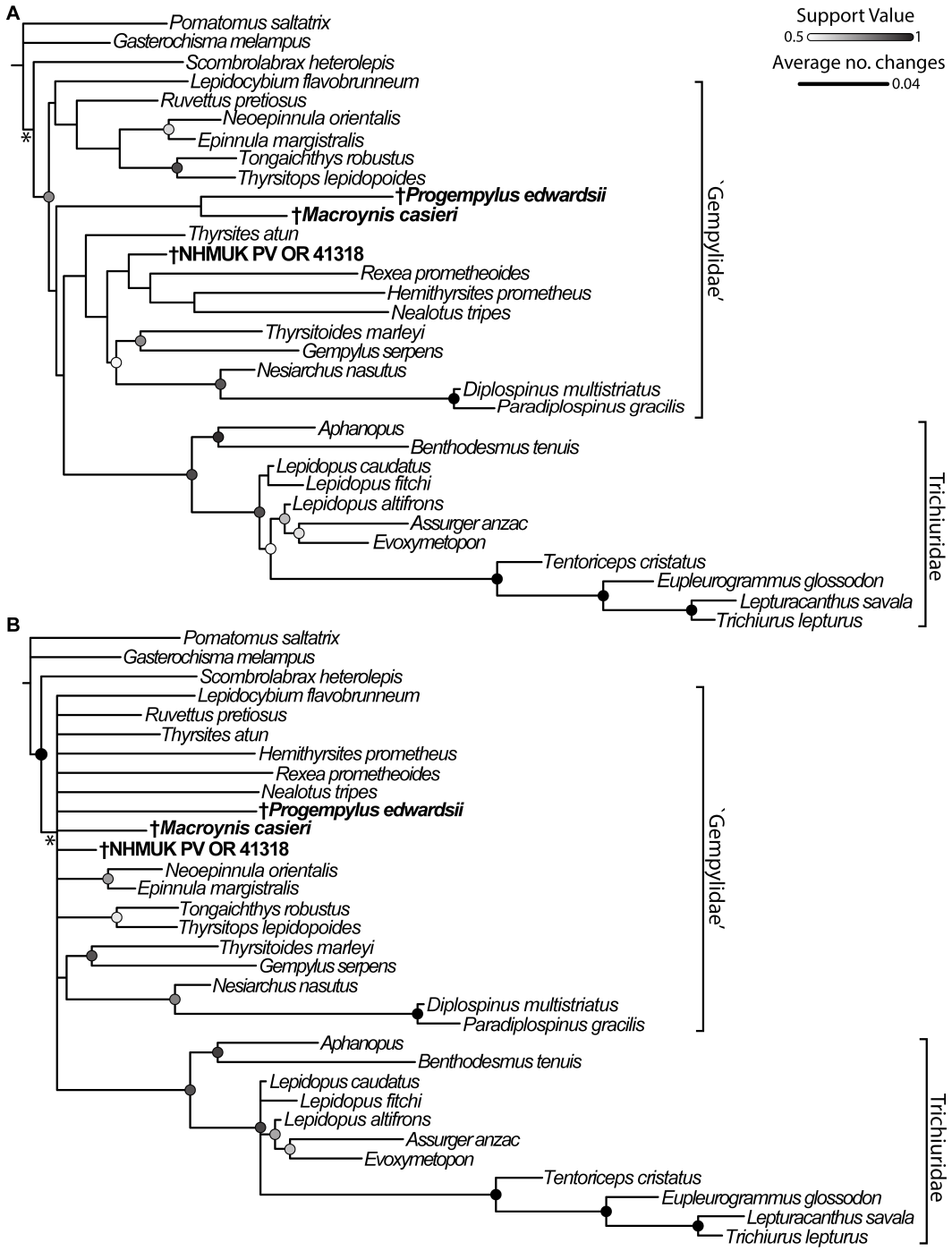


Figure 3.14: Relationships of Trichiuroidea based on the Bayesian analysis of the combined morphology and molecular dataset (mitochondrial data from Miya et al. 2013): A, the maximum clade credibility tree; B, the majority-rule consensus tree. Circles at nodes indicate Bayesian posterior probabilities above 0.5. Starred nodes are enforced. Fossil taxa in **bold**.

3.5 Discussion

3.5.1 Relationships within Trichiuroidea

Across all analyses, our results consistently recover a monophyletic Trichiuridae nested within poorly supported grade of 'gempylids'. This result is in line with previous morphological (Tucker, 1956; Johnson, 1986; Patterson and Rosen, 1986; Carpenter et al., 1995; Gago, 1997) and molecular (Orrell et al., 2006; Betancur-R et al., 2013, 2017; Miya et al., 2013; Near et al., 2013) analyses. Within this, relationships among 'gempylids' are highly variable, but *Lepidocybium* and *Ruvettus* are consistently recovered as the earliest diverging extant taxa. While trichiurids are consistently monophyletic, some relationships within the clade vary compared to previous hypotheses.

In our analyses of morphological characters (under both parsimony and Bayesian frameworks; Figs 3.12, 3.13), relationships among 'gempylids' agree broadly (and unsurprisingly) with those reported by Russo (1983), a major source of our characters. *Lepidocybium* and *Ruvettus* are recovered in both morphological analyses (Figs 3.12, 3.13) as successively branching sister taxa to the remaining ingroup. This deep split between *Lepidocybium* and all remaining trichiuroids was argued by Johnson (1986), but is not routinely supported by molecular analyses (Orrell et al., 2006; Miya et al., 2013) or our combined analysis (Fig. 3.14). *Paradiplospinus* + *Diplospinus* is recovered in all analyses as the most nested 'gempylid' clade (Russo, 1983) and the sister clade to trichiurids in the morphology analyses (Gago, 1997, 1998). *Diplospinus* has historically been closely aligned with trichiurids, and was initially placed within the group (Tucker, 1956) before

its subsequent removal (Parin and Becker, 1972). The elongate body plan of *Diplospinus* resembles that of trichiurids, lending support to a close relationship. However, *Paradiplospinus* and *Diplospinus* are rarely included in molecular analyses, so molecular support for this hypothesis is sparse (Orrell et al., 2006; Miya et al., 2013; Near et al., 2013; Betancur-R et al., 2017). Addition of molecular data to our analyses results in a different pattern of relationships among 'gempylids'. Rather than comprising numerous successive outgroups to trichiurids, 'gempylids' remain a grade but fall within a more restricted set of clades. However, the monophyly and mutual relationships of these clades are poorly supported in analyses that include fossil taxa. Removal of fossils from the combined dataset results in a well-supported pair of 'gempylid' clades (Beckett et al. 2018, S5), containing similar constituent taxa to those recovered in previous molecular analyses (Orrell et al., 2006; Miya et al., 2013), but showing different internal relationships. Other published molecular analyses including multiple 'gempylid' taxa likewise show little agreement between inferred relationships either within the assemblage or to trichiurids (Orrell et al., 2006; Betancur-R et al., 2013, 2017; Miya et al., 2013; Near et al., 2013). Satisfactory resolution of 'gempylid' interrelationships remains elusive, and we anticipate that molecular studies targeting additional lineages and increased number of loci might provide increased clarity (see Harrington et al. 2016 for a similar case).

In contrast to the ambiguity concerning 'gempylid' relationships, we find good support for Trichiuridae (cf. Gago 1998; Betancur-R et al. 2013, 2017; Miya et al. 2013; Near et al. 2013) and broadly consistent patterns of relationships within the group between analyses. Our results provide a test of the division of trichiurids into three 'tribes' by Tucker (1956): Aphanopodinae (*Diplospinus*,

Aphanopus and *Benthodesmus*), Lepidopodinae (*Assurger*, *Tentoriceps*, *Lepidopus*, *Evoxymetopon* and *Eupleurogrammus*), and Trichiurinae (*Trichiurus* and *Lepturacanthus*). Of these historically recognized 'tribes' *sensu* Tucker (1956) only the Trichiurinae are consistently recovered as monophyletic. All of our analyses resolve Lepidopodinae (*sensu* Tucker, 1956) as paraphyletic with respect to his Trichiurinae. In particular, we find that *Eupleurogrammus* and *Tentoriceps* are always successive sister groups of trichiurines. Gago (1998) recovered a similar arrangement and moved *Eupleurogrammus* to the Trichiurinae, to which we also add *Tentoriceps*. This group of four genera is a consistent feature across our analyses. The remaining 'lepidopodines' fall as a grade in Bayesian analyses (3.13, 3.14), in agreement with (Gago, 1997, 1998). Tucker (1956) evolutionary tree of trichiurids implies that Aphanopodinae are a grade, with *Diplospinus* being the deepest branch (Tucker 1956, fig. 23). Parin and Becker (1972) removed *Diplospinus* to the 'gempylids', a result supported by (Gago, 1997, 1998) and our analyses. The core 'aphanopodines' are paraphyletic in our morphological analyses as well as those of Gago (1998), but our combined analysis supports monophyly of *Aphanopus* + *Benthodesmus*, a result also recovered in previous molecular analyses (Miya et al., 2013; Betancur-R et al., 2017). In sum, we consistently recover three trichiurid assemblages across our analyses: *Aphanopus* and *Benthodesmus* at the base of Trichiuridae; 'Lepidopodinae', either as the monophyletic sister to trichiurines (in the parsimony analysis) or a paraphyletic grade with respect to trichiurines (in the Bayesian analyses); a monophyletic Trichiurinae (Fig. 3.12, node E), which falls as the most nested trichiurid clade in the Bayesian analyses. Further morphological and molecular studies should target the relationships of the 'Lepidopodinae', which are particularly unstable.

3.5.2 Placement of London Clay fossils within Trichiuroidea

†*Progempylus* was aligned with 'gempylids' and trichiurids by Casier (1966), who noted its similarity to Gempylus. Monsch (2000, 2005) also placed †*Progempylus* with 'gempylids' because of its recurved conical teeth. In his unpublished analysis, Monsch (2000, fig. 8.1) recovered †*Progempylus* in a basal polytomy uniting several fossil taxa with Trichiuroidea and a clade containing scombrids and xiphioids. In our analyses, †*Progempylus* is consistently recovered as a 'gempylid'. In the parsimony analysis, †*Progempylus* is recovered near the base of the tree in a clade with *Ruvettus* (supported by: ch. 10[1], rounded anterior process of subopercle; ch. 66[1], bifurcation of supraoccipital ridge on the supraoccipital). †*Progempylus* is nested within 'gempylids' in both Bayesian analyses, with no particular relationship to *Ruvettus*. In the morphology analysis, it falls in a clade with *Epinnula*, *Neoepinnula* and NHMUK PV OR 41318. Conversely, in the combined analysis maximum clade credibility tree †*Progempylus* is recovered with †*Macroynis*, albeit with very weak support (BPP < 0.5). We consider †*Progempylus* to be a deeply diverging trichiuroid but can propose no more precise assignment at present.

NHMUK PV OR 41318 has been interpreted as a trichiurid based on association with †*Macroynis* (Casier 1966, p. 249, fig. 56). Despite this, Casier (1966, p. 249, fig. 56) described the morphology of this braincase as intermediate between scombrids (e.g. *Scombrinus*) and trichiurids (e.g. *Lepidopus*), and Monsch (2005) assigned it to 'Gempylidae' *incertae sedis*. In our parsimony analysis (Fig. 3.12) NHMUK PV OR 41318 is recovered as the sister taxon of Rexea (supported by

a single homoplastic character: ch. 61[1], narrowing of frontals above the orbit). NHMUK PV OR 41318 is excluded from the trichiurid crown by character 67[0], as it displays the primitive state of the pterotic ending before the posterior margin of the neurocranium (ch. 67[1]: the pterotic extends beyond the posterior margin of the braincase in trichiurids). The braincase shows more general similarities with *Rexea*, including a 'box-like' lateral profile and extension of the supraoccipital crest over the posterior margin of the exoccipitals. NHMUK PV OR 41318 is recovered as sister to †*Progempylus* in our Bayesian morphology analysis (Fig. 3.13A), and as sister to a clade comprising *Rexea* and other 'gempylids' in our combined analysis (Fig. 3.14A), although collapses into the 'gempylid' polytomy in the majority-rule consensus tree of both analyses (Figs 3.13B, 3.14B). The placement of NHMUK PV OR 41318 outside the trichiurid clade in phylogenetic analyses supports its historical placement in the paraphyletic 'Gempylidae'. We consider NHMUK PV OR 41318 Trichiuroidea *incertae sedis*, but are confident it can be excluded from Trichiuridae.

The specimen renamed here as †*Macroynis* has historically been considered to be a trichiurid (Leriche, 1910; Arambourg and Signeux, 1952; Casier, 1966; Monsch, 2000, 2005) due to its straight serial teeth. Casier (1966) and Monsch (2005) suggested a series of characters tying †*Macroynis* to 'gempylids' and trichiurids more generally: premaxillary fangs (seen elsewhere in *Scombrolabrax* but not scombrids), an elongated skull (typically associated with an elongate body), and a tightly bound maxilla and premaxilla (seen elsewhere in scombrids but not *Scombrolabrax*). Despite this, no formal phylogenetic analyses have been conducted that incorporate either this specimen or †*Eutrichiurides* (with which it was previously associated) more generally. In our parsimony analysis, †*Macroynis* is resolved

as highly nested within Trichiuridae as the sister taxon to *Evoxymetopon* (based on the reversal of two highly homoplastic characters). However, this relationship is not upheld in our Bayesian analyses where it is recovered as a 'gempylid' (Bayesian morphology: Fig. 3.13A; Bayesian combined: Fig. 3.14A). While this contradicts previous assessments of its placement, this is perhaps unsurprising given the limited character information that can be obtained for †*Macroynis*. The highly fragmented braincase of †*Macroynis* results in a large number of uncodeable characters in a morphological matrix that largely targets the braincase, suggesting that its nested position in the parsimony analysis may be due to a "path of least resistance" rather than any meaningful support. However, visual inspection of †*Macroynis* indicates similar jaw proportions to extant trichiurids such as *Aphanopus* and *Evoxymetopon*, with the upper jaw extending notably anterior to the braincase and the articulation of the lower jaw behind the midpoint of the orbit. A similar morphology is seen in some elongate 'gempylids' (e.g. *Nesiarchus*, *Diplospinus*, *Paradiplospinus*), in particular those that have previously been either included in (*Diplospinus*: Tucker 1956, or closely associated with, Trichiuridae in the past (Carpenter et al., 1995; Gago, 1998). †*Macroynis* can be confidently placed in Trichiuroidea, but is of uncertain placement within this group. The morphological analysis suggests a close association with those species with an elongate body plan, either trichiurids or a subset of 'gempylids' sometimes recovered as closely related to trichiurids. However, there is greater uncertainty associated with this placement due to the ambiguities in the relationships of 'gempylids'. As with †*Progempylus*, we consider †*Macroynis* to be *incertae sedis* within Trichiuroidea, but unlike that genus we cannot exclude the possibility of placement within Trichiuridae.

3.5.3 An overview of the fossil record of Trichiuroidea, with comments on the placement of key fossil taxa

Fossil trichiuroids can broadly be categorized in two groups: firstly, those assigned to extant genera; and secondly, those representing extinct lineages. Extant trichiuroid genera with a fossil record include *Lepidopus* (†*L. lateralis* from the Miocene of Azerbaijan, †*L. albyi* from the Miocene of Italy and †*L. proargenteus* from the Miocene of Algeria: Arambourg 1927), here we follow (Bannikov and Parin, 1995) in synonymizing some members of *Lepidopus*and †*Anenchelum*as outlined below; *Thyrsitoides* (†*T. zarathoustrae* from the Eocene of Iran: Arambourg 1943); *Epinnula* (†*E. cancellata* from the Eocene of Iran: Arambourg 1967); and *Hemithyrsites*(†*H. armatus* from the Miocene of Italy: Sauvage 1873; here we follow Monsch and Bannikov 2012 in synonymizing *Hemithyrsites* and *Promethichthys*).

In addition to the taxa described in this paper, trichiuroids assigned to fossil genera include: †*Argestichthys* from the earliest Eocene (Ypresian) of Turkmenistan (Prokofiev, 2002); †*Abadzekhia* from the early-late Oligocene (Rupelian-Chattian) of the Caucasus (Bannikov, 2005) and Germany (Bannikov, 2000*a*); †*Chelifichthys* from the late Miocene (Messinian) of Algeria (Carnevale, 2006); †*Anenchelum* from the middle Eocene to early Miocene of Europe; †*Eutrichiurides* from the early Oligocene (Rupelian) of Belgium (we refer to skeletal remains only; isolated teeth attributed to the genus are more widespread but their attributions are questionable) and †*Musculopedunculus* from the early Oligocene (Rupelian) of Germany (Parin and Astakhov, 2007). Although several of these genera are represented by near-complete fossils, lateral compression and associated concealment of the braincase and gill arches means that relatively few

morphological characters can be scored. We comment below on possible placements of these genera based on previously published descriptions and character optimizations (Appendix A.1) from our phylogenetic analyses. Several as-yet undescribed Eocene trichiuroids have been figured in the literature (Bonde, 2008; Zorzin et al., 2011; Giusberti et al., 2014), but published photographs reveal too little detail to meaningfully comment on their placements.

†*Argestichthys* is the oldest described trichiuroid body fossil (Prokofiev, 2002). Prokofiev noted a series of primitive features shared by †*Argestichthys* and gempylids, and argued for a similar insertion pattern of anal-fin pterygiophores in the genus and *Ruvettus* (questioned by Monsch and Bannikov 2012, p. 264). However, Prokofiev later suggested that †*Argestichthys* shows "proximity to the generalised ancestor of Trichiuridae" (Prokofiev 2002, p. 233), implying a position on the trichiurid stem. Monsch and Bannikov (2012) classified †*Argestichthys* as Trichiuroidea *incertae sedis*, but tentatively placed it as a stem trichiurid in their composite tree. A combination of premaxillary fangs and a short ascending process of the premaxilla are consistent with a trichiuroid placement of †*Argestichthys*. Both features are present in other lineages of Pelagiaria (e.g. Scombridae, *Scombrolabrax*) but not in conjunction. However, the postmaxillary process is not well developed (ch. 21[0]), unlike the condition in trichiuroids but similar to that of outgroups. The reduced supraoccipital crest (ch. 63[1]) is found in 'gempylids' excluding *Lepidocybium* and *Ruvettus*, however the distribution among trichiurids is more complex, with a reversal in *Assurger*, *Eupleurogrammus*, *Evoxymetopon* and *Lepidopus*. Spine-like external elements of the pelvic-fin spine restrict †*Argestichthys* to

outside Trichiuridae + (*Diplospinus* + *Paradiplospinus*) (ch. 91[0]; they are scale-like in Trichiuridae + (*Diplospinus* + *Paradiplospinus*). This combination of primitive characters suggest that †*Argestichthys* is a very deeply diverging member of crown Trichiuroidea, or possibly even on the trichiuroid stem.

†*Abadzekhia* has been assigned to 'Gempylidae' (Bannikov, 1985; Bannikov and Fedotov, 1989) close to *Tongaichthys*, *Thyrsitops*, *Ruvettus* and *Lepidocybium* (Bannikov, 2005). It can be placed within Trichiuroidea on the basis of the short ascending process of the premaxilla (ch. 18[0]; also seen in scombrids), and a low but distinct postmaxillary process (Bannikov, 2017) (ch. 21[0]; a well developed process is a synapomorphy of Trichiuroidea). Within the trichiuroids, †*Abadzekhia* can be further constrained outside of Trichiuridae + (*Diplospinus* + *Paradiplospinus*)) based on the absence of two nonhomoplastic characters which support this clade: two radials are reported in the soft dorsal fin pterygiophores by Bannikov (2005) (ch. 101[0]; three are seen in Trichiuridae although given the size of the additional radial (Johnson 1986, ch. 30) it is difficult to distinguish genuine absence from taphonomic loss in fossils) and the external elements of the pelvic-fin are spine-like (ch. 91 [0] they are scale like in Trichiuridae + (*Diplospinus* + *Paradiplospinus*)).

†*Chelifichthys* was assigned to 'Gempylidae' by Carnevale (2006), and described as closely related to *Nealotus*, *Hemithyrsites*, *Rexea* and *Rexichthys*. It cannot be evaluated for any of the synapomorphies that support Trichiuroidea, however it has a moderately sized supraoccipital crest (ch. 63[1]; found in 'gempylids' excluding *Lepidocybium* and *Ruvettus*; trichiurids are characterized by further reduction of the crest, ch. 63[2]). †*Chelifichthys* also has a preopercle that is widest at the angle of the bone (ch. 5[0]), which excludes it from the clade comprising *Nesiarchus* +

((*Diplospinus* + *Paradiplospinus*) + Trichiuridae). †*Chelifichthys* shows a weakly splintered preopercle (ch. 1[0]) and two radials in the soft dorsal fin pterygiophores (ch. 101[0]; Carnevale 2006, fig. 4C; see caveats above for fossils in discussion of †*Abadzekhia*), two primitive features that show derived states in Trichiuridae. Limitations in preserved anatomy preclude precise placement within Trichiuroidea but †*Chelifichthys* can be placed within the 'gempylid'-grade in a position more closely related to trichiurids than *Lepidocybium* and *Ruvettus*, but outside of the clade comprising *Nesiarchus*, *Diplospinus*, *Paradiplospinus* and Trichiuridae.

The oldest body fossil associated with trichiurids is a specimen similar to †*Anenchelum* from the Ypresian of Monte Solane, Italy (Zorzin et al., 2011) that shows the elongate body plan associated with trichiurids. †*Anenchelum* itself is known from a number of sites, with nominal species ranging in age from Eocene to Miocene. The taxonomic history of †*Anenchelum* is complicated, largely due to reclassification of species between this genus and the extant *Lepidopus*. Woodward (1901) synonomized these two genera, but Bannikov and Parin (1995) upheld the validity of †*Anenchelum* and recognized the following species: the type †*Anenchelum glarisianum* (Blainville, 1818) from several deposits of Oligocene age; †*Anenchelum eocaenicus* (Daniltshenko, 1962) from the middle Eocene of Georgia; †*Anenchelum paucivertebrale* from the middle Eocene of the Northern Caucasus (Bannikov and Parin, 1995); †*Anenchelum angustum* (Daniltshenko, 1980) from the early Oligocene of the Caucasus and †*Anenchelum lednevi* (Menner, 1949) from the early Miocene (upper Maikopian) of Caucasus. These authors also suggest that the Oligocene †*Lepidopus hungaricus* and †*L. brevicauda* might belong to †*Anenchelum*. Many of the diagnostic features of †*Anenchelum* are admittedly generalized trichiuirid characters (Bannikov and Parin 1995, p. 186).

Most species of †*Anenchelum* are poorly known, or descriptions are largely meristic counts with few details of the skull, so here we restrict consideration to the most completely described species: †*A. paucivertebrale* and †*A. glarisianum* Bannikov and Parin (1995); Gregorova (2010). Bannikov and Parin (1995) considered †*A. paucivertebrale* to be the ancestor of 'Aphanopodinae' and 'Lepidopodinae', effectively suggesting a placement close to the crown trichiurid node. †*A. paucivertebrale* has premaxillary fangs and a short ascending process of the premaxilla, which occur together in trichiuroids. As noted by Bannikov and Parin (1995) it shows a differentiated soft and spinous portion of the dorsal fin (ch. 99[0]; a primitive feature retained by 'gempylids' + *Aphanopus* and *Benthodesmus*). The preopercle is widest opposite the dorsal arm (ch. 5[1]; observed in trichiurids, *Diplospinus* + *Paradiplospinus*, *Nesiarchus*). No epineurals are observed in the material (Bannikov and Parin 1995; ch. 98[2]; the absence of epineurals is a trichiurid synapomorphy). The caudal complex is well developed (ch. 107[0]; seen in 'gempylids', 'Aphanopodinae', and 'Lepidopodinae'). †*A. paucivertebrale* also has a slightly lower vertebral count (ch. 76: Bannikov and Parin 1995) than extant Trichiuridae (typically around 100: Nakamura and Parin 1993, but higher than even the most elongated 'gempylids' (*Paradiplospinus*: 60-64). Collectively, these features suggest a position on the trichiurid stem. †*A. glarisianum* has a more typical vertebral count for a trichiurid (110; ch. 95[2]) and shows three derived features of trichiurids in its opercular series: ch. 1[1], the opercular series is strongly fimbriate; ch. 6[0], the posterior opercular spine is absent; and ch. 10[1], the anterior process of the subopercle is rounded. It can also be excluded from the Trichiurinae + 'Lepidopodinae' based on the presence of a notch between the soft

and spinous portions of the dorsal fin (ch. 99[0]). While it is clear that the affinities of †*Anenchelum* lie with Trichiuridae, it is less clear whether its constituent species form a clade given the meristic variation observed among them.

†*Musculopedunculus* was previously assigned to its own monotypical family, Musculopedunculidae, by Parin and Astakhov (2007), who suggested affinities with *Lepidopus* and †*Anenchelum*. The specimen has some taphanomic uncertainty associated with it, the caudal fin being at an angle to the rest of the specimen, and slightly raised above the plane. It has been suggested that this could be the result of two specimens overlaid, †*Anenchelum* and the caudal fin of a thunnine (Carnevale 2018 pers. coms.). The following discussion of character placement should be considered with this in mind. Within the context of the synapomorphy scheme generated by the present study, the genus can be constrained within Trichiuroidea based on the short ascending process of the premaxilla (ch. 18[0]). An elongate bodyform with a high number of vertebrae (ch. 95[2]) and the absence of attached epineurals and epicentrals in the caudal region (ch. 98[2]) place it in Trichiuridae. The plesiomorphic presence of a flexed ultimate centrum forming a urostyle (ch. 108[0]) and a well-developed caudal fin in †*Musculopedunculus* exclude the genus from Trichiurinae. Additionally, †*Musculopedunculus* shows no division between the spinous and soft parts of the dorsal fin (ch. 99[1]), a derived feature seen in all trichiurids apart from *Aphanopus* and *Benthodesmus*. A well-developed supraoccipital crest (ch. 63 [0]) suggests placement within the 'Lepidopodinae'. Here, †*Musculopedunculus* is therefore considered to be a crown trichiurid, however some uncertainty is associated with this assignment given the taphonomy of the specimen.

†*Eutrichiurides delheidi*, from the Boom Clay of Belgium, is the type species of

the genus, and is represented by a premaxilla, dentary and teeth. The premaxilla shows a fang, seen in Scombrolabrax and trichiuroids (Johnson, 1986), but no other characters exclusive to trichiuroids are apparent. Within trichiuroids, the dentary shows an anteroventral projection at the tip of the jaws as seen in the trichiurids *Assurger* and *Evoxymetopon*. Based on this admittedly scant evidence, we consider †*Eutrichiurides delheidi* Trichiuroidea *incertae sedis*. These body fossils show that probable 'gempylids' appear in the geological record (†*Argestichthys*) before anatomically primitive trichiurids (†*Anenchelum*, including the undescribed specimen). This pattern is consistent with the sequence of evolutionary origins implied by past morphological and molecular analyses that reconstruct 'gempylids' as a grade (Collette et al., 1984; Johnson, 1986; Patterson and Rosen, 1986; Carpenter et al., 1995; Orrell et al., 2006; Miya et al., 2013; Near et al., 2013), as well as with our own results. Formal assessment of trichiuroid body fossils requires a molecular dataset with broad sampling across the trichiuroids, in addition to an improved morphological dataset, with particular focus on characters not pertaining to the braincase. Lacking new specimens, future work on placing fossil trichiuroid taxa should target well-preserved or geologically older specimens, especially those that are as yet undescribed (e.g. Zorzin et al. 2011).

3.6 Conclusions

Computed tomography has revealed novel character information for †*Macroynis casieri*, †*Progempylus edwardsii* and NHMUK PV OR 41318, allowing these fossils to be coded into a matrix of Recent taxa and phylogenetically assessed for the first time. In these phylogenetic analyses, trichiurids are consistently resolved

as a monophyletic group nested within a paraphyletic grade of 'gempylids' and we support the term Trichiuroidea for the group as a whole. †*Progempylus edwardsii* is recovered as deeply nested within Trichiuroidea within the 'gempylid' grade. The isolated braincase previously associated with 'gempylids', NHMUK PV OR 41318, is recovered within the 'gempylid' grade, sometimes in association with Rexea. NHMUK PV P26904 is reassigned from †*Eutrichiurides winkleri* to the new genus and species †*Macroynis casieri* and considered to be Trichiuroidea *incertae sedis*. Laterally compressed body fossils associated with Trichiuroidea are informally placed within the clade based on phylogenetic patterns of character distribution implied by our analyses.

3.7 Acknowledgements

The authors thank Farah Ahmed, Amin Garbout, Rebecca Summerfield, Dan Sykes, Emma Bernard, James MacLaine and Oliver Crimmen for access to the collections and assistance with scanning at the Natural History Museum, London. For access to specimens we also thank Doug Nelson at the University of Michigan Museum of Zoology, Caleb McMahan at the Field Museum of Natural History and Christine Thacker, Rick Feeney and Javier Gago at the Los Angeles County Museum of Natural History. We thank Thodoris Argyriou for his help in deriving the Greek name of †*Macroynis*. This study includes data produced in the CTEES facility at University of Michigan, supported by the Department of Earth & Environmental Sciences and College of Literature, Science, and the Arts. This research was supported by a NERC studentship to HB on the DTP Environmental Research (NE/L0021612/1), a Leverhulme Project Grant (RPG-2012-658) and

Leverhulme Prize (PLP-2012-130), both to MF, and a Junior Research Fellowship from Christ Church, Oxford, to SG. The authors would like to thank Eric Hilton and an anonymous reviewer for their thorough and constructive comments on an earlier version of this manuscript, and to Sally Thomas for her help with copy editing and production.

Chapter 4

The oldest fossil mackerel and the Paleocene origin of modern percomorph families

Abstract

Relatively little is known of the fossil record of marine fishes between the latest Cretaceous and the Paleocene-Eocene boundary, despite it being an important interval in the diversification of many modern groups. The scombrid †*Landanichthys* is a three-dimensionally preserved Selandian fossil from Angola. Unusually for the Paleocene fossil record †*Landanichthys* has been historically interpreted as deeply nested within a crown percomorph family. Here I use micro-computed tomography to redescribe †*Landanichthys* in order to place it in a formal phylogenetic analysis for the first time. The results show that †*Landanichthys* is nested within the scombrid crown group, within the Scombrinae. The placement of †*Landanichthys* as a deeply nested member of a percomorph family has implications for the rapid

diversification of Scombridae in the aftermath of the K-Pg extinction, suggesting that by the Paleocene-Eocene boundary modern phenotypes have been established, providing further support for a postulated adaptive radiation in Pelagiaria.

4.1 Introduction

The aftermath of the Cretaceous-Paleogene (K-Pg) mass extinction is marked by rapid radiation in major tetrapod groups including mammals (Simpson, 1937; Alroy, 1999; Wilson, 2014) and birds (Ksepka et al., 2017; Prum et al., 2015). Substantial changes in marine vertebrate assemblages also occurred around the K-Pg, including major shifts in the composition of fish faunas mediated by extinction and subsequent evolutionary recovery (Friedman, 2009, 2010; Sibert and Norris, 2015). Paleontological (Patterson, 1993*c*,*a*; Friedman, 2010; Friedman et al., 2016; Friedman and Carnevale, 2018) and molecular (Alfaro et al., 2018; Price et al., 2014 but see Near et al., 2013; Betancur-R et al., 2013, 2017) lines of evidence point to this interval as an important episode in the diversification of percomorphs, a species-rich clade of acanthomorph, or spiny-rayed, fishes, a group that today includes nearly one in every three vertebrate species (Nelson, 2006). Definitive Cretaceous percomorphs are restricted to the latest Cretaceous (ca. 72 Ma), and are either "perciforms" *sensu lato* (Gayet, 1991; Gayet and Meunier, 1998; Arratia and Cione, 1996; including material assigned more precisely but inadequately described) or belong to deeply diverging lineages like ophidiiforms (Carnevale and Johnson, 2015), batrachoidiforms (Bannikov, 2000*c*; Carnevale and Collette, 2014), and syngnathiforms (Sorbini, 1981). Percomorphs, like Cretaceous acanthomorphs more generally, are often rare within their respective faunas. By contrast, marine

fossil localities at (Bannikov, 2000*b*; Prokofiev, 2002) and shortly after (Monte Bolca: Friedman and Carnevale (2018); London Clay: Friedman et al. (2016)) the Paleocene-Eocene boundary are dominated by percomorphs, yielding diverse fish assemblages containing abundant members of living percomorph families that clearly foreshadow modern diversity (Patterson, 1993*c*).

Calibrating the tempo of percomorph diversification requires paleontological information between these two snapshots. However, the fossil record of percomorphs during much of the critical 10 million year Paleocene interval is poor (Patterson, 1993*c*). Only a handful of articulated or associated percomorph skeletons are known from this span, with most interpreted as Percomorpha *incertae sedis* (Davis, 1890; Adolfssen et al., 2017; Arratia et al., 2004; Alaniz-Galvan, 2011; Cantalice and Alvarado-Ortega, 2017). Exceptions include a sygnathiform assigned to an extinct monotypic family (Cantalice and Alvarado-Ortega, 2016), a fossil assigned to the stem of the monotypic menids (Friedman and Johnson, 2005), a serranid (Alaniz-Galvan, 2011; Alvarado-Ortega et al., 2015; Cantalice et al., 2018), and a scombrid (Dartevelle and Casier, 1949, 1959).

The latter of these, the scombrid †*Landanichthys*, is remarkable among Paleocene taxa on two counts. First, unlike its severely compressed or disrupted contemporaries, remains of †*Landanichthys*, from Angolese deposits historically regarded as Danian in age (Dartevelle and Casier, 1949, 1959), are partially inflated. Second, and more significantly, †*Landanichthys* has repeatedly been interpreted as being highly nested within a crown percomorph family (Bannikov, 1981; Monsch and Bannikov, 2012), although it has never been included in a formal phylogenetic analysis. Scombrids branch within the major percomorph clade Pelagiaria, which is postulated to have radiated in the early Cenozoic in response to new ecological

opportunities following the K-Pg extinction (Miya et al., 2013). With the loss of pelagic predators such as pachicormiforms and aulopiforms in line with wider biodiversity, particularly at higher tropic levels (Friedman, 2010; Friedman and Sallan, 2012), this particular ecospace was ripe with opportunity. Diverse pelagiarian fossils are known from sites at and above the Paleocene-Eocene boundary (Prokofiev, 2002; Monsch, 2005; Monsch and Bannikov, 2012; Beckett and Friedman, 2016; Friedman et al., 2016), representing a microcosm of the broader percomorph pattern. By virtue of its age and purported phylogenetic position, †*Landanichthys* is potentially a pivotal fossil in constraining divergences within Pelagiaria and among percomorphs more broadly. Despite its importance it has not been studied since the middle of the last century. Here I examine the three-dimensionally preserved †*Landanichthys* using micro-computed tomography (μCT) in order to critically test its phylogenetic placement, with the central goal of assessing its impact on our understanding of the timeline of percomorph radiation and its relationship to the K-Pg boundary.

4.2 Methods

4.2.1 Micro-computed tomography

RG 5166 from the Museum for Central Africa, Teryuren, Belgium was scanned using a Metris X-Tek HMX ST 225 CT scanner (Imaging and Analysis Centre, Natural History Museum, London) and segmented using Mimics Innovation Suite Version 18.0-19.0 (http://biomedical.materialise.com/mimics). Images were obtained by exporting meshes as .ply files to Blender (blender.org).

4.2.2 Phylogenetic dataset assembly and analysis

I amalgamated the datasets of Johnson (1986; table. 1) and Collette et al. (1984, fig. 312 and appendix) to create a single morphological character list and character matrix of 23 taxa (15/15 scombrid genera, some represented by multiple species, and two outgroups) and 103 characters. To this matrix I then added three fossil taxa; †*L. lusitanicus*, †*Eocoelopoma portentosum* PIN 1762 (coded based on my translation of Bannikov (1985)) and †*Eocoelopoma curvatum*(NHMUK PV 9455). 19 characters from Collette, Reeb and Block (2001) were added based on their discussions (no formal matrix is provided in that study). Character states were assessed with reference to the morphological literature available for scombrids (Matsui, 1967; Collette and Chao, 1975; Collette and Russo, 1984; Collette et al., 1984; Johnson, 1986; Collette and Gillis, 1992; Collette et al., 2001) and μCT scans of museum specimens see Appendix B.1. Full characters are available in Appendix B.4. The dataset includes two outgroups: *Pomatomus saltatrix* and *Scombrolabrax heterolepis*. The molecular dataset is based on that of Santini (2013), and comprises 2 nuclear (tmo4c4: 530bp; and Rh: 508bp) and 5 mitochondrial (cox1: 652bp; cytb: 1144bp; atp6: 1046bp; 12s: 479bp; and 16s: 661bp) markers. To obtain sequences for additional taxa and outgroups I constructed a new dataset from GenBank. Sequences were downloaded using BLAST (https://blast.ncbi.nlm.nih.gov/Blast.cgi), and aligned using Muscle (https://www.ebi.ac.uk/Tools/msa/muscle/). Partitions and models were used as in Santini et al. (2013), specifying a GTR+gamma model for Cox1, cytB, atp6 and tmo4c4, and HKY+gamma model for 12s, 16s and

rhod. Networks were rooted on *Pomatomus saltatrix* based on broader hypotheses of percomorph phylogeny (Orrell et al., 2006; Betancur-R et al., 2013; Near et al., 2013; Betancur-R et al., 2017). Parsimony analysis of the morphological dataset was undertaken in PAUP* v.4.0b10 (Swofford, 2001), using a heuristic search (addseq=random hold=5 nreps=500, unweighted and unordered characters and tree bisection and reconstruction strategy enabled). Bootstrap (nreps=1000 search=heuristic/ addseq=simple nreps=5 swap=tbr hold=1 rearrlimit=5000000 limitperrep=yes) and Bremer support values were calculated in PAUP*. Bayesian analysis of the morphological and combined datasets was undertaken in MrBayes v. 3.2.6 (Huelsenbeck and Ronquist, 2001). The analysis was performed with two independent runs with four chains over 15 million generations, sampling every 500 generations with a 25% burn in. Convergence was indicated by average standard deviation of split frequencies < 0.01, effective sample sizes > 200 and visual inspection of the marginal probability distribution and trace of the analyses in Tracer v 1.6 (Drummond and Rambaut, 2007).

4.3 Systematic Palaeontology

Percomorpha Rosen, 1973

Scombridae Rafinesque-Schmaltz, 1815

†*Landanichthys* Dartevelle & Caiser, 1949

Landanichthys lusitanicus Dartevelle and Casier, 1949

4.3.1 Material

†*Landanichthys* (Dartevelle and Casier, 1949, 1959) is represented by multiple specimens divided between several species: the type species †*L. lusitanicus* RG 4.614 (holotype) and RG 9.165; †*L. moutai* RG 4.617 and RG 5.695 (holotype); and †*L.* sp. RG 9.166. The specimens †*L. lusitanicus* RG 4.614, and †*L. moutai* RG 4.617 and RG 9.695 are missing. Of the two remaining specimens represented in the collections of the Museum for Central Africa, I do not consider RG. 9.165 a scombrid and it is removed from the genus †*Landanichthys* (see Remarks below). I regard the second remaining specimen, RG 9.166 previously identified as †*L.* sp., as attributable to the type species, †*L. lusitanicus* (see Remarks below).

4.3.2 Locality and horizon

All known examples of †*Landanichthys* derive from the Landana Formation in the Cabinda enclave of Angola, Africa. This formation is divided into distinctive beds. The holotype specimen, RG 4.614 and two referred specimens RG 4.617 and RG 5.695 were recovered from bed 5. The specimen studied here, RG 9.166, is from bed 8. Beds 2-12 are in the planktonic foraminifera assemblage P3b which corresponds to the early Selandian (61.33-60.52 Ma; Gradstein et al., 2012; Solé et al., 2018).

4.3.3 Diagnosis

A scombrid characterised by: absence of teeth on the vomer, a scalloped mesethmoid in dorsal view, lower jaw with parallel dorsal and ventral margins and a prominent ornamented “chin”, posterior position of jaw articulation, pronounced

premaxillary process, highly ornamented frontals with a relatively straight anterior margin, broad hyomandibular head and narrow preoperculum.

4.3.4 Remarks

†*L. lusitanicus* (Fig. 4.1A) and †*L. moutai* are distinguished by Dartevelle and Casier (1949) based on the 'remarkable ornamentation of the elements of the oral apparatus' (my translation of Dartevelle and Casier 1949, p. 237). As far as I can observe this refers to a set of radiating ridges around the "chin" on the lower jaw and a set of ridges extending linearly along the maxilla and premaxilla. This ornamentation is visible in both species of †*Landanichthys* with no clear difference and I therefore transfer specimens of †*L. moutai* into †*L. lusitanicus*. RG 9.165 assigned to †*L. lusitanicus* by Dartevelle and Casier (1959), possesses several characters at odds with a scombrid identification, including broad bands of denticles rather than a single row of teeth on its jaws (see Appendix B.3). I remove it from †*Landanichthys* and Scombridae, but cannot identify its likely affinities beyond Percomorpha *incertae sedis* at present. RG 9.166, †*L.* sp., is a skull with a single row of large slightly compressed peg-like teeth, box shaped lower jaw with a pronounced and ornamented "chin", and highly ornamented frontals. In the absence of RG4.614, I designate RG 9.166 as the neotype of †*Landanichthys lusitanicus*. †*Landanichthys* has been associated previously with the scombrid tribe Eocoelopomini based on: large fossae posterior to the frontals, which extend to the middle of the orbit; and thick, highly ornamented frontals (Monsch and Bannikov, 2012). As previously noted (Beckett and Friedman, 2016; Chapter 2) the group Eocoelopomini needs taxonomic revision, and my discussion here is mindful of this

uncertainty. †*Landandicthys* clearly differs from the type species of †*Eocoelopoma*, †*Eocoelopoma colei* (NHMUK PV P623a), in the jaw shape and proportions. It also differs from the referred specimen of †*E. colei* NHMUK PV P1755 in the geometry of the postero-superior fossae (see Appendix B.2). I note that †*Eocoelopoma portentosum* (Monsch and Bannikov, 2012), from the Paleocene-Eocene boundary of Turkmenistan, shows some correspondences with †*Landanichthys* to the exclusion of †*E. colei* (see Supplementary Information), an association that merits further investigation in future work.

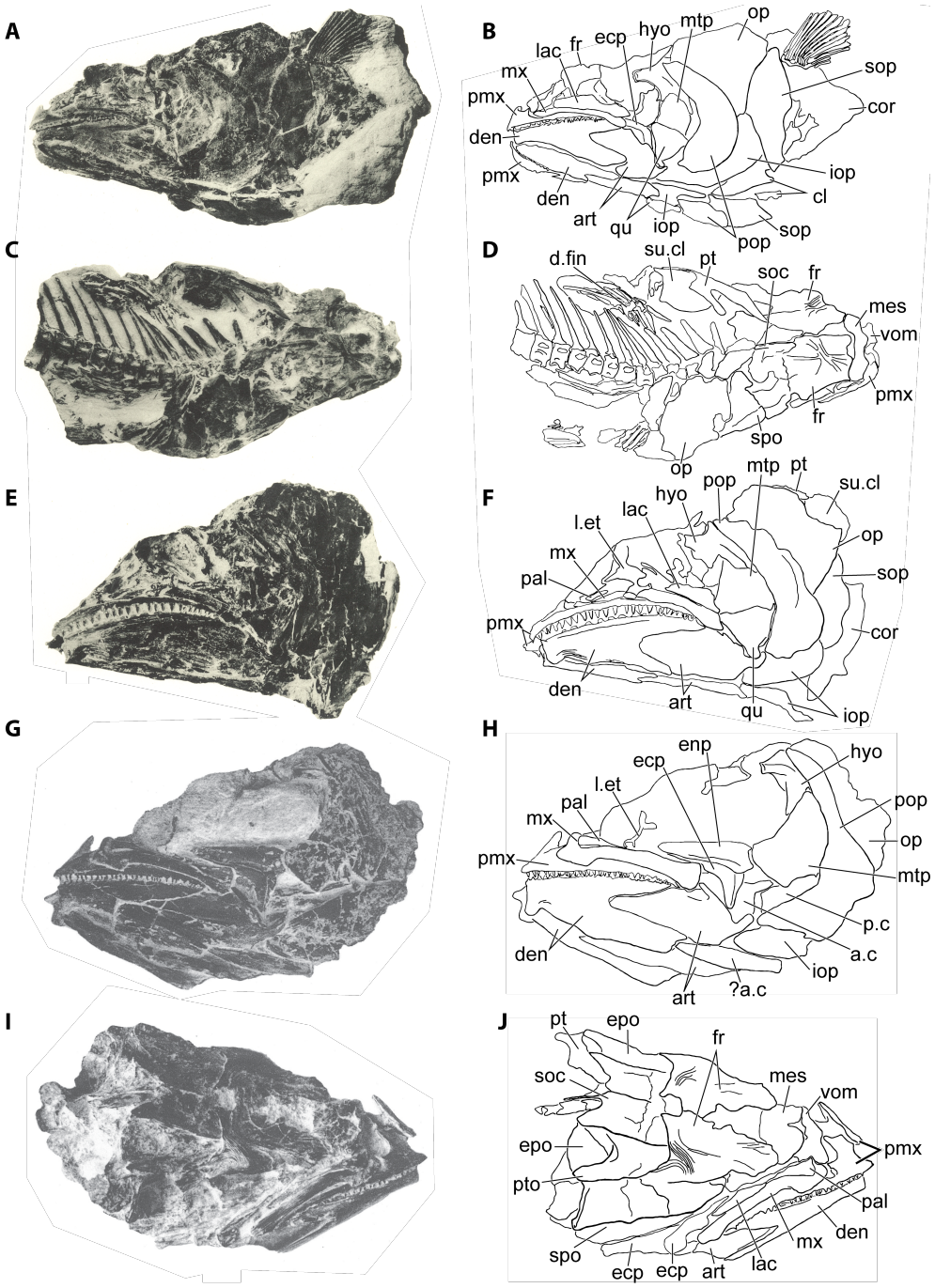


Figure 4.1: Missing specimens of †*Landanichthys*. Specimen RG 4.614 (holotype) photograph (A) and interpretive drawing (B) in left lateral view and photograph (C) and interpretive drawing (D) in right lateral view. Specimen RG 4.617 (E) photograph in left lateral view and (F) interpretive drawing in left lateral view. Specimen RG 5.695 photograph (G) and interpretive drawing (H) in left lateral view and photograph (I) and interpretive drawing (J) in right lateral view. Specimen photographs taken from Dartevelle and Casier (1959).

4.3.5 Description

The anatomical description is largely based on examination of RG 9.166 using μCT and fossil observation. Further information is drawn from published (Dartevelle and Casier, 1949, 1959), but lost, material where relevant.

Braincase: The braincase is well ossified, although in RG 9.166 the dorsal surface is highly fragmented and sutures between ossifications are not apparent. Sutures have previously been indicated in other specimens (Dartevelle and Casier, 1959). The supraoccipital is square in shape, bounded anteriorly by the frontal, and laterally by a pronounced epiotic ridge. Deep fossae sit either side of this ridge, posterior to the frontals. The pterotic fossa, broken at the external margin of RG 9.166 but visible in RG 4.614 (Fig. 4.1G&H), is present lateral to this ridge. By comparing to RG 5.695 and RG 4.614, the dermal ornament anterior to the supraoccipital region indicates the position of the frontals in RG 9.166, where only the left frontal is preserved. This ornament covers the frontals of RG 5.695, forming a swirl shape on the posterior part of the frontals, which is truncated sharply by a prominent perpendicular ridge. The mesethmoid is wide, with a scalloped anterior margin in dorsal view, and is overlain posteriorly by the frontal. The nasal, which is tube-shaped with a flattened posterior extension, flanks the mesethmoid laterally. The parasphenoid of RG 9.166 bears a dorsal interorbital ridge projecting some way between the orbits, and a ventral depression below the basioccipital. The parasphenoid widens posteriorly with a notched posterior margin marking the position of the dorsal aorta. Teeth are not present on the vomer, and no suture with the parasphenoid is apparent. The lateral ethmoid is tripartite, with two facets for articulation with apparatus of the upper jaw.

Infraorbital bones: A large expanded lacrimal is present on the right side of the specimen, overlapping the mid-point of the maxilla. It has a rolled and thickened dorsal margin and forms a broad plate which narrows anteriorly and posteriorly to form a broad plate.

Jaws: The premaxilla and maxilla are tightly bound and extend the full length of the lower jaw. The premaxilla has a poorly developed premaxillary process and bears a single row of 11 large conical posteriorly recurved teeth. These are mostly broken, and only the bases of an additional four are preserved. No supramaxilla is apparent. The lower jaw is upright and square in shape with a small ventral projection at the anterior tip with a ridged ornament (Fig 4.2E-F). The dentary bears a single row of 15 large, slightly compressed conical teeth plus an additional tooth base along its dorsal margin. The ventral arm of the dentary makes a "v"-shaped contact with the articular, with the latter forming the posterior head of the lower jaw. The articulation with the quadrate is missing and no retroarticular is preserved.

Suspensorium: A pronounced lateral head on the palatine articulates with the anterior head of the maxilla. A row of small pointed teeth is borne on the palatine, which articulates posteriorly with a long splint-like ectopterygoid. The posterior margin of the ectopterygoid expands to form a triangular plate that underlaps the quadrate mesially. The fan-shaped quadrate has a notched dorsal margin that articulates with the ventral margin of the metapterygoid, and bears a well-developed condyle for articulation with the lower jaw. A rod like symplectic is preserved but cannot be separated from the mesial surface of the quadrate (RG 9.166). Two facets for articulation with the neurocranium are borne on the hyomandibular head, which expands into a plate-like structure anteroventrally (RG

5.695, RG 4.617).

Hyoid and Gill Arches: The hyoid and branchial arches are partially articulated in RG 9.166. A triangular posterior ceratohyal sutures tightly to the approximately square anterior ceratohyal which bears a ceratohyal window. An anterior projection of the anterior ceratohyal articulates with a posterior extension of the ventral hypohyal. A small oval dorsal hypohyal is preserved dorsal to the ventral hypohyal. Numerous bones of the gill skeleton are preserved, but the specific arch to which individual bones belong is not always clear. A short hypobranchial 1 articulates via a pronounced head with the base of the small basibranchial 1. Ceratobranchials are elongate, straight and robust, with 5 clearly preserved and additional fragments also present. The dorsal gill skeleton preserves epibranchials 3 and 4 and pharyngobranchial 3. Epibranchials 3 and 4 are plate like with expanded medial arms while pharyngobranchial 3 is elongate with a broad midline expansion.

Opercular Series: The preoperculum is an expanded crescent shape, widest at the curve of the bone. The broad, flat opercular bone is a blunted triangle shape, widest dorsally, articulating posteroventrally with the elongate suboperculm (RG 4.614). The interoperculum contacts the ventral tip of the operculum and the dorsal margin of the suboperculum (RG 4.614).

Post-cranial anatomy: Some postcranial anatomy is visible in RG 4.614, including the pectoral fin girdle, elements of the dorsal fin, and anterior vertebral column. The posttemporal is forked, the longer arm articulating with the dorsal surface of the braincase (Fig. 4.1A). Posteriorly the posttemporal articulates with the dorsolateral surface of the oval, plate-like supracleithrum (Fig. 4.1A). The

triangular coracoid has a notch on the anterodorsal surface which may be preservational (Fig. 4.1A-B). At least 15 pectoral fin rays are present. The cleithrum is preserved beneath the coracoid, extending anteriorly in an elongate spur, with a pronounced notch on its ventral margin. Elements of the anterior portion of the laterally compressed dorsal fin are preserved, but specific neural insertion points are difficult to identify. No supraneurals (predorsal bones) appear to be preserved.

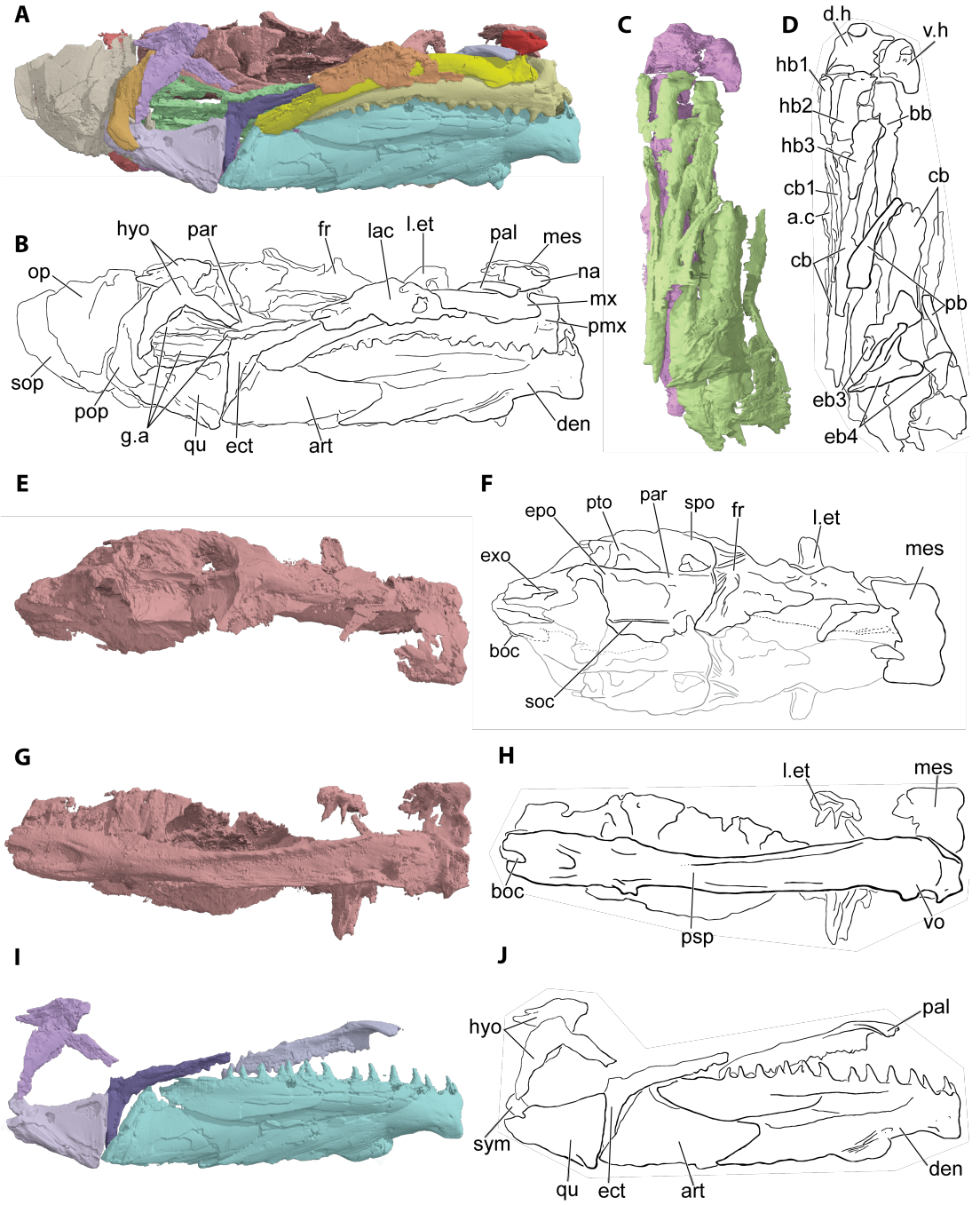


Figure 4.2: Renderings (A, C, E, G, I) and drawings (B, D, F, H, J) of †*L. lusitanicus* RG 9.166, in right lateral view (A-B). Gill skeleton and hyoid arch in dorsal view (C-D). Braincase in dorsal view; grey lines indicate mirrored and inferred areas of the braincase, dotted lines indicate bones visible that are not on the dorsal surface of the specimen (E-F). Braincase in ventral view (G-H). Suspensorium and lower jaw in right lateral view (I-J). See List of Abbreviations.

4.4 Phylogenetic results

†*Landanichthys* is recovered in a polytomy with Scomberomorini, Sardini and Thunnini (and the two other fossil taxa †*Eocoelopoma curvatum*and †*Eocoelopoma portentosum*) in both parsimony strict consensus and Bayesian 50% majority-rule analyses. Much of the uncertainty in these trees concerns the relationships of extant taxa, particularly within the Scombrini and the Thunnini (see Appendix B.7, Fig. B.14). Individual parsimony trees place †*Landanichthys* as the sister taxon of †*Eocoelopoma portentosum*, together the sister group to *Allothunnus*. †*Eocoelopoma curvatum*is recovered as a deeply diverging member of the Scomberomorini.

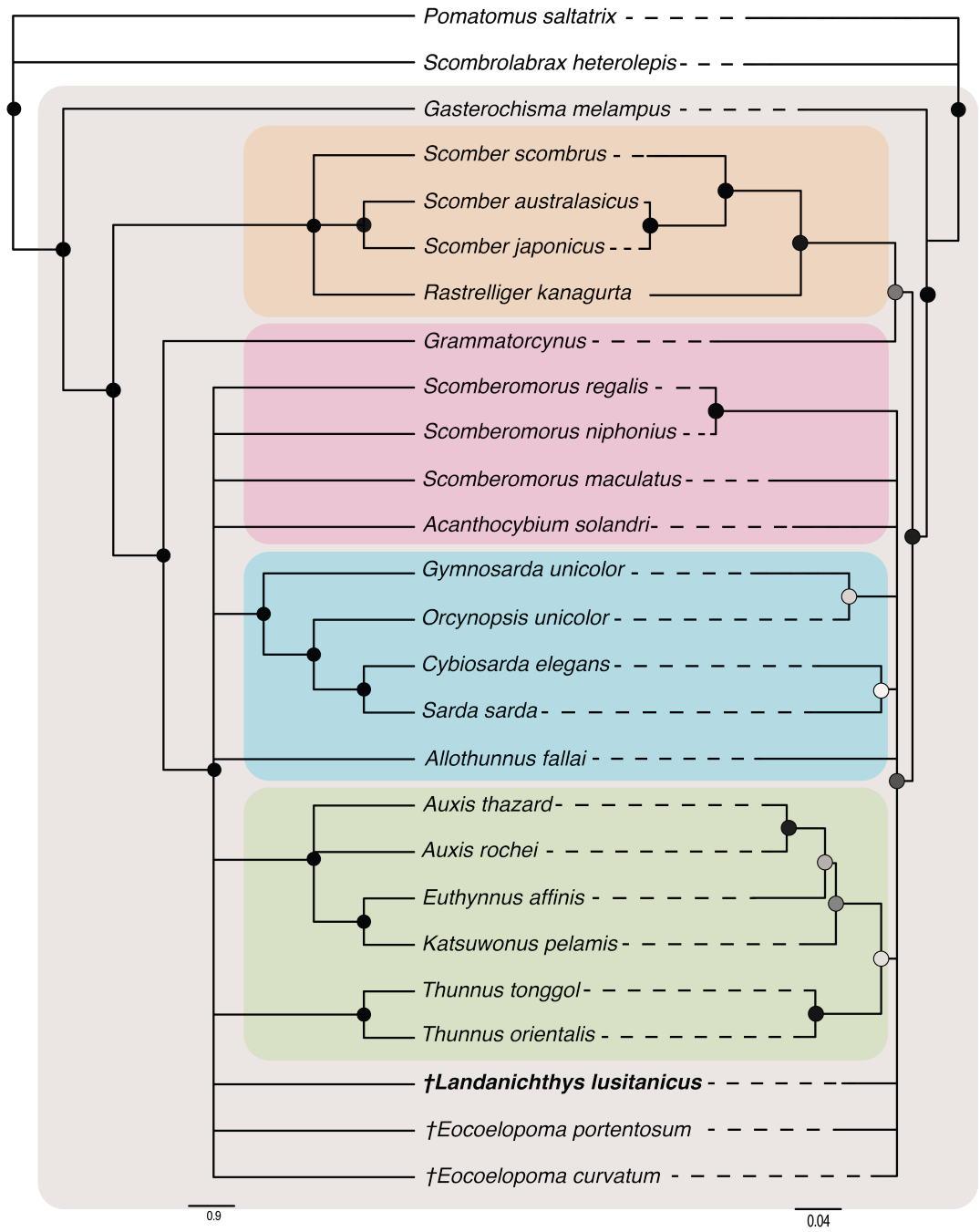


Figure 4.3: Phylogenetic placement of †*L. lusitanicus* RG 9.166; left, parsimony strict consensus and right, Bayesian 50% majority rule consensus tree for combined analysis. Circles at nodes indicate posterior probabilities above 50%.

4.5 Discussion

4.5.1 Morphological framework for Scombridae

†*Landanichthys* has important implications for the tempo and timing of the pelagiarian, and by extension percomorph, radiation. It is unique in its place as a fossil member of a crown percomorph family (Dartevelle and Casier, 1949, 1959; Bannikov, 1981). No other specimens from the early Paleocene are known that can be assigned to crown families within percomorphs, although one, †*Mene purdyi* can be assigned to the stem of the monotypic menids (Friedman and Johnson, 2005) and two can be assigned to the stem of extant percomorph families: †*Eekaulostomus cuevasae*, a syngnathiform (Cantalice and Alvarado-Ortega, 2016) and †*Palaeoserranus*, tentatively interpreted as belonging to the family Serranidae (Alaniz-Galvan, 2011; Alaniz-Galvan and Alvarado-Ortega, 2011; Alvarado-Ortega et al., 2015; Cantalice et al., 2018).

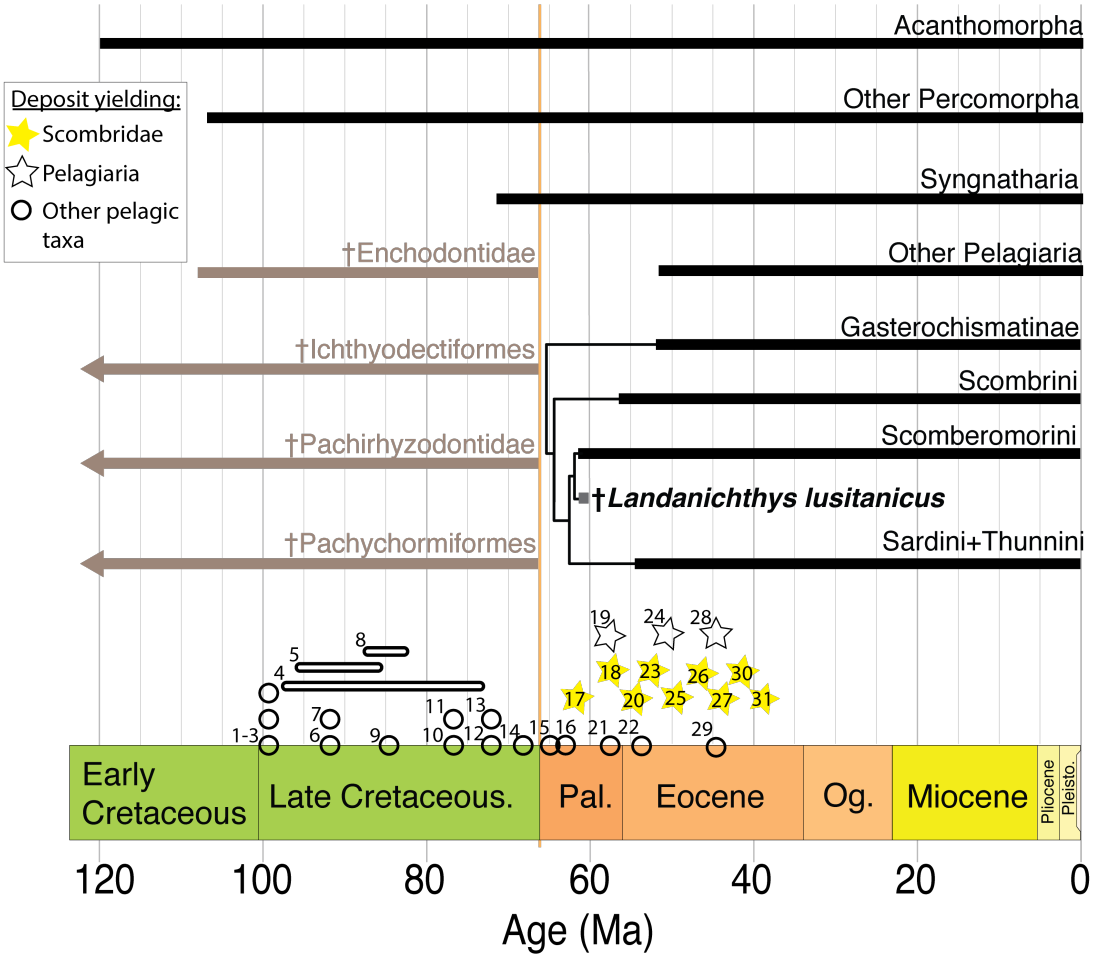
In creating a new morphological framework for Scombridae I confirm a sombrid identify for †*Landanichthys*, most likely affiliated with the Sardini (see Fig. 4.3 and additional figures in Appendix B.7). This is in keeping with previous verbal hypotheses that have suggested a nested placement within Scombrinae (Dartevelle and Casier, 1949, 1959; Bannikov, 1981). Historically the characters supporting Scombridae are: expanded infraorbital bones (Collette et al. 1984 [9]), inner row of premaxillary teeth absent (Collette et al., 1984; Johnson, 1986), and pair of epurals (Collette et al., 1984; Johnson, 1986). The first two of these are readily identifiable in †*Landanichthys*. Placement of †*Landanichthys* as a member of Scombrinae (i.e. scombrids to the exclusion of Gasterochisma) is also supported by the presence

of teeth on the palatine (Fig. 4.2) and the absence of supraneurals (Figure 1). The characters supporting Scomberomorini, Thunnini and Sardini (see Appendix B.8) cannot be assessed in †*Landanichthys*; but the group including *Allothunnus*, †*Eocoelopoma portentosum*and †*L. lusitanicus*is supported a reversal, the absence of teeth on the vomer (ch. 33 [0]). †*Eocoelopoma curvatum*acts as a wildcard taxon.

4.5.2 Fossil evidence for rapid diversification in Pelagiaria

The recognition of †*Landanichthys* as a crown scombrid indicates that the major morphological features associated with this radiation were assembled by the end of the Selandian (early Paleocene). Indeed, a mere 8 million years later, the London Clay Formation bears a diverse scombrid fauna containing members of all modern tribes (Monsch, 2005; Friedman et al., 2016). With modern body plans established so early in the group's history there is much truth to Patterson (1993; p.53) off-the-cuff statement that subsequent percomorph evolution is "mere tinkering". The presence of a definitive crown scombrid in the middle Paleocene suggests two possible explanations: morphological diversity in Scombridae was acquired very rapidly at the beginning of the Paleocene; or the origins of scombrids lie prior to the K-Pg boundary, with critical fossil evidence missing or unrecognised. The total absence of scombrids in the Cretaceous record, despite an abundance of pelagic predatory teleosts including aulopiforms, ichthyodectiforms and pachyrhizodontids (Shimada, 2015) and pachychormiforms (Friedman, 2010), see Figure 4.4, suggests that the former hypothesis is likely to be more accurate.

Rapid divergences between scombrids and other families within Pelagiaria have



been indentified as part of large-scale molecular studies of the group (Miya et al., 2013). These have estimated the origin of scombrids to be shortly before (Santini, 2013) or after (Alfaro et al., 2018) the K-Pg boundary, although some studies have recovered ages as young as the Oligocene-Miocene boundary (Near et al., 2013; Betancur-R et al., 2013, 2017) in direct opposition to clear fossil evidence. Explosive diversification following the K-Pg has also been suggested in other fishes (Betancur-R et al., 2013, 2017; Near et al., 2013; Harrington et al., 2016; Alfaro

Figure 4.4: Previous page. Localities indicated with [P] and [S] have pelagiarians and scombrids present respectively, where no superscript is given, neither are found. **Cretaceous localities**: 1-3. Hakel, Hadjula and Namoura, Lebanon (Cenomanian (Forey et al., 2003)); 4. English Chalk Group, UK (Cenomanian – middle Maastrichtian (Friedman et al., 2015)); 5. Komen, Slovenia (Cenomanian-Santonian (Palci et al., 2008)); 6. Goulmima, Morocco (Turonian (Cavin, 1999)); 7. Teplice Formation, Czech Republic (Turonian (Ekrt et al., 2008)); 8. Smoky Hill Chalk, USA (latest Conacian–earliest Campanian (Shimada and Fielitz, 2006)); 9. Sahel Alma, Lebanon (Santonian (Forey et al., 2003)); 10. Ripley Formation, US (Campanian (Schein and Lewis, 2007)); 11. Westphalia, Germany (Campanian (Dietze, 2009)); 12. Nard, Italy (Campanian – Maastrichtian boundary (Friedman, 2009; Friedman et al., 2016)); 13. Trebiciano, Italy (Campanian-Maastrichtian (Carnevale and Collette, 2014)); 14. Ciply – Malogne Phosphatic Chalk Formation, Belgium and Maastricht Formation of the Netherlands (Maastrichtian (Friedman, 2012). **Paleogene Localities**: 15. Limhman Quarry, Sweeden (Danian (Adolfssen et al., 2017)); 16. Chiapas, Mexico (Danian (Cantalice and Alvarado-Ortega, 2016, 2017; Cantalice et al., 2018)); 17. Landana Formation, Angola[P,S] (Danian/Selandian (Solé et al., 2018)); 18. Danata Formation, Turkmenistan[P,S] (Paleocene – Eocene (Bannikov, 1996)); 19. Marh Formation, Khuiala Formation, Rajasthan[P] (Paleocene-lower Eocene (Sahni and Choudhary, 1972; Kumar et al., 2005, 2007)); 20. Fur Formation (Mo Clay)[P,S] and 21. Stolle Klint Clay, Denmark (earliest Ypresian (Bonde et al., 2008)); 22. Flanders Clay, Belgium (Ypresian (Casier, 1946)); 23. London Clay[P,S] (Ypresian (Friedman et al., 2015)); 24. Monte Solane, Italy[P] (Ypresian (Monsch and Bannikov, 2012)); 25. Monte Postale and Pesciara, Bolca[P,S] (Ypresian (Friedman and Carnevale, 2018)); 26. Habib Rahi Formation, uncatalogued specimens at UMMP, Pakistan[P,S] (Lutetian (Friedman pers comms)); 27. Lilleblt Clay, Denmark[P,S] (Lutetian (Bonde et al., 2008)); 28. Dabakhana Svita, Georgia[P] (Lutetian (Monsch and Bannikov, 2012)); 29. Lede and Wemmel sands (Lutetian), Belgium (Taverne and Nolf, 2010); 30. Ilam, Iran[P,S] (Mid-Late Eocene (Afsari et al., 2014)); 31. Kuma, North Caucasus[P,S] (Bartonian (Monsch and Bannikov, 2012)).

et al., 2018), birds (Ksepka et al., 2017; Prum et al., 2015), and mammals (Simpson, 1937; Alroy, 1999; Wilson, 2014). Well-established Mesozoic pelagic predatory teleosts including alepisauroids, ichthyodectiforms and pachyrhizodontids and pachychormiforms disappear at the K-Pg boundary (Friedman, 2010; Friedman et al., 2013a; Friedman and Sallan, 2012), with pelagic predatory percomorphs diversifying to fill these gaps. This pattern is not mirrored to the same extent in non-predatory taxa; Aulopiformes, for example, survive the K-Pg extinction,

but their pelagic predatory component, †Enchodontidae is seemingly replaced by Scombridae and other percomorph lineages. Indeed, †*Landanichthys* is the first of these pelagic predatory taxa to appear in the record, with other groups not appearing until the Paleocene-Eocene boundary.

Irrespective of the age of origination of scombrids, prior to or after the K-Pg, the alignment of †*Landanichthys* with Scombridae supports the hypothesis that fast morphological diversification is likely to have occurred within the families of Pelagiaria.

4.6 Conclusion

Reassessment of the fossil †*Landanichthys* confirms its placement as the oldest fossil scombrid. Furthermore, its likely alignment with the Sardini makes it unique in being assigned beyond the family level among fossil percomorphs. Fitting into the fossil 'gap' of the early Paleocene, †*Landanichthys* suggests crown scombrids established their morphological bodyplan within 5-10 million years of the K-Pg boundary, supporting the suggestion of a rapid radiation in Pelagiaria and adding to our understanding of the tempo of the percomorph radiation.

4.7 Acknowledgements

I thank Farah Ahmed, Amin Garbout, Rebecca Summerfield, Dan Sykes, Emma Bernard, James MacLaine and Oliver Crimmen for access to the collections and assistance with scanning at the Natural History Museum, London. For access to specimens we also thank Doug Nelson at the University of Michigan Museum of

Zoology, Caleb McMahan at the Field Museum of Natural History and Christine Thacker, Rick Feeney and Javier Gago at the Los Angeles County Museum of Natural History. This study includes data produced in the CTEES facility at University of Michigan, supported by the Department of Earth & Environmental Sciences and College of Literature, Science, and the Arts.

Chapter 5

Patterns of phenotypic evolution in Pelagiaria

Abstract

Adaptive radiation, the rapid diversification of species into new niches using key innovations, is a widely used term in biological literature. However, our understanding of the morphological patterns of evolution that produce an 'adaptive radiation' is relatively limited, especially when comparing radiations typically studied in the biological literature to those typically studied in the paleontological literature. Comparative methods in evolutionary biology provide an opportunity to investigate these patterns where phylogenetic and morphological datasets exist. Here I use micro-computed tomography to assemble a three-dimensional cranial dataset of extant and extinct Pelagiaria, a group of open-ocean fishes thought to have undergone an ancient adaptive radiation in the early Cenozoic. 68 pelagiarian fishes are represented, sampling 53 of 73 extant genera and approximately one third of all species. 4 fossil taxa are added to create a second, combined (fossil

and extant taxa), dataset. I use a time-calibrated molecular tree inferred from ultra-conserved elements and their flanking regions as a backbone for the analysis. I apply disparity through time and model-fitting approaches to investigate the evolutionary patterns in the group, specifically whether they are consistent with those associated with adaptive radiation. Disparity through time analyses reveal a deviation from a null model of Brownian motion evolution (MDI values < 0). Rank envelope DTT analysis indicates a pattern of deviations from a BM model of evolution early in the history of the clade, around 50 Ma. I also applied a model-fitting approach to assess support for Brownian motion, Early Burst or a new SHIFT model, where the mode of evolution shifts from Brownian motion to an Ornstein-Uhlenbeck process. The latter model best fits the data, with the age at which this shift occurs inferred as mid-Ypresian ($\sim$51Ma) in both analyses. The addition of fossil taxa to the analysis does not significantly alter the results. Pelagiaria appear to show a change in evolutionary mode consistent with some models of adaptive radiation, but differences to the observed patterns in mammals make it unclear whether the evolutionary dynamics of postulated adaptive radiations are the same. Phenotypes in Pelagiaria appear to have diversified rapidly in the aftermath of the Cretaceous-Paleogene boundary before becoming phenotypically constrained as ecological niches become filled in the early Eocene, adding quantitative support to previous hypotheses of adaptive radiation in the group.

5.1 Introduction

First proposed by Osborn in a series of papers at the turn of the 20th century (Osborn, 1893, 1899, 1902), 'adaptive radiation' has become a central concept

in evolutionary biology. Osborn (1902) rooted this idea in the proliferation and differentiation of mammals after the end-Cretaceous extinction, describing "two great periods of placental radiation" (Osborn, 1893) with "focal types, or most primitive forms" (Osborn, 1899) giving rise to the origins of diversity in radiations. In aiming to synthesise palaeontology and biology, Simpson (1944) expanded on Osborn's concept of adaptive radiation, providing early explanatory models of evolutionary processes. Simpson later defined his concept of adaptive radiation as the "more or less simultaneous divergences of numerous lines from more or less the same ancestral adaptive type" (Simpson, 1953). This pattern of widespread and apparently rapid origination of multiple disparate lineages appears many times in the fossil record (Schluter, 2000; Erwin, 2001; Glor, 2010), often associated with the time period immediately following a mass extinction event (Erwin, 2015; Hull, 2015).

Despite an overwhelming emphasis of foundational studies on ancient divergences in the fossil record, most contemporary studies of adaptive radiations overwhelmingly consider geologically ephemeral and spatially constrained examples associated with heterogeneous and isolated environments. Classic examples of adaptive radiations studied in the recent literature include *Geospiza* finches (Grant and Grant, 2008), *Anolis* lizards (Losos and Ricklefs, 2009; Losos, 2011), Hawaiian honeycreepers (Sibley and Ahlquist, 1982), Silverswords (Baldwin and Sanderson, 1998) and cichlids (Seehausen, 2006). All of these radiations occur on geographically isolated islands or, in the case of cichlids, in equally isolated East African rift lakes. These modern examples have virtually no fossil records making them very difficult to study over geological timescales, in contrast to the classical idea of adaptive radiation envisaged by Osborn and Simpson. Additionally, while there

is no doubt that there is a diversity of species associated with each of these modern radiations, their morphologies are relatively limited when compared to the huge morphological disparity associated with the mammal radiation (Nowak and Walker, 1999), even accounting for the problem of comparing across timescales in these groups.

The development of a battery of comparative tools over the past decade has resulted in a revolution in macroevolutionary studies, permitting more direct interrogation of questions relating to the rate and mode of evolution (Felsenstein, 1985; McShea, 1994; Pagel, 1998, 1999; Harmon et al., 2003, 2010; Hunt and Rabosky, 2014; Harmon, 2018). These are key fixtures in the concept of adaptive radiation and even gave Simpson's 1944 book its name – but contemporary methods were not capable of assessing them. With phylogenetic trees, coupled with trait data in the form of either molecular or morphological data, we can now investigate these evolutionary patterns for both extant and extinct taxa (Felsenstein, 1985; Pagel, 1998; Harmon, 2018).

Early models of evolution in the phylogenetic setting focus on a Brownian motion model of evolution (Felsenstein, 1985): this describes a random walk model, where trait values change randomly through time according to some variance (rate) parameter σ^2. The theory of adaptive radiation however, predicts an early phase of evolution marked by a period of high morphological and ecological divergence between lineages (Harmon et al., 2003; Simões et al., 2016) followed by a period of stasis, with ecomorphological differences between clades persisting (Foote, 1997; Jackson and Cheetham, 1999; Schluter, 2000; Hansen and Houle, 2004; Estes and Arnold, 2007). Broadly speaking, with respect to recent literature on models of adaptive radiation, this pattern has come to be interpreted as changing rates of

evolution (e.g. Harmon et al., 2010). The most commonly used class of models to explain adaptive radiation are those of Pagel's δ (Pagel, 1998), ACDC (accelerating and decelerating rates; Blomberg et al., 2003), and the "Early Burst" model (Harmon et al., 2010), all of which modify the branch lengths of a tree to create variable rates, concentrating evolutionary change towards the root (or indeed the tips) of a tree. The most common of this suite of models now discussed in the literature is the "Early Burst" model which concentrates rates at the root of the tree, with the rate of evolution decaying exponentially through time.

However as the title of Simpson's (1944) *"Tempo and mode in Evolution"* suggests, evolutionary patterns arise from the interplay between these two factors, rate and mode. Although Simpson's 1944 model is largely visual (Figure 5.1), he describes an early "explosive" phase of evolution with "great variation [in phenotype] and many intermediate types" followed by a period of "normal" evolution with "reduced variation [in phenotype] and no intermediate types". This model suggests a change in the mode of evolution at some point in time, but not necessarily the rate. A model of evolution commonly used to implement constraint, or optima, is the Ornstein-Uhlenbeck (OU) model of evolution, where traits evolve through time with a constant rate and a constraint parameter, which always draws evolution back to an optimum value. Where this constraint parameter is 0 the model is that of Brownian motion. OU models can be implemented either as single peak models, with a single optimum value, or as multi-peak models, where the optima more directly compare to phenotypic peaks. These peaks or constraints "may result from intrinsic factors (the genetic covariation patterns) or extrinsic factors (the array of selective pressures impinging on diverse members of a clade)" (Derrickson and Ricklefs, 1988). Despite the root of adaptive radiation in both

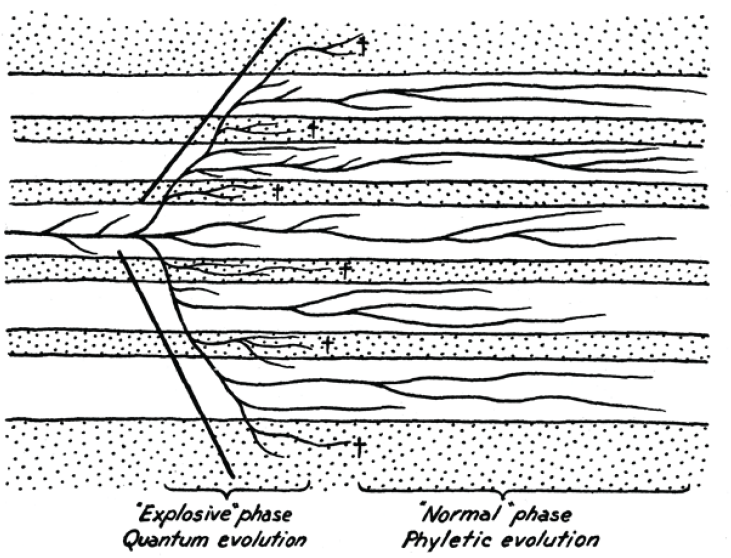


Figure 5.1: Figure 35 from Simpson's 1944 paper where he outlines a model that today might be called a model of adaptive radiation. In this model, Simpson describes a change in rate over time, but also indicates the role that adaptive zones may play in evolution. This figure appears to indicate an early phase of diffusive evolution is followed by a period of constraint within adaptive zones.

rate and mode, few studies investigate both rate and mode of evolution (but see Slater, 2013). Additionally, despite their impact on resolving patterns of radiation among taxa (Slater et al., 2012) few studies include fossil taxa.

Recent molecular studies of fish evolution have highlighted patterns suggested to indicate potential radiations (Harrington et al., 2016; Alfaro et al., 2018). Acanthomorph, and within them percomorph, fishes show a pattern of rapid radiation close to and after the K-Pg boundary (Friedman, 2009, 2010; Miya et al., 2013). Analagous to stem and crown eutherians, acanthomorphs and percomorphs are moderately diverse up until the end of the Cretaceous, where there is rapid appearance of new families and phenotypes among percomorph clades, including

the Pelagiaria, Eupercaria, Ovalentaria and Carangaria (Miya et al., 2013; Harrington et al., 2016; Alfaro et al., 2018). Pelagiaria are a group of anatomically disparate yet closely related percomorph taxa, united by a pelagic ecology (Miya et al., 2013). Emerging in the fossil record in the Paleocene, a literal reading of the record indicates that by the Paleocene-Eocene boundary, a diversity of recognisably modern phenotypes has been established (Miya et al., 2013), suggesting a relative stasis in phenotype in each family after this period. Molecular studies investigating the relationships and divergence times of Pelagiaria, informed by the fossil record, suggest very short internodes on the order of 1-2 Ma early in the history of the group, indicating a pattern of possible adaptive radiation (Miya et al., 2013). Additionally, many predatory pelagic fishes, including those within Pelagiaria (e.g. tunas), seem to fulfil the ecological and functional roles occupied by predatory pelagic fishes that became extinct by the end of the Cretaceous (e.g. alepisauroids, pachichormiforms) (Friedman, 2009, 2010), clearing the way for possible 'adaptive radiation'-like dynamics in the early Paleocene: indicative of an ecological release model of adaptive radiation. In contrast to 'model' examples, this ecological opportunity is being provided by the clearance of niches resulting from a mass extinction event, rather than colonisation of geographically isolated areas (Stroud and Losos, 2016).

Pelagiaria provide an excellent study system on which to test models of adaptive radiation. They have a well-established molecular framework (Near et al., 2012; Miya et al., 2013; Betancur-R et al., 2013, 2017; Alfaro et al., 2018; Friedman et al., Submitted), a good fossil record particularly for the Scombridae and Trichiuroidea (Miya et al., 2013), and are phenotypically diverse but contain a tractable number of species (around 236 species, compared to 5000 mammal

species and 17,000 percomorph). Here I investigate evolutionary patterns of phenotypical diversification in both extinct and extant Pelagiaria using a combination of three-dimensional landmark, molecular and morphological data. The aim of this study is to establish: (1) whether patterns of phenotypic evolution deviate from a global Brownian Motion (BM) model and if so when; (2) if deviation from a BM model is observed, what model best describes the patterns of phenotypic evolution in the group, specifically testing the most commonly considered model of adaptive radiation, the Early Burst model (Slater et al., 2010; Harmon et al., 2010) against a Simpsonian model of evolution (Simpson, 1944) here called the SHIFT model; (3) the implications of such a deviation on phenotypic diversification within the group.

5.2 Material and Methods

5.2.1 Institutional Abbreviations

BMNH, Life Sciences collections, Natural History Museum, London, UK; FMNH, Division of Fishes, Field Museum, Chicago, USA; LACM, Natural History Museum of Los Angeles County, Los Angeles, USA; NHMUK, Earth Sciences collections, Natural History Museum, London, UK; UMMZ, Division of Fishes, University of Michigan Museum of Zoology, Ann Arbor, USA.

5.2.2 Landmark dataset assembly

We assembled a landmark dataset of skull shape, an anatomical structure linked to ecology and post-cranial body shape, using micro-computed tomography (μCT)

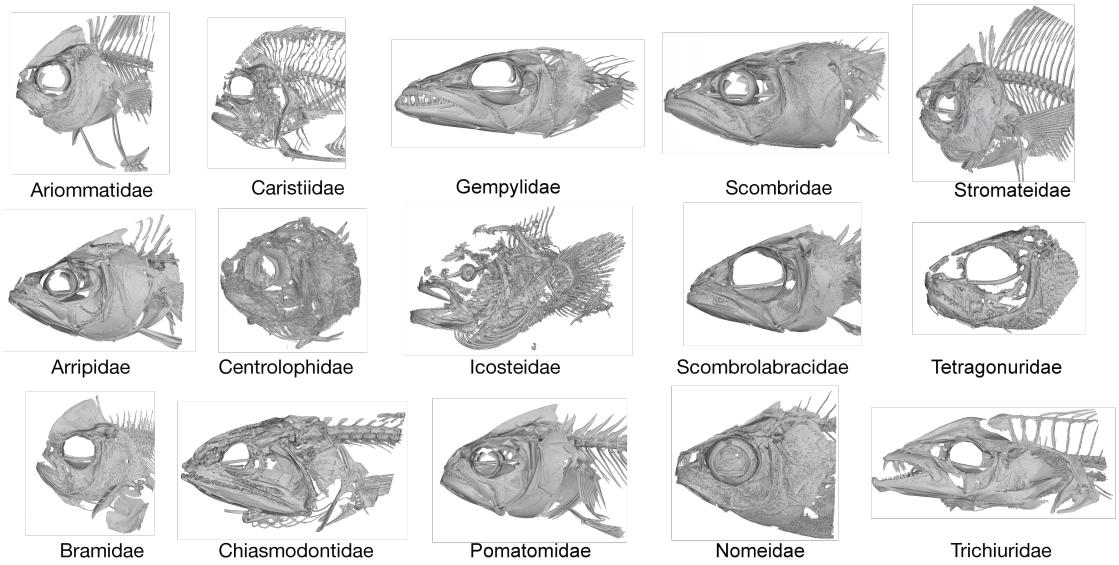


Figure 5.2: Representative skulls for 15 families of Pelagiaria. Amarsipidae, a monospecific family, is not represented.

scanning.

The combined dataset consists of 68 extant and 4 fossil specimens, representing 53/74 extant genera and one third of extant species. Extant specimens were investigated from museum wet collections in the UK and US. Fossil specimens and Recent BMNH specimens were scanned using the Metris X-Tek HMX ST μCT scanner in the Imaging and Analysis Centre of the Natural History Museum, London. FMNH, LACM and UMMZ specimens were scanned using the Metris X-Tek XT H 225ST μCT scanner at the CTEES facility in the Department of Earth and Environmental Sciences, University of Michigan. Scan settings are provided in Appendix C. Specimens used in the course of the study are listed below.

Specimens Examined

Arriommatidae *Ariomma bondi* UMMZ 228950; *Ariomma indica* UMMZ 219645; *Ariomma melanum* MCZ 168623_6.

Arripidae *Arripis trutta* UMMZ 209265.

Bramidae *Brama dussumieri* UMMZ 234770; *Brama japonica* UMMZ 191017; *Eumegistus illustris* LACM 38573; *Pterycombus brama* BMNH 1979.3.21.393; *Taractes asper* BMNH 1953.10.28.2; *Taractes rubescens* MCZ 148060_5; *Taractichthys steindachneri* FMNH 63863.

Caristiidae *Caristius macropus* FMNH 76316; *Chiasmodon niger* UMMZ 228958.

Centrolophidae *Hyperoglyphe japonica* UMMZ 233106; *Psenopsis anomala* UMMZ 182977; *Schedophilus medusophagus* BMNH 1972.2.22.101.

Chiasmodontidae *Dysalotus oligoscolus* BMNH 2002.3.2.86; *Kali macrodon* BMNH 1996.2.14.15; *Kali normani* FMNH 88149; *Pseudoscopelus altipinnis* BMNH 2004.8.17.10; *Pseudoscopelus astronesthidens* MCZ 161417; *Pseudoscopelus pierbartus* MCZ 164590; *Pseudoscopelus scutatus* FMNH 99160.

Icosteidae *Icosteus aenigmaticus* UMMZ 1900048.

Nomeidae *Cubiceps baxteri* BMNH 1997.9.17.27; *Cubiceps whiteleggi squamiceps* BMNH 1986.10.6.37-40; *Psenes arafurensis* BMNH 1997.9.17.10; *Psenes cyanophrys* UMMZ 86219.

Scombridae *Acanthocybium solandri* FMNH 44400; *Auxis rochei* UMMZ 250172; *Auxis thazard* UMMZ 238740; †*Bramoides brieni* NHMUK PV P 47851, cranium from the Eocene (Ypresian, 52-49 Ma) London Clay Formation, UK; *Euthynnus affinis* UMMZ222134; †*Eocoelopoma curvatum* NHMUK PV OR 44877a, historically prepared cranium from the Eocene (Ypresian, 52-49 Ma)

London Clay Formation, UK; *Gasterochisma melampus* BMNH 1868.6.22.21; *Gymnosarda unicolor* FMNH 89962; *Katsuwonus pelamis* FMNH 41899; *Rastrelliger kanagurta* UMMZ 226911; *Sarda sarda* UMMZ 145849; *Scomber australiasicus* UMMZ250152; *Scomber japonicus* UMMZ 250083; *Scomber scombrus* UMMZ 214543; *Scomberomorus maculatus* UMMZ 199143; *Scomberomorus niphonius* UMMZ 167374; *Scomberomorus regalis* UMMZ 143137; *Thunnus orientalis* FMNH 58745; *Thunnus tonggol* UMMZ 225078; †*Wetherellus cristates* NHMUK OR PV 28498 historically prepared cranium from the Eocene (Ypresian, 52-49 Ma) London Clay Formation, UK.

Scombrolabracidae *Scombrolabrax heterolepis* FMNH 65350.

Stromateoidae *Pampus argenteus* UMMZ 335567; *Peprilus alepidotus* UMMZ 199053; *Peprilus burti* UMMZ 249257; *Peprilus tricanthus* UMMZ 244723.

Tetragonuridae *Tetragonurus atlanticus* FMNH 88285.

Trichiuroidea *Aphanopus carbo* BMNH 2006.6.27.1; *Benthodesmus simonyi* BMNH 1972.1.10.64; *Benthodesmus taenius* FMNH 88043; *Diplospinus multistriatus* LACM 45473; *Gempylus serpens* FMNH 71423; *Lepidocybium flavobrunneum* LACM 36320-1; *Lepidopus altifrons* FMNH 64102; *Lepidopus caudatus* BMNH 1928.6.27.22; *Lepturacanthus savala* UMMZ 219522; *Neoepinnula americana* FMNH 65717; *Nesiarchus nasutus* FMNH 71422; *Paradiplospinus antarcticus* LACM 10908_5; †*Progempylus edwardsii* PV OR 32388 historically prepared cranium from the Eocene (Ypresian, 52-49 Ma) London Clay Formation, UK (Friedman et al., 2016); *Paradiplospinus gracilis* BMNH 2009.5.18.143; *Promethichthys prometheus* UMMZ 250143; *Rexea prometheoides* FMNH 120779; *Ruvettus pretiosus* BMNH 1938.6.23; *Tentoriceps cristatus* BMNH 1987.1.23-28; *Thyrsitoides marleyi* BMNH 1986.9.8.147; *Trichiurus lepturus* UMMZ 219710.

Pomatomidae *Pomatomus saltatrix* UMMZ 111069.

5 additional fossil specimens (†*Duplexdens macropomus*, †*Tamesichthys decipiens*, †*Woodwardella patellifrons*, †*Micrornatus hopwoodi*, and an addition specimen assigned to †*Eocoelopoma curvatum*) were scanned, segmented and landmarked but are either poorly constrained phylogenetically or relatively incomplete and are therefore not included in the analysis (see Appendix D.2).

Computed tomography

Tomogram stacks were segmented using Mimics Innovation Suite Version 18.0-19.0 (http://biomedical.materialise.com/mimics) and Avizo v.8 (https://www.fei.com/software/amira-avizo/) to remove soft tissue features and any mineralised scales that obscure cranial structures. Three-dimensional point cloud meshes were exported as .ply files to Avizo v.8 for landmarking. Two dimensional images were obtained by exporting meshes as .ply files to Blender (blender.org).

Landmarking

All specimens were landmarked in Avizo v.8 using 66 left and right landmarks, and 7 midline landmarks (Figure 5.3, Appendix D). Landmarks were chosen to represent the pattern of skull variation across Pelagiaria indicating points of articulation and homology.

Landmark positions were imported into R (see code Appendix D) for post-processing. Left and right landmarks were mirrored and averaged using the package `StereoMorph` (Olsen and Westneat, 2015). The resulting matrix was then submitted to a Procrustes alignment and a PCA analysis using `Geomorph` (Adams

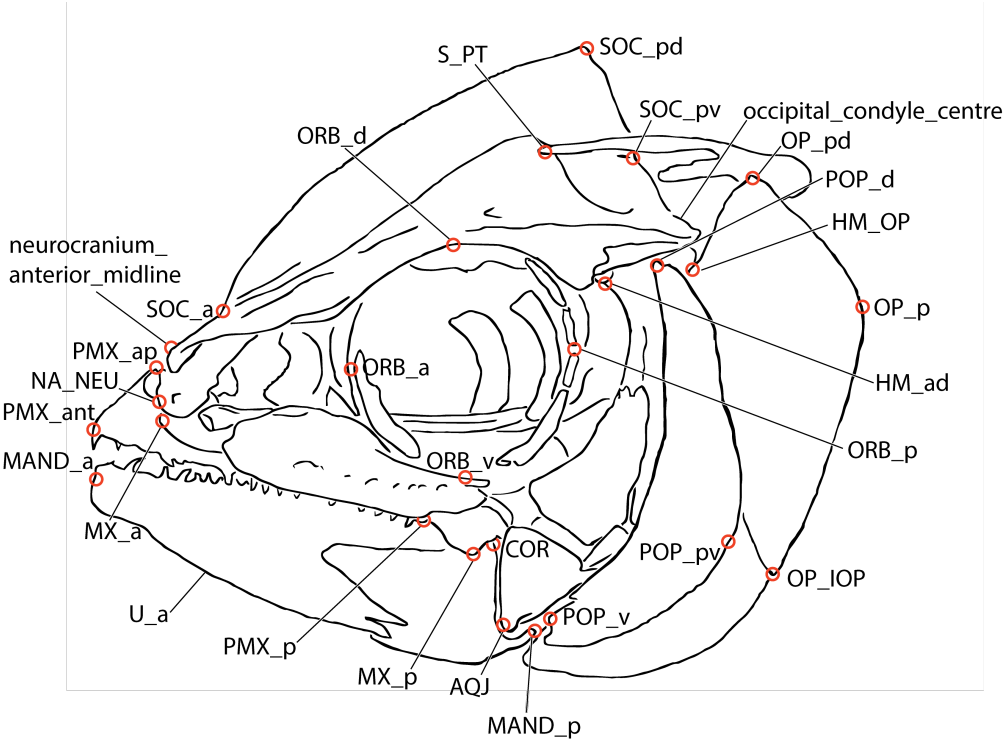


Figure 5.3: Landmark Scheme for evolutionary analyses, for descriptions of landmarks see Appendix D.

et al., 2018). The first 5 axes accounted for 95% of variation and all analyses were performed on PCs 1 to 5. Two datasets assembled: an extant only dataset comprising 68 taxa and a combined (extant + fossil) dataset comprising 72 taxa. A phylomorphospace of the first two axes is plotted using `Geomorph` (Adams et al., 2018) to visualise the main axes of variation (Figure 5.5).

5.2.3 Tree assembly

A time calibrated posterior distribution of trees is taken from Friedman et al. (Submitted) and comprises 94 pelagiarian taxa and 12 acanthomorph outgroup species. This tree has advantages over previously published mitogenomic trees

(Miya et al., 2013) in having multiple loci, and being internally calibrated. However to account for the sensitivity of inferences of phenotypic evolution to variations in topology and branch durations in comparative analyses, all analyses are carried out across the same sample of 100 trees, drawn from the posterior distribution from a topologically unconstrained BEAST divergence dating analysis Friedman et al. (Submitted). The BEAST analysis of Friedman et al. (Submitted) was performed as a relaxed molecular clock dating analysis, on 10 independent subsets of 25 randomly selected UCE loci, for 10 million generations, with 10 replicates. This sample of 100 trees is imported into R and tips with no associated landmark data available are pruned out of all trees using `drop.tip` in `ape` (Paradis et al., 2004). Confidence intervals were estimated empirically for calibrated nodes based on outgroups to Pelagiaria resulting in inclusive priors, in most cases the 95% confidence intervals permitted divergences in the Cretaceous.

For the combined analysis, four fossil taxa (Appendix D) were placed in each of the 100 trees using the maximum likelihood (ML) implementation of `locate.fossil` in `phytools` (Revell, 2012). The four fossil taxa are placed based on argumentation put forward by Monsch (2005), Monsch and Bannikov (2012) and personal observations (see Appendix D.3). `Locate.fossil` places fossils under a conservative Brownian model of evolution into a user specified tree using trait data, in this case landmark data. Additionally the placement can be further constrained by an age constraint (given as the age range of the fossil; taken from Friedman et al. 2016) and a phylogenetic constraint. Because the posterior distribution of trees have different ages and branch lengths, there are some instances where the age of the fossils (the age constraint) is older than the age of the branch on which they are to be placed (the phylogenetic constraint). In

situations such as these, the age constraint is relaxed to allow the fossil to be constrained phylogenetically and a notification message produced. In practice, for the fossils being placed in this analysis with a time constraints of 49-52 Ma, the constraint is relaxed to 47.5-53.5 Ma. `Locate.fossil` produces a ML placement for each fossil, independent of the others, in the form of a phylo object. Occasionally trees with an equal likelihood are found, and a single random tree is chosen. The function `bind_successive_trees` (see Appendix F) uses `bindPaleoTip` from `PaleoTree` (Bapst, 2012) to insert fossils based on their phylogenetic placement in the `locate.fossil` analysis. All code for placement of fossils is available in Appendix F.

5.2.4 Disparity through time analysis

Disparity through time analyses have emerged as a method for investigating changes in morphological diversity (disparity) across the timescale of a phylogenetic tree, particularly for investigating adaptive radiations (Harmon et al., 2003; Slater et al., 2010). I conducted a disparity through time (DTT) analysis (Harmon et al., 2003) to investigate the relative partitioning of disparity between versus to within subclades through the history of Pelagiaria, and whether the acquisition of this disparity varies from a Brownian motion model of evolution. In addition to the morphological and phylogenetic data included in a DTT analysis, the timeslicing approach allows the phylogeny to be investigated with a temporal element (Hunn and Upchurch, 2001; Turner, 2004). DTT calculates disparity for the entire clade, followed by each subclade (defined by a node) in the phylogeny. To do this, a timeslice is taken at each branching event (see Fig 5.4), with disparity for each

subclade calculated at this point. This subclade disparity is then given as a ratio relative to the disparity of the entire clade; the relative disparity. Relative disparity for each timeslice is calculated by taking the average of the relative disparity for all subclades for which an ancestral lineage is present in the timeslice. Disparity is

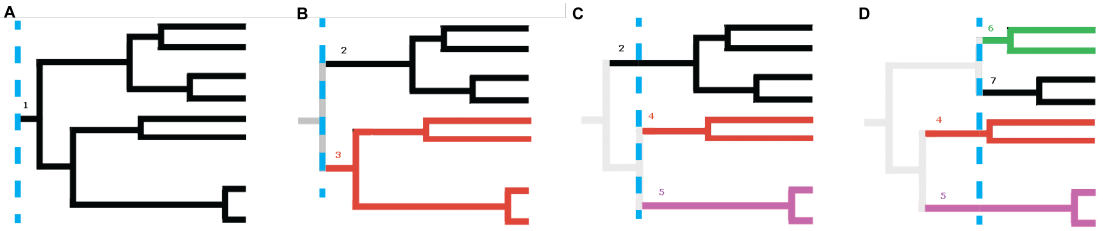


Figure 5.4: Modified figure S1 from Harmon et al. (2010). Dashed blue line indicates the timeslice for which disparity is calculated, colours indicate successively more nested subclades. Time A is calculating the disparity of the whole tree, at B, the relative disparity of two subclades (black and red) are calculated and the average taken. This process continues for each timeslice in the tree (C and D).

expected to vary between 1 at the point of origin, where all disparity is contained within a single clade, and 0 at the present, where each tip is in effect its own clade and therefore encompasses no disparity. A DTT analysis therefore provides an opportunity to examine whether disparity is partitioned largely between clades – as expected for the morphologically distinct groups predicted by an adaptive radiation – or largely within clades. Two DTT analyses were run, each with 2500 simulations. The first, using the extant only dataset, was processed through `dtt` in `GEIGER` (Harmon et al., 2008; Pennell et al., 2014), and the second, which used the combined dataset, through `fossilDTT` (Slater et al., 2010).

Each dataset was investigated via two different methods in order to investigate empirical deviations from the null model of Brownian motion. First, I applied a point envelope test, as in the standard implementation of DTT (Harmon et al., 2003), from which a morphological disparity index (MDI) is calculated. DTT is

applied to data simulated under Brownian motion to form a confidence envelope of null model simulations. From this the MDI is calculated as the sum of deviations of the empirical curve from the median of null model simulations. Values of MDI < 0 suggest that there is greater variation between the clades rather than within them. Greater variation between, rather than within, clades than expected under BM has been suggested to be consistent with adaptive radiation, particularly early in the history of a group (Harmon et al., 2003; Slater et al., 2010). Because of prior hypotheses of adaptive radiation in Pelagiaria (Miya et al., 2013; Friedman et al., Submitted) we specifically test for this scenario using a one-tailed test implemented in `GEIGER` to test for negative deviations in MDI. The results are reported as a distribution of p values. Second, I applied a one-tailed rank envelope test (Murrell, 2018), which ranks the empirical curve relative to each simulated curve, is implemented (code in Appendix F based on Friedman et al., Submitted). A rank envelope test assigns ranks to each Brownian motion simulated curve at each timepoint, and then ranks the empirical curve in the same framework to investigate a deviation from the null (Murrell, 2018). A rank envelope test allows isolation of the deviations to a specific interval in the timeseries, and if scaled relative to the age of the origin of the tree allows the deviations to be timescaled. The proportion of trees showing deviations from a null model of BM at specific time periods in the history of the clade are calculated by scaling the relative timescale against the root ages of the tree.

5.2.5 Model-fitting analyses

DTT analysis can suggest that there is a deviation in evolution from a Brownian motion process, but it cannot attribute this change to either the rate or the mode of evolution. Model-fitting is applied to both the extant and the combined datasets to test specific models of evolution. Three models, outlined below, were applied using the package `mvMORPH` in R (Clavel et al., 2015): (1) a Brownian motion model (BM) using `mvBM`; (2) an Early Burst model using `mvEB`; and (3) a SHIFT model using `mvSHIFT`.

1. BM is the most commonly used model in comparative phylogenetics (Felsenstein, 1985), and expresses evolution as an unconstrained stochastic process where each tip (taxon) is free to move through trait-space without constraint according to a rate parameter σ^2. The observable pattern is one of increasing dispersal away from a mean (ancestral state value μ or θ_0) through time. It is implemented here using the standard parameters in `mvBM`. These assume a single ancestral state and no selective regime, therefore fitting a model of Brownian motion across the whole tree to give a single rate matrix σ.

2. The "early burst" (EB) model, implemented by Harmon et al. (2010) allows decelerating rates through time, and is therefore a special implementation of the ACDC model of Blomberg et al. (2003), which allows for the acceleration or deceleration (ACDC) of rates of character evolution. Where the rate parameter in an EB model is constant it becomes a Brownian motion model. An interpretation of Simpson's (1944) model, the EB model predicts that as ecological niches open up and lineages diversify into them, morphological

evolution should be rapid. As taxa occupy this niche space, there is less ecological opportunity and the rate of morphological evolution slows (Foote, 1994; Schluter, 2000; Blomberg et al., 2003). In the EB model implemented here decelerating rates are modelled as an exponential decay process β with the standard bounds implemented: an upper bound of 0 and a lower bound of $\frac{\log(min.rate)}{T}$ where $min.rate$ is the minimum rate that can be assumed for the model on the tree and T is the depth of the tree.

3. A SHIFT model assumes a change in the mode of evolution at some period in the history of the group, much like the change suggested by Simpson (1944) from an early "'Explosive' phase" of evolution to a "'Normal' phase" of evolution. Similar to the Early Burst model, the SHIFT model is predicated on the theory of opening of niches at some point in time after which taxa are free to evolve in an unconstrained manner (in a Brownian motion type pattern) until some point at which the niche spaces became saturated (where evolution is constrained as in an OU model), whether due to morphological limitations or some external constraint. As such the implementation of the SHIFT model in `mvSHIFT` assumes an early phase of Brownian motion and a second phase of OU, specified using "BMOU" in the model argument. During the OU phase of the model, in addition to the σ parameter representing drift, a selection parameter α is also estimated, with high values of α indicating strong selection.

   Previous implementations (Slater, 2013; Vidal-García and Keogh, 2017) of this model have specified the timing of the shift point *a priori*, however this involves an assertion by the investigator, rather than allowing the data to

influence the most appropriate point for the shift to occur. I have therefore implemented an optimisation search using the base package `optim` for the shift point of the model, which is free to vary from the age of the oldest node in the tree to the modern day. `Optim` maximises the value of the likelihood function $\hat{L}$, and the age estimate of this most likely model. I am therefore implementing an optimisation for the model-fitting parameters for each of the BM and OU elements of the model in addition to the shift point, to obtain a model likelihood as with all implementations of models in `mvMORPH`, and also an estimate for the age at which the shift in evolution occurs.

A model likelihood value (logLik) is obtained for all of the models fit in `mvMORPH` in addition to an Akaike information criterion (AIC) and an AICc value (Akaike, 1974). The AIC can be defined as:

$$\text{AIC} = 2k - 2\ln(\hat{L}),$$

where k is the number of estimated parameters in the model and $\hat{L}$ is the maximum value of the likelihood function. For the models presented here k is 20 for BM, 21 for EB and 36 for the SHIFT model. AICc is a similar information criterion which achieves a balance between selecting the most likely model and the simplest model. An additional term in AICc effectively penalises more highly parameterised models, particularly where the sample size is low. It can be defined as:

$$\text{AICc} = \text{AIC} + \frac{2k^2 + 2k}{n - k - 1},$$

where n is the sample size, which for the case of comparative methods is the number

of taxa (Butler and King, 2004; O'Meara et al., 2006) and all other parameters remain the same as for AIC.

More negative values of AICc favour one model over another. Data are initially compared and visualised using raw AICc values, but model fits are compared using Akiake Weights. The Akiake Weights are given by the relative likelihood $\mathcal{L}$ of a model (Burnham and Anderson, 2003) divided by the sum of the relative likelihood values for all models. That is

$$\mathcal{L}_j = \exp\left(-\frac{1}{2}\Delta\text{AIC}_j\right),$$

where $\mathcal{L}_j$ is the model relative likelihood, ΔAIC_j is the difference in AIC values for model j relative to the null model, and the corresponding Akiake weight is given by

$$\text{Akaike Weight for model 1} = \frac{\mathcal{L}_1}{\sum_j \mathcal{L}_j},$$

where j is the number of models to be compared over. The Akaike weights are calculated using the `akaike.weights` function in the `qpcR` package in R (Spiess, 2014), an Akaike weight of close to 1 indicates a more favoured model.

In addition to log likelihood and AICc values, parameter values (Butler and King, 2004), σ θ_0, α and β, are reported for each model as applicable.

5.2.6 Parametric bootstrapping

Recent studies have shown that assessment of multivariate data (for example landmark data) can be fraught with problems. There is a tendency to overestimate the prevalence of "Early Burst"-type models both when using multivariate data

(Adams and Collyer, 2017) and a subset of lower PC axes. Furthermore when using a subset of the lower PC axes (Uyeda et al., 2015), often a necessity when using high dimensional data due to computing power limitations, there is an additional bias towards "Early Burst" type models. Put in statistical terms, there are high rates of type-one error, falsely rejecting the null hypothesis when it is true.

I performed parametric bootstrapping to check if the observed result could be obtained with a dataset known to exhibit BM, which would indicate model misspecification, either because of using multivariate data or a subset of PC axes. For each tree the covariance matrix was estimated from the empirical trait data under a process of BM. Using the base package `simulate`, 100 datasets for each of the 100 trees were simulated with the same covariance matrix as that estimated from the empirical data. This process is repeated for both the extant only and combined datasets. The BM and SHIFT models in `mvMORPH` are then fitted to the 100 simulated datasets for each tree and maximum likelihood estimates for each dataset are obtained, recording the AIC and AICc. The difference in AIC values between the SHIFT model and the BM model for a given dataset, the ΔAIC, indicates the favoured model. The ΔAIC is calculated as:

$$\Delta\text{AIC} = \text{AIC}_{SHIFT} - \text{AIC}_{BM}.$$

A distribution of ΔAIC values is calculated from the simulated data and a single ΔAIC value is calculated from the empirical data and compared to this distribution. Given the synthetic data was simulated under BM, the expectation is that when the models are fitted to the synthetic data the BM model will be favoured over the SHIFT model, and the ΔAIC value will be positive, whereas if the SHIFT

model is favoured the ΔAIC value will be negative. If the ΔAIC of the empirical data falls outside of the distribution of that obtained for the simulated data, the result is considered robust to type-1 errors.

Due to the high computational requirements of each bootstrap replicate, only 100 bootstrap replicates were applied to all trees, but 1000 bootstrap replicates were run on selected trees to confirm the pattern is not dependent on the number of bootstrap replicates.

5.3 Results

5.3.1 Morphospace

The phylomorphospace presented uses tree 1 from the distribution of 100 trees. The placement within the morphospace is not affected by the choice of tree. PC1 and PC2 (36.69% and 19.72% of variance) correlate most closely to skull aspect ratio and position of jaw joint respectively. Families cluster in particular areas of the morphospace. Trichiuroids, with their elongate skulls and anteriorly positioned (below the orbit) jaw joint, plot in the upper left hand corner of the morphospace. Chiasmodontids, with their slightly less elongate skulls, but highly modified jaw apparatus and posteriorly positioned jaw joint, plot on the lower left hand quadrant of the morphospace. Bramids and caristiids, which possess a high supraoccipital crest on top of the neurocranium occupy the upper right hand portion of the morphospace, with some stromateoids and arripids in a less extreme position. Scombrids, with a more generalised skull shape occupy the central portion of the morphospace.

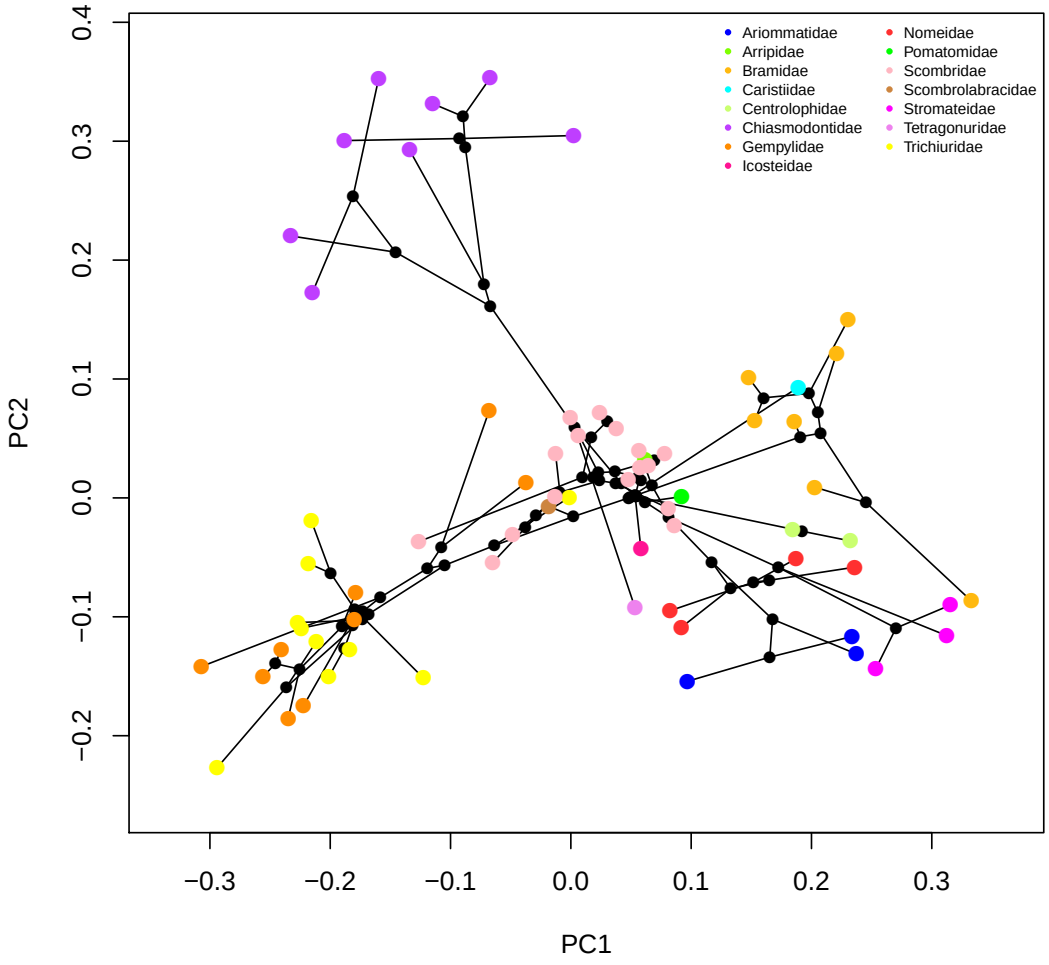


Figure 5.5: Phylomorphospace for the families in Pelagiaria with the first tree from the distribution of 100 trees used as the backbone.

5.3.2 Disparity through time analysis

Both disparity through time (DTT) analyses show a deviation from the null model of BM in the MDI statistic, for all trees (MDI value < 0). However this deviation is not time calibrated, so it is not possible to know where the deviation occurs. This mirrors the results observed in the rank envelope test, which also shows deviations in the empirical data from the simulations obtained under a Brownian motion null. The p-values from the rank envelope test also show significance in 95% of the trees at the 99.5% significance level and all trees show a deviation from the null above the 95% significance level. This result is repeated for both the extant only and combined datasets. In order to account for uncertainty, p-values in the rank test envelope are also reported as p-intervals (see Fig 5.6A). These also show significance at the 95% confidence interval for both the extant only and combined datasets.

In both datasets, the majority of these deviations occur in a broad peak between 50 and 55 Ma, corresponding to the Ypresian, with a second, smaller peak between 39 and 42 Ma (see Figure 5.6A).

5.3.3 Model-fitting analyses

In the extant only dataset the SHIFT model is favoured in 88% of trees, with an Akiake weight of 1. In the remaining 12% of trees a combination of BM and the EB model are favoured with Akiake weights of $\sim$0.75 and $\sim$0.25 respectively depending on the tree, with the exception of tree 73 where a EB model is favoured with an Akiake weight of 1 (Fig. 5.7C). The median values for parameters obtained for the models are reported in Appendix E. The estimated values for σ and θ_0 are

	BM	EB	SHIFT
Extant	0.087	0.033	0.880
Combined	0.057	0.013	0.930

Table 5.1: The average Akaike weights for the extant and combined (including fossils) datasets for the three models.

very similar for the BM and EB models (Appendix Table E.1). This is because the rate parameter of the BM model is 0, at which point the EB model is the same as the BM model, but with an additional parameter. σ and θ_0 are broadly similar for the SHIFT model, although σ is slightly weaker. After the shift point, α is consistent with strong selection acting broadly on all PCs, strongest on PC1 (0.136), PC3 (0.151) and PC4 (0.361) (Appendix Table E.1). The results for the combined dataset are broadly similar; the SHIFT model is favoured in 93% of trees, and a combination of BM and EB in the remaining 7% (Fig. 5.7D). While the parameters for each model (Appendix Table E.2) vary slightly for the combined dataset relative to the extant only dataset, this difference is not significant. The average Akaike weights for each model are shown in Table 5.1. The age estimates obtained in both analyses closely correspond to the model favoured. In those trees where a SHIFT model is not favoured, a very young (<10 Ma) age estimate is found. As the age of the shift moves towards the modern the amount of time that the clade is undergoing a constant-rate BM regime is maximised, such that the model begins to converge on a BM model. There is no obvious topological differences between these trees, other than in those trees where a BM model is favoured the length of each of the nodes in the tree is slightly longer, pushing the ages of the nodes within the tree towards the present. However, in both the extant and combined datasets where a SHIFT model is favoured, the age estimate for this

shift occurs around 50 Ma (Fig. 5.7C) which corresponds to the middle Ypresian. The combined analysis showing a slightly older age estimate (∼1 Ma), but this difference is not significant.

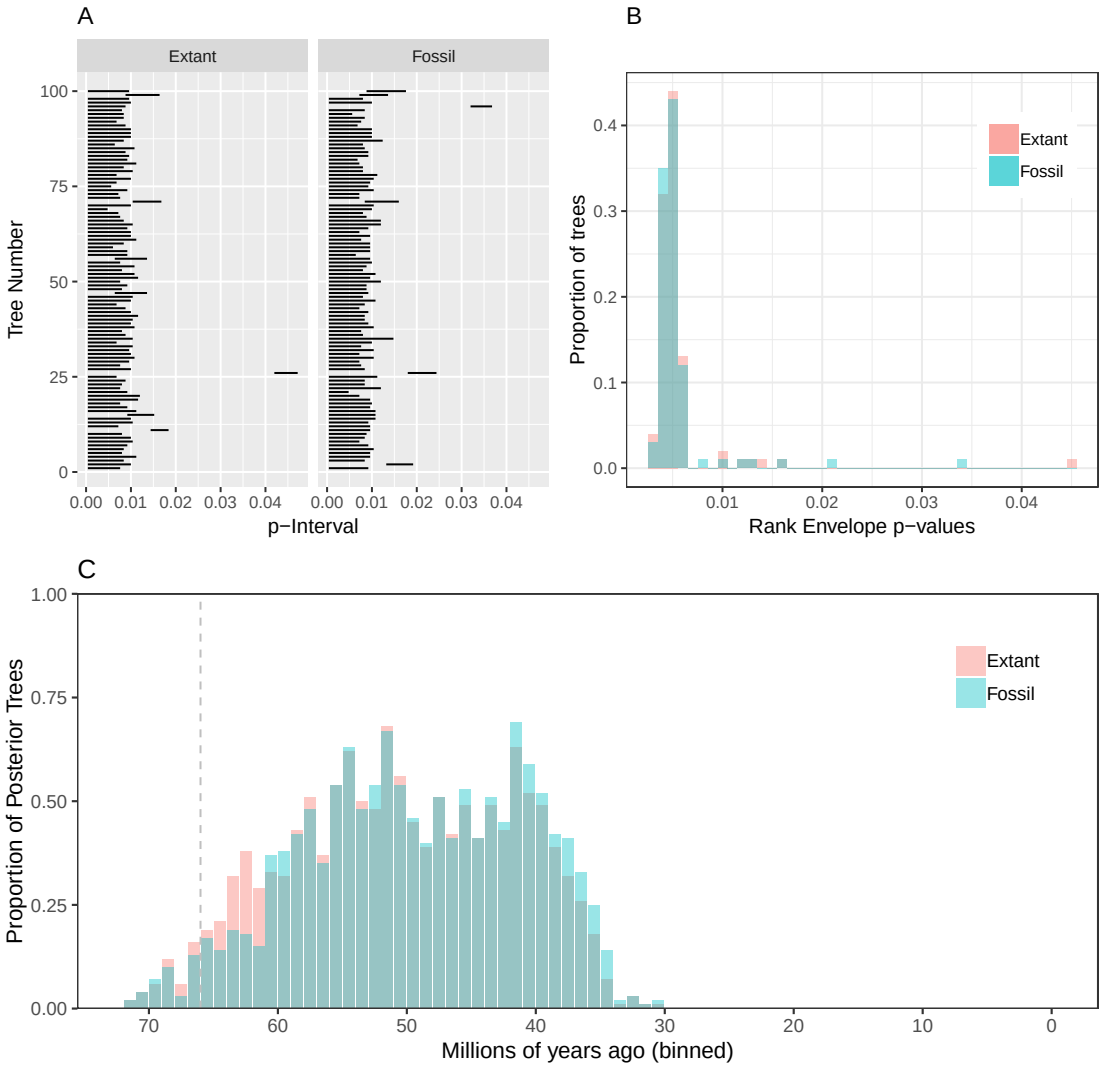


Figure 5.6: Results of the disparity through time analysis for both datasets, extant and combined (fossil). A) p-intervals for extant and combined datasets, B) proportion of trees that show p-values, C) Time calibrated deviations from the null for the rank envelope tests. Red: extant only dataset, blue: combined (fossil) dataset.

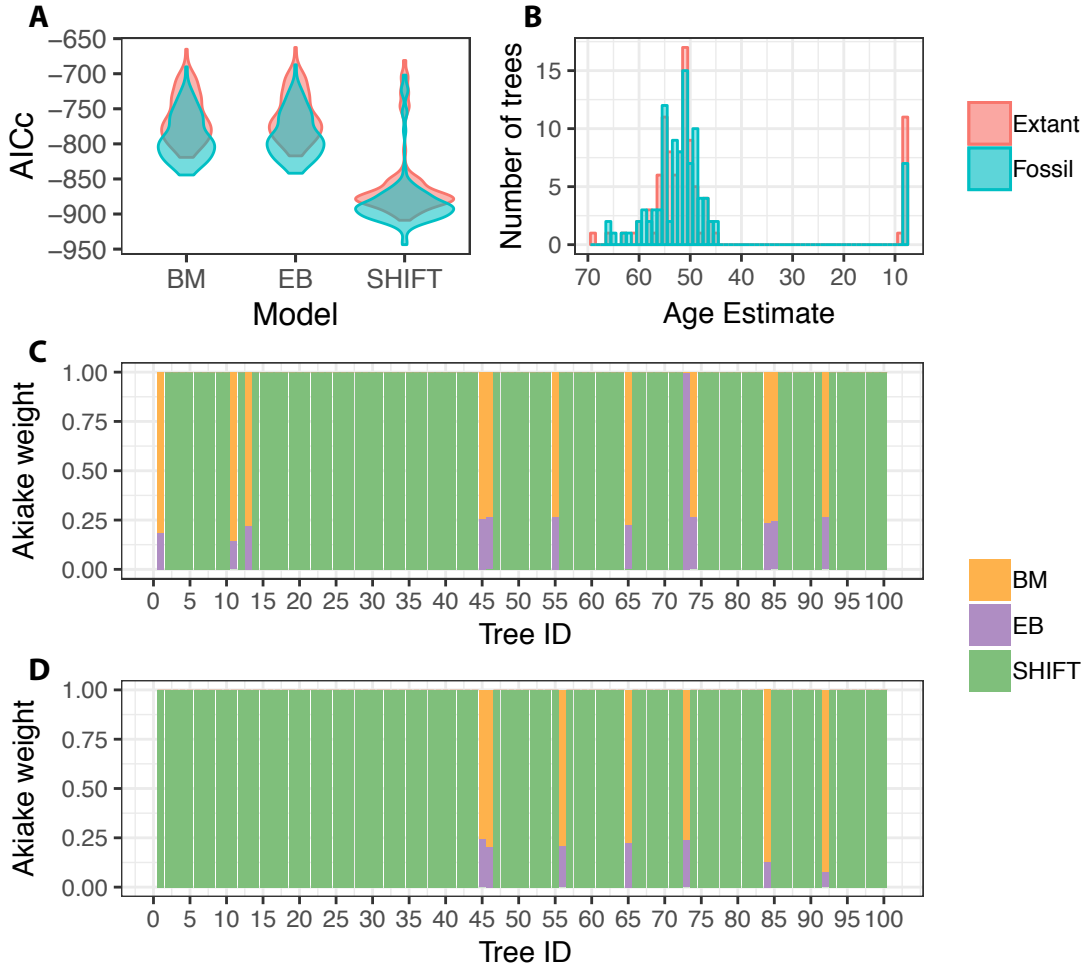


Figure 5.7: Results from the model-fitting analysis run in `mvMORPH`. A. Distribution of AICc values for all 100 trees, B. distribution of age estimates obtained from the SHIFT model. C and D, Akiake weights of the BM, EB and SHIFT models for each of the 100 trees for the extant only and combined datasets respectively.

5.3.4 Parametric bootstrapping

Parametric bootstrapping shows that for all trees where a SHIFT model is favoured the ΔAIC sits well outside of the distribution obtained for the datasets simulated under a process of brownian motion (Fig. 5.8). This is true for both datasets. The exception is where a BM model is favoured in the empirical data. In these cases the empirical data sits within the distribution of that which could be obtained under data simulated from Brownian motion, although it is in the tails of the distribution outside of the 95% confidence interval. This result is unsurprising; where a BM model is favoured for a tree, this suggests there is some large BM signal in the data, and it follows that the same signal could be obtained from data simulated under BM. Running 1000 replicates on multiple trees confirmed that this pattern is robust to number of simulations.

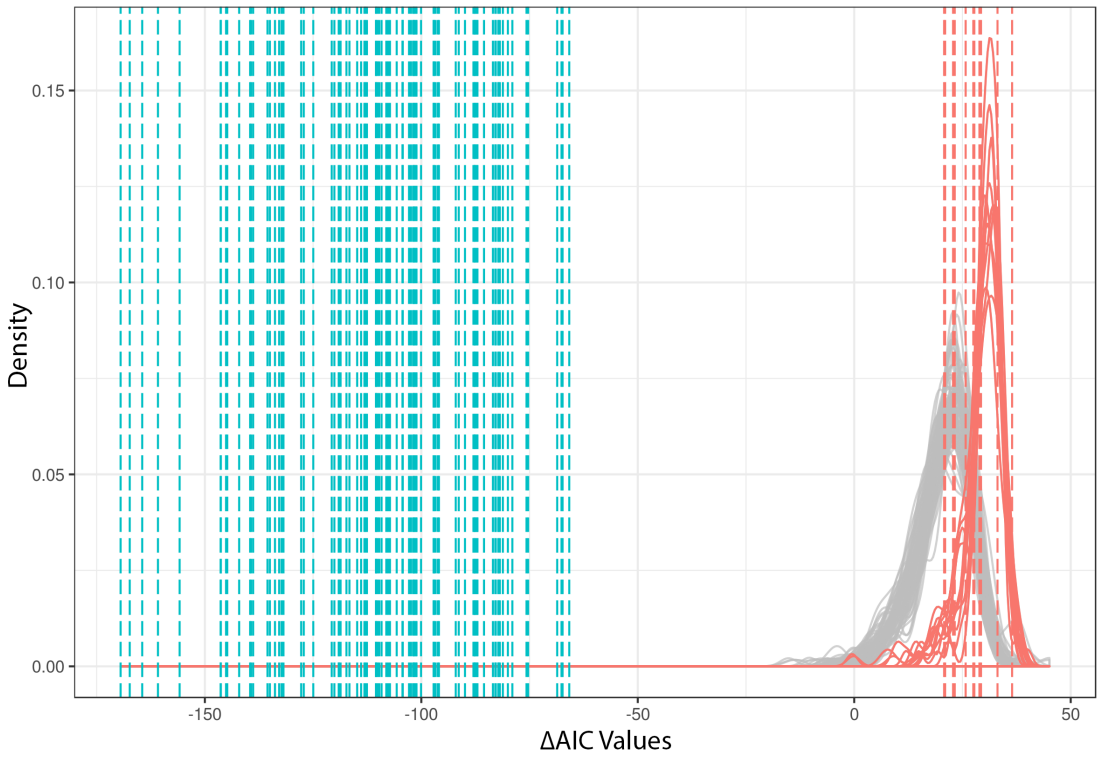


Figure 5.8: Results for the parametric boostrapping of 100 trees. Trees for which the empirical data falls significantly outside of the distribution of the data simulated under brownian motion are indicated in blue. Trees for which the empirical data falls inside of the distribution of the data simulated under brownian motion are indicated in red, with their distribution correspondingly indicated.

5.4 Discussion

A central tenet of the thesis of adaptive radiation *sensu* Schluter (2000) is that adaptive radiation is a biological response to natural selection, with ecological opportunity providing the possibility of rapid diversification of species and key biological adaptations. This study reveals evidence that Pelagiaria undergo a change in the rate and mode of evolution by the end of the Eocene, resulting in a diversity of phenotypes soon after the origin of the group. This diversification occurs rapidly after the K-Pg extinction, suggesting that the further condition of

ecological opportunity is met.

5.4.1 Deviations from a Brownian motion model of evolution

Evidence supports the hypothesis that phenotypic evolution in pelagiarian fishes deviates from a null model of Brownian motion. This concurs with previous suggestions of an adaptive radiation in the group (Miya et al., 2013; Alfaro et al., 2018; Friedman et al., Submitted) and provides evidence that Pelagiaria show non-Brownian patterns of morphological evolution through time. DTT rank envelope analyses support this deviation, in both the MDI statistic and the rank envelope test suggesting this partitioning of disparity between clades is higher early in the history of the clade (see Fig. 5.6C). This pattern is consistent with or without the inclusion of selected fossils, all of which show a broadly similar age distribution for the timing of the deviation in the rank envelope DTT analysis, i.e. a broad peak around the Ypresian (∼50 Ma). Model-fitting analysis supports the deviation from a null model of evolution observed in these analyses, favouring a SHIFT model, where there is a change in mode of evolution, over a BM model in around 90% of the trees. The parameters obtained from the models support this, with a strong selection pressure after the shift point of the SHIFT model. The addition of fossils to the model-fitting analysis does not have a significant effect on the number of trees that favour a SHIFT model relative to the extant dataset. For the fossil dataset, there was a small shift towards more negative AICc values for all trees, the addition of four fossils to the dataset will have changed the parameters and could account for this variation.

This muted effect of the addition of the fossils was somewhat surprising, given studies that show that inclusion of fossils in this way can affect results (Slater et al., 2012). In the analysis presented here, the addition of fossils slightly increases the recovery of a SHIFT (i.e. BM to OU) process, and moves the age estimate of the shift by approximately 1 Ma. That is not to say that the addition of fossils is unwarranted if they are available, but the data presented here suggests that the sensitivity of the analysis to the inclusion or exclusion of fossils is clade dependent, for Pelagiaria the pattern of a SHIFT model over BM is strong irrespective of the inclusion of fossil data. It may also be that the addition of more fossil data, with tighter constraints on their phylogenetic relationships, would have a greater effect on the model likelihoods recovered. Additionally, there are two things to note with the process of placing fossils with maximum likelihood: firstly, as the analysis involves placing fossils into a tree with a fixed topology and branch lengths it is not possible for the fossil to inform these as it would in a formal phylogenetic analysis. Secondly, in placing fossils according to a BM model of evolution the model testing is becoming implicitly biased towards a BM result. Fossils make up a very small percentage of the total combined dataset, less than 10%, and yet they increase the number of trees on which a SHIFT model is favoured.

Two estimates are obtained for the age at which this deviation from the null model occurs; from the DTT rank envelope analysis (Fig. 5.6C) and from the age of the shift from a BM mode of evolution to an OU mode of evolution (SHIFT model; Fig. 5.7A). These estimates have broadly similar distributions peaking between 50-55 Ma for the DTT analyses and around 50 Ma for the SHIFT model, with a slightly older age estimate recovered from analysis of the combined dataset. In combination with the shift to an OU process, these age estimates suggest that

by the mid Eocene Pelagiaria were phenotypically constrained, and that evolution prior to and after this point proceeded in a different way. This mirrors the pattern seen in the fossil record, with the first occurrences of body fossils of many extant pelagiarian families at or around the Paleocene-Eocene boundary, many with strikingly similar morphologies to the modern day, and an established fauna of recognisably modern taxa by the end of the Eocene. In contrast, there are no pelagiarian fossils found prior to the K-Pg boundary (Miya et al., 2013, fig. 7) giving very tight bounds on the possible evolutionary timescale over which this phenotypic diversity can have been obtained.

5.4.2 *Lagerstätten* effects

Lagerstätten effects, biases in the fossil record caused by episodes of exceptional preservation that result in higher sampling in one interval than another, were first recognised half a century ago (Raup, 1972; Raup and Sepkoski, 1982; Sepkoski, 1996). Since the realisation of the effect of such sites on diversity analyses, attempts have been made to ameliorate the problem, initially on taxonomic occurrence data (Sepkoski, 1996; Briggs and Gall, 1990), and then through phylogenetic correction (Cavin and Forey, 2007; Benson et al., 2009) or comparison of exceptional sites only (Briggs and Gall, 1990).

The influence of *Lagerstätten* effects on phenotypic patterns are less well discussed and understood. There has however been some attempt to assess the contribution of *Lagerstätten* and other exceptional sites to patterns of morphological diversity either through jackknifing (Friedman, 2010; Clarke and Friedman, 2018), or by including a *Lagerstätten* variable in linear models when using a modelling

approach (Butler et al., 2013; Lloyd and Friedman, 2013).

Even less considered is the role that exceptional preservation might play in comparative analyses, specifically those that integrate phylogenetic data. One might be tempted to conclude that since such analyses might not include fossils directly as terminals there are no biasing factors; however, this is likely a simplistic view, because fossils are likely to have some influence, particularly when it comes to estimating the specific timing of evolutionary events.

The most obvious inclusion of a possible *Lagerstätten* effect in such analyses is obtained from calibrations drawn from specific time periods of exceptional preservation. Both the London Clay (Friedman et al., 2016) and Bolca (Friedman and Carnevale, 2018) are described as *Lagerstätten*, with exceptional 3D and 2D preservation respectively. These are joined by less famous deposits like the Fur and Danata formations that could rightly be considered exceptional. This period of exceptional preservation around the Paleocene-Eocene boundary marks a minima for the origin of many families with Pelagiaria. Around half of the families within Pelagiaria have first appearances within this interval. Additionally many of the calibrations for nodes within some of these families derive from these localities (20% of calibrations in pelagiarian tree). It is possible that the origin of families represents a true biological pattern, and it is coincidentally viewed this through the lens of exceptional preservation. However, it would be overly optimistic to dismiss this pattern as completely free of any bias. As discussed in Chapter 4, the percomorph fossil record is lacking during the Paleocene, but despite biological (distinctive skeletal components) and ecological (geographically widespread taxa) factors supporting high preservation potential no pelagiarian fossils are known prior to the K-Pg boundary, even with an abundance of fossil deposits in the late

Cretaceous that preserve other pelagic predatory teleosts (see Figure 4.4).

Accepting that a theoretical bias as a result of *Lagerstätten* could affect a comparative analysis like that presented here, the sensitivity of the results to these biasing factors must be considered. A deviation from a BM model of evolution is found relatively early in the clades history in all analyses, and in the mvMORPH analysis a shift is found from a BM to an OU model of evolution at a similar time. This might be interpreted as the discovery of multiple optima early in the history of the clade, "locking it in" to a series of general morphologies without further expansion. However it is possible this result is amplified by calibrations of a similar age for each distinctive crown group, giving them potentially spurious first appearances.

There are two consequences of possible *Lagerstätten* effects. Firstly, the possible bias acting on the dataset to create a pattern of fast evolution early in the history of the clade. Of the 20 calibrations used in the pelagiarian tree, 7 are from the Paleocene-Eocene time interval; 3 from the Danata Formation (calibrating nodes within syngnathiforms, scombrids, and between *Scombrolabrax* and the Trichiuroidea) and one from the London Clay Formation (calibrating the MRCA of *Acanthocybium* and *Scomberomorus*). In the pelagiarian tree the crown nodes of only 4 supra-families are calibrated, stromateoids, scombrids, scombrolabracids + trichiuroids, and tetragonurids + chiasmodontids and only one of these with a fossil from a site of exceptional preservation. Additionally, across all the calibrations obtained from the Paleocene-Eocene interval, the 95% CI extends to 75.14 Ma (for the Danatinsk Formation) and 66.85 Ma for the London Clay formation, both in the Late Cretaceous. This suggests that the calibrations are not creating an analysis that is highly dependent on a 'literal' reading of the fossil record, as they

do not impose tight constraints on the origins of families. There are additional reasons to suggest that the origin of families during the Paleocene-Eocene period is not as dependent on calibrations. Many of the deep internodes in the tree are very short even when the tree is uncalibrated, indicating that it is probable that many of these divergences took place rapidly (i.e. early in the clades history). This suggests that the appearance of these distinctive bodyplans at similar times is not inconsistent with patterns apparent from a non-fossil calibrated tree. Trees without pelagiarian calibrations (Miya et al., 2013) also show distributions of branch lengths consistent with an early establishment of morphological body plans. In future work, there are additional strategies that could be implemented to test the robustness of evolutionary patterns to the calibrations used in the tree and seeing if the pattern of an early shift in evolution is maintained. It would be possible to use external calibrations (outside of the group of interest), a rate smoothed tree with a relative (rather than absolute) timescale, or the use of simulated data to test changes in calibrations and the effect of this on evolutionary analysis.

The second bias introduced by possible *Lagerstätten* effects concerns the timing of a shift in mode of evolution or the deviation from a BM model of evolution. For the reasons outlined above, a shift early in the history of the group is relatively robust. However, the timing of this shift is more open to the impact of biases, since calibrations are used to tie the tree to an absolute rather than relative timescale. In a more general context, one of the ways to test this would be to use external calibrations only. In the case of Pelagiaria however, a substantially older timing of the deviation from a BM model and shift in mode of evolution seems improbable given our knowledge of the fossil record.

It is impossible to unpick fully whether the peak of deviations from a BM

model of evolution around the Paleocene-Eocene boundary is the result of increased sampling around this time. The *Lagerstätten* effect from calibrations used in the phylogenetic tree are likely to be minimal, although cannot be excluded, and no observable difference is identified from using London Clay fossils in the combined analysis versus the extant analysis presented here.

5.4.3 Implications for models of radiation

While the early Paleocene fossil record is sparse (Chapter 4), those taxa that are recovered in Paleocene deposits seem to reveal a highly altered pelagic predatory fauna to that of the Late Cretaceous (Cavin, 2002). Pelagic predatory teleosts including the alepisauroids (aulopiforms), ichthyodectiforms, pachirhyzodontids and pachychormiforms are lost at the K-Pg boundary, with the establishment of, among other groups, the pelagic predatory Scombridae in the early Paleocene (Friedman, 2010; Friedman and Sallan, 2012). This rapid overturning of taxa has been suggested to support indications of adaptive radiation in Pelagiaria, as in other percomorph groups (Miya et al., 2013; Alfaro et al., 2018). Model-fitting results in this analysis support the concept of adaptive radiation within Pelagiaria.

Adaptive radiation within Pelagiaria

In over a century of discussion and debate our understanding of adaptive radiation has come to encompass different things (Givnish and Sytsma, 2000, Table 1.2). The most widely used definition refers to Schluter (2000) and includes three facets: that adaptive radiation is a response to both natural selection and ecological opportunity, involving diversification of species, and their associated adaptations (Glor,

2010; Schluter, 2000). The term adaptive radiation is used to describe groups as diverse in time and space as the worldwide mammal radiation after the K-Pg and cichlid fishes in North African Rift lakes in the last 5 million years. There is little clarity however of the underlying evolutionary dynamics of these radiations and whether they are in fact comparable.

Despite a number of studies in the literature investigating models of changing rate to explain evolutionary patterns, studies testing changes in mode are comparatively rare (Slater, 2013). This is despite the biological reality that shifts in mode of evolution are for some groups a more realistic explanation for observed phenotypes than changes in rate. In order to produce the pattern observed in the pelagiarian fossil record and suggested in molecular phylogenies, there would need to be rapid rates of evolution early in the history of the group, followed by a significant slowing of rates towards the present. Alternatively, the rate change could be less extreme but would have needed to start accumulating earlier than the K-Pg boundary, which as discussed in Chapter 4 is unlikely. The results of our model-fitting do not support an "Early Burst" model, and Akiake weights were low in trees where a Brownian motion model was favoured. This adds to evidence put forward by Harmon et al. (2010) in a wide-scale study of multiple clades, in which models of adaptive radiation displaying an early burst of morphological evolution followed by a period of slow down in morphological rate are rarely found. This is in despite Harmon et al. (2010) using only the first shape axis, which should be biased towards finding an EB model (Uyeda et al., 2015). For morphological evolution of skull shape in Pelagiaria a model of evolution where there is an early period of unconstrained evolution followed by a period of constraint, whether by intrinsic or extrinsic factors, is the most favoured model. A pattern of unconstrained followed

by constrained evolution has a broadly similar morphological pattern to that predicted by an "early burst" type model but has no change in rate. However the definition of adaptive radiation does not actually specify how the morphological diversity is obtained, just that it has a diversification of species and adaptions for key niches.

Favouring a model where there is a shift from a period of unconstrained evolution to a period of constraint fits into Simpson's (1944) concept of adaptive zones. In the period of constraint an ecological mode of life is imposing constraint on a phenotype. The SHIFT model applied here is a simplification of the model of adaptive zones, the ideal model being a multi-peak OU model where each peak corresponds to a group of taxa with similar phenotypes. For the example presented here, the Pelagiaria, there might be one adaptive peak for chiasmodontids, another for trichiuroids, and so on (Fig 5.5). While the persistence of a stable optima over 50 Ma could be difficult to accept when only considering genetic traits and variation (Hansen and Houle, 2004), palaeontological and morphological evidence suggests stability over geological timescales is not unsurprising (Estes and Arnold, 2007; Jackson and Cheetham, 1999). Marine environments tend to be relatively stable over geological timescales, in direct contrast to those changing or heterogenous environments typically associated with adaptive radiations e.g. colonisation of East African rift lakes by cichlids.

Comparisons with the mammal radiation

One of the few analyses to test changes in mode is Slater (2013) who investigated the classical example of adaptive radiation, the mammal radiation. Slater tested 8 models including some that varied rate, some mode and some both. He modelled

a BM process, an OU model, and various shift models, with the shift always constrained to occur at the K-Pg boundary. The basic shift model he tests is one of varying rates before and after the K-Pg boundary, named the "K-Pg shift model". This model is then subjected to two modifications: the first constrains the mode of evolution prior to the shift as OU, followed by BM, the "ecological release model"; and the second allows rate and mode to change at the shift point: the "release and radiate model". In contrast to the results recovered here for Pelagiaria, Slater concluded that a constrained model of evolution, followed by a BM model of evolution, was the best fit model for his mammal dataset. He also recovered a change in the rate across the K-Pg boundary, something not tested here. However, in contrast to Pelagiaria, mammals have a longer fuse to their evolution, with stem placentals known from the late Jurassic (Luo et al., 2011), suggesting some period of constraint when non-avian dinosaurs were the dominant fauna. In an attempt to more directly compare the mammal radiation to the pelagiarian radiation, I ran a brief test of the SHIFT model presented in this chapter on the dataset of Slater (2013). I tested the BM and the SHIFT model on three subsets of their data: the whole dataset, crown Eutheria and Placental mammals (see Appendix G.1 for Tree; nodes 6 and 5 respectively). The last of these truncates the dataset to only include the taxa thought to have radiated at or around the K-Pg, making the dataset more directly comparable to that of Pelagiaria. Of these three datasets, only Placental mammals did not include any fossil samples. In agreement with Slater, I also found that the BM model was favoured over the SHIFT model for all three mammal datasets (see Appendix G; Fig. G.2) with an Akaike weight of $\sim$0.75 across all subsets of the analysis. These results, in conjunction with those of Slater (2013), suggest that Pelagiaria show a different evolutionary pattern to the

'classic' mammal radiation. This conclusion, however, comes with some caveats. Firstly, Slater's dataset considers only body size, rather than the morphological dataset assembled here, and it is not unreasonable to expect that body size and morphology might have different evolutionary pressures acting upon them. Skull shape and in particular jaw morphology have a strong link to function (Westneat, 2005; Anderson et al., 2011; MacLaren et al., 2017). This is also true of body size to an extent, however there are many more possible morphologies than there are body sizes, providing much more opportunity for diversification and consequently constraint than when investigating only body size. The second caveat is that there were no fossils included in the placental mammal subset of the dataset, where most of the modern diversity is partitioned. While this did not affect our results for Pelagiaria, previous analyses have suggested that fossils are important in assessing the fitting of OU models (Hansen, 1997; Hunt et al., 2008). Finally, the sample of mammals represented in Slater's dataset is limited in comparison to Pelagiaria, about 3% extant mammal species compared to the sample of around 30% of Pelagiaria, an order of magnitude difference. Further work, particularly morphological studies on mammals aimed at assessing the mode and rate of evolution, is needed before concluding there are significant differences between clades exhibiting adaptive radiation.

Modern 'model' radiations provide almost the opposite end of the spectrum to the mammal radiation. While studies targeting the mammal radiation are comparatively rare in the literature (but see for example Slater, 2013), modern 'model' radiations are relatively well-understood and well-studied (Baldwin and Sanderson, 1998; Gillespie, 2004; Grant and Grant, 2008; Losos and Ricklefs, 2009; Losos,

2011; Stroud and Losos, 2016). However they do not appear to be followed by a period of stasis, most likely because they haven't had time to "play the tape through to the end". This perspective is roughly equivalent to truncating the evolutionary history of Pelagiaria ∼10 Ma after the origination of the group; no doubt the evolutionary pattern that would be observed in such circumstances would be different. It is therefore with caution that we should compare evolutionary patterns across such diverse groups for which the term 'adaptive radiation' is currently employed.

5.5 Conclusion

Pelagiaria provide a new study system to test changes in rate and mode of evolution across the Cenozoic. They provide insight into a alternative model for how an adaptive radiation-like pattern can be obtained by changing the mode of evolution in a group. With and without fossils the most likely model for evolutionary dynamics within Pelagiaria is a model with a shift in the mode of evolution around the early Eocene. Patterns of evolutionary dynamics appear to be relatively specific to the group being tested, with Pelagiaria showing a different mode of evolution to mammals. There are a wide variety of groups that have been suggested to be undergoing adaptive radiation, but until we know what the processes generating these adaptive radiations are they are difficult to compare. The outcomes obtained can be generated under different processes, and different radiations may be driven by different aspects of rate and mode. A synthetic analysis of a range of radiations under the same methodological framework is required to investigate if patterns of adaptive radiation are similar across groups.

Chapter 6

Conclusions and Further Work

This thesis has sought to investigate evolutionary patterns in the group Pelagiaria, integrating fossil data into a modern phylogenetic framework to investigate changes in rate and mode of evolution in the group. Utilising the relatively good fossil record of Pelagiaria, particularly three-dimensionally preserved examples from the Paleocene Landana Formation and Eocene London Clay Formation in conjunction with emerging molecular datasets, progress is being made towards a better understanding of the morphologies characterising this group.

6.1 Morphological understanding in Pelagiaria and its implications for evolutionary analyses

While molecular relationships among Pelagiaria are now relatively well resolved (Miya et al., 2013; Campbell et al., 2018; Alfaro et al., 2018; Friedman et al., Submitted), morphological relationships within the group remain poorly understood.

Efforts to rectify this are hampered by a lack of rigorous morphological datasets that can be interrogated by statistical methods. Existing morphological synapomorphy schemes in Pelagiaria are based on historical analyses and are restricted to individual families within the group.

One of the core groups of families previously associated with one another is the 'classical' Scombroidei (Regan, 1909; Gosline, 1968; Collette et al., 1984; Johnson, 1986), comprising scombrids, trichiuroids, and xiphioids (billfishes). However, morphological analyses of Scombroidei are predicated on an assumption of monophyly. This assumption has been violated by the recent removal of billfishes from the group, on the basis of multiple molecular markers (e.g. Near et al., 2013; Alfaro et al., 2018). This has made placing putative scombrid fossils into an extant framework challenging, as evidenced by attempts to manually place †*Micrornatus* and other taxa from the London Clay (Chapter 2). Establishment of a formal character set for scombrids independent of Scombroidei (Chapter 4 and Appendix B.4) goes some way to solving these problems, although this list still requires development, and would most likely be sensitive to placement of many fossils.

With the establishment of a scombrid character matrix in this thesis, it has been possible to investigate key fossils associated with the group, particularly in the poorly constrained Paleocene record. Despite being hypothesised as an important interval in the diversification of many modern groups, very few percomorph fossils from this time period have been found, and fewer still have been aligned with modern groups. Placement of the three-dimensionally preserved †*Landanichthys* from the Selandian of Angola as a deeply diverging member member of the Scomberomorini in phylogenetic analyses (Chapter 4). Its placement within this highly nested tribe within a percomorph family strongly indicates that morphological

evolution in the immediate aftermath of the Cretaceous-Paleogene mass extinction was rapid, establishing modern phenotypes by the Paleocene-Eocene boundary. These results provide further evidence for a postulated adaptive radiation in Pelagiaria.

As with Scombridae, our morphological understanding of other families in Pelagiaria is constrained based on their previous associations. 'Gempylids' and trichiurids have been frequently linked, but their precise relationships based on morphological and molecular studies are highly variable (Johnson, 1986; Patterson and Rosen, 1986; Carpenter et al., 1995; Orrell et al., 2006; Collette et al., 1984; Betancur-R et al., 2013; Miya et al., 2013; Near et al., 2013; Betancur-R et al., 2017). However these two families have a relatively rich fossil record, both two- and three-dimensional. In combining morphological character sets for trichiuroids in addition to published molecular data I provide a template for the combination of morphological matrices across Pelagiaria. Despite remaining uncertainties, this morphological framework is now relatively well estabilised for placement of new and previously described fossil taxa, including flattened specimens that were only informally placed.

Character sets for families and Pelagiaria as a whole are required independently of one another due to the sensitivities of analyses to the addition of fossils. Both of the character matrices presented here (Chapters 3 and 4) can be sensitive to the addition of multiple fossils into the analysis. This is particularly a problem without the addition of a robust molecular framework when including fossils with large percentages of missing data, or without exclusively creating and defining characters designed for placement of fossil taxa.

Critical advances have been made in resolving relationships within Scombridae

and Trichiuroidea, and in placing three-dimensional fossils of these two families. The initial integration of datasets for 'gempylids' and trichiurids in Chapter 3 provides a template for the integration of the remaining character sets in Pelagiaria. A morphological framework for Scombridae and Trichiuroidea will provide an opportunity to simultaneously analyse molecular, morphological and fossil data in a fossilised-birth-death framework (Heath et al., 2014). Resolving the morphological relationships between the other families within Pelagiaria is beyond the scope of this thesis, but presents an obvious next step for reconciling molecular and anatomical arguments of relationships. Critically, morphological evidence for pelagiarian monophyly is lacking, although potential candidates include elevated vertebral counts (Haedrich, 1967; Collette et al., 1984; Johnson, 1986; Melo, 2009*b*; Friedman et al., Submitted). In addition to potentially resolving some of the more uncertain nodes at the base of the molecular tree (Friedman et al., Submitted), this will lead to important implications for our understanding of evolutionary patterns in the earliest Cenozoic.

This thesis focusses on the scombrid and trichiurid fossil records, as they are by far the best known for Pelagiaria, but extinct members of other pelagiarian families would benefit from a morphological framework in which to be studied. An obvious place to start with this would be for those groups where character matrices already exist. Chiasmodontids have character matrices (Melo, 2009*b*, 2010) and are relatively well studied, although there remains debate concerning the number of species within *Chiasmodon* (Prokofiev and Kukuev, 2009). Chiasmodontids + tetragonurids have been suggested as sister to Scombridae (Friedman et al., Submitted), an interesting relationship given their divergent life habits. Scombrids are found at the surface of the ocean, whereas chiasmodontids occupy meso – bathy

pelagic waters. The two groups also have divergent feeding behaviours and associated skeletal modifications, likely linked in part to their habitat. In order to swallow their prey whole, chiasmodontids have a highly modified skull, with a extremely posteriorly placed posterior jaw joint, elongate recurved teeth, and reduced cranial bones for increased movement (*pers. obvs* and Melo, 2009*b*, 2010). Published character matrices for chiasmodontids provide a starting point for a study of chiasmodontid fossils. Particularly of interest would be progression from a generalised percomorph body plan to that of Chiasmodontidae, and the timing of these modifications. However, the only known fossil chiasmodontid appears to already show these substantial changes and is likely a member of the crown radiation. Character discussions and matrices also exist for stromateoids (Ariommatidae, Centrolophidae, Nomeidae, Stromateidae and Tetragonuridae) (Haedrich, 1967; Doiuchi et al., 2004; Jawad and Jig, 2017) which have a series of associated fossils (Bannikov, 1985; Bonde et al., 2008; Bannikov, 2012; Přikryl et al., 2014). Molecular evidence suggests that the monophyly of Stromateoidei is not robust, placing tetragonurids as the sister to chiasmodontids, centrolophids as an individual clade and leaving only ariommatids, nomeids and stromateids as a group. A unified character matrix across Pelagiaria would be beneficial in investigating these more surprising aspects of molecular phylogeny. The addition of morphological data may alter the arrangement of short internodes at the base of the molecular phylogeny, or the molecular phylogeny may continue to be supported.

In addition to the significant outstanding areas of uncertainty in extant Pelagiaria (e.g. the lack of character matrices or analyses in caristiids and bramids), aspects of fossil relationships relative to extant taxa remains controversial. Without a molecular framework, many fossil taxa have not had their placements reassessed

relative to Pelagiaria as a whole. Some, for example the †Euzaphlegidae, are of initial uncertain placement, or indeed phylogenetic coherence. †Euzaphlegidae are associated with 'gempylids' but may in fact be polyphyletic (Patterson, 1993*b*; Monsch, 2000; Monsch and Bannikov, 2012). The situation is further complicated by the lack of morphological character sets for Pelagiaria as a whole, as it is impossible to test their relationships to 'gempylids' without first assuming their monophyly with them *a priori*.

6.2 Evolutionary patterns in Pelagiaria

More than half a century after *Tempo and Mode in Evolution* (Simpson, 1944), there remains debate about the underlying evolutionary processes underpinning adaptive radiation, particularly the interplay between rate and mode which can produce broadly similar evolutionary patterns with small changes of evolutionary parameters (Foote, 1997). Although the effect of rate has received far more attention (Schluter, 2000; Harmon et al., 2003; Farrell and Sequeira, 2004; Kocher, 2004; Gavrilets and Losos, 2009; Slater et al., 2010; Harmon et al., 2010; Cantalapiedra et al., 2017), research into mode is starting to gain ground (e.g. Slater, 2013; Vidal-García and Keogh, 2017) and Chapter 5 suggests patterns of mode are of key importance in describing evolutionary dynamics, especially for Pelagiaria. However, there is as yet no consensus on the evolutionary dynamics of adaptive radiation and Simpson's model remains open to interpretation.

Pelagiaria show a pattern of phenotypic evolution that initially follows a Brownian motion process, with a subsequent shift to an Ornstein-Uhlenbeck model.

This means that early in the history of Pelagiaria, evolution proceeded in an unconstrained fashion. This is hypothesized to represent a consequence of a lack of incumbent taxa occupying major ecological niches. By the mid-Eocene, around 50 million years ago, this pattern of phenotypic evolution shifted, becoming constrained. However, it seems obvious from the variety of ecological niches Pelagiaria have occupied that there is not a single constraint acting on the group. Despite an apparently homogenous open ocean, Pelagiaria have occupied a variety of niches along gradients of depth (e.g. Scombridae versus Chiasmodontidae) and diet (e.g. Scombridae versus Tetragonuridae) and have also created niches based on relationships with other pelagic taxa (e.g. species of Nomeidae are found in association with siphonophores). While the analysis presented here fits a basic BM to OU shift model, a potentially more elaborate and accurate application of Simpson's (1944) model would be to fit a multi-peak OU model after the shift point. An additional variation would be to test a change in rate across the shift, similar to the release and radiate model of Slater (2013).

As discussed in Chapter 5, the SHIFT model recovered for phenotypic evolution in Pelagiaria is opposite to the pattern recovered for body shape in mammals, where Slater (2013) found overwhelming support for a OU followed by BM model, with a change in rate in some datasets (see Slater, 2014). It is easy to understand a model of constraint for mammals during the Mesozoic, given the saturation of niche spaces by non-avian dinosaurs (Slater, 2013). However, the observation of Brownian motion for mammals in the Cenozoic is surprising and would appear to be in contrast to other studies investigating body size in the same time period for mammals (Alroy, 1999). While body size may evolve in a different framework to that of skull morphology, this difference is stark and highlights how dependent the

recovery of evolutionary patterns is to the group and trait studied.

Research into adaptive radiation, currently focused on isolated modern radiations which are relatively well characterised, would benefit from a change in focus to radiations like that of Pelagiaria or other geographically non-isolated continental radiations. As less isolated radiations their evolutionary patterns are slightly more difficult to untangle, but they provide a different and more analogous perspective to large-scale radiations like the 'classical' mammal radiation. However even this change in focus would be scratching the surface of the bigger problem, which is the lack of understanding in whether the evolutionary dynamics of these radiations are in fact comparable. To answer this question requires comparison of patterns across groups and timescales under the same experimental framework to establish if their evolutionary dynamics overlap. A dataset of radiations on different scales, but where all other variables remain relatively constant would be a resource with which to investigate similarities and differences between radiations. This would represent an extension of work done by Harmon et al. (2010) but including a greater range of phenotypic variability. Building up such a dataset would allow comparison of the evolutionary dynamics of radiations.

Investigating a pair of radiations, one modern and one ancient, utilising instances where there is significant phenotypic overlap between taxa in two such radiations, would provide a complementary approach to a dataset of radiations. Pelagiaria, in combination with cichlids, could provide an opportunity for such a study. As ancient and modern radiations within Percomorpha respectively, they nonetheless share broadly similar morphologies, and could therefore be compared with the same, or an expanded, landmark set as used in this study. Studying two groups such as these under the same morphological framework, with the same

evolutionary models, would go some way to testing if the evolutionary dynamics of young modern 'model' radiations are the same as those that occured tens of millions of years ago on broader spatial scales. In conjunction with a synthetic analysis across postulated radiations, equivalent to that of Harmon et al. (2010) but incorporating modern multivariate and variable mode models there is potential to build a framework for thinking about the general rules–if any–of adaptive radiation. In presenting Pelagiaria as a non-analogue adaptive radiation I show a study system, globally distributed and yet tractable in its species richness, that provides an opportunity to investigate evolutionary radiations and the dynamics underpinning them.

6.3 Inclusion of fossils in evolutionary analyses

The ability to introduce fossils into morphological character matrices that encompass all of Pelagiaria is important for two reasons. Firstly, a morphological framework in which to place fossils can be used in combination with a molecular framework to perform total-evidence phylogenetic and dating approaches, including fossilised-birth-death analyses. Secondly, in obtaining estimates of both morphological relationships and branch lengths simultaneously the problems associated with placing fossils *a posteriori* using maximum likelihood are overcome. However, to accurately reconstruct the evolutionary history of Pelagiaria the fossil records of a wider sample of the families need to be understood, and these fossils incorporated into evolutionary analyses. Previous analyses have suggested that the inclusion of fossils improves the recovery of evolutionary patterns relative to extant data only (Slater et al., 2012). While I found that including fossils in the

analysis did slightly change the number of trees for which a SHIFT model was favoured the difference was not significant. Additionally, a SHIFT model was recovered as the favoured model in ∼90% of the trees even without the inclusion of fossil data, indicating a robust evolutionary pattern.

An potential bias in Chapter 5 is the inclusion of fossils in Scombridae and Trichiuroidea only. This is limited by the availability of three-dimensional fossils beyond those considered here; with the exclusion of scombrids and trichiuroids the remainder of the families in Pelagiaria almost exclusively have two-dimensional fossil records. It may therefore only be possible to include a balanced fossil sample if phenotypic measures are applicable to laterally compressed fossils, for example a body size or shape dataset, such as that used in Friedman et al. (Submitted). An extension of the work of Friedman et al. (Submitted) would be to use the two-dimensional landmark dataset to test the models of evolution investigated in Chapter 5. This dataset includes sampling across the Pelagiarian tree, but again would be limited by a lack of understanding of where the fossils are placed relative to extant species. In addition to the lack of character datasets, placing two-dimensional fossils phylogenetically can be a challenge as some information about bone relationships and internal structure is lost relative to three-dimensional data. Additionally, two-dimensional datasets are limited in their ability to account for all of the morphological variation associated with phenotype, for example jaw morphology, and largely account for overall shape variation.

6.4 Evolution in percomorphs

The diversification of pelagiarians in the Paleocene aligns with wider patterns of replacement in early Cenozoic oceans (Robertson et al., 2013; Sibert and Norris, 2015). While scombrids and trichiuroids, along with other pelagic predatory forms, diversify into a previously occupied and recently vacated niche (Friedman, 2010), such a clear pattern of ecological replacement is not evident for other groups in Pelagiaria. It may be that they obtained key innovations to capitalise on niches not previously occupied, or that the replacement pattern is not as clear as for pelagic predatory taxa. Alternatively they could have evolved in response to environmental change in the immediate aftermath of the K-Pg boundary, perhaps in response to an abundance of particular prey.

The diversification of percomorphs is striking in that their morphologies are hugely variable, even among sister lineages. Molecular studies consistently recover Syngnatharia (seahorses, pipefishes and their kin) as the sister lineage to Pelagiaria (Miya et al., 2013; Near et al., 2013; Alfaro et al., 2018), despite their highly divergent morphologies and a lack of obvious morphological evidence to support the relationship. There are no candidate fossils that capture the phenotypic divergence between these two lineages, but the fossil record of syngnatharians with recognisably modern morphologies extends back to the Late Cretaceous (Sorbini, 1981). It is plausible that it would not be possible to identify the key fossils linking pelagiarians and syngnatharians, such are the differences in their morphology.

Multiple radiations have been identified within Percomorpha (e.g. Harrington et al., 2016; Alfaro et al., 2018), all of which have the potential to be investigated in a framework similar to that presented here. However there remains similar

problems to overcome. Molecular studies (Near et al., 2012; Betancur-R et al., 2013, 2017; Alfaro et al., 2018) reshuffle percomorph taxa and highlight associations that have not previously been recovered based on morphological analyses. Consequently morphological datasets may also be lacking in these families. However, there are molecular frameworks that exist for families within percomorphs (Carangimorpha for example: Harrington et al., 2016), and these would provide an opportunity for comparisons of adaptive radiations on similar scales in a similar study system to that of Pelagiaria.

6.5 Summary

In using μCT to investigate three-dimensional fossils, I have created character sets for Scombridae and Trichiuroidea, the most speciose and fossil-rich families in Pelagiaria. This has fed into a cross-family evolutionary analysis of Pelagiaria which has revealed that they show a pattern of adaptive radiation consistent with a change in mode of evolution, rather than a change in rate. Pelagiaria present a study system on which to investigate evolutionary diversification, to develop an understanding of adaptive radiation-like patterns on broad spatial scales.

Chapter 7

Bibliography

Adams, D. C. and Collyer, M. L. (2017), Multivariate phylogenetic comparative methods: evaluations, comparisons, and recommendations, *Systematic biology* **67**(1), 14–31.

Adams, D., Collyer, M. and Kaliontzopoulou, A. (2018), Geomorph: Software for geometric morphometric analyses. R package version 3.0.6. https://cran.r-project.org/package=geomorph.

Adolfssen, J. S., Milan, J. and Friedman, M. (2017), Review of the Danian vertebrate fauna of southern Scandinavia., *Bulletin of the Geological Society of Denmark* **65**(1).

Afsari, S., Yazdi, M., Bahrami, A. and Carnevale, G. (2014), A new deep-sea hatchetfish (Teleostei: Stomiiformes: Sternoptychidae) from the Eocene of Ilam, Zagros Basin, Iran., *Bollettino Della Societa Paleontologica Italiana* **53**(1), 27–37.

Akaike, H. (1974), A new look at the statistical model identification, *IEEE transactions on automatic control* **19**(6), 716–723.

Alaniz-Galvan, A. (2011), Primer registro de perciformes fósiles paleocénicos de Palenque, *Chiapas, México* .

Alaniz-Galvan, A. and Alvarado-Ortega, J. (2011), Un 'Serranido' del Paleoceno de Palenque, Chiapas, y sus implicaciones en la comprensión de la evolución de los Percomorfos, *in* XII Congreso Nacional de Paleontología; Sociedad Mexicana de Paleontología; Libro de Resúmenes, 22–25 February 2011, Puebla, Mexico. Edificio Carolino, Benemérita Universidad Autónoma de Puebla Puebla, México, pp. 22–25.

Alfaro, M. E., Faircloth, B. C., Harrington, R. C., Sorenson, L., Friedman, M., Thacker, C. E., Oliveros, C. H., Černỳ, D. and Near, T. J. (2018), Explosive diversification of marine fishes at the Cretaceous–Palaeogene boundary, *Nature ecology & evolution* p. 1.

Alfaro, M. E., Santini, F., Brock, C., Alamillo, H., Dornburg, A., Rabosky, D. L., Carnevale, G. and Harmon, L. J. (2009), Nine exceptional radiations plus high turnover explain species diversity in jawed vertebrates, *Proceedings of the National Academy of Sciences* **106**(32), 13410–13414.

Alfaro, M. and Santini, F. (2010), A flourishing of fish forms, **464**, 840–842.

Allis, E. P. (1903), The skull and the cranial and first spinal muscles and nerves in *Scomber Scomber*.

Alroy, J. (1999), The fossil record of North American Mammals: Evidence for a Paleocene Evolutionary Radiation, *Systematic biology* **48**(1), 107–118.

Alvarado-Ortega, J., Cuevas-García, M., del Pilar Melgarejo-Damián, M., Cantalice, K. M., Alaniz-Galvan, A., Solano-Templos, G. and Than-Marchese, B. A. (2015), Paleocene fishes from Palenque, Chiapas, southeastern Mexico, *Palaeontologia Electronica* **18**(2), 1–22.

Anderson, P. S., Friedman, M., Brazeau, M. D. and Rayfield, E. J. (2011), Initial radiation of jaws demonstrated stability despite faunal and environmental change, *Nature* **476**(7359), 206.

Arambourg, C. (1927), Les poissons fossiles d'Oran., *Materiaux Pour la Carte Geologique de L'Algerie, 1re Serie: Paleontologie* **6**, 1–298.

Arambourg, C. (1943), Note preliminaire sur quelques Poissons fossiles nouveaux, *Bulletin de la Société Géologique de France* **43**, 281–288.

Arambourg, C. (1967), Résultats scientifiques de la mission C. Arambourg en Syrie et en Iran:(1938-1939)., *Les poissons oligocènes de l'Iran.* **2**.

Arambourg, C. and Signeux, J. (1952), Les vértébres fossiles des gisements de phosphates (Maroc - Algérie - Tunisie), *Mémoires du Service Géologique Marocco* **92**, 1–372.

Arratia, G. and Cione, A. (1996), The record of fossil fishes of southern South America, *Münchner Geowissenschaftliche Abhandlungen* **30**, 9–72.

Arratia, G., López-Arbarello, A., Prasad, G. V., Parmar, V. and Kriwet, J. (2004), Late Cretaceous-Paleocene percomorphs (Teleostei) from India-early radiation

of perciformes, *Recent Advances in the Origin and Early Radiation of Vertebrates* pp. 635–663.

Baciu, D. and Bannikov, A. (2003), *Paucaichthys neamtensis* gen. et sp. nova-the First Discovery of Sea Breams (Bramidae) in the Oligocene of Romania, *Journal of Ichthyology* **43**(8), 598–602.

Baldwin, B. G. and Sanderson, M. J. (1998), Age and rate of diversification of the Hawaiian silversword alliance (Compositae), *Proceedings of the National Academy of Sciences* **95**(16), 9402–9406.

Bannikov, A. F. (1981), Sistematicheskoye polozheniya sostav i proiskhozhdenikye semeystva. Scombridae., *Voprosy Ikhtiologii* **21**, 200–208.

Bannikov, A. F. (1985), Iskopayemye skumbrievye SSSR [Fossil scombrids of the USSR], *Trudy Paleontologicheskogo Instituta: Akademiya Nauk SSSR* **210**, 1–111.

Bannikov, A. F. (1996), The list of marine fishes from Cenozoic (upper Paleocene-middle Miocene) localities in southern European Russia and adjacent countries., *Journal of Ichthyology* **37**, 133–146.

Bannikov, A. F. (2000*a*), *Fossil vertebrates of Russia and adjacent countries: Fossil Spiny Rayed Fishes (Teleostei, Acanthopterygii)*, GEOS, Moscow. [in Russian].

Bannikov, A. F. (2000*b*), New Data on Late Paleocene Marine Percoids (Perciformes) of Turkmenistan, *Journal of Ichthyology* **40**(8), 564–570.

Bannikov, A. F. (2000*c*), A new genus and species of putative centrolophid fish (Perciformes, Stromateoidei) from the Eocene of Bolca, northern Italy., *Bollettino del Museo Civico di Storia Naturale di Verona* **24**, 37–46.

Bannikov, A. F. (2005), A new species of the snake mackerel genus *Abadzekhia* (Perciformes, Gempylidae) from the lower Oligoene of the Northern Caucasus., *Paleontologicheskii Zhurnal* **1**, 65–68.

Bannikov, A. F. (2012), The first record of the genus *Isurichthys* (Perciformes, Ariommatidae) in the lower Oligocene of the northern Caucasus., *Paleontological Journal* **46**(2), 171–176.

Bannikov, A. F. (2017), New data on the morphology of the snake mackerel *Abadzekhia tarletskovi* Bannikov (Perciformes, Gempylidae) from the Lower Oligocene of the Northern Caucasus., *Paleontological Journal* **39**(1), 62–65.

Bannikov, A. F. (2018), A New Genus and Species of Stromateoid Fishes (Perciformes, Stromateoidei) from the Lower Oligocene of the Northern Caucasus, *Paleontological Journal* **52**(6), 631–638.

Bannikov, A. F. and Fedotov, V. F. (1989), On the taxonomic position of the Perciform Genera *Lednevia* and *Abadzekhia* from the Maikopian of the Southern USSR., *Byulleten, Moskovskogo Obschestva Ispytateliy Prirody, Odtel Geologicheskii* **64**, 85–90.

Bannikov, A. F. and Parin, N. V. (1995), Description of the new species of scabbardfish (Aphanopinae: Trichiuridae) from the Middle Eocene of the northern Caucasus, with restoration of the validity of the fossil genus *Anenchelum.*, *Journal of Ichthyology* **35**, 183–192.

Bannikov, A. F. and Tyler, J. C. (2004), A revision of the Eocene fish family Exellidae (Perciformes)., *Paleontological Journal* **27**, 128–140.

Bannikov, A. and Sorbini, C. (2000), Preliminary note on a lower Paleocene fish fauna from Trebiciano (Trieste–North-Eastern Italy), *Atti del Museo civico di storia naturale di Trieste* **48**, 15–30.

Bapst, D. W. (2012), paleotree: an R package for paleontological and phylogenetic analyses of evolution., *Methods in Ecology and Evolution* **3**, 803–807.

Beckett, H. T. and Friedman, M. (2016), The one that got away from Smith Woodward: cranial anatomy of *Micrornatus* (Acanthomorpha: Scombridae) revealed using computed microtomography, *Geological Society, London, Special Publications* **430**.
URL: *http://sp.lyellcollection.org/cgi/doi/10.1144/SP430.16*

Beckett, H. T., Giles, S., Johanson, Z. and Friedman, M. (2018), Morphology and phylogenetic relationships of fossil snake mackerels and cutlassfishes (Trichiuroidea) from the Eocene (Ypresian) London Clay Formation., *Papers in Palaeontology* .

Benson, R. B., Butler, R. J., Lindgren, J. and Smith, A. S. (2009), Mesozoic marine tetrapod diversity: mass extinctions and temporal heterogeneity in geological megabiases affecting vertebrates, *Proceedings of the Royal Society of London B: Biological Sciences* p. rspb20091845.

Betancur-R, R., Broughton, R. E., Wiley, E. O., Carpenter, K., López, J. A., Li, C., Holcroft, N. L., Arcila, D., Sanciangco, M., Cureton II, J. C., Zhang,

F., Buser, T., Campbell, M. A., Ballesteros, J. A., Roa-varon, A., Willis, S., Borden, W. C., Rowley, T., Reneau, P. C., Hough, D. J., Lu, G., Grande, T., Arratia, G. and Orti, G. (2013), The Tree of Life and a New Classification of Bony Fishes, *PLOS Currents Tree of Life* (0732988).

Betancur-R, R., Wiley, E. O., Arratia, G., Acero, A., Bailly, N., Miya, M., Lecointre, G. and Orti, G. (2017), Phylogenetic classification of bony fishes, *BMC evolutionary biology* **17**(1), 162.

Blainville, H. D. D. (1818), Sur les ichthyolites ou les poissons fossiles, *in* Nouveau dictionnaire d'histoire naturelle, Vol. 27, Deterville, Paris, pp. 310–395.

Block, B. A., Finnerty, J. R., Stewart, A. F. and Kidd, J. (1993), Evolution of endothermy in fish: mapping physiological traits on a molecular phylogeny, *Science* **260**, 210–214.

Blomberg, S. P., Garland, T. and Ives, A. R. (2003), Testing for phylogenetic signal in comparative data: behavioral traits are more labile, *Evolution* **57**(4), 717–745.

Blot, J. (1969), *Les poissons fossiles du Monte Bolca: classés jusqu'ici dans les familles des Carangidae, Menidae, Ephippidae, Scatophagidae*, Vol. 1, Museo Civico di Storia Naturale di Verona.

Bonde, N. (2008), Osteoglossomorphs of the marine Lower Eocene of Denmark–with remarks on other Eocene taxa and their importance for palaeobiogeography., *Geological Society, London, Special Publications* **295**, 253–310.

Bonde, N., Anderson, S., Hald, N. and Jakobsen, S. (2008), *Danaekræ - Denmark's best fossils [in danish]*, Vol. 226pp, Gyldendal, Copenhagen.

Briggs, D. E. G. and Gall, J.-C. (1990), The continuum in soft-bodied biotas from transitional environments: a quantitative comparison of Triassic and Carboniferous Konservat-Lagerstätten, *Paleobiology* **16**(2), 204–218.

Brusatte, S. L., Benton, M. J., Ruta, M. and Lloyd, G. T. (2008), Superiority, competition, and opportunism in the evolutionary radiation of dinosaurs, *Science* **321**(5895), 1485–1488.

Brusatte, S. L., Nesbitt, S. J., Irmis, R. B., Butler, R. J., Benton, M. J. and Norell, M. A. (2010), The origin and early radiation of dinosaurs, *Earth-Science Reviews* **101**(1-2), 68–100.

Burnham, K. P. and Anderson, D. R. (2003), *Model selection and multimodel inference: a practical information-theoretic approach*, Springer Science & Business Media.

Butler, M. A. and King, A. A. (2004), Phylogenetic comparative analysis: a modeling approach for adaptive evolution, *The American Naturalist* **164**(6), 683–695.

Butler, R. J., Benson, R. B. and Barrett, P. M. (2013), Pterosaur diversity: untangling the influence of sampling biases, Lagerstätten, and genuine biodiversity signals, *Palaeogeography, Palaeoclimatology, Palaeoecology* **372**, 78–87.

Campbell, M. A., Sado, T., Shinzato, C., Koyanagi, R., Okamoto, M. and Miya, M. (2018), Multilocus phylogenetic analysis of the first molecular data from the rare and monotypic Amarsipidae places the family within the Pelagia and highlights limitations of existing data sets in resolving pelagian interrelationships, *Molecular phylogenetics and evolution* **124**, 172–180.

Cantalapiedra, J., Prado, J., Fernández, M. H. and Alberdi, M. (2017), Decoupled ecomorphological evolution and diversification in Neogene-Quaternary horses, *Science* **355**(6325), 627–630.

Cantalice, K. M. and Alvarado-Ortega, J. (2016), *Eekaulostomus cuevasae* gen. and sp. nov., an ancient armored trumpetfish (Aulostomoidea) from Danian (Paleocene) marine deposits of Belisario Domínguez, Chiapas, southeastern Mexico, *Palaeontologia Electronica* **18**(3), 1–24.

Cantalice, K. M. and Alvarado-Ortega, J. (2017), *Kelemejtubus castroi*, gen. et sp. nov., an ancient percomorph (Teleostei, Actinopterygii) from the Paleocene marine deposits near Palenque, Chiapas, southeastern Mexico, *Journal of Vertebrate Paleontology* p. e1383265.

Cantalice, K. M., Alvarado-Ortega, J. and Alaniz-Galvan, A. (2018), *Paleoserranus lakamhae* gen. et sp. nov., a Paleocene seabass (Perciformes: Serranidae) from Palenque, Chiapas, southeastern Mexico, *Journal of South American Earth Sciences* **83**, 137–146.

Carnevale, G. (2006), A new snake mackerel from the Miocene of Algeria, *Palaeontology* **49**, 391–403.

Carnevale, G. (2007), Fossil fishes from the Serravallian (Middle Miocene) of Torricella Peligna, Italy, *Palaeontographia Italica* **91**, 1–67.

Carnevale, G. and Collette, B. B. (2014), † *Zappaichthys harzhauseri*, gen. et sp. nov., a new Miocene toadfish (Teleostei, Batrachoidiformes) from the Paratethys (St. Margarethen in Burgenland, Austria), with comments on the fossil record of batrachoidiform fishes, *Journal of Vertebrate Paleontology* **34**(5), 1005–1017.

Carnevale, G. and Johnson, G. D. (2015), A Cretaceous cusk-eel (Teleostei, Ophidiiformes) from Italy and the Mesozoic diversification of percomorph fishes, *Copeia* **103**(4), 771–791.

Carpenter, K. E., Collette, B. B. and Russo, J. L. (1995), Unstable and stable classifications of scombroid fishes., *Bulletin of Marine Science* **56**, 379–405.

Casier, E. (1944), Contributions à l'étude des poissons fossiles de la Belgique. V. – Les genres *Trichiurides* Winkler (s.str.) et *Eutrichiurides* nov., leurs affinites respectives., *Bulletin du Musée royal d'histoire naturelle de Belgique,* **20**, 1–9.

Casier, E. (1946), La faune ichthyologique de l'Yprésien de la Belgique., *Mémoires du Musee royal d'histoire naturelle de Belgique* **104**, 1–267.

Casier, E. (1966), *Faune icthyologique du London Clay: Atlas*, Vol. 2, British Museum (Natural History).

Cavin, L. (1999), Occurrence of a juvenile teleost, *Enchodus* sp., in a fish gut content from the Upper Cretaceous of Goulmima, Morocco, *Special Papers in Palaeontology* **60**, 57–72.

Cavin, L. (2002), Effects of the Cretaceous-Tertiary boundary event on bony fishes, *in* Geological and biological effects of impact events, Springer, pp. 141–158.

Cavin, L. and Forey, P. L. (2007), Using ghost lineages to identify diversification events in the fossil record, *Biology Letters* **3**(2), 201–204.

Clarke, J. T. and Friedman, M. (2018), Body-shape diversity in Triassic–Early Cretaceous neopterygian fishes: sustained holostean disparity and predominantly gradual increases in teleost phenotypic variety, *Paleobiology* pp. 1–32.

Clavel, J., Escarguel, G. and Merceron, G. (2015), mvMORPH: an R package for fitting multivariate evolutionary models to morphometric data, *Methods in Ecology and Evolution* **6**(11), 1311–1319.

Collette, B. B. (1999), Mackerels, molecules, and morphology, *5th Indo-Pac Fish Conference Noumea* pp. 149–164.

Collette, B. B. and Chao, L. N. (1975), Systematics and morphology of the Bonitos (Sarda) and their relatives (Scombridae, Sardini), *Fishery Bulletin* **73**(3), 516–625.

Collette, B. B. and Gillis, G. (1992), Morphology, systematics, and biology of the double-lined mackerels (Grammatorcynus, Scombridae), *Fishery Bulletin* **92**, 13–53.

Collette, B. B., Potthoff, T., Richards, W. J., Ueyanagi, S., Russo, J. L., Nishikawa, Y. and Moser, H. G. (1984), Scombroidei: Development and Relationships, *in* H. G. Moser, W. J. Richards, D. M. Cohen, M. P. Fahay, A. W. Kendall and S. L. Richardson, eds, Ontogeny and Systematics of Fishes, Vol. Spec. Pub. 1, American Society of Ichthyologists and Herpetologists, pp. 591–620.

Collette, B. B., Reeb, C. and Block, B. A. (2001), Systematics of the tunas and mackerels (Scombridae), *in* B. A. Block and D. E. Stevens, eds, Tuna: physiology, ecology and evolution, Vol. 19 of *Fish Physiology*, London: Academic Press, pp. 1–33.

Collette, B. B. and Russo, J. L. (1984), Morphology, systematics and biology of the Spanish Mackerels (Scomberomorus, Scombridae), *Fishery Bulletin* **82**(4), 545–692.

Daniltshenko, P. G. (1960), Bony fishes of the Maikop deposits of the Caucasus., *Trudy Paleontologicheskogo Instituta: Akademiya Nauk SSSR* **78**, 3–207.

Daniltshenko, P. G. (1962), Fishes of the Dabakhanskaya formation of Georgia., *Paleontologicheskii Zhurnal* **1**, 111–126.

Daniltshenko, P. G. (1980), Order Perciformes, *in* L. I. Novitskaya, ed., Iskopayemye kostistye ryby SSSR, Vol. 178, Trudy Paleontologicheskogo Instituta Akademii Nauk SSSR, pp. 115–169.

Dartevelle, E. and Casier, E. (1943), Les Poissons fossils du Bas-Congo et des regions voisines, *Annales du Musée du Congo Belge* **1**, 1–200.

Dartevelle, E. and Casier, E. (1949), Les poissons fossiles du Bas-Congo et des régions voisines., *Annales du Musée du Congo Belge* **2**, 201–256.

Dartevelle, E. and Casier, E. (1959), Les poissons fossiles du Bas-Congo et des régions voisines., *Annales du Musée du Congo Belge* **3**, 257–568.

Davesne, D., Friedman, M., Barriel, V., Lecointre, G., Janvier, P., Gallut, C. and Otero, O. (2014), Early fossils illuminate character evolution and interrelationships of Lampridiformes (Teleostei, Acanthomorpha), *Zoological Journal of the Linnean Society* **172**(2), 475–498.

David, L. R. (1943), Miocene fishes of southern California, *Geol. Soc. Am. Spec. Pap.* **43**, 1–193.

Davis, J. W. (1890), On the fossil fish of the Cretaceous formations of Scandinavia., *Scientific Transactions of the Royal Dublin Society* **4**.

Derrickson, E. and Ricklefs, R. (1988), Taxon-dependent diversification of life-history traits and the perception of phylogenetic constraints, *Functional Ecology* pp. 417–423.

Dietze, K. (2009), Morphology and phylogenetic relationships of certain neoteleostean fishes from the Upper Cretaceous of Sendenhorst, Germany, *Cretaceous Research* **30**(3), 559–574.

Doiuchi, R., Sato, T. and Nakabo, T. (2004), Phylogenetic relationships of the stromateoid fishes (Perciformes), *Ichthyological Research* **51**(3), 202–212.

Drummond, A. J. and Rambaut, A. (2007), BEAST: Bayesian evolutionary analysis by sampling trees, *BMC evolutionary biology* **7**(1), 214.

Ekrt, B., Košt'ák, M., Mazuch, M., Voigt, S. and Wiese, F. (2008), New records of teleosts from the late Turonian (Late Cretaceous) of the Bohemian Cretaceous Basin (Czech Republic), *Cretaceous Research* **29**(4), 659–673.

Erwin, D. H. (2001), Lessons from the past: biotic recoveries from mass extinctions, *Proceedings of the National Academy of Sciences* **98**(10), 5399–5403.

Erwin, D. H. (2015), Novelty and innovation in the history of life, *Current Biology* **25**(19), R930–R940.

Estes, S. and Arnold, S. J. (2007), Resolving the paradox of stasis: models with stabilizing selection explain evolutionary divergence on all timescales, *The American Naturalist* **168**(2), 227–244.

Farrell, B. D. and Sequeira, A. S. (2004), Evolutionary rates in the adaptive radiation of beetles on plants, *Evolution* **58**(9), 1984–2001.

Felsenstein, J. (1985), Phylogenies and the comparative method, *The American Naturalist* **125**(1), 1–15.

Fierstine, H. L., Huddleston, R. W. and Takeuchi, G. T. (2012), *Catalog of the Neogene bony fishes of California: A systematic inventory of all published accounts*, California Academy of Sciences.

Fink, W. L. (1981), Ontogeny and Phylogeny of Tooth Attachment Modes in Actinopterygian Fishes, *Journal of Morphology* **167**(2), 167–184.

Finnerty, J. R. and Block, B. A. (1995), Evolution of cytochrome b in the Scombroidei (Teleostei): molecular insights into billfish (Istiophoridae and Xiphiidae) relationships, *Fishery Bulletin* **93**, 78–96.

Foote, M. (1994), Morphological disparity in Ordovician-Devonian crinoids and the early saturation of morphological space, *Paleobiology* **20**(3), 320–344.

Foote, M. (1997), The evolution of morphological diversity, *Annual Review of Ecology and Systematics* **28**(1), 129–152.

Forey, P. L., Yi, L., Patterson, C. and Davies, C. E. (2003), Fossil fishes from the Cenomanian (Upper Cretaceous) of Namoura, Lebanon, *Journal of Systematic Palaeontology* **1**(4), 227–330.

Friedman, M. (2008), The evolutionary origin of flatfish asymmetry., *Nature* **454**(7201), 209–212.

Friedman, M. (2009), Ecomorphological selectivity among marine teleost fishes during the end-Cretaceous extinction., *Proceedings of the National Academy of Sciences of the United States of America* **106**(13), 5218–23.

Friedman, M. (2010), Explosive morphological diversification of spiny-finned teleost fishes in the aftermath of the end-Cretaceous extinction., *Proceedings. Biological sciences / The Royal Society* **277**(1688), 1675–83.

Friedman, M. (2012), Ray-finned fishes (Osteichthyes, Actinopterygii) from the type Maastrichtian, the Netherlands and Belgium, *Scripta Geologica Special Issue* pp. 113–142.

Friedman, M., Beckett, H. T., Close, R. A. and Johanson, Z. (2015), The English Chalk and London Clay: two remarkable British bony fish *Lagerstätten*, *Geological Society, London, Special Publications* **430**.

Friedman, M., Beckett, H. T., Close, R. A. and Johanson, Z. (2016), The English chalk and London Clay: two remarkable British bony fish Lagerstätten, *Geological Society, London, Special Publications* **430**(1), 165–200.

Friedman, M. and Carnevale, G. (2018), The Bolca Lagerstätten: shallow marine life in the Eocene, *Journal of the Geological Society* pp. 1–164.

Friedman, M., Harrington, R. C., Beckett, H. T., Feilich, K., Near, T. J., Alfaro, M. E., Faircloth, B. C., Cerny, D. and Miya, M. (Submitted), Ancient diversification in the open ocean: phylogenomic analysis reveals rapid divergences in Pelagiaria (Acanthomorpha: Percomorpha) near the Cretaceous-Paleogene boundary, *Proceedings of the Royal Society B* .

Friedman, M. and Johnson, G. (2005), A new species of Mene (Perciformes: Menidae) from the Paleocene of South America, with notes on paleoenvironment and a brief review of menid fishes, *Journal of Vertebrate Paleontology* **25**(December), 770–783.

Friedman, M. and Sallan, L. C. (2012), Five hundred million years of extinction and recovery: a phanerozoic survey of largescale diversity patterns in fishes, *Palaeontology* **55**(4), 707–742.

Friedman, M., Shimada, K., Everhart, M. J., Irwin, K. J., Grandstaff, B. S. and Stewart, J. D. (2013a), Geographic and stratigraphic distribution of the Late Cretaceous suspension-feeding bony fish *Bonnerichthys gladius* (Teleostei, Pachycormiformes), *Journal of Vertebrate Paleontology* **33**(1), 35–47.

Fujita, K. (1990), *The caudal skeleton of teleostean fishes*, Tokai University Press, Tokyo, 897 pp.

Gago, F. J. (1997), Character evolution and phylogeny of the cutlassfishes, an ontogenetic perspective (Scombroidei: Trichiuridae), *Bulletin of Marine Science* **60**(1), 161–191.

Gago, F. J. (1998), Osteology and Phylogeny of the Cutlassifshes (Scombroidei: Trichiuridae), *Contributions in Science* **476**, 1–79.

Gavrilets, S. and Losos, J. B. (2009), Adaptive radiation: contrasting theory with data, *Science* **323**(5915), 732–737.

Gayet, M. (1991), "Holostean" and teleostean fishes of Bolivia, *Revista Técnica de YPFB* **12**(3-4), 453–494.

Gayet, M. and Meunier, F. J. (1998), Maastrichtian to early late Paleocene freshwater Osteichthyes of Bolivia: additions and comments, *Phylogeny and classification of Neotropical fishes* pp. 85–110.

Gibbs, R. H. and Collette, B. B. (1967), Comparative anatomy and systematics of the tunas, genus Thunnus, *Fish Bull* **66**(1), 65–130.

Gill, T. N. (1862), On the limits and arrangements of the family of scombroids., *Proceedings of the Academy of Natural Sciences of Philadelphia* **14**, 124–127.

Gillespie, R. (2004), Community assembly through adaptive radiation in Hawaiian spiders, *Science* **303**(5656), 356–359.

Giusberti, L., Bannikov, A. F., Galazzo, F. B., Fornaciari, E., Frieling, J., Luciani, V., Papazzoni, C. A., Roghi, G., Schouten, S., Sluijs, A., Bosellini, F. R. and Zorzin, R. (2014), A new Fossil-Lagerstätte from the Lower Eocene of Lessini Mountains (northern Italy): a multidisciplinary approach., *Palaeogeography, Palaeoclimatology, Palaeoecology* **403**, 1–15.

Givnish, T. J. and Sytsma, K. J. (2000), *Molecular evolution and adaptive radiation*, Cambridge University Press.

Glor, R. E. (2010), Phylogenetic insights on adaptive radiation, *Annual Review of Ecology, Evolution, and Systematics* **41**, 251–270.

Gosline, W. A. (1968), The suborders of perciform fishes., *Proceedings of the United States National Museum* **3647**, 1–78.

Gradstein, F. M., Ogg, G. and Schmitz, M. (2012), *The Geological Timescale 2012*, Vol. 2-Volume set, Elsevier.

Grant, B. R. and Grant, P. R. (2008), Fission and fusion of Darwin's finches populations, *Philosophical Transactions of the Royal Society of London B: Biological Sciences* **363**(1505), 2821–2829.

Gregorova, R. (2010), Osteological and morphological analysis of the scabbardfish *Anenchelum glarisianum* BLAINVILLE, 1818 (Trichiuridae) from the Menilitic Formation of the Moravian part of West Carpathians (Oligocene, Rupelian)., *Acta Musei Moraviae, Scientiae Geologicae* **95**, 141–149.

Grey, M. (1955), The fishes of the genus *Tetragonurus* Risso., *Dana-Rep.* pp. 1–75.

Grey, M. (1960), Description of a western Atlantic specimen of Scombrolabrax heterolepis Roule and notes on fishes of the family Gempylidae, *Copeia* **1960**(3), 210–215.

Haedrich, R. L. (1967), The stromateoid fishes: systematics and a classification, *Bulletin of the Museum of Comparative Zoology* **135**, 31–139.

Hansen, T. F. (1997), Stabilizing selection and the comparative analysis of adaptation, *Evolution* **51**(5), 1341–1351.

Hansen, T. F. and Houle, D. (2004), Evolvability, stabilizing selection, and the problem of stasis, *Phenotypic integration: Studying the ecology and evolution of complex phenotypes* pp. 130–150.

Harmon, L. J. (2018), *Phylogenetic Comparative Methods: learning from trees*, https://lukejharmon.github.io/pcm/.

Harmon, L. J., Losos, J. B., Jonathan Davies, T., Gillespie, R. G., Gittleman, J. L., Bryan Jennings, W., Kozak, K. H., McPeek, M. A., Moreno-Roark, F.,

Near, T. J. and Purvis, A. (2010), Early bursts of body size and shape evolution are rare in comparative data., *Evolution* **64**(8), 2385–2396.

Harmon, L. J., Schulte, J. A., Larson, A. and Losos, J. B. (2003), Tempo and mode of evolutionary radiation in iguanian lizards, *Science* **301**(5635), 961–964.

Harmon, L., Weir, J., Brock, C., Glor, R. and Challenger, W. (2008), GEIGER: investigating evolutionary radiations, *Bioinformatics* **24**, 129–131.

Harrington, R. C., Faircloth, B. C., Eytan, R. I., Smith, W. L., Near, T. J., Alfaro, M. E. and Friedman, M. (2016), Phylogenomic analysis of carangimorph fishes reveals flatfish asymmetry arose in a blink of the evolutionary eye, *BMC evolutionary biology* **16**(1), 224.

Heath, T. a., Huelsenbeck, J. P. and Stadler, T. (2014), The fossilized birth-death process for coherent calibration of divergence-time estimates, *Proceedings of the National Academy of Sciences* **111**(29), E2957–2966.

Huelsenbeck, J. P. and Ronquist, F. (2001), MRBAYES: Bayesian inference of phylogenetic trees, *Bioinformatics* **17**(8), 754–755.

Hull, P. (2015), Life in the aftermath of mass extinctions, *Current Biology* **25**(19), R941–R952.

Hunn, C. A. and Upchurch, P. (2001), The importance of time/space in diagnosing the causality of phylogenetic events: towards a 'chronobiogeographical'paradigm?, *Systematic Biology* **50**(3), 391–407.

Hunt, G., Bell, M. A. and Travis, M. P. (2008), Evolution toward a new adaptive optimum: phenotypic evolution in a fossil stickleback lineage, *Evolution* **62**(3), 700–710.

Hunt, G. and Rabosky, D. L. (2014), Phenotypic Evolution in Fossil Species: Pattern and Process, *Annual Review of Earth and Planetary Sciences* **42**(1), 421–441.

Jackson, J. B. and Cheetham, A. H. (1999), Tempo and mode of speciation in the sea, *Trends in Ecology & Evolution* **14**(2), 72–77.

Jawad, L. A. and Jig, L. (2017), Comparative osteology of the axial skeleton of the genus Pampus (Family: Stromateidae, Perciformes), *Journal of the Marine Biological Association of the United Kingdom* **97**(2), 277–287.

Johnson, G. D. (1986), Scombroid Phylogeny: an alternative hypothesis, *Bulletin of Marine Science* **39**(1), 1–41.

Johnson, G. D. and Patterson, C. (1993), Percomorph phylogeny: a survey of acanthomorphs and a new proposal, *Bulletin of Marine Science* **52**(1), 554–626.

Kocher, T. D. (2004), Adaptive evolution and explosive speciation: The cichlid fish model, *Nature Reviews Genetics* **5**(4), 288–298.

Kohno, H. (1984), Osteology and Systematic Position of the Butterfly Mackerel, Gasterochisma melampus, *Japenese Journal of Ichthyology* **31**(3), 268–286.

Komori, K. (1993), Osteological development of ragfish (*Icosteus aenigmaticus* Lockington)., PhD thesis, Humboldt State Univ., Arcata, Calif, MS Thesis, 116 p.

Kriwet, J. and Benton, M. J. (2004), Neoselachian (chondrichthyes, elasmobranchii) diversity across the cretaceous–tertiary boundary, *Palaeogeography, Palaeoclimatology, Palaeoecology* **214**(3), 181–194.

Ksepka, D. T., Stidham, T. A. and Williamson, T. E. (2017), Early Paleocene landbird supports rapid phylogenetic and morphological diversification of crown birds after the K–Pg mass extinction, *Proceedings of the National Academy of Sciences* p. 201700188.

Kukuev, E., Parin, N. and Trunov, I. (2012), Materials for the revision of the Family Caristiidae (Perciformes). 2. Manefishes from the East Atlantic (Redescription of Platyberyx opalescens Zugmayer and description of two new species Platyberyx mauli sp. n. and Caristius andriashevi sp. n.), *Journal of Ichthyology* **52**(3), 185–199.

Kukuev, E., Parin, N. and Trunov, I. (2013), Materials for the revision of the family Caristiidae (Perciformes): 3. Manefishes (genus Caristius) from moderate warm waters of the Pacific and Atlantic oceans with a description of three new species from the southeast Atlantic (C. barsukovi sp. n., C. litvinovi sp. n., C. walvisensis sp. n.), *Journal of ichthyology* **53**(8), 541–561.

Kumar, K., Rana, R. and Paliwal, B. (2005), Osteoglossid and lepisosteid fish remains from the Paleocene Palana Formation, Rajasthan, India, *Palaeontology* **48**(6), 1187–1209.

Kumar, K., Rana, R. S. and Singh, H. (2007), Fishes of the Khuiala Formation (Early Eocene) of the Jaisalmer Basin, Western Rajasthan, India, *Current Science* pp. 553–559.

Landini, W. and Sorbini, L. (1992), Données récentes sur les téléostéens du Miocene et du Pliocéne d'Italie, *Geobios* **25**, 151–157.

Last, P. and Moteki, M. (2001), Bramidae, *FAO species identification guide for fishery purposes. The living marine resources of the Western Central Pacific* **5**, 2824–2836.

Leapley, W. T. (1952), The cranial osteology of the Blue-fish: *Pomatomus saltatrix* (Linnaeus)., PhD thesis, Unpublished PhD Dissertation, The George Washington University, Washington DC, 65pp, 3pl.

Leriche, M. (1905), Les Poissons Eocenes de la Belgique., *Mémoires du Musée royal d'histoire naturelle de Belgique* **11**(3), 51–228.

Leriche, M. (1910), Les poissons Oligocènes de la Belgique., *Mémoires du Mus ee Royal d'Histoire Naturelle de Belgique* **5**, 1–363.

Lloyd, G. T. and Friedman, M. (2013), A survey of palaeontological sampling biases in fishes based on the Phanerozoic record of Great Britain, *Palaeogeography, Palaeoclimatology, Palaeoecology* **372**, 5–17.

Losos, J. B. (2011), *Lizards in an evolutionary tree: ecology and adaptive radiation of anoles*, Vol. 10, Univ of California Press.

Losos, J. B. and Ricklefs, R. E. (2009), Adaptation and diversification on islands, *Nature* **457**(7231), 830.

Luo, Z.-X., Yuan, C.-X., Meng, Q.-J. and Ji, Q. (2011), A Jurassic eutherian mammal and divergence of marsupials and placentals, *Nature* **476**, 442 EP –.

MacLaren, J. A., Anderson, P. S., Barrett, P. M. and Rayfield, E. J. (2017), Herbivorous dinosaur jaw disparity and its relationship to extrinsic evolutionary drivers, *Paleobiology* **43**(1), 15–33.

Matsui, T. (1967), Review of the mackerel genera *Scomber* and *Rastrelliger* with description of a new species of Rastrelliger, *Copeia* pp. 71–83.

McShea, D. W. (1994), Mechanisms of large-scale evolutionary trends, *Evolution* **48**(6), 1747–1763.

Mead, G. W. (1972), Bramidae, *The Carlsberg Foundation's oceanographical expedition round the World 1928-30 and previous Dana-expeditions. Dana-Report* .

Melo, M. (2009*a*), Taxonomic and Phylogenetic Revision of the Family Chiasmodontidae (Perciformes: Acanthomorpha), PhD thesis, Auburn University.

Melo, M. R. (2009*b*), Revision of the genus *Chiasmodon* (Acanthomorpha: Chiasmodontidae), with the description of two new species, *Copeia* **2009**(3), 583–608.

Melo, M. R. (2010), A revision of the genus *Pseudoscopelus* Lütken (Chiasmodontidae: Acanthomorphata) with descriptions of three new species, *Zootaxa* **2710**, 1–78.

Menner, V. V. (1949), Class Pisces. Fishes., *Atlas Rukovodyashchikh Form Iskopayemykh Faun SSSR* **13**, 346–360.

Milner, A. C. and Walsh, S. A. (2009), Avian brain evolution: new data from Palaeogene birds (Lower Eocene) from England., *Zoological Journal of the Linnean Society* **155**, 198–219.

Miya, M., Friedman, M., Satoh, T. P., Takeshima, H., Sado, T., Iwasaki, W., Yamanoue, Y., Nakatani, M., Mabuchi, K., Inoue, J. G., Poulsen, J. Y., Fukunaga, T., Sato, Y. and Nishida, M. (2013), Evolutionary origin of the scombridae (tunas and mackerels): members of a paleogene adaptive radiation with 14 other pelagic fish families., *PloS one* **8**(9), e73535.

Monsch, K. A. (2000), The phylogeny of the scombroid fishes., PhD thesis, University of Bristol.

Monsch, K. a. (2005), Revision of the scombroid fishes from the Cenozoic of England, *Transactions of the Royal Society of Edinburgh: Earth Sciences* **95**(3-4), 445–489.

Monsch, K. a. and Bannikov, A. F. (2012), New taxonomic synopses and revision of the scombroid fishes (Scombroidei, Perciformes), including billfishes, from the Cenozoic of territories of the former USSR, *Earth and Environmental Science Transactions of the Royal Society of Edinburgh* **102**(04), 253–300.

Müller, J. (1845), Über den Bau und die Grenzen der Ganoiden, und über das natürliche System der Fische, *Arch Naturgesch* **11**(91-141).

Murrell, D. J. (2018), A global envelope test to detect non-random bursts of trait evolution, *Methods in Ecology and Evolution* .

Nakamura, I. (1983), Systematics of the billfishes (Xiphiidae and Istiophoridae), *Publications of the Seto Marine Biological Laboratory* **28**, 255–396.

Nakamura, I. and Parin, N. V. (1993), Snake mackerels and cutlassfishes of the world, *FAO Fisheries Synopsis* **15**(125).

Near, T. J., Dornburg, A., Eytan, R. I., Keck, B. P., Smith, W. L., Kuhn, K. L., Moore, J. a., Price, S. a., Burbrink, F. T., Friedman, M. and Wainwright, P. (2013), Phylogeny and tempo of diversification in the superradiation of spiny-rayed fishes, *Proceedings of the National Academy of Sciences of the United States of America* **110**(31), 12738–12743.

Near, T. J., Eytan, R. I., Dornburg, A., Kuhn, K. L., Moore, J. A., Davis, M. P., Wainwright, P. C., Friedman, M. and Smith, W. L. (2012), Resolution of ray-finned fish phylogeny and timing of diversification, *Proceedings of the National Academy of Sciences* **109**(34), 13698–13703.

Nelson, J. (2006), *Fishes of the World*, John Wiley & Sons.

Nolf, D. and Stringer, G. L. (1996), Cretaceous fish otoliths – a synthesis of the North American record., *in* G. Arratia and G. Viohl, eds, Mesozoic fishes: systematics and paleoecology., Friedrich Pfeil, Munich., pp. 433–459.

Nowak, R. M. and Walker, E. P. (1999), *Walker's Mammals of the World*, Vol. 1, JHU Press.

Ohe, F. (1993), Deep fish assemblage from the Middle Miocene Morozaki group, southern part of Chita Peninsula, Aichi Prefecture, central Japan, *in* Fossils from the Miocene Morozaki Group, Nagoya, Japan, The Tokai Fossil Society, pp. 199–262.

O'Leary, M. A., Bloch, J. I., Flynn, J. J., Gaudin, T. J., Giallombardo, A., Giannini, N. P., Goldberg, S. L., Kraatz, B. P., Luo, Z.-X., Meng, J. et al. (2013), The placental mammal ancestor and the post–K-Pg radiation of placentals, *Science* **339**(6120), 662–667.

Olsen, A. and Westneat, M. (2015), StereoMorph: an R package for the collection of 3D landmarks and curves using a stereo camera set-up, *Methods in Ecology and Evolution* **6**, 351–356.

O'Meara, B. C., Ané, C., Sanderson, M. J. and Wainwright, P. C. (2006), Testing for different rates of continuous trait evolution using likelihood, *Evolution* **60**(5), 922–933.

Orrell, T. M., Collette, B. B. and Johnson, G. D. (2006), Molecular data support separate scombroid and xiphioid clades, *Bulletin of Marine Science* **79**(3), 505–519.

Osborn, H. F. (1893), The Rise of the Mammalia in North America., *Proceedings of the American Association for the Advancement of Sciences* **42**, 187–227.

Osborn, H. F. (1899), The Origin of Mammals, *American Journal of Science (1880-1910)* **7**(38), 92.

Osborn, H. F. (1902), The Law of Adaptive Radiation, *The American Naturalist* **36**(425), 353–363.

Owen, R. (1854), *Descriptive catalogue of the Fossil Organic Remains of Reptilia and Pisces contained in the Museum of the Royal College of Surgeons of England.*, Taylor and Francis, London.

Pagel, M. (1998), Inferring evolutionary processes from phylogenies, *Zoologica Scripta* **26**(4), 331–348.

Pagel, M. (1999), Inferring the historical patterns of biological evolution, *Nature* **401**(6756), 877.

Palci, A., Jurkovšek, B., Kolar-Jurkovšek, T. and Caldwell, M. W. (2008), New palaeoenvironmental model for the Komen (Slovenia) Cenomanian (Upper Cretaceous) fossil lagerstätte, *Cretaceous Research* **29**(2), 316–328.

Paradis, E., Claude, J. and Strimmer, K. (2004), APE: analyses of phylogenetics and evolution in R language, *Bioinformatics* **20**, 289–290.

Parin, N. V. and Astakhov, D. A. (2007), New fossil fish *Musculopedunculus micklichi* (Trichiuroidei) from the Lower Oligocene of Germany., *Journal of Ichthyology* **47**, 547–554.

Parin, N. V. and Becker, V. E. (1972), Materials on taxonomy and distribution of some trichiuroid fishes (Pisces, Trichiuroidae: Scombrolabracidae, Gempylidae, Trichiuridae)., *Transactions of the P.P. Shirshov Institute of Oceanology* **93**, 110–204.

Patterson, C. (1964), A review of Mesozoic Acanthopterygian Fishes, with Special Reference to Those of the English Chalk, **247**(739), 213–482.

Patterson, C. (1993*a*), Osteichthyes: Teleostei, *in* M. J. Benton, ed., The fossil record 2, London, UK: Chapman & Hall, pp. 621–656.

Patterson, C. (1993*b*), An overview of the early fossil record of acanthomorphs, *Bulletin of Marine Science* **52**(1), 29–59.

Patterson, C. (1993*c*), An overview of the early fossil record of acanthomorphs, *Bulletin of Marine Science* **52**(1), 29–59.

Patterson, C. and Rosen, D. E. (1977), Review of ichthyodectiform and other Mesozoic teleost fishes and the theory and practice of classifying fossils., *Bulletin of the American Museum of Natural History* **158**, 81–172.

Patterson, C. and Rosen, D. E. (1986), Review of ichthyodectiform and other Mesozoic teleost fishes and the theory and practice of classifying fossils., *Bulletin of the American Museum of Natural History* **158**, 81–172.

Pennell, M., Eastman, J., Slater, G., Brown, J., Uyeda, J., FitzJohn, R., Alfaro, M. and Harmon, L. (2014), geiger v2.0: an expanded suite of methods for fitting macroevolutionary models to phylogenetic trees., *Bioinformatics* **15**, 2216–2218.

Potthoff, T., Richards, W. J. and Ueyanagi, S. (1980), Development of *Scombrolabrax heterolepis* (Pisces, Scombrolabracidae) and comments on familial relationships., *Bulletin of Marine Science* **30**, 329–357.

Price, S., Schmitz, L., Oufiero, C., Eytan, R. I., Dornburg, A., Smith, W. L., Friedman, M., Near, T. J. and Wainwright, P. (2014), Two waves of colonization straddling the K–Pg boundary formed the modern reef fish fauna, *Proceedings of the Royal Society of London B: Biological Sciences* **281**(1783), 20140321.

Přikryl, T. and Bannikov, A. F. (2014), A new species of the Oligocene pomfret fish Paucaichthys (Perciformes; Bramidae) from Iran, *Neues Jahrbuch für Geologie und Paläontologie-Abhandlungen* **272**(3), 325–330.

Přikryl, T., Bannikov, A. F., Grădianu, I., Kania, I. and Krzemiński, W. (2014), Revision of the family Propercarinidae (Perciformes, Stromateoidei) with description of a new species from the Oligocene of the Carpathians, *Comptes Rendus Palevol* **13**(8), 691–700.

Prokofiev, A. and Kukuev, E. (2009), Systematics and distribution of black swallowers of the genus *Chiasmodon* (Perciformes: Chiasmodontidae), *Journal of Ichthyology* **49**(10), 899.

Prokofiev, A. M. (2002), A new genus of cutlassfish from the upper Paleocene of Turkmenistan (Scombroidei: Trichiuroidea)., *Zoosyst Ross 11: 229–233.* **11**(229-233).

Prum, R. O., Berv, J. S., Dornburg, A., Field, D. J., Townsend, J. P., Lemmon, E. M. and Lemmon, A. R. (2015), A comprehensive phylogeny of birds (Aves) using targeted next-generation DNA sequencing, *Nature* **526**(7574), 569.

Purdy, R., Schneider, V., Applegate, S., McLellan, J., Meyer, R. and Slaughter, B. (2001), The Neogene sharks, rays, and bony fishes from Lee Creek Mine, Aurora, North Carolina, **90**, 71–202.

Rafinesque-Schmaltz, C. S. (1815), *Analyse de la Nature, ou Tableau de l'Univers et de Corps Organisées*, Palermo.

Raup, D. M. (1972), Taxonomic diversity during the Phanerozoic, *Science* **177**(4054), 1065–1071.

Raup, D. M. and Sepkoski, J. J. (1982), Mass extinctions in the marine fossil record, *Science* **215**(4539), 1501–1503.

Regan, C. T. (1909), XII.—The classification of Teleostean fishes, *Journal of Natural History Series 8* **3**(13), 75–86.

Revell, L. J. (2012), phytools: An R package for phylogenetic comparative biology (and other things)., *Methods in Ecology and Evolution* **3**, 217–223.

Robertson, D. S., Lewis, W. M., Sheehan, P. M. and Toon, O. B. (2013), K-Pg extinction patterns in marine and freshwater environments: The impact winter model, *Journal of Geophysical Research: Biogeosciences* **118**(3), 1006–1014.

Rosen, D. E. (1973), Interrelationships of higher euteleostean fishes., *in* P. H. Greenwood, R. S. Miles and C. Patterson, eds, Interrelationships of Fishes, Academic Press, London, pp. 297–513.

Russo, J. L. (1983), Interrelationships of the gempylid fishes (Teleostei, Scombroidei), PhD thesis, The George Washington University.

Sahni, A. and Choudhary, N. (1972), Lower Eocene fishes from Barmer, Southwestern Rajasthan, India, *in* Proc. Indian Natl. Sci. Acad. Part A, Vol. 38, pp. 97–102.

Santini, F. (2013), First molecular scombrid timetree (Percomorpha: Scombridae) shows recent radiation of tunas following invasion of pelagic habitat, *Italian Journal of Zoology* **80**(2), 210–221.

Sauvage, H.-E. (1873), Memoire sur la faune ichtyologique de la periode tertiaire, et plus specialement sur les Poissons fossiles d'Oran (Algerie) et sur ceux decouverts par M. R. Alby a Licata en Sicile., *Annales des Sciences Geologiques* **4**, 1–272.

Schein, J. P. and Lewis, R. D. (2007), Actinopterygian fishes from Upper Cretaceous rocks in Alabama, with emphasis on the teleostean genus *Enchodus*, *Paludicola* **6**, 41–86.

Schluter, D. (2000), *The ecology of adaptive radiation*, OUP Oxford.

Schwartzhans, W., Beckett, H. T., Schein, J. D. and Friedman, M. (2018), Computed tomography scanning as a tool for linking the skeletal and otolith-based fossil records of teleost fishes., *Palaeontology* **61**(4), 511–541.

Seehausen, O. (2006), African cichlid fish: a model system in adaptive radiation research, *Proceedings of the Royal Society B* **273**, 1987–1998.

Sepkoski, J. J. (1996), Patterns of Phanerozoic extinction: a perspective from global data bases, *in* Global events and event stratigraphy in the Phanerozoic, Springer, pp. 35–51.

Shimada, K. (2015), Body form and paleoecology of the large Late Cretaceous bony fish, *Pachyrhizodus caninus*, *Cretaceous Research* **52**, 286–291.

Shimada, K. and Fielitz, C. (2006), Annotated checklist of fossil fishes from the Smoky Hill Chalk of the Niobrara Chalk (Upper Cretaceous) in Kansas, *Bulletin of the New Mexico Museum of Natural History* **35**, 193–213.

Sibert, E. C. and Norris, R. D. (2015), New Age of Fishes initiated by the Cretaceous- Paleogene mass extinction, *Proceedings of the National Academy of Sciences* **112**(28), 8537–8542.

Sibley, C. G. and Ahlquist, J. E. (1982), The relationships of the Hawaiian honeycreepers (Drepaninini) as indicated by DNA-DNA hybridization, *The Auk* pp. 130–140.

Simões, M., Breitkreuz, L., Alvarado, M., Baca, S., Cooper, J., Heins, L., Herzog, K. and Lieberman, B. (2016), The evolving theory of evolutionary radiations, *Trends in ecology & evolution* **31**(1), 27–34.

Simpson, G. G. (1937), The beginning of the age of mammals, *Biological Reviews* **12**(1), 1–46.

Simpson, G. G. (1944), *Tempo and mode in evolution*, number 15, Columbia University Press.

Simpson, G. G. (1953), *Major features of evolution*, Columbia University Press: New York.

Slater, G. J. (2013), Phylogenetic evidence for a shift in the mode of mammalian body size evolution at the Cretaceous-Palaeogene boundary, *Methods in Ecology and Evolution* **4**(8), 734–744.

Slater, G. J. (2014), Correction to 'Phylogenetic evidence for a shift in the mode of mammalian body size evolution at the Cretaceous–Palaeogene boundary', and a note on fitting macroevolutionary models to comparative paleontological data sets, *Methods in Ecology and Evolution* **5**(7), 714–718.

Slater, G. J., Harmon, L. J. and Alfaro, M. E. (2012), Integrating fossils with molecular phylogenies improves inference of trait evolution, *Evolution: International Journal of Organic Evolution* **66**(12), 3931–3944.

Slater, G. J., Price, S. A., Santini, F. and Alfaro, M. E. (2010), Diversity versus disparity and the radiation of modern cetaceans, *Proceedings of the Royal Society of London B: Biological Sciences* **277**(1697), 3097–3104.

Smith, J. (1953), V.—The genus *Tetragonurus* Risso, 1810, *Annals and Magazine of Natural History* **6**(61), 53–66.

Smith, W. L. and Wheeler, W. C. (2006), Venom evolution widespread in fishes: a phylogenetic road map for the bioprospecting of piscine venoms, *Journal of Heredity* **97**, 206–217.

Solé, F., Noiret, C., Desmares, D., Adnet, S., Taverne, L., De Putter, T., Mees, F., Yans, J., Steeman, T., Louwye, S. et al. (2018), Reassessment of historical sections from the Paleogene marine margin of the Congo Basin reveals an almost complete absence of Danian deposits, *Geoscience Frontiers* .

Sorbini, L. (1981), cretaceous fishes of Nardo. I. Order Gasterosteiformes (Pisces), *Bollettino-Museo civico di storia naturale di Verona* .

Spiess, A.-N. (2014), *qpcR: Modelling and analysis of real-time PCR data*, https://CRAN.R-project.org/package=qpcR. R package version 1.4-0.

Starks, E. C. (1910), The osteology and mutual relationships of the fishes belonging to the family Scombridae., *Journal of Morphology* **21**(77-99).

Stevenson, D. E. and Kenaley, C. P. (2011), Revision of the manefish genus *Paracaristius* (Teleostei: Percomorpha: Caristiidae), with descriptions of a new genus and three new species, *Copeia* **2011**(3), 385–399.

Stevenson, D. E. and Kenaley, C. P. (2013), Revision of the manefish genera *Caristius* and *Platyberyx* (Teleostei: Percomorpha: Caristiidae), with descriptions of five new species, *Copeia* **2013**(3), 415–434.

Stringer, G. L., Oman, L. D. and Badger, R. F. (2016), Woodbury Formation (Campanian) in New Jersey yields largest known Cretaceous otolith assemblage

of teleostean fishes in North America., *Proceedings of the Academy of Natural Sciences of Philadelphia* **165**, 15–36.

Stroud, J. T. and Losos, J. B. (2016), Ecological opportunity and adaptive radiation, *Annual Review of Ecology, Evolution, and Systematics* **47**, 507–532.

Swofford, D. L. (2001), Paup*: Phylogenetic analysis using parsimony (and other methods) 4.0. B5.

Swofford, D. L. and Sullivan, J. (2003), Phylogeny inference based on parsimony and other methods using PAUP*, *The Phylogenetic Handbook: A Practical Approach to DNA and Protein Phylogeny, cáp* **7**, 160–206.

Taverne, L. and Nolf, D. (2010), Les Priacanthidae (Teleostei, Perciformes) des Sables de Lede (Éocène moyen, Belgique): ostéologie et otolithes, *Bulletin de l'Institut Royal des Sciences Naturelles de Belgique: Sciences de la Terre* **80**, 187–243.

Trunov, I., Kukuev, E. and Parin, N. (2006), Materials for the revision of the family Caristiidae (Perciformes): 1. Description of *Paracaristius heemstrai* gen. et sp. nov., *Journal of Ichthyology* **46**(6), 441–446.

Tucker, D. W. (1956), Studies on trichiuroid fishes-3. A preliminary revision of the family Trichiuridae, *Bulletin of the British Museum of Natural History* **4**, 73–130.

Turner, A. H. (2004), Crocodyliform biogeography during the Cretaceous: evidence of Gondwanan vicariance from biogeographical analysis, *Proceedings of the Royal Society of London B: Biological Sciences* **271**(1552), 2003–2009.

Tyler, J. C., Johnson, G. D., Nakamura, I. and Collette, B. B. (1989), Morphology of Luvarus imperialis (Luvaridae), with a phylogenetic analysis of the Acanthuroidei (Pisces), *Smithsonian Contributions to Zoology* **485**, 1–78.

Uyeda, J. C., Caetano, D. S. and Pennell, M. W. (2015), Comparative analysis of principal components can be misleading, *Systematic Biology* **64**(4), 677–689.

Vidal-García, M. and Keogh, J. S. (2017), Phylogenetic conservatism in skulls and evolutionary lability in limbs–morphological evolution across an ancient frog radiation is shaped by diet, locomotion and burrowing, *BMC evolutionary biology* **17**(1), 165.

Walsh, S. and Milner, A. (2011), *Halcyornis toliapicus* (Aves: Lower Eocene, England) indicates advanced neuromorphology in Mesozoic Neornithes., *Journal of Systematic Palaeontology* **9**, 173–181.

Westneat, M. W. (2005), Skull biomechanics and suction feeding in fishes, *Fish Physiology* **23**, 29–75.

White, E. I. (1931), *From the thanet sands to the basement bed of the London Clay. The vertebrate Faunas of the English Eocene.*, Vol. 1, British Museum (Natural History), London.

Wilson, G. P. (2014), Mammalian extinction, survival, and recovery dynamics across the Cretaceous-Paleogene boundary in northeastern Montana, USA, *Geological Society of America Special Papers* **503**, 365–392.

Winkler, T. C. (1876), *Deuxième mémoire sur des dents de poissons fossiles du terrain bruxellien.*, Vol. 4, Archives du Musée Teyler.

Woodward, A. S. (1891), *Catalogue of fossil fishes in the British Museum (Natural History). Part II. Containing the Elasmobranchii (Acanthodii), Holocephali, Ichthyodorulites, Ostracodermi, Dipnoi, and Teleostomi (Crossopterygii and Chondrostean Actinopterygii).*, Trustees of the British Museum - (Natural History), London.

Woodward, A. S. (1901), *Catalogue of the Fossil Fishes in the British Museum (Natural History). Part IV. Containing the Actinopterygian Teleostomi of the Suborders Isospondyli (in Part), Ostariophysi, Apodes, Percesoces, Hemibranchii, Acanthopterygii, and Anacanthini.*, Trustees of the British Museum - (Natural History), London.

Yagishita, N., Miya, M., Yamanoue, Y., Shirai, S., Nakayama, K., Suzuki, N., Satoh, T., Mabuchi, K., Nishida, M. and Nakabo, T. (2009), Mitogenomic evaluation of the unique facial nerve pattern as a phylogenetic marker within the perciform fishes (Teleostei: Percomorpha)., *Molecular Phylogenetics and Evolution* **53**, 258 – 266.

Zorzin, R., Bannikov, A. F., Fornaciari, E., Giusberti, L., Papazzoni, C. A. and Roghi, G. (2011), Il giacimento a pesci e piante fossili dell'Eocene inferiore di Monte Solane (Verona)., *Bollettino del Museo Civico di Storia Naturale di Verona. Geologia Paleontologia Preistoria* **35**, 57–64.

Appendix A

Supplementary Information associated with Chapter 3 'Morphology and phylogenetic relationships of fossil snake mackerels and cutlassfishes (Trichiuroidea) from the Eocene (Ypresian) London Clay formation'

This appendix contains the supplementary information for the paper: **Beckett, H.T.**, Giles, S., Johanson, Z. and Friedman, M., Morphology and phylogenetic relationships of fossil snake mackerels and cutlassfishes (Trichiuroidea) from the Eocene (Ypresian) London Clay Formation. *Papers in Palaeontology.* https://doi.org/10.1002/spp2.1221.

A digital copy of the data included here, including character list, matrix, a Mimics file, .vol file, .ply files and other information are available in the Dryad Digital Repository: https://doi.org/10.5061/dryad.7722q.

A.1 Scan Parameters

A.1.1 Radiography

Specimen Name	Specimen Number	mA	kV	Time (s)	Dist. (cm)
Aphanopus carbo	BMNH 1961.6.20.1	3	30	60	75
Benthodesmus simonyi	BMNH 1972.1.10.64	3	30	60	30
Eupleurogrammus glossodon	BMNH 1955.5.13.3	3	30	75	30
Lepidopus caudatus	BMNH 1864.10.5.7	3	30	90	75
Lepturacanthus savala	BMNH 51.19.27.14.3	3	30	75	75
Nealotus tripes	BMNH 2016.4.14.59	3	30	90	75
Neoepinnula orientalis	BMNH 1986.9.8.164.5	3	30	90	75
Nesiarchus nasutus	1998.8.9.127.37-38	3	30	90	75
Paradiplospinus gracilis	BMNH 2009.5.18.74-75	3	30	90	75
Promethichthys prometheus	BMNH 1906.9.8.149	3	30	90	75
Ruvettus pretiosus	BMNH 1997.5.21.40	3	40	180	75
Tentoriceps cristatus	BMNH 1974.3.5.1-3	3	30	90	75
Thyrsites prometheus	BMNH 99.1.16.4	3	30	90	75
Thyrsitoides marleyi	BMNH 1986.9.8.147	3	30	60	75
Trichiurus lepturus	BMNH 1897.12.1.343	3	30	75	75

A.1.2 Computed Tomography

All specimens below were reconstructed based on 3142 projections, with the exception of *Gempylus serpens* which was reconstructed using 4000 projections.

Specimen Name	**Specimen No.**	**Filter (mm)**		**mA**	**kV**	**Res. (mm)**
†*Macroynis casieri*	NHMUK PV P 26904	Copper	2	200	210	0.067
†*Progempylus edwardsii*	NHMUK PV OR 32388	Copper	2	200	210	0.066
Aphanopus carbo	BMNH 2006.6.27.1	Copper	0.25	175	175	0.072
Benthodesmus simonyi	BMNH 1972.1.10.64	Copper	0.1	190	95	0.045
Gempylus serpens	FMNH 71423	None		160	75	0.039
Lepidopus caudatus	BMNH 1903.6.27.22	Copper	0.1	180	190	0.051
Lepturacanthus savala	UMMZ 219522	Copper	0.1	255	105	0.052
Nesiarchus nasutus	FMNH 71422	Copper	0.1	250	100	0.053
Paradiplospinus gracilis	BMNH 2009.5.18.143	Copper	0.1	175	190	0.029
Pomatomus saltatrix	UMMZ 111069	Copper	0.1	255	100	0.042
Promethichthys prometheus	UMMZ 250143	Copper	0.1	255	105	0.076
Rexea prometheoides	FMNH 120779	Copper	0.1	250	100	0.042
Ruvettus pretiosus	BMNH 1938.6.23	Copper	0.25	205	95	0.064
Tentoriceps cristatus	BMNH 1987.1.23:28	None		180	75	0.039
Thyrsitoides marleyi	BMNH 1986.9.8.147	Copper	0.1	180	185	0.066
Trichiurus lepturus	UMMZ 219710	Copper	0.1	255	105	0.052

A.2 Character List

Opercular series

1. Posterior and ventral margins of opercle, subopercle, and interopercle: Complete; only the dorsal flap of the opercle and the posterior corner of the subopercle may be slightly splintered (0). Strongly splintered or fimbriate (1). [Gago, 1998 (1)]

2. Lateral process on articular head of the opercle: Plate-like and covering most of the articular fossa of the bone (0). Elongate and flat in cross section (1); Elongate and round in cross section (2). [Gago, 1998 (2)]

3. Fimbriations on posteroventral corner of the subopercle: not much longer than the preceding ventral ones, giving a convex appearance to the ventral margin of the bone (0); much more elongate than the preceding ventral ones, giving a slightly concave appearance to the ventral margin of the bone (1). [Gago, 1998 (3)]

4. Posterodorsal margin of preopercle: convex (0); concave (1). [Gago, 1998 (5); Russo, 1983 (48)]

5. Preopercle width: widest at angle (0); widest opposite dorsal arm (1). [Russo, 1983 (47)]

6. Posterior opercular spine: absent (fimbriate in lateral view) (0); absent (pointed but not spinous) (1); present (pointed and spinous) (2). [Russo, 1983 (56)]

7. Dorsal protuberance on articular fossa of opercle: present (0); absent (1). [Russo, 1983 (57)]

8. Protuberance on ventral margin of opercular fossa: absent (0); present (1). [Russo, 1983 (58)]

9. Position of articular fossa of opercle: fossa in mid-region of anterior margin (0); fossa at dorsal corner of anterior margin (1). [Russo, 1983 (59)]

10. Anterior process of subopercle: pointed (0); rounded (1). [Russo, 1983 (60)]

Circumorbital Series

11. Circumorbital series: complete (0); incomplete with a short gap between the first infraorbital elements and the postorbitals (1); extremely reduced; only the lachrymal and jugal are present (2). [Gago, 1998 (6); Russo 1983 (33, 35)]

12. Shape of ventral wing of lachrymal: Ovoid; fimbriations in the anterior and posterior margins of the ventral wing are not perpendicular to the dorsal, longitudinal, lateral-line canal (0). Quadrilateral; fimbriations in the anterior and posterior margins of the ventral wing are nearly perpendicular to the dorsal, longitudinal, lateral-line canal (1). Elongate; with a straight ventral margin and no fimbriations (2). [Gago, 1998 (7)]

13. Posterodorsal plate of lachrymal: Short; ends before or above the posterior pore of the longitudinal, dorsal lateral-line canal (0). Elongate; extends past

the posterior pore of the longitudinal, dorsal lateral-line canal ending above the jugal (1). [Gago, 1998 (8)]

14. Dorsal extent of medial articular process of first lachrymal: low and rounded (0); long and pointed (1). [Russo, 1983 (31)]

15. Posteroventral corner of first infraorbital: blunt, no specialized process (0); splint-like process coming off first infraorbital, extending under second infraorbital (1). [Russo, 1983 (34)]

16. Infraorbital canal pore openings: lateral or aborbital (0); adorbital (1). [Russo, 1983 (36)]

Jaws

17. Dentary and premaxillary fangs and serial teeth: smooth (0); serrate (1). [Gago, 1998 (10); Russo, 1983 (38)]

18. Ascending process of premaxilla: elongate (0); short (1). [Russo, 1983 (39)]

19. Posterior arm of premaxilla: expanded posteriorly and extending under and beyond the maxilla (0); not expanded posteriorly, extending under but not beyond the maxilla (1). [Russo, 1983 (40)]

20. Cartilaginous projection at tip of jaws: absent (0); present (1). [Russo, 1983 (41)]

21. Postmaxillary process: not well-developed (not high above dorsal margin of maxilla) (0); well-developed (arched high above most of dorsal margin of

maxilla) (1); very well-developed, occupying area about 2/3 of the anterior part of the maxilla (2). [Russo, 1983 (42)]

22. Supramaxilla: moderate in size (0); greatly reduced (small and splint-like) (1). [Russo, 1983 (43)]

23. Anterior tooth on dentary: in line with rest of dentary teeth (0); emerges from lateral surface, not in line with other dentary teeth (1). [Russo, 1983 (44)]

Suspensorium

24. Posterodorsal process of quadrate: has a smooth dorsal margin, process extends past the ventral margin of the metapterygoid (0); has a notch in the dorsal margin, with a shorter process extending below the ventral margin of the metapterygoid (1). [Gago, 1998 (11)]

25. Posteromedial arm of ectopterygoid: does not reach the metapterygoid (0); reaches the metapterygoid (1). [Gago, 1998 (12)]

26. Well-developed condyle posterior to anteromedial shelf of palatine: absent (0); present and visible in lateral view (1). [Gago, 1998 (13)]

27. Teeth on ventral margin of palatine: large and few; a single row covering only a very small portion of the ventral margin of the bone (0). Small and numerous; in several rows covering most of the ventral margin of the bone (1). [Gago, 1998 (14)]

28. Lateral and medial processes of metapterygoid: moderate sized (separate, joining hyomandibular laterally and medially) (0); greatly reduced (dorsal margin of metapterygoid appears to come to a single point) (1). [Russo, 1983 (45)]

29. Posterior process of hyomandibular head: drawn out into a more or less blunt point (0); rounded (1). [Russo, 1983 (46)]

Hyoid complex

30. Anterodorsal corner of ceratohyal: not pointed; does not extend anteriorly (0); pointed; extends anteriorly abutting the dorsal margin of the dorsal hypohyal (1). [Gago, 1998 (15)]

31. Shape of posteroventral processes of basihyal in ventral view: neither triangular nor quadrilateral; do not have their lateral corners pointing posteriorly (0); wing-like, with corners pointed posteriorly (1); quadrilateral (2); triangular (3). [Gago, 1998 (16), who modified Russo, 1983 (50, 51)]

32. Dorsoanterior end of basihyal: dorsal profile concave (0); dorsal profile convex (1). [Russo, 1983 (49)]

33. Ceratohyal window: present (0); absent (1). [Russo, 1983 (52)]

34. Number of branchiostegals on epihyal: two (0); three (1). [Russo, 1983 (53)]

35. Dorsal process of urohyal: present (0); absent (1). [Russo, 1983 (54)]

Branchial complex

36. Shape of articular head of first basibranchial: tapers to a point; not knob-like (0). Knob-like, but not bearing dorsolateral processes (1). Knob-like and bearing dorsolateral processes (2). [Gago, 1998 (17)]

37. Length of first basibranchial: short to moderate sized (0); very elongate (1). [Russo, 1983 (61)]

38. Laterally pointed processes on second basibranchial: absent (0); present (1). [Gago, 1998 (18)]

39. Anterior process of first hypobranchial: present (0); absent (1). [Russo, 1983 (63)]

40. Shape of fourth ceratobranchial: straight (0); sigmoidal (1). [Gago, 1998 (19); Russo, 1983 (64)]

41. Teeth on third epibranchial: two rows (0); one row (1); absent (2). [Russo, 1983 (65)]

42. Shape of anterior end of second pharyngobranchial; wide (0); narrow (1). [Russo, 1983 (66)]

43. Process for interarcaal cartilage and process for articulation with anterior pharyngobranchial cartilage of second pharyngobranchials: joined (0); separate (1). [Russo, 1983 (67)]

Neurocranium

Ethmoidal Region

44. Anterior tip of nasal: straight (0); curved; giving the bone a concave lateral margin in dorsal view (1). [Gago, 1998 (20)]

45. Dorsal ridges on ethmoid: absent or reduced; do not extend well above the nasals in lateral view (0); present; extend well above the nasals in lateral view (1). [Gago, 1998 (21)]

46. Ethmoid shape: relative!y short (much less than twice as long as wide) (0); relatively elongate (about 2 or more times longer than vide) (1). [Russo, 1983 (1)]

47. Anterior protuberance of ethmoid: large (0); small (inconspicuous) (1); absent (anterior end of ethmoid rounded) (2). [Russo, 1983 (3)]

48. Lateral process of ethmoid: large (0); small (inconspicuous) (1); absent (2). [Russo, 1983 (4)]

49. Palatal process of ethmoid: rounded and knob-like (0); elongated anteroposteriorly (1). [Russo, 1983 (5)]

50. Lateral ethmoid: not elongate (length ¡90

51. Articular cartilage for first infraorbital and palatine on lateral ethmoid: separated by bony ridge (0); continuous (1). [Russo, 1983 (8)]

52. Posterolateral process of lateral ethmoid: absent (0); present (1). [Russo, 1983 (9)]

53. Vomerine teeth: patch or single row (0); one or two pair (1); absent (2). [Russo, 1983 (11)]

54. Lateral process of vomer: absent (0); present (1). [Russo, 1983 (12)]

55. Extent of anterior end of vomer: extends beyond anterior end of ethmoid (0); extends to a point under the anterior end of ethmoid (1); behind anterior end of ethmoid (2). [Russo, 1983 (13)]

56. Nasal: a simple tube with a moderately sized laminar plate (0; anterior end of nasals tubular and elongate while posterior end is broad and flat (1). [Russo, 1983 (14)]

57. Medially directed nasal canal pores: absent (0); present (1). [Russo, 1983 (15)]

Orbital Region

58. Connection of supraorbital and infraorbital lateral-line canals: supraorbital lateral-line canal connects with the infraorbital canal through a dorsally or laterally directed pore (0); lateral bony tubular extension of supraorbital lateral-line canal to orbital rim (1). [Gago, 1998 (22)]

59. Elevation of frontal ridges on ethmoidal region: not elevated (0); elevated; laterally convex (1); extremely elevated; appear as laterally flat sheets (2). [Gago, 1998 (23)]

60. Sclerotics: present (0); absent (1). [Gago, 1998 (24)]

61. shape of lateral margin of frontals in dorsal view: parallel or become closer anteriorly (0); narrow, above the orbit and again widening above the lateral ethmoid (1). [Russo, 1983 (16)]

62. Basioccipital fossa: not greatly extended anteriorly (0); narrows and is extended anteriorly along the ventral margin of the basioccipital (1). [Russo, 1983 (28)]

Otic Region

63. Size of supraoccipital crest: (0) large (extends high above neurocranium); (1) moderate (extends we11 above epiotic ridge); (2) small (a thin ridge). [Russo, 1983 (20); modified Gago, 1998 (25)]

64. Highest point of supraoccipital crest: posterior to the orbits (0); above the orbits (1). [Gago, 1998 (26)]

65. Supraoccipital strut coming off posterior end of main body of supraoccipital extending onto crest: (0) present; (1) absent. [Russo, 1983 (21)]

66. Position of bifurcation of supraoccipital ridge: (0) on frontal; (1) on supraoccipital. [Russo, 1983 (22)]

67. Pterotic: ends before the posterior margin of the neurocranium (0); ends well past the posterior margin of the neurocranium (1). [Gago, 1998 (27)]

68. Canal pores in the pineal region: present (0); absent (1). [Russo, 1983 (17)]

69. Origin of infraorbital branch of laterosensory system: from depression in wall of trough for supraorbital branch (0); from discrete pore on pterotic ridge on frontal (1). [Russo, 1983 (18)]

70. Canal pore on frontal portion of pterotic ridge: does not open to sphenotic fossa (0); opens to sphenotic fossa (1). [Russo, 1983 (19)]

71. Posterodorsal pterotic canal pore: branches directly from main pterotic canal (0); separate canal extended away from main canal by bony shelf (1). [Russo, 1983 (23)]

72. Pterotic fossa: divided by a step into high anterior and low posterior regions (0); step absent, gradually slopes posteriorly (1). [Russo, 1983 (24)]

73. Anterior prootic arch: arch absent (0); anterior edge of prootic forms an arch encircling a foramen which connects the trigeminofacial chamber with the anterior portion of the myodome (1). [Russo, 1983 (25)]

74. Intercalar: visible dorsally (0); not visible dorsally (1). [Gago, 1998 (28)] [Russo, 1983 (26)]

75. Exoccipital ridge: reaches the vagus foramen (0); does not reach the vagus foramen (1). [Gago, 1998 (29); Russo, 1983 (29)]

Pectoral girdle

76. Length of dorsal articular process of posttemporal: short; ends before or slightly past the anterior margin of the supratemporal (0); more than twice the length of the supratemporal (1). [Gago, 1998 (30)]

77. Posteroventral process of posttemporal: absent (0); reduced, flat in cross section; comes in contact or close association with the articular head of the supracleithrum (1); long, round in cross section; does not come in contact or close association with the articular head of the supracleithrum (2). [Gago, 1998 (31)]

78. Anteroventral process of posttemporal: originates on the posterior corner of the bone (0); shares a common origin with the posteroventral process; close to or on the anterior half of the canal-bearing portion of the bone (1); separate from the posteroventral process; originates close to or on the anterior half of the canal- bearing portion of the bone (2). [Gago, 1998 (32)]

79. Posterodorsal corner of posttemporal: not expanded (0); expanded (1). [Gago, 1998 (33)]

80. Lateral protuberance of posttemporal: present (0); absent (1). [Russo, 1983 (70)]

81. Articular head of the supracleithrum; posteriorly expanded; bears a completely enclosed canal that transmits the lateral line to the posttemporal (0); posteriorly expanded; bears an open canal or shelf connect- ing the lateral line to the posttemporal (1); not expanded; lacks a canal (2). [Gago, 1998 (34)]

82. Lateral process on articular head of supracleithrum: absent (0); present (1). [Gago, 1998 (35)]

83. Posteroventral plate on coracoid: absent; ventral margin of coracoid is flat; its posterior corner ending before the fourth radial (0); present; ventral margin is round; its posterior corner ending past the fourth radial (1). [Gago, 1998 (37)]

84. Length of pectoral-fin rays: posterior fin rays are longer (0); anterior fin rays are longer (1). [Gago, 1998 (38)]

85. Medial extrascapular canal tube: present (0); absent (1). [Russo, 1983 (68)]

86. Dorsal articular process of cleithrum: short (0); elongate (1). [Russo, 1983 (73)]

87. Posterior protuberance on cleithrum: present (0); absent (1). [Russo, 1983 (74)]

88. Dorsal postcleithrum: flat (0); rounded in cross-section (1). [Russo, 1983 (75)]

89. Shape of ventral postcleithrum: flat or with knife-like posterior edge (0); rounded in cross section (1). [Russo, 1983 (76)]

Pelvic girdle

90. Basipterygium: present (0); absent (1). [Gago, 1998 (39)]

91. External spinous elements of pelvic fin: spine-like (0); scale-like (1). [Gago, 1998 (40)]

92. Position of basipterygium: thoracic; articular facet is anterior to distal tip of ventral postcleithrum (0); abdominal; articular facet is posterior to distal tip of ventral postcleithrum (1). [Gago, 1998 (41)]

93. Central part of basipterygium: dorsally inclined (0); nearly parallel to the ventral body wall (1). [Gago, 1998 (42)]

94. Central part of basipterygium: bilaterally divided (0); longitudinally fused (1). [Gago, 1998 (43)]

Axial skeleton

Vertebral Column

95. Total number of vertebrae: 30-55 (0); 57-67 (1); 84-198 (2). [Gago, 1998 (44)]

96. First neural spine: not distally bifurcate (0); distally bifurcate (1). [Gago, 1998 (45)]

97. Anterior neural spines; not expanded or forked distally (0); expanded and forked distally (1). [Gago, 1998 (46)] lntermusculars

98. Series of unattached epineurals and epicentrals extending into caudal region: both present (0); only the epineural series present (1); both absent (2). [Gago, 1998 (47)]

Dorsal and Anal Fins

99. Notch in the fin membrane separating the spinous and soft portions of the dorsal fin: present (0); absent (1). [Gago, 1998 (48)]

100. Spinous portion of the dorsal fin: XIX-XXXIX spines; its base is longer than that of the soft portion (0). XXXVIII-XLV spines; its length is only slightly shorter than length of soft portion (1); XXXI-XLVI spines; its base is less than half of the length of the soft portion but not extremely short (2); only III-X spines; its base is extremely short compared to the base of the soft portion (3). [Gago, 1998 (49)]

101. Number of radials in soft dorsal-fin pterygiophores: 2; proximal-middle and distal (0). 3; proximal, middle, and distal (1). [Gago, 1998 (50)]

102. Proximal-middle radial of first dorsal pterygiophore: does not extend above occiput (0); extends above occiput (1). [Gago, 1998 (51)]

103. Foramen at anteroventral corner between the proximal and distal portions of the dorsal-fin proximal radials: absent (0); present (1). [Gago, 1998 (52)]

104. Number of supernumerary elements on first anal-fin pterygiophore: two (0); one (1). [Gago, 1998 (53)]

105. Anal-fin soft rays: well-developed soft rays throughout the whole length of the anal fin (0); well-developed soft rays only in the posterior portion of the anal fin (1); modified as small spinule-like elements (2); reduced to small scale-like ossifications that do not penetrate the epithelium (3); modified

into small fused knobs that barely penetrate the epithelium (4). [Gago, 1998 (54)]

106. Anal-fin pterygiophores: two (proximal-middle and distal) or three (proximal, middle, and distal) radials present (0); the proximal, middle, and distal radials are fused with each other and appear as a single unit (1). [Gago, 1998 (55)]

Caudal complex

107. Caudal complex: well developed (0); reduced to a few small internal elements (1); absent (2). [Gago, 1998 (56)]

108. Ultimate centrum: flexed and forming a urostyle (0); not flexed (1). [Gago, 1998 (57)]

109. Number of epurals: three (0); two (1); one (2). [Gago, 1998 (58); Russo, 1983 (84)]

110. Haemal and neural spines of preural centrum 4: long; extends past or as far as the posterior margin of the preural centrum 3 (0); short; does not extend well past the anterior margin of the preural centrum 3 (1). [Gago, 1998 (59)]

111. Upper hypural fusion: hypurals 3, 4 and 5 separate (0); 3 and 4 fused (1); 5 also fused to 3 and 4 (2). [Russo, 1983 (79)]

112. Hypurals 1 and 2: separate (0); fused (1). [Russo, 1983 (81)]

113. Hypural notch: large (0); small (1). [Gago, 1998 (61); Russo, 1983 (80)]

114. Parhypural and hypural 1: separate (0); fused (1). [Russo, 1983 (82)]

115. Upper and lower halves of the hypural plate: separate (0); fused (1). [Russo, 1983 (83)]

116. Number of autogenous haemal spines: two (0); one (1). [Russo, 1983 (85)]

117. Median caudal cartilage (CMC cartilage): absent (0); present (1). [Gago, 1998 (62)]

118. Cartilaginous postneural spine element on the third preural vertebrae (CP-NPU3 cartilage): present (0); absent (1). [Gago, 1998 (63)]

Otoliths

119. Excisura: delimited by a well-developed rostrum and antirostrum (0); delimited by a reduced rostrum and antirostrum (1). [Gago, 1998 (64)]

120. Cristae superior and inferior: reduced (0); well developed and overhanging (1). [Gago, 1998 (65)]

121. Longitudinal ridge on the ostium: absent (0); present (1). [Gago, 1998 (66)]

Ontogenetic characters

122. Number of external nares during development: two external nares retained during development (0); posterior external naris is lost during development (1). [Gago, 1997 (1)]

123. Spinous dorsal fin: high and steeply graduated (0); low and not steeply graduated (1). [Gago, 1997 (2)]

124. Morphology and development of the soft dorsal and anal-fin pterygiophores: proximal and middle radials become fused during development (0); proximal, middle and distal radials remain separate during development (I). [Gago, 1997 (3)]

125. Direction of development of the pterygiophores and rays of the dorsal and anal fins: spinous dorsal develops posteriotly; soft-dorsal and anal fins develop both anteriotly and posteriotly (0); both spinous and soft-dorsal, and anal fins develop posteriotly (1). [Gago, 1997 (4)]

126. Shape of the initial ossifications of the vertebrae: saddle-shaped (0); thin lateral strips (I). [Gago, 1997 (5)]

127. Dorsal or ventral patches of pigment at tip of notochord: absent (0); present (1). [Gago, 1997 (6)]

128. Inclination of the central part of basipterygium: dorsally inclined; extends well-between the cleithrum and coracoid (0); parallel to ventral body wall; does not extend well-between cleithrum and coracoid (1). [Gago, 1997 (7)]

129. Reduction of the caudal-fin complex: caudal-fin complex is well developed with a full complement of internal and external elements (0); caudal-fin complex reduced; the urostyle does not undergo flexion and only a few reduced hypurals and pseudo-rays remain in the adult (1); caudal-fin complex is lost in the adults; the urostyle does not undergo flexion; the presence of a few reduced hypurals and pseudo-rays is only temporary (2). [Gago, 1997 (8)]

130. Fusion of the radials in the anal-fin pterygiophores: radials in anal fin remain separate (0); radials in anal fin become fused (1). [Gago, 1997 (9)]

131. Longitudinal ventral keel of the supernumerary spines of first anal pterygiophore: smooth or with extremely reduced serrations (0); with well-developed serrations (1). [Gago, 1997 (10)]

132. Supracleithral spine: present (0); absent (1). [Gago, 1997 (11)]

133. Pelvic-fin spine shape: elongated; posterolateral and posteromedial keels are approximately equal in width (0); short; posteriolateral keel is much wider than posteromedial keel (1). [Gago, 1997 (12)]

134. Posterolateral keels of dorsal-fin spines; serrated (0); smooth (1). [Gago, 1997 (13)]

135. Pigment patch on the opercular-preopercular area: absent (0); present (I). [Gago, 1997 (14)]

136. Spinous projections on the anteroventral margin of the bases of anal-fin soft rays: absent (0); present (1). [Gago, 1997 (15)]

137. Pelvic fin development: pelvic fin is well developed and present throughout development (0); pelvic fin becomes reduced in the adult, the external fin rays are lost (1); pelvic fin is never present during development (2). [Gago, 1997 (16)]

138. Length of first dorsal-fin spine: short; shorter than or slightly past the tip of the second dorsal-fin spine (0); long; well past the tip of the second dorsal-fin spine (1). [Gago, 1997 (17)]

139. Longitudinal anterior keel of dorsal-fin spines: serrated (0); smooth (1). [Gago, 1997 (18)]

140. Longitudinal ventral keel of pelvic-fin spine: serrated (0); smooth (I). [Gago, 1998 (19)]

141. Supraorbital ridge: serrated or spinous (0); smooth (1). [Gago, 1997 (20)]

142. Preopercular spine(s): serrated (0); smooth (1). [Gago, 1997 (21)]

143. Pigment patch(es) on dorsal finfold: absent (0); present (1). [Gago, 1997 (22)]

144. Pigment patch(es) on anal finfold: absent (0); present (1). [Gago, 1997 (23)]

A.3 Character Matrix

The character matrix in nexus format can be found at:
DOI: https://doi.org/10.5061/dryad.7722q.

	1-10										11-20										21-30									
Pomatomus_saltatrix	0	0	0	0	0	1	0	0	1	0	0	0	0	0	0	0	0	0	0	0	0	0	0	1	0	1	1	0	0	0
Gasterochisma_melampus	0	0	0	0	0	0	0	0	1	0	0	0	0	0	0	0	0	0	1	0	0	1	0	0	1	0	0	1	0	0
Scombrolabrax_heterolepis	0	0	0	0	0	1	0	0	0	0	0	2	0	0	0	0	0	0	0	0	0	0	0	0	0	0	1	0	0	0
Lepidocybium_flavobrunneum	0	?	0	0	0	1	0	0	0	0	1	2	0	0	0	0	0	1	1	0	1	0	0	0	0	0	?	1	0	0
Ruvettus_pretiosus	0	0	0	0	0	2	0	0	1	1	0	2	0	0	0	0	0	1	1	0	1	0	1	0	0	0	0	0	0	0
Thyrsites_atun	0	?	0	0	0	1	0	0	1	0	0	2	0	1	0	0	1	1	1	0	1	0	0	0	0	0	?	0	0	0
Hemithyrsites_prometheus	0	0	0	0	0	2	0	1	1	1	0	2	0	1	1	0	0	1	1	0	1	0	1	0	0	0	1	0	0	0
Rexea_prometheoides	0	0	0	0	0	1	0	1	1	0	0	2	0	1	1	0	0	1	1	0	1	0	1	0	0	0	0	0	0	0
Nealotus_tripes	0	?	0	0	0	1	1	1	1	0	0	2	0	1	1	0	0	1	1	1	1	0	1	0	0	0	?	0	0	0
Thyrsitoides_marleyi	0	0	0	0	0	1	1	1	1	1	0	2	0	1	0	0	0	1	1	1	1	0	1	0	0	0	0	0	0	0
Nesiarchus_nasutus	0	0	0	0	1	1	0	1	1	0	0	0	0	1	0	0	0	1	1	1	1	0	1	0	0	0	0	0	0	0
Gempylus_serpens	0	0	0	0	0	1	0	1	1	0	0	0	0	1	1	0	1	1	1	1	2	1	0	0	0	0	0	0	0	0
Diplospinus_multistriatus	0	0	0	1	1	1	1	1	1	0	1	0	0	1	0	1	0	1	1	0	1	1	1	0	0	0	0	1	0	0
Paradiplospinus_gracilis	0	0	0	1	1	2	1	1	1	0	1	0	0	1	0	1	0	1	1	0	1	1	1	0	0	0	0	1	0	0
Neoepinnula_orientalis	0	0	0	0	0	2	1	0	1	1	0	2	0	1	1	0	0	1	1	0	1	0	1	0	0	0	1	0	1	0
Epinnula_margistralis	0	?	0	0	0	2	1	0	1	1	0	2	0	1	1	0	0	1	1	0	1	0	1	0	0	0	1	0	0	0
Tongaichthys_robustus	0	?	?	0	0	2	0	0	1	0	?	2	?	1	1	0	0	1	1	0	1	0	0	0	?	0	?	0	1	0
Thyrsitops_lepidopoides	0	?	0	0	0	1	0	0	1	0	0	2	0	1	1	0	0	1	1	0	1	0	1	0	0	0	1	0	1	0
Aphanopus	1	0	0	1	1	0	1	1	1	1	2	0	0	1	0	-	1	1	1	1	0	1	1	0	1	0	0	0	0	0
Assurger_anzac	1	1	0	1	1	0	0	1	1	1	2	0	1	1	0	-	0	1	1	1	1	1	1	0	1	0	0	0	1	0
Benthodesmus_tenuis	1	2	0	1	1	0	0	1	1	1	2	0	0	1	0	-	0	1	1	1	1	1	1	0	1	0	0	1	0	0
Eupleurogrammus_glossodon	1	2	0	1	1	0	0	1	1	?	2	0	1	1	0	-	0	1	1	1	1	0	1	1	1	0	1	0	0	1

	1-10										**11-20**										**21-30**									
Evoxymetopon	1	2	0	1	1	0	0	?	1	1	2	0	1	1	0	-	0	1	1	1	1	1	0	0	1	0	0	0	0	0
Lepidopus_altifrons	1	2	0	1	1	0	0	0	1	1	2	0	1	?	?	-	0	1	1	1	1	1	?	0	1	0	0	0	0	0
Lepidopus_caudatus	1	2	0	1	1	0	0	0	1	1	2	0	1	?	?	-	0	1	1	1	1	1	1	0	1	0	0	0	0	0
Lepidopus_fitchi	1	2	0	1	1	0	0	1	1	1	2	0	1	1	0	-	0	1	1	1	1	1	1	0	1	0	0	1	0	0
Lepturacanthus_savala	1	2	1	1	1	0	0	0	1	1	2	1	1	1	1	-	0	1	1	1	0	1	1	1	1	1	1	1	0	1
Tentoriceps_cristatus	1	2	0	1	1	0	0	1	1	1	2	0	1	1	0	-	0	1	1	1	1	1	1	0	1	0	0	0	1	1
Trichiurus_lepturus	1	2	1	1	1	0	0	1	1	1	2	1	1	1	0	-	0	1	1	1	0	1	1	1	1	1	1	0	0	1
†*Progempylus_edwardsii*	0	?	?	?	0	1	1	0	1	1	?	?	?	?	?	?	0	?	?	?	?	?	0	1	?	0	?	?	0	0
†*Macroynis_casieri*	?	?	?	?	?	?	?	?	?	?	?	?	?	?	?	?	?	?	?	?	?	?	0	?	?	0	0	?	?	0
†*NHMUK_PV_OR_41318*	?	?	?	?	?	?	?	?	?	?	?	?	?	?	?	?	?	?	?	?	?	?	?	?	?	?	?	?	?	?

	31-40										**41-50**										**51-60**									
Pomatomus_saltatrix	1	1	0	0	1	0	0	0	0	1	0	0	?	0	0	0	0	0	0	0	?	0	0	0	0	0	0	0	0	0
Gasterochisma_melampus	3	0	0	0	1	1	0	0	1	0	0	0	?	0	-	0	?	?	?	0	?	0	0	0	0	0	0	0	?	0
Scombrolabrax_heterolepis	0	0	1	0	0	1	0	1	0	0	0	0	0	0	0	0	0	0	0	0	0	0	0	0	0	0	0	0	0	0
Lepidocybium_flavobrunneum	0	0	1	1	0	?	0	1	0	0	1	0	0	0	0	0	0	0	0	0	1	0	0	0	1	1	0	0	0	2	?
Ruvettus_pretiosus	0	0	0	1	1	1	0	1	1	0	2	0	0	1	0	0	0	0	0	0	1	0	1	0	0	1	0	0	0	0
Thyrsites_atun	0	0	0	1	1	?	0	1	1	0	2	0	0	0	0	1	1	0	1	2	1	1	1	0	0	0	0	0	0	0
Hemithyrsites_prometheus	0	0	1	1	1	0	0	1	1	0	1	0	0	0	0	1	0	0	0	1	1	0	2	0	0	0	0	0	0	1
Rexea_prometheoides	0	0	0	1	1	0	0	1	1	0	1	0	1	0	0	1	0	0	0	1	0	1	2	0	0	0	0	0	0	0
Nealotus_tripes	0	0	0	1	1	?	0	1	1	0	1	0	0	1	0	1	1	0	0	1	0	0	2	0	0	0	0	0	0	?
Thyrsitoides_marleyi	0	1	1	1	0	0	0	1	1	0	1	1	0	1	0	1	2	0	1	1	0	1	2	0	1	0	0	0	0	?
Nesiarchus_nasutus	0	0	1	1	1	0	0	0	1	0	1	1	0	0	0	1	2	2	1	1	1	1	2	1	2	0	0	0	0	0
Gempylus_serpens	1	1	1	1	1	0	0	0	0	0	2	1	0	0	0	1	2	0	1	2	1	1	2	0	0	0	0	0	0	0
Diplospinus_multistriatus	2	1	1	1	1	0	1	0	0/1	1	1	1	0	0	1	1	2	2	0	1	1	1	2	0	0	0	0	0	0	1
Paradiplospinus_gracilis	2	1	1	1	0	0	1	0	1	1	0	1	0	0	1	1	1	1	0	1	1	1	2	0	0	0	0	0	0	1
Neoepinnula_orientalis	1	1	1	1	1	0	0	1	1	0	1	0	1	1	0	1	0	0	0	0	1	0	1	0	0	1	0	0	0	0
Epinnula_margistralis	1	1	1	1	0	?	0	1	1	0	0	0	1	0	0	0	0	0	0	0	1	0	2	0	1	1	0	0	0	?
Tongaichthys_robustus	1	0	1	1	1	?	0	1	0	0	1	0	0	?	0	1	0	0	0	0	0	0	0	0	0	0	1	1	0	0	?
Thyrsitops_lepidopoides	0	0	1	1	0	?	0	1	1	0	0	0	0	0	0	1	0	0	0	0	1	0	0	0	0	1	1	0	0	?
Aphanopus	2	0	1	1	1	1	1	1	1	0	?	1	?	1	0	1	0	1/2	0	1	1	1	2	1	0	0	0	1	0	1
Assurger_anzac	2	1	1	1	1	1	1	1	0	0	?	?	?	1	1	1	1	?	?	0	1	1	2	1	1	0	?	1	2	1
Benthodesmus_tenuis	2	1	1	1	1	1	1	1	1	0	1	0	?	1	0	1	2	0	?	1	1	1	2	1	1	0	0	1	0	1
Eupleurogrammus_glossodon	3	1	0	1	1	2	0	1	0	0	?	?	?	1	0	1	1	?	?	0	1	1	2	1	1	0	?	1	1	1
Evoxymetopon	2	1	0	1	1	1	0	1	0	0	?	?	?	1	1	1	1	?	?	2	1	1	2	1	1	0	?	1	2	1
Lepidopus_altifrons	2	?	1	1	1	1	0	1	0	0	0	0	?	1	1	1	0	0	0	2	1	1	2	1	1	0	0	1	2	1
Lepidopus_caudatus	2	?	1	1	1	1	0	1	0	0	0	0	?	1	0	1	0	0	0	2	1	1	2	1	1	0	0	1	0	1

	31-40										41-50										51-60									
Lepidopus_fitchi	2	1	1	1	1	1	0	1	0	0	?	?	?	1	0	1	0	?	?	2	1	1	2	1	1	0	?	1	0	1
Lepturacanthus_savala	3	1	0	1	1	1	2	0	1	0	0	0	2	0	?	1	0	1	1	2	0	2	1	1	2	1	1	1	0	1	0	1
Tentoriceps_cristatus	3	1	0	1	1	1	2	0	1	0	0	0	1/2	0	?	1	1	1	1	2	0	?	1	1	1	2	1	1	1	1	?	1	2	1
Trichiurus_lepturus	3	1	1	1	1	1	2	0	1	0	0	0	0	1	0	1	0	1	1	2	0	0	0	2	1	1	2	1	1	1	1	?	1	0	1
†*Progempylus_edwardsii*	?	?	1	0	1	?	?	?	?	0	2	?	?	?	?	0	?	?	?	?	?	?	?	?	1	1	0	?	?	?	?	?	0
†*Macroynis_casieri*	?	?	0	?	?	?	?	?	?	?	?	?	?	?	?	?	?	?	?	?	?	?	?	?	2	1	0/1	?	?	?	?	?	?
†*NHMUK_PV_OR_41318*	?	?	?	?	?	?	?	?	?	?	?	?	?	?	?	0	?	?	?	?	?	?	?	?	?	?	?	?	?	?	?	0	?

	61-70										**71-80**										**81-90**									
Pomatomus_saltatrix	0	0	0	0	?	0	0	0	0	0	?	0	0	0	?	0	0	0	0	0	0	0	0	1	?	0	0	?	?	0
Gasterochisma_melampus	0	?	0	0	?	1	0	?	0	?	?	1	1	0	0	0	0	1	0	0	2	0	0	1	?	?	0	0	1	0
Scombrolabrax_heterolepis	0	0	0	0	0	0	0	0	0	0	0	0	0	0	0	0	0	1	0	0	2	0	0	1	0	0	0	1	0	0
Lepidocybium_flavobrunneum	0	0	0	0	1	0	0	0	1	0	0	1	0	0	0	0	0	0	1	0	2	0	0	1	1	1	1	1	0	0
Ruvettus_pretiosus	0	0	0	0	1	1	0	0	1	1	1	0	0	0	0	0	0	0	0	0	2	0	0	1	1	1	0	0	0	0
Thyrsites_atun	0	0	1	0	1	0	0	0	1	0	1	0	1	0	0	0	0	0	0	0	0/1	0	0	1	1	1	0	0	0	0
Hemithyrsites_prometheus	0	0	1	0	1	1	0	1	0	0	1	0	1	0	0	0	0	0	0	0	0/1	0	0	1	1	1	0	0	0	1
Rexea_prometheoides	1	0	1	0	1	1	0	0	0	0	1	0	1	0	0	0	1	0/1	0	0	2	0	0	1	0	1	0	0	0	1
Nealotus_tripes	0	0	2	0	1	1	0	1	0	0	1	1	1	0	1	0	0	0	0	0	2	0	0	1	1	1	0	0	0	0
Thyrsitoides_marleyi	0	1	1	0	1	1	0	0	1	0	0	1	1	0	0	0/1	0	0	0	0	2	0	0	1	1	1	0	0	0	0
Nesiarchus_nasutus	0	1	2	0	1	1	0	0	0	0	0	1	1	0	0	0	0	0	0	1	0	0	0	0	1	1	0	0	0	0
Gempylus_serpens	0	1	1	0	1	1	0	0	0	0	1	1	1	0	0	0	2	0	0	1	2	0	0	1	1	1	0	0	1	0
Diplospinus_multistriatus	1	0	2	0	1	1	0	1	0	0	0	1	1	1	1	0	0	0	0	1	0	0	0	0	1	1	1	0	1	0
Paradiplospinus_gracilis	1	0	2	0	1	1	0	1	1	0	0	1	1	1	1	0	0	0	0	1	0	0	0	0	1	1	1	0	1	0
Neoepinnula_orientalis	0	1	1	0	1	0	0	0	0	0	1	0	1	0	0	0	1	1	0	0	2	0	0	1	0	1	0	0	0	0
Epinnula_margistralis	0	0	1	0	1	0	0	0	0	0	1	0	1	0	0	0	?	0/1	0	0	2	0	0	1	0	1	1	0	0	0
Tongaichthys_robustus	0	0	1	0	1	1	0	0	0	1	1	0	0	0	0	0	?	0	0	0	2	0	0	1	0	1	0	0	0	0
Thyrsitops_lepidopoides	0	1	1	0	1	0	0	0	0	1	1	0	0	0	0	0	?	0	0	1	2	0	0	1	0	1	0	0	0	0
Aphanopus	0	0	2	0	?	1	1	?	1	0	0	0	1	0	0	0	0	0	0	0	0	0	0	1	0	?	1	1	?	?	0
Assurger_anzac	1	?	0	1	?	?	1	?	1	0	1	?	1	0	0	1	1	1	1	?	1	0	1	0	?	1	0	?	?	0
Benthodesmus_tenuis	1	0	2	0	?	0	1	?	1	0	0	0	1	0	0	0	1	1	0	?	1	0	1	0	?	1	1	?	?	0
Eupleurogrammus_glossodon	1	?	0	0	?	0	1	?	1	0	1	?	1	0	0	0	1	2	1	?	2	1	1	1	?	1	1	?	?	0
Evoxymetopon	1	?	0	1	?	0	1	?	1	0	1	?	1	0	0	1	1	1	1	?	1	0	1	0	?	1	0	?	?	0
Lepidopus_altifrons	0	?	0	1	?	0	1	?	1	0	1	1	1	0	0	1	1	1	1	0	1	0	1	0	?	1	1	0	1	0
Lepidopus_caudatus	0	?	0	0	?	0	1	?	1	0	1	1	1	0	0	1	1	1	1	0	1	0	1	0	?	1	1	0	1	0
Lepidopus_fitchi	0	?	1	0	?	0	1	?	1	0	1	?	1	0	0	1	1	1	1	?	1	0	1	0	?	1	1	?	?	0

	61-70										71-80										81-90									
Lepturacanthus_savala	0	0	1	0	?	0	1	0	1	0	?	1	1	0	0	0	1	2	1	0	2	1	1	1	?	1	1	1	?	1
Tentoriceps_cristatus	0	1	2	1	?	0	1	?	1	0	1	1	1	1	0	0	1	1	2	1	0	1	0	1	1	?	1	1	1	1	0
Trichiurus_lepturus	0	0	2	0	?	0	1	?	1	0	?	1	1	0	0	0	0	1	2	1	0	2	1	1	1	1	?	1	1	1	1
†*Progempylus_edwardsii*	1	?	2	0	?	1	0	0	?	?	?	0	?	0	?	?	?	?	?	?	?	?	?	?	?	?	?	?	?	?	?
†*Macroynis_casieri*	?	?	?	?	?	?	?	?	?	?	?	?	?	?	?	?	?	?	?	?	?	?	?	?	?	?	?	?	?	?	?
†*NHMUK_PV_OR_41318*	1	0	1	0	?	1	0	0	?	?	?	0	?	0	?	?	?	?	?	?	?	?	?	?	?	?	?	?	?	?	?

	91-100										**101-110**										**111-120**									
Pomatomus_saltatrix	?	0	0	0	0	0	0	?	0	4	0	?	?	0	0	?	0	0	0	0	2	1	0	0	0	?	0	?	?	?
Gasterochisma_melampus	?	0	0	1	0	0	0	?	0	0	?	?	?	?	?	?	0	0	1	0	2	1	0	1	1	?	0	?	?	?
Scombrolabrax_heterolepis	0	0	0	0	0	0	0	?	0	0	0	?	?	?	0	0	0	0	0	?	0	0	0	0	0	0	0	?	?	?
Lepidocybium_flavobrunneum	0	?	?	?	0	0	0	?	0	0	0	?	?	?	0	0	0	0	0	1	2	0	0	1	1	0	0	?	?	?
Ruvettus_pretiosus	0	0	0	0	0	0	0	1	0	0	0	?	?	1	0	0	0	0	0	0	0	0	0	0	0	0	0	1	?	?
Thyrsites_atun	0	1	0	0	0	0	0	2	0	0	0	0	?	0	0	0	0	0	0	0	1	0	0	1	1	0	0	?	?	?
Hemithyrsites_prometheus	0	0	0	0	0	0	0	0	0	0	0	0	?	0	0	0	0	0	0	0	0	0	0	0	0	0	0	0	?	?
Rexea_prometheoides	?	0	0	0	0	0	0	0	0	0	0	0	?	1	0	0	0	0	0	0	1	0	0	1	0	0	0	?	?	?
Nealotus_tripes	0	0	0	?	0	0	0	0	0	0	0	0	?	0	0	0	0	0	0	0	1	0	0	1	0	0	0	1	?	?
Thyrsitoides_marleyi	0	0	1	0	0	0	0	0	0	0	0	0	?	0	0	0	0	0	0	1	0	0	0	0	0	0	0	?	?	?
Nesiarchus_nasutus	0	0	0	0	0	0	0	1	0	0	0	0	0	0	0	0	0	0	0	0	0	0	0	0	0	0	0	0	0	0
Gempylus_serpens	0	0	0	0	0	0	0	0	0	0	0	0	0	0	0	0	0	0	0	0	1	0	0	1	0	0	0	0	0	0
Diplospinus_multistriatus	1	0	0	0	1	0	0	0	0	0	0	0	0	0	0	0	0	0	0	1	0	2	1	1	1	1	1	0	0	1	0
Paradiplospinus_gracilis	?	0	0	0	1	0	0	0	0	0	0	0	0	0	0	0	0	0	0	1	0	2	1	1	1	1	1	0	0	1	0
Neoepinnula_orientalis	0	0	0	0	0	0	0	2	0	0	0	0	?	0	0	0	0	0	0	0	0	1	1	0	1	0	0	0	0	?	?
Epinnula_margistralis	0	?	?	?	0	0	0	?	0	0	0	0	?	?	0	0	0	0	0	0	0	0	0	0	0	0	0	?	?	?
Tongaichthys_robustus	0	?	?	?	0	0	0	?	0	0	0	0	?	0	0	0	0	0	0	0	?	2	1	0	0	0	0	0	?	?	?
Thyrsitops_lepidopoides	0	?	?	?	0	0	0	?	0	0	0	0	?	?	0	0	0	0	0	0	1	0	0	1	0	0	0	?	?	?
Aphanopus	?	0	1	0	2	1	0	2	0	1	1	0	0	0	0	0	0	0	0	2	1	2	1	1	1	?	2	1	1	1	1
Assurger_anzac	1	0	1	0	2	1	1	2	1	2	1	1	0	0	1	0	0	0	2	1	2	1	1	0	?	2	1	1	0	1	
Benthodesmus_tenuis	1	0	1	0	2	1	0	2	0	2	1	0	0	0	0	0	0	0	2	1	2	1	1	1	1	2	1	1	1	0	
Eupleurogrammus_glossodon	1	1	1	1	2	1	1	2	1	3	1	1	1	1	4	1	2	1	?	?	?	?	?	1	-	2	-	-	?	?	
Evoxymetopon	1	0	1	0	2	1	0	2	1	3	1	1	0	0	1	0	0	0	2	1	2	1	1	1	?	2	1	1	?	?	
Lepidopus_altifrons	1	0	1	0	2	1	0	2	1	3	1	1	0	0	1	0	0	0	2	1	2	1	1	1	?	2	1	1	?	?	
Lepidopus_caudatus	1	0	1	0	2	1	0	2	1	3	1	1	0	0	1	0	0	0	2	1	2	1	1	1	?	2	1	1	0	1	

	91-100	101-110	111-120
Lepidopus_fitchi	1 0 1 0 2 1 0 2 1 3 1 1 0 0 1 0 0 0 2 1 2 1 1 1 1 ? 2 1 1 0 1
Lepturacanthus_savala	- - - - 2 1 1 2 1 3 1 1 1 1 2 1 2 1 ? ? ? ? ? 1 - 2 - - 0 1
Tentoriceps_cristatus	1 1 1 1 2 1 1 2 1 3 1 1 1 1 3 1 1 1 ? ? ? ? ? 1 - 2 - - ? ?
Trichiurus_lepturus	- - - - 2 1 1 2 1 3 1 1 1 1 2 1 2 1 ? ? ? ? ? 1 - 2 - - 0 1
†*Progempylus_edwardsii*	? ?
†*Macroynis_casieri*	? ?
†*NHMUK_PV_OR_41318*	? ?

	121-130										131-140										141-144			
Pomatomus_saltatrix	?	?	?	?	?	?	?	?	?	?	?	?	?	?	?	?	?	?	?	?	?	?	?	?
Gasterochisma_melampus	?	?	?	?	?	?	?	?	?	?	?	?	?	?	?	?	?	?	?	?	?	?	?	?
Scombrolabrax_heterolepis	?	?	?	?	?	?	?	?	?	?	?	?	?	?	?	?	?	?	?	?	?	?	?	?
Lepidocybium_flavobrunneum	?	0	0	0	0	0	0	?	0	0	0	0	0	0	0	0	0	0	0	0	0	0	0	0
Ruvettus_pretiosus	?	0	0	0	0	0	0	?	0	0	0	0	0	0	1	0	0	0	0	0	0	1	0	0
Thyrsites_atun	?	0	0	0	0	0	0	?	0	0	0	0	0	0	1	0	0	0	1	0	1	1	0	0
Hemithyrsites_prometheus	?	0	0	0	0	0	0	?	0	0	0	0	0	0	1	0	1	0	0	0	0	1	0	0
Rexea_prometheoides	?	0	0	0	0	0	0	?	0	0	0	0	0	0	1	0	0/1	0	0	0	0	0	0	0
Nealotus_tripes	?	0	0	0	0	0	0	?	0	0	0	0	0	0	0	0	0	0	0	0	0	0	0	0
Thyrsitoides_marleyi	?	?	?	?	?	?	?	?	?	?	?	?	?	?	?	?	?	?	?	?	?	?	?	?
Nesiarchus_nasutus	0	0	0	0	0	0	0	0	0	0	0	0	0	0	1	0	0	0	0	0	0	1	0	0
Gempylus_serpens	0	0	0	0	0	0	0	0	0	0	0	0	0	0	1	0	0	0	0/1	0	1	0	0	?
Diplospinus_multistriatus	0	0	0	0	0	0	0	0	0	0	0	0	0	0	1	0	0	0	0	0	0	?	?	?
Paradiplospinus_gracilis	0	0	0	?	?	0	0	0	0	0	0	0	0	0	1	0	1	0	0	0	0	0	0	0
Neoepinnula_orientalis	?	0	0	0	0	0	0	?	0	0	0	0	0	0	1	0	0	0	0	0	0	0	0	0
Epinnula_margistralis	?	0	0	?	?	?	0	?	0	0	?	0	0	0	1	0	0	0	0	0	0	0	?	?
Tongaichthys_robustus	?	?	?	?	?	?	?	?	?	?	?	?	?	?	?	?	?	?	?	?	?	?	?	?
Thyrsitops_lepidopoides	?	0	0	0	0	0	0	?	0	0	0	0	0	1	1	0	0	0	1	1	1	1	0	0
Aphanopus	0	1	1	1	1	1	?	0	0	0	0	0	0	1	1	0	1	0	0	0	1	1	0	?
Assurger_anzac	0	1	1	1	1	1	?	1	0	0	0	0	0	0	1	0	0	1	0	0	0	0	?	?
Benthodesmus_tenuis	0	1	1	1	1	1	0	1	0	0	0	0	0/1	0	1	0	0	1	1	1	0/1	1	0	0
Eupleurogrammus_glossodon	?	1	1	1	?	?	?	?	2	1	1	1	1	1	0	0	0	0	0	0	1	1	?	0
Evoxymetopon	?	?	?	?	?	?	?	?	?	?	?	?	?	?	?	?	?	?	?	?	?	?	?	?
Lepidopus_altifrons	?	?	?	?	?	?	?	?	?	?	?	?	?	?	?	?	?	?	?	?	?	?	?	?
Lepidopus_caudatus	0	?	?	?	?	?	?	?	?	?	?	?	?	?	?	?	?	?	?	?	?	?	?	?
Lepidopus_fitchi	0	1	1	1	1	1	1	1	0	0	0	0	0	0	1	0	0	1	1	1	0	1	1	1

	121-130	131-140	141-144
Lepturacanthus_savala	1 1 1 1 1 1 1 1 ? 2	1 1 1 ? 1 0 1 2 0 0	? 0 1 0 0
Tentoriceps_cristatus	? 1 1 1 1 1 1 1 1 1	1 1 1 0 1 0 0 0 0 0	1 0 1 ?
Trichiurus_lepturus	1 1 1 1 1 1 1 1 ? 2	1 1 1 ? 1 0 1 2 0 0	? 0 1 0/1 0/1
†*Progempylus_edwardsii*	? ? ? ? ? ? ? ? ? ?	? ? ? ? ? ? ? ? ? ?	? ? ? ?
†*Macroynis_casieri*	? ? ? ? ? ? ? ? ? ?	? ? ? ? ? ? ? ? ? ?	? ? ? ?
†*NHMUK_PV_OR_41318*	? ? ? ? ? ? ? ? ? ?	? ? ? ? ? ? ? ? ? ?	? ? ? ?

A.4 Character Optimisations

The character optimisation is included below, but is too small to be interpretable, it is included as a large size pdf at DOI: https://doi.org/10.5061/dryad.7722q.

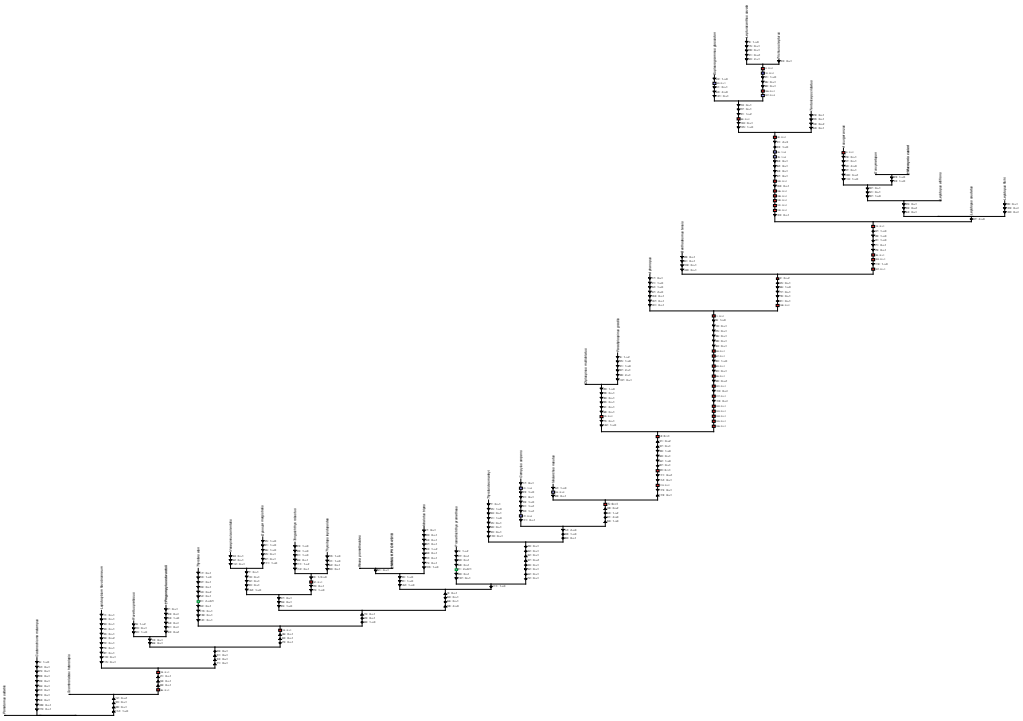


Figure A.1: Trichiuroid optimisations from morphological parsimony analysis. This pdf file is output from MacClade. A key is included.

A.5 Extant Mr Bayes tree



Figure A.2: Maximum clade credibility tree from the Bayesian analysis of the combined morphology and molecular dataset (mitochondrial data from Miya et al. 2013) for extant trichiuroids. Bayesian posterior probabilities are indicated on nodes.

Appendix B

Supplementary Information associated with Chapter 4 'The oldest fossil mackerel and the Paleocene origin of modern percomorph families'

B.1 Specimens studied using μCT

The following specimens were investigated in the course of this study for character codings or information, including fossil specimens. *Acanthocybium solandri* FMNH 44400; *Auxis rochei* UMMZ 250172; *Auxis thazard* UMMZ 238740; *Euthynnus affinis* UMMZ222134; †*Eocoelopoma curvatum* NHMUK PV OR 44877a, P623a, P9455; crania from the Eocene (Ypresian, 52-49 Ma) London Clay Formation, UK; *Gasterochisma melampus* BMNH 1868.6.22.21; *Gymnosarda unicolor* FMNH 89962; *Katsuwonus pelamis* FMNH 41899; †*L. lusitanicus* RG 9.166 a laterally

sheared cranium from the Paleocene (Selandian, 61.33-60.52 Ma) Landana Formation, Angola and RG 9.165 previously associated with †*L. lusitanicus*, a laterally sheared cranium from the same deposit; †*Micrornatus hopwoodi* NHMUK PV OR 36136 a cranium from the Eocene (Ypresian, 52-49 Ma) London Clay Formation, UK; *Rastrelliger kanagurta* UMMZ 226911; *Sarda sarda* UMMZ 145849; *Scomber australiasicus* UMMZ250152; *Scomber japonicus* UMMZ 250083; *Scomber scombrus* UMMZ 214543; *Scomberomorus maculatus* UMMZ 199143; *Scomberomorus niphonius* UMMZ 167374; *Scomberomorus regalis* UMMZ 143137; *Thunnus orientalis* FMNH 58745; *Thunnus tonggol* UMMZ 225078; and the outgroups *Scombrolabrax heterolepis* FMNH 65350; *Pomatomus saltatrix* UMMZ 111069.

B.2 Comparisons with Eocoelopomini

Tribe †Eocoelopomini Monsch and Bannikov 2012 pp.277

Diagnosis Taken from Monsch and Bannikov (2012). Frontal with postero-superior fossae extending to near middle of orbit. Frontals anterior of these fossae thickened and ornamented with more or less coarse grooves (Monsch and Bannikov, 2012, figs 26-27). About 40 vertebrae.

B.2.1 Original description of †*Landanichthys*

†*Landanichthys* was originally diagnosed by Dartevelle and Casier (1949) with the characters (our translation): "relatively short cranium, slightly elongated frontal with prominent rough lateral and posterior parts. Promiment supraoccipital but little elongated. Deep fossa extending barely in front of the anterior end of the supraoccipital. Premaxilla with rostrum protruding past the anterior end of the

teeth. No free space between the premaxilla and maxilla. Small, conical, slender teeth only seen on the premaxilla. Operculum higher than it is long, preoperculum strongly indented. Vertebrae slightly elongated, round articular faces, bear upper fossa laterally, deep pit separated by a thick longitudinal septum." We add (see Chapter 4) that it is characterised by a very upright square jaw, a pronounced ornamented chin, the dentary forms more than half of the jaw, frontals highly ornamented and truncated sharply posteriorly. Has a scalloped posterior margin of the mesethmoid.

B.2.2 Comparisons with London Clay Eocoelopomines

The taxonomy of †*Eocoelopoma* and †*Micrornatus* needs reassessment ((Beckett and Friedman, 2016), Chapter 2). †*Micrornatus hopwoodi* is remarkably similar to the neotype specimen of †*Eocoelopoma curvatum*, both of which differ considerably to the remainder of the specimens referred to †*Eocoelopoma curvatum* which bear more similarity to †*Eocoelopoma colei* (see Beckett and Friedman 2015; fig. 10). †*Eocoelopoma gigas* appears to be the adult form of those specimens similar to †*Eocoelopoma curvatum*/†*Micrornatus hopwoodi*. One further specimen, from the Danata Formation, Turkmenistan, is referred to †*Eocoelopoma*, †*Eocoelopoma portentosum* (Monsch and Bannikov 2012, pp 278-279, fig. 26). The similarities and differences of †*Landanichthys* to the three 'groups' of Eocoelopomines are discussed below. †*Eocoelopoma portentosum* shows similarities to †*L. lusitanicus* and beyond the similarities outlined below; this association merits further consideration.

Similarities to †*Micrornatus* (NHMUK PV P36136)/†*Eocoelopoma curvatum* (NHMUK PV OR44877a) neotype

†*Landanichthys* shows ornamentation on the jaws and braincase as in †*Micrornatus* and the †*Eocoelopoma curvatum* holotype, however the ornamented frontals are not truncated posteriorly in †*Micrornatus* as in †*Landanichthys*. The posterior margin of the mesethmoid is similar in †*Landanichthys* and †*Micrornatus*. However in †*Landanichthys* the dentary forms a larger portion of the lower jaw (2/3) than in †*Micrornatus* where it is approximately 1/2.

Similarities to †*Eocoelopoma curvatum* referred specimen NHMUK PV OR 24613

The ornament on the frontals is truncated posteriorly in NHMUK PV OR 24613 as in †*Landanichthys* (RG 5.695), they also both bear a trough in the underside of the vomer. However the mesethmoid shape differs, scalloped in †*Landanichthys*, but with a significant posterior extension in NHMUK PV OR 24613.

Similarities to †*Eocoelopoma colei* (NHMUK PV P623a) Holotype of †*Eocoelopoma*

Both †*Eocoelopoma colei* and †*Landanichthys* show ornamentation on the preoperculum and the frontals, however the posterior articulation of the lower jaw in †*Eocoelopoma colei* is beneath the orbit compared to posterior to the orbit in †*Landanichthys*. This also corresponds to a longer relative jaw length in †*Landanichthys*. There is no evidence of a 'chin' in †*Eocoelopoma colei* (although it could be broken off) and no evidence of ornament on the dentary. There is a

large fossa anterior to the supraoccipital in †*Eocoelopoma colei*, behind the frontals, which is not present in †*Landanichthys*.

The holotype specimen is missing a large part of the neurocranium but further comparisons with the referred specimen of †*Eocoelopoma colei* P1755 reveals a deep fossal just behind the frontals not present in †*Landanichthys*, and also no evidence of the clear truncation of the frontals in †*Eocoelopoma colei* as in †*Landanichthys*.

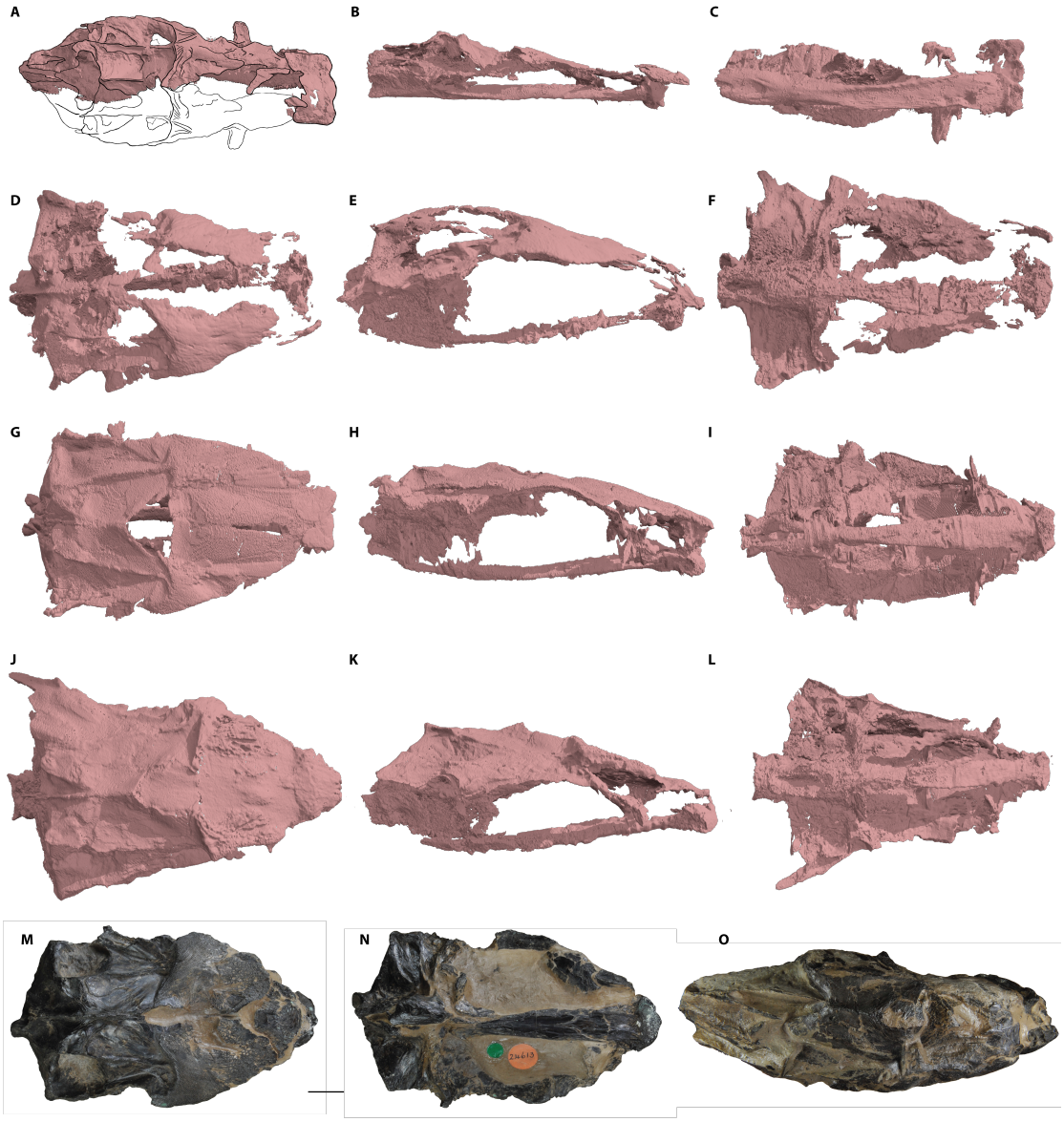


Figure B.1: Braincases of: †*L. lusitanicus* in A. dorsal view (with reconstruction overlain), B. in lateral view, C. in ventral view; †*Eocoelopoma curvatum* in dorsal D., lateral E. and ventral F. view; †*Eocoelopoma curvatum*NHMUK PV P623a in dorsal G, lateral H and ventral I view; †*Eocoelopoma curvatum* NHMUK PV P7455 in dorsal J, lateral K and ventral L view; †*Eocoelopoma curvatum*NHMUK PV in dorsal M and ventral N view; and †*Eocoelopoma gigas* in dorsal view O.

B.2.3 Comparisons to †*Eocoelopoma portentosum*

We note that †*Eocoelopoma portentosum* (Monsch and Bannikov, 2012), from the Paleocene-Eocene boundary of Turkmenistan, shows some correspondences with †*Landanichthys* to the exclusion of *E. colei*, including: a posterior position of the jaw articulation; pronounced ornamented 'chin' at the anteroventral tip of the dentary; pronounced premaxillary process; a maxilla extending to the posterodorsal corner of the dentary; slightly compressed large teeth on the premaxilla (described as small and conical by Monsch and Bannikov (2012), but here changed to represent the comparison to extant taxa) and relatively straight anterior margin of the preoperculum.

These observations suggest †*Eocoelopoma portentosum* may in fact belong within †*Landanichthys*rather than †*Eocoelopoma*, but this relationship needs further revision, as does the wider eocoelopomine group.

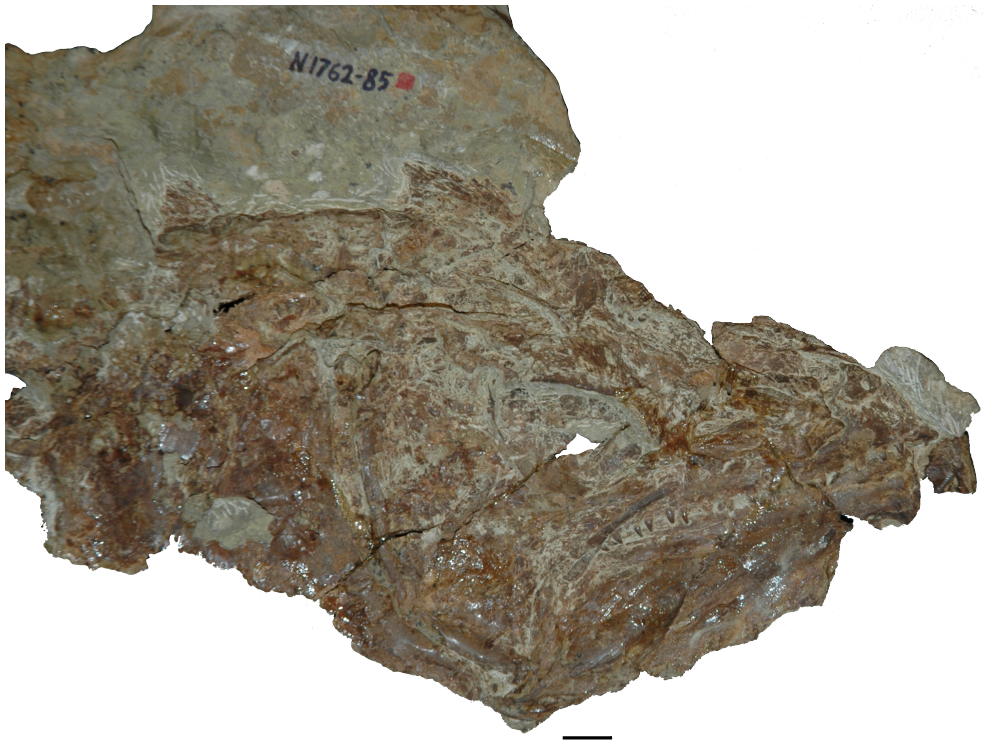


Figure B.2: †*Eocoelopoma portentosum* PIN 1762/85 (Monsch and Bannikov, 2012) from the Paleocene-Eocene boundary of Turkmenistan. Photograph (MF) of the right side of the cranium.

B.3 Percomorpha *incertae sedis* RG 9.165

Formerly associated with †*L. lusitanicus* RG 9.165 (Fig. B.3A-B) is here removed from Scombridae as it's jaws bear broad bands of denticles rather than a single row of teeth, suggesting a filter feeding approach. A single row of teeth is a synapamorphy of Scombridae (Johnson, 1986). Additionally gill rakers are preserved on the first arches of the specimen. We now consider RG 9.165 a generalised percomorph, and it's affinities are unclear. A brief description is given below.

B.3.1 Brief Description

The braincase is robust but sheared laterally and broken at the midlength (Fig. B.3C,E). The frontal is highly fragmented and ornamentation is lacking, although how much this is a result of preservation is unclear. It is not possible to see sutures between the bones on the dorsal surface of the braincase, but based on relative positions, the fragmented remains of the supraoccipital, exoccipitals, pterotics, epiotics and parietals are preserved. Both lateral ethmoids are preserved, they are robust hourglass shaped. The parasphenoid is well preserved and sutures to the underside of the basioccipital which is laterally compressed. The parasphenoid is elongate, widest anteriorly at the suture to the parasphenoid and coming to a point at its posteiror end. Where the lateral commisure contacts the braincase the parasphenoid constricts significantly. Anterior to this the parasphenoid bears a pronounced ridge on its midline. The vomer is well preserved, is an elongate kite-shape with a thickened and rolled anterior margin. On the underside of the vomer a rough triangular area may be a tooth patch.

The complex of the upper jaw is short relative to the lower jaw, which extends past the posterior margin of the supramaxilla. The maxilla articulates with the premaxillary process anteriorly and the flat supramaxilla posteriorly. The supramaxilla is expanded posteriorly and articulates with the posterior-dorsal margin of the dentary. The lower jaw is triangular and flat extending on the ventral surface of the skull, with a small ventral projection at the anterior tip (Fig. B.3D). The dentary forms the dorsal margin of the jaw, bearing several rows of denticles.

The suspensoria (Fig. B.3G-H) preserves the palatine, pterygoid bones, hyomandibular, quadrate and symplectic. The palatine has a pronounced lateral

head that articulates with the anterior head of the maxilla. The palatine meets the ectopterygoid posteriorly. The ectopterygoid is a long splint-like bone, curving down posteriorly to form a triangular expansion where it articulates with the quadrate. The quadrate of both specimens is triangular in shape with a head for articulation with the posterio-ventral corner of the lower jaw and a notch on the dorsal margin behind which the symplectic, a splint like bone, is housed. The endopterygoid is a flat plate-like bone broken by the shearing of the specimen. The metapterygoid is a triangular ossification which overlaps the dorsal margin of the quadrate ventrally and bifurcates to articulate with the hyomandibular dorsally. The hyomandibular has a large articular head with a well developed ventral plate like extension with a notch just above the articulation with the metapterygoid. On the surface of the hyomandibular extending down the ventral arm is a lateral plate like expansion.

The hyoid and gill arches are robust and preserved in partial articulation (Fig. B.3F). A ceratohyal window is preserved in the anterior ceratohyal and the posterior ceratohyal is triangular. The hypohyals are tightly sutured. The gill arches preserve elements of both the central and dorsal gill skeleton and gill rakers are preserved on the first arch.

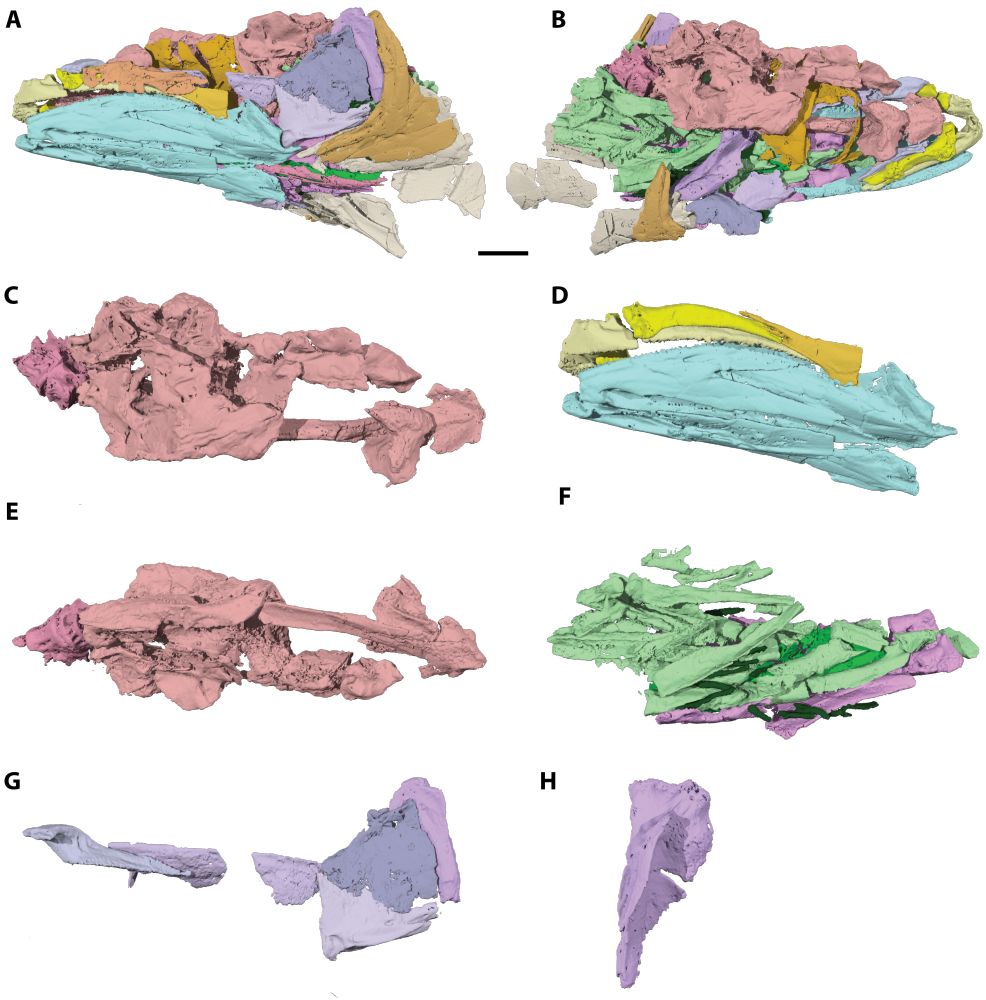


Figure B.3: μCT renderings of Percomorpha *incertae sedis* RG 9.165. A, Left and B, right lateral view of whole specimen, scale bar 10mm. C, dorsal view of braincase, D, left lateral view of jaw apparatus, E, ventral view of braincase. F, right lateral view of hyoid and gill arches. G, left lateral view of suspensorium and H, right lateral view of right hyomanidbular, broken on the left side of the specimen. Panels C-H not to scale.

B.4 Scombrid character list

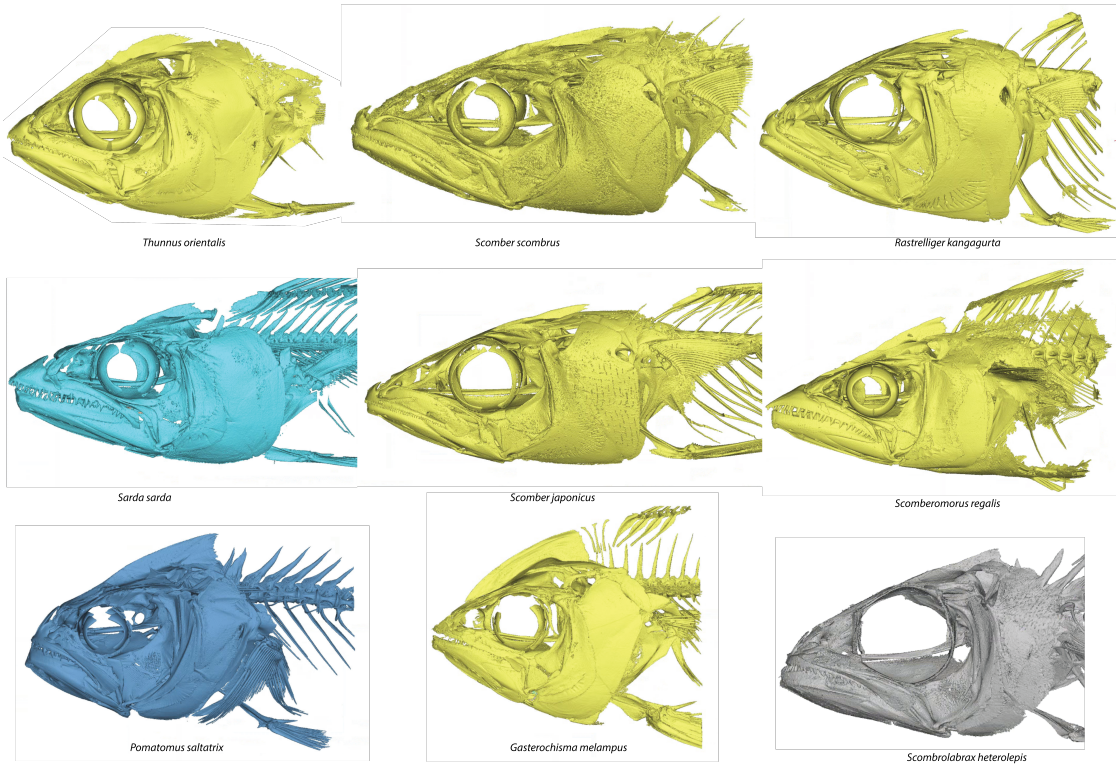


Figure B.4: Left lateral views of a sample of Scombridae and outgroups studied in this analysis.

Gill Arches

1. Epibranchials. Tip of 2nd epibranchial short (0); 2nd epibranchial extends over top of 3rd infrapharyngobranchial to connect with 3rd epibranchial (1); tip of 2nd epibranchial greatly expanded to articulate with both the 2nd and 3rd pharyngobranchials. (Collette et al 1984 [1], Johnson 1986 [6])

This character is used in a couple of different analyses to mean different things. I have used the character states from Johnson, but included the uncertainty of of Collette and Russo 1984 [48] "Anterior process of second epibranchial. Elongate (0); not elongate (1)" (but see Pg 49 which gives a different character state to the one in the character list). Collette and Russo (1984) state that a shortened anterior process is a character uniting Acanthocybium *and* Scomberomorus.

2. Triangular stay extending anteriorly from anteromedial corner of fourth pharyngeal toothplate. Stay absent, anterior margin of toothplate truncate, no bony contact between it and PB3 (0); anteromedial corner of toothpla.e gives rise to large laminar, approximately triangular bony stay that extends anteriorly along ventromedial side of PB3 (1). (Collette et al 1984 [3], Johnson 1986 [31])

3. Fourth pharyngobranchial cartilage. Present, abuts posterior cartilaginous margin of PB3 and is main surface of articulation for EB4 (0), absent, EB4 articulates directly with the posterior cartilaginous portion of PB3 (1) (Johnson 1986 [7])

4. Third pharyngobranchial and fourth pharyngeal toothplate. short, with broad rounded flat shelf along anteromedial margin of third pharyngobranchial (0); PB3 and fourth pharyngeal toothplate elongate, lateral shelf on PB3 reduced, medial margin of bone straight (1). (Johnson 1986 [8])

   In my opinion this could be a function of the previous character, however I have left it in the analysis and scored it. I would want to study cleared

and stained specimens, in addition to higher resolution CT scans in a wider range of taxa to build up a character distribution.

5. Shape of the fourth epibranchial. Medial arm slightly expanded (0), medial arm elongate and circular in cross section (1); Medial arm dorso-ventrally expanded (2). (Collette, Reeb and Block 2001)

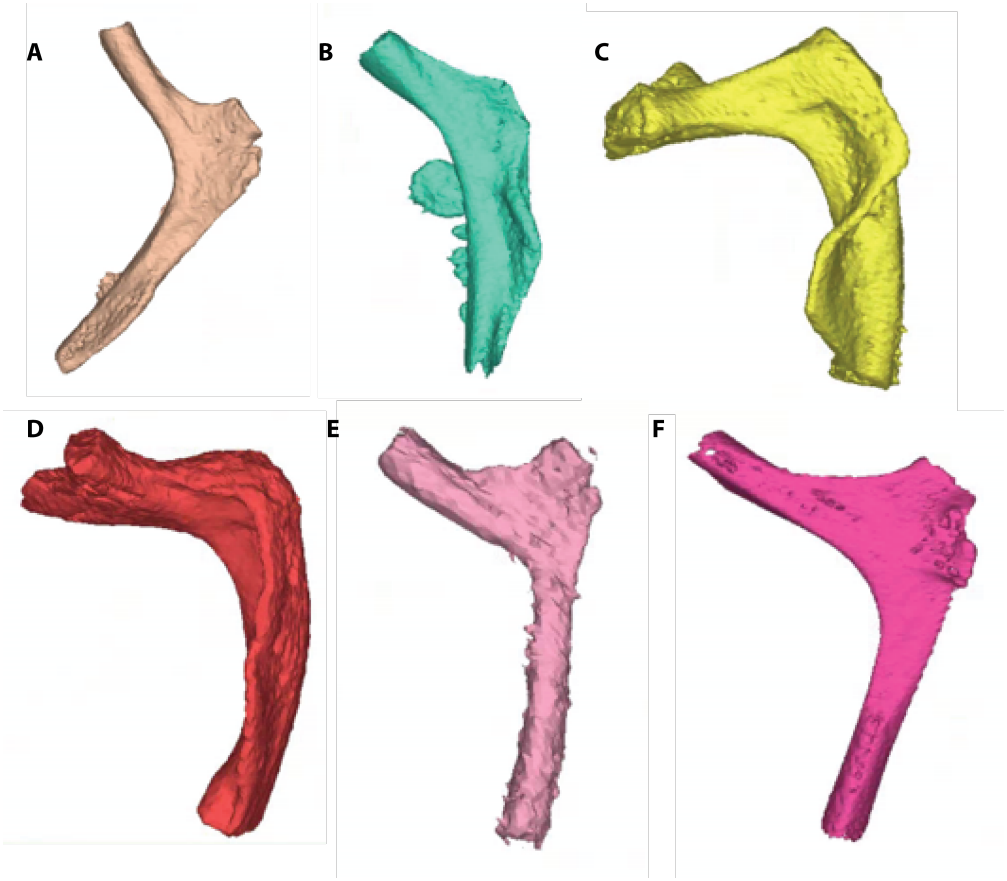


Figure B.5: A, *Scomberomorus regalis* (1), B, *Pomatomus saltatrix* (0), C, *Scomber japonicas* (2), D, *Rastrelliger kangagurta* (2), E, *Sarda sarda* (1), F, *Thunnus orientalis* (0).

6. Tongue teeth. None fused to glossohyal (0); patch of teeth on the glossohyal (1); two patches fused to glossohyal (2). (Collette et al 1984 [40])

*"*Orcynopsis*,* Cybiosarda *and* Gymnosarda *have two patches of tongue teeth, but the patches are attached to the glossohyal bone in the former two genera and on separate plates that fit over the bone in* Gymnosarda*" (Collette, Reeb and Block 2001)*

7. Cross-connections of gill filaments. No cross-connections (0); cross-connections present (I). (Collette et al 1984 [6])

   Only seen in Thunnus *according to the tree in Collette et al. 1984. No other evidence clear in the literature or in scans.*

8. Fifth branchiostegal borne posterior to anterior ceratohyal. Fifth branchiostegal expanded head inserts on the posteroventral corner of anterior ceratohyal (0); fifth branchiostegal ray narrow head, displaced posteriorly and inserting on the anteroventral corner of posterior ceratohyal (1). (Johnson 1986 [10])

9. Gill rakers: few (0); many short (1); many elongate (2); few elongate (3). (formalised from Collette, Reeb and Block, 2001)

   This character is from Collette, Reeb and Block 2001, who describe it both in terms of few and many, and also in terms of numbers, which makes it confusing. I have coded these in combination of the scanned specimens and these descriptions. Collette, Reeb and Block 2001 p. 7 indicate Rastrelliger *(44ish) has more numerous and elongate gill rakers than* Scomber *(which has 30 from my count).* Grammatorcynus *(Scomberomorini) has fewer rakers (Collette, Reeb and Block 2001, p. 8)* Scomberomorus regalis *has 13 gill rakers (my count UMMZ 143137).* Allothunnus *(Thunnini) has a "very high*

number of gill rakers" (Collette, Reeb and Block 2001 p. 12). Auxis *has 37-47 gill rakers (*Auxis thazard *47-43,* Auxis rochei *40-47).* Katsuwonus *(53-63).* Euthynnus *(29-40).* Thunnus atlanticus *(19-25),* Thunnus tonggol *19-28 both in the subgenus (*Neothunnus*). In the subgenus* Thunnus *(*Thunnus thynnus, T orientalis*, and* T maccoyii *(31-43) and* T. alalunga, T. obesus *(23-31)).*

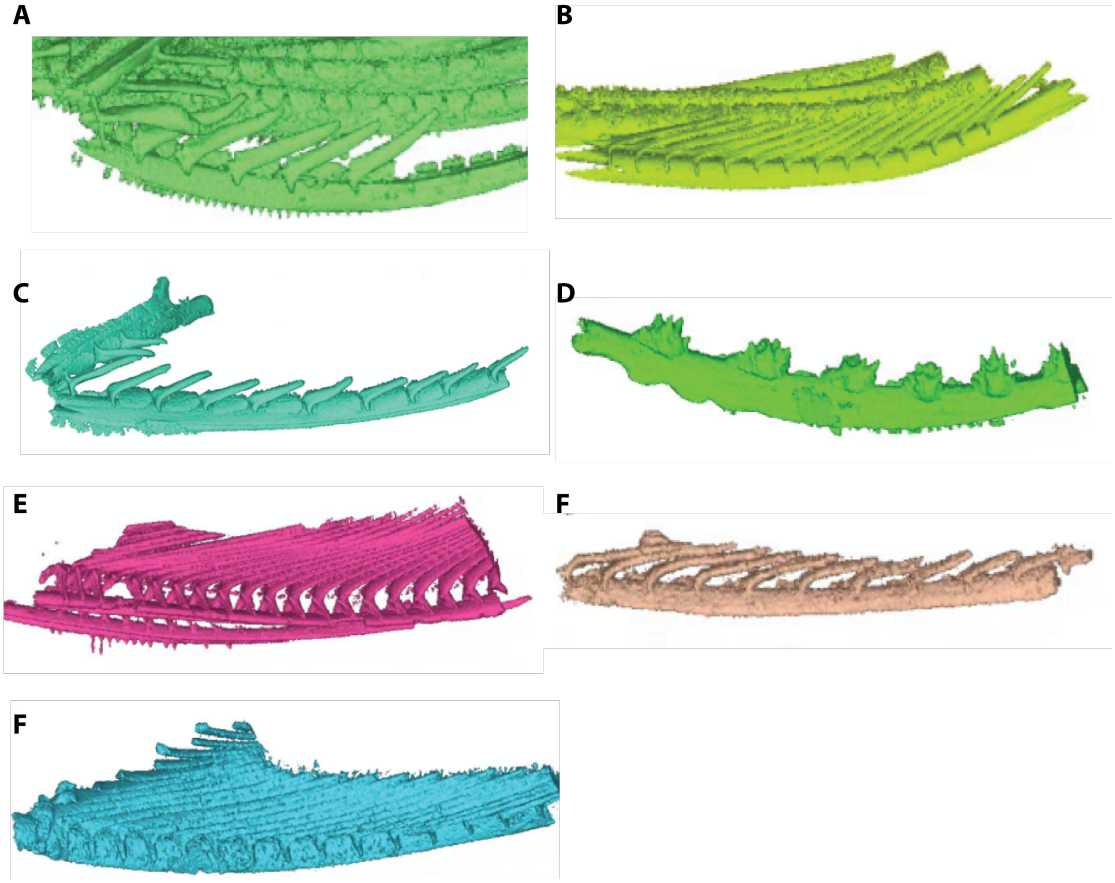


Figure B.6: A, *Pomatomus saltatrix* (3), B, *Thunnus orientalis* (1), C, *Scomberomorus regalis* (3), D, *Gasterochisma melampus* (0), E, *Rastrelliger kangagurta* (2), F, *Sarda sarda* (1), G, *Scomber japonicus* (1).

10. Dorsally projecting ridges on the upper surface of the tongue: Absent (0), Present (1). (formalised from Collette, Reeb and Block, 2001)

    Collette, Reeb and Block, 2010 (p.12) indicate Thunnini are the only scombrids to show the presence of this character. Collette and Chao 1975 (p. 75) describe Sardini as "lack[ing] dorsally projecting lateral cartilaginous ridges on tongue".

11. Last branchiostegal ray: Rounded (0); Flattened (1); only slightly flattened (2). (formalised from Collette, Reeb and Block, 2001)

    Collette, Reeb and Block list a slightly flattened branchiostegal ray as a unique synapomorphy of Scomber*.*

12. Shape of posterior end of dorsal margin of urohyal Tripartite (0); Forked (1); Simple (2) (Collette and Russo 1984 [44])

    Tripartate posterior ends of dorsal margin of urohyal is seen in most outgroups and some scombrids. Thunnus *has a simple rounded posterior end of the urohyal, and is not tripartite or forked.*

Infraorbital bones

13. Anterior end of infraorbital bone. Not tubular (0); tubular (I). (Collette et al 1984 [15])

    Invariant in Scombridae, but this character remains in the matrix as if you want to compare more widely across Pelagiariaria it is variant e.g. it is tubular in gempylids and trichiurids.

14. lnfraorbital bones. Not expanded into large plates (0); expanded into large plates (1). (Collette et al 1984 [9])

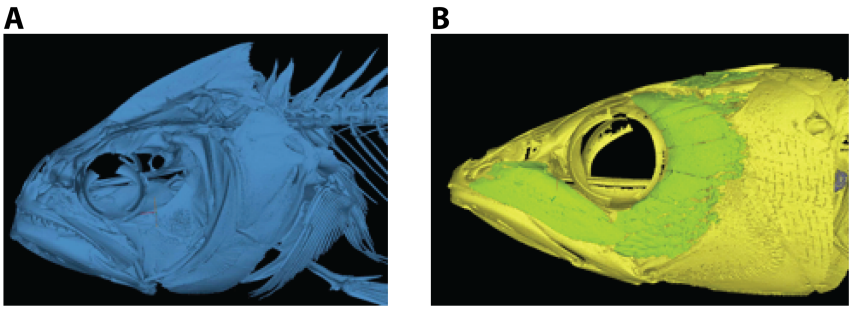


Figure B.7: A, *Pomatomus saltatrix* (0), B, *Scomber japonicas* (1).

15. Joint between first and second infraorbital bones. Simple contact (0); tightly bound (I). (Collette et al 1984 [28])

    Seen in all Scombridae, independently acquired in some (?) gempylids, see tree Collette et al. 1984, however not clear which from this tree. In future analyses of Pelagiariaria this character would need detailed investigation.

Jaws

16. Inner row of premaxillary teeth. Single row of premaxillary teeth (0); additional row of teeth present on antero-medial end of premaxilla (1). (Collette et al 1984 [18], Johnson 1986 [32])

    "A single row of premaxillary teeth is seen in all scombrids [and also in billfishes]. Scombrops*,* Scombrolabrax *and Trichiuroidea have a short inner row of two or three enlarged fang like teeth near the premaxillary symphysis" (Johnson 1986 pg 21).*

17. Protrusability of premaxilla. Upper jaw protrusible, premaxilla free from maxilla (0); premaxilla anchored to maxilla (1). (Collette et al 1984 [19], Johnson 1986 [9])

18. Tooth shape. Small conical (0); large conical (1) large compressed (2). (Collette et al 1984 [25])

    Collette, Reeb and Block 2001 (p. 7) indicate all Scomberomorini have large compressed teeth, which are serrate in some species. They also describe Scombrini as having small conical teeth. Scombrini have small conical teeth. (Collette, Reeb and Block 2001 pp 5). In Collette et al. (1984 fig. 312), character state 1 is only seen in Scomberomorus *and* Acanthocybium*, all other taxa have a character state 0.*

19. Length of maxillary head. Short (0); Medium (1); Long (2); very long (3). (Collette and Russo 1984 [6])

    Coded for Scomberomorines from Fig 70 (Collette and Russo, 1984). He states the plesiomorphic condition as 2.

20. Distinctive Development, Replacement Mode and Adult Configuration of Primary Jaw Dentition. Several large ankylosed teeth on dentary amidst the usual bands of Type 2 teeth (0); Single row of ankylosed (Type 1) teeth (1). (Johnson 1986 [1])

    See (Fink, 1981). State (0) is seen in outgroups to Scombrops + Scombrolabrax + Pomatomus + *Scombridae*

21. Ventral process of angular relative to the length of the dorsal process. Short, 42-80% (0); moderate, 87-93% (1); long, 117-126% (2). (Collette and Russo 1984 [6])

    This character refers to the relative length of the ventral process of the angular to the dorsal process of the angular. The ventral process of Acanthocybium *is longer than the dorsal process, the ventral process of* Grammatorcynus *is shorter than the dorsal process, and the two processes are relatively equal in scomberomorines generally.*

22. Relative length of arms of the dentary. Lower arm longest (0); approximately equal (1); upper arm longer than lower arm (2). (Collette and Russo 1984 [56])

    Collette and Russo list Grammatoryncus *as having a slightly longer lower arm than upper arm. Collette and Chao (1975) say they are usually about equal in length (pg 557) but that the ventral branch is slightly longer in* Gymnosarda *and* Allothunnus *and sometimes* Sarda.

23. Posterior-dorsal limb of the articular relative to the main body of the articular: small posterior-dorsal limb of the articular with a small notch anterior to it (0); large posterior-dorsal limb of the articular robust with a large notch anterior to it (1). (New Character)

    A large posterior-dorsal limb on the articular is found in Scombrini to the exclusion of other scombrids. The outgroups Scombrolabrax *and* Pomatomus *also show a small notch on the articular.*

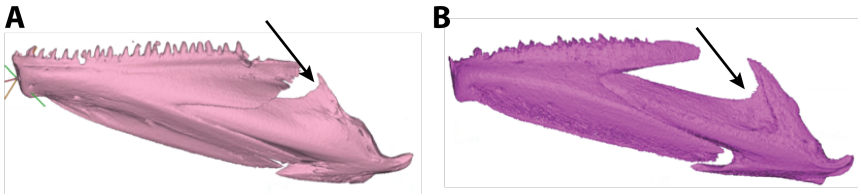


Figure B.8: A, *Thunnus orientalis* (0), B, *Scomber scomber* (1).

24. Snout: short (0); elongate (1). (Collette, Reeb and Block 2001)

    Scomberomorus *lacks the elongate snout characteristic of* Acanthocybium. *This is in many ways a weak character, as length is never a a particularly good indicator.*

Suspensorium

25. Teeth on palatine: Absent (0); Present (1). (Collette, Reeb and Block 2001)

    Teeth are present on the palatine of Scomber, *but not* Rastrelliger *(Collette, Reeb and Block 2001). Palatine teeth are present in* Sarda sarda *(8-21; table 17 Collette and Chao 1975). Present in all of* Cybiosarda, Orcynopsis, Gymnosarda *and* Allothunnus *(figure 35 Collette and Chao, 1975). Seen in* Scomberomorus, Acanthocybium *and* Grammatorcynus. *(Gibbs and Collette, 1967) describes a "dentigerous palatine" in Thunnini.*

26. Large ventral extension of the hyomandibular head. Absent (0); Present (1) (New Character)

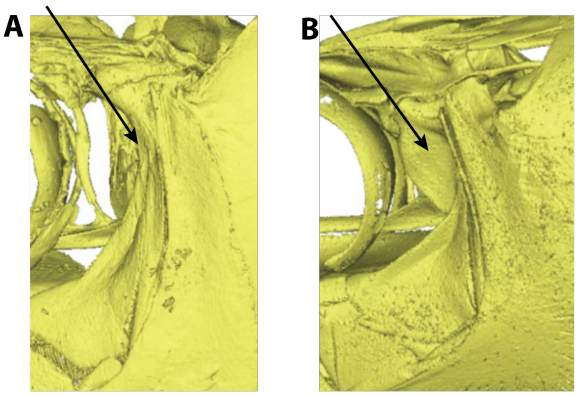


Figure B.9: A, *Gasterochisma melampus* (0), B, *Scomber scombrus* (1).

27. Length of posterior arm of ectopterygoid. Posterior edge long, 64-68% of ventral length (0); posterior edge short, 41-62% of ventral length (1). (Collette and Russo 1984 [57])

    Grammatorcynus *has a long posterior edge which is listed as the plesiomorphic condition.* Acanthocybium *and* Scomberomorus *have a short posterior edge. Sardini coded from Collette and Chao (1975)*

Neurocranium

28. Fronto-parietal fenestra. Absent (0); present (1). (Collette et al 1984 [24])

    Seen in Euthynnus, Katsuwonus *and* Thunnus *(fig. 312).*

29. Paired frontoparietal foramina: lacking (0), prominent (1). (Collette, Reeb and Block 2001)

    Collette, Reeb and Block (2001) describe a prominent pair of frontoparietal foramina on the dorsal surface of the skull as seen in all Thunnini except Auxis *and* Allothunnus.

30. Prootic pits (on ventral surface of skull). Absent (0); present (1). (Collette et al 1984 [26])

    Collette and Chao (1975; p. 75) and Collette, Reeb and Block (2001) describe the absence of well developed prootic pits as a character uniting all Sardini. Collette, Reeb and Block (2001; p. 12) suggest well developed prootic pits are seen in all Thunnini. In Collette et al. (1984 fig. 312) this character is optimised below the Thunnini, suggesting all other scombrids and outgroups show no prootic pits.

31. Subocular shelf on the third infraorbital. Present (0); absent (1). (Collette et al 1984 [10], Johnson 1986 [37])

    *Johnson 1986 [37], Collette et al 1984 [10] discusses the presence/absence of a subocular shelf. The presence of a subocular shelf on the third infraorbital is seen in generalised percoids. The distribution of this shelf is variable in scombrids, absence is seen some gempylids (*Rexea, Thyrsitops, Thyrsitoides *and* Tongaichthys*) and Scombrini and a subocular shelf originating from the posterior portion of the third infraorbital is seen in Sardini, Thunnini and Scomberomorini.*

32. Enlarged and reoriented fronto-sphenotic shelf forms floor of large fossa. Junction of infraorbital and supraorbital sensory canals is at posterior margin of orbit, uppermost infraorbital resting in an expanded, trough like area or notch on the more or less vertically oriented lateral margin of the sphenotic (0); supraorbital canal separated from dorsolateral margin of the orbit by large fossa which houses enlarged levator arcus palatini, horizontally

orientated fronto-sphenotic shelf is thick and rounded, not modified to accommodate dorsal-most infraorbital. (1); supraorbital canal separated from dorsolateral margin of the orbit by large fossa which houses enlarged dilatator opercula, horizontally orientated fronto-sphenotic shelf is thin and not modified to accommodate dorsal-most infraorbital. (2) (Johnson 1986 [3])

Johnson notes that this character is long and could probably be split into multiple characters.

33. Teeth on vomer: Absent (0); Present (1). (Collette, Reeb and Block 2001)

    Gasterochisma *and* Scomber *coded from Collette, Reeb and Block 2001. Sardini coded from images in Collette and Chao 1975.* Scomberomorus*,* Acanthocybium *and* Grammatorcynus *coded from Collette and Russo 1984 (fig. 18-19). Additionally observations are made of scanned material.*

34. Pineal window: Absent (0); Present (1); Reduction in bone thickness (2). (Collette, Reeb and Block 2001)

    Collette, Reeb and Block 2001 - "Grammatorcynus *differs from* Scomberomorus *in having [...] a pineal window". Collette and Chao 1975 p.21 - "A prominent pineal foramen (Figures 10-14) is present anterior to the supraoccipital crest between the median edges of the frontal bones. Among the bonitos, it is most prominent in* Allothunnus*. Other scombrids either have a reduction in the thickness of the bone in this area (*Scomber, Rastrelliger*, and* Scomberomorus*) or a similar pineal foramen (*Grammatorcynus, Acanthocybium, Auxis, Euthynnus, Katsuwonus*, and* Thunnus*)."*

35. Position of nasal. Protrude far beyond ethmoid region (0); do not protrude further than adjacent to the ethmoid region (1). (Collette and Russo 1984 [43])

Shoulder Girdle

36. Width of supracleithrum. Wide (0); Narrow (1). (Collette and Russo 1984 [41])

37. Pores on dorsal arm of supratemporal. Absent (0); Present (1). (Collette and Russo 1984 [42])

Post-cranial

38. Predorsal bones. Present (0); absent (1). (Collette et al 1984 [2], Johnson 1986 [11])

39. Number of epurals. Three (0); two (1). (Collette et al 1984 [7], Johnson 1986 [36])

40. Number of ossifications in last dorsal and anal pterygiophores. A single ossification (0); two ossifications (1) (Collette et al 1984 [20])

    This is optimised in Collette et al (1984) fig. 312 as relating to all gempylids and scombrids.

41. Relationship of second dorsal fin pterygiophores to neural spines. Relationship 2:1 (0) 1:1 (1). (Collette et al 1984 [21])

Interpreted as referring to two pterygiophores associated the neural spines.

42. Single supernumerary spine on first spinous dorsal pterygiophore; Two supernumerary spines, primitive "chain link" articulation (Bridge 1896) (0); Single supernumerary spine, no chain link articulation (1). (Johnson 1986 [2])

    Single supernumary spine seen in Scombrolabrax + Pomatomus *and the scombroids.*

43. Vertebral trellis work. Absent (0); present (1); present, reduced (2). (modified from Collette et al 1984 [27])

    Vertebral trellis work is scored as seen in all Thunnini except Allothunnus *in Collette et al (1984 fig. 312). However Collette, Reeb and Block (2001) provide more detail, stating that vertebral trelliswork is present in* Euthynnus *and* Katsuwonus*, it is reduced (yellowfins) or absent (bluefins) in* Thunnus*. No mention is made of trelliswork either present or absent in* Auxis*, which is therefore coded as in Collette et al. (1984).*

44. Number of vertebrae. 24-26 (0), 30-31 (1); 32-67 (2); 98-192 (3). (Johnson 1986 [16], Collette et al 1984 [29])

    Johnson 1986 changes the states from Collette et al 1984. Character coding has been carried out based on Johnson's character.

45. Number of pectoral fin rays. 10-17 (0); 17-19 (1); and along another transition series to 17-23 (2), 20-27 (3), 25-29 (4), and 30-36 (5). (Collette et al 1984 [39])

    Coded from Table 155 Collette et al 1984.

46. Dorsal and anal fin stay bifrurcated posteriorly. Stay simple, flat vertical plate (0); posterior end of stay bilaterally bifurcated (1). (Johnson 1986 [4])

    Bifurcate stay synapomorphy of Pomatomus *and scombrids, reversal in trichiurids.*

47. Finlets. Absent (0); present (1). (Johnson 1986 [12]).

    Present in scombrids, absent in percoids and Sphyraena*, independently lost in some gempylids/trichiurids.*

48. Interneural bones under the first dorsal fin: 11 (0); 12-28 (1). (Collette, Reeb and Block 2001)

    Collette, Reeb and Block (2001) describe these in Rastrelliger *and* Scomber *based on Matsui 1967 Table 4. A literature search does not reveal any record of interneurals in other tribes.*

49. Precaudal vertebrae: 12-14 (0); 13 (1); 14 (2); 16-19 (3); 20-21 (4); 22-28 (5); 16-32 (6); 30-32 (7). (Collette, Reeb and Block 2001)

    Collette, Reeb and Block (2001) describe 13 precaudal vertebrae in Scomber scombrus*, and 14 in the other species of* Scomber*. These are maintained and then added to using Table 154 from Collette et al 1984.*

Caudal fin

50. Number of vertebrae supporting caudal fin. Two (0); 3-4 (1). (Collette et al 1984 [8], Johnson 1986 [40])

51. Mid-lateral keel on caudal peduncle. Absent (0); present (1). (Collette et al 1984 [11], Johnson 1986 [38])

    A fleshy mid lateral keel on the caudal peduncle is seen in Lepidocybium*, and all scombrids above the Scombrini (i.e. it is absent in Scombrini).*

52. Median keel on caudal peduncle: Well developed with no bony support (0), partially developed bony keel (1), fully developed bony keel supports fleshy median keel on the caudal peduncle (2). (Collette, Reeb and Block 2001)

    Gasterochisma *lacks a median keel on the caudal peduncle (Collette, Reeb and Block 2001, p. 5) It is also absent in Scombrini. This character is therefore inapplicable to these taxa. Scomberomorini have a well-developed median keel on the caudal peduncle, but with no bony support (Collette, Reeb and Block 2001). In Sardini and Thunnini there is a developed bony keel, which is partially developed in Sardini and fully developed in Thunnini (Collette and Chao, 1975 (p75); Collette, Reeb and Block, 2001). This character has been merged with Collette et al. (1984) [16] and [17].*

53. Pair of small keels at base of caudal fin. Absent (0); present (1). (Collette et al 1984 [12], Johnson 1986 [14])

    In Gasterochisma*, this character is coded in Johnson 1986 as 0 (absent), but Collette, Reeb and Block (2001) say "has only the pair of small keels on each side of the base of the caudal fin that are characteristic of all scombrids", and Collette et al. (1984 fig. 312) optimises this character as present in* Gasterochisma *(and all Scombridae). This character is therefore updated for this taxon.*

54. Extension of caudal fin rays over hypural plate. Not overlapping or slightly overlapping plate (0); completely covering plate (1). (Collette et al 1984 [14], Johnson 1986 [33])

55. Number of uroneurals in adult. Two (0); one (1). (Collette et al 1984 [30], Johnson 1986 [34]) Fusion of uroneural to urostyle. No fusion (0); fused (I). (Collette et al 1984 [31])

56. Bony shelf divides the neural canal of anterior six vertebrae into dorsal and ventral portions: Absent (0), Present (1).

    A bony shelf dividing the neural canal of the anterior six vertebrae into dorsal and ventral portions is absent in Thunnus*, but seen in all other Thunnini. (Collette and Chao 1975 pp 76)*

57. Preural centra two and three: not greatly shortened (0), shortened (1). (Collette and Chao 1975, Collette, Reeb and Block 2001)

    Preural central two and three not greatly shortened in Scombrini and Scomberomorini (Collette and Chao 1975 pp 75, Collette, Reeb and Block 2001 pp 5)

58. Fifth hypural fuses to uroneural, but not to hypural plate. Distal ends of uroneural embrace and eventually fuse with the proximal portion of the fifth hypural forming a hockey-stick-shaped strut (0); ventral margin of the fifth hypural remains separate from the hypural plate (1). (Johnson 1986 [35])

    Replaces Collette et al 1984 [31]

59. Fusion of upper hypural bones. Hypurals 3, 4, and 5 separate (0): 3 and 4 fused (1); 3, 4, and 5 fused (2). (Collette et al 1984 [32], Johnson 1986 [13]1, Russo 1983 [79])

60. Fusion of lower hypural bones. Hypurals l and 2 separate (0); fused (1). (Collette et al 1984 [35], Johnson 1986 [13]1, Russo 1983 [81])

    Johnson 1986 amalgamates Collette et al 1984 [32] and [35] as the fifth hypural doesn't fuse to the fourth in scombroids. Russo (1983) also has these two characters for gempylids, and they are both variable and fusion of the fifth hypural is seen, and the separation is therefore preserved.

61. Notch in hypural plate. Large (0): small (1); absent (2). (Collette et al 1984 [33])

    Collette, Reeb and Block 2001 p. 10 say a notch in the hypural plate is absent in Sardini. There is a distinct notch in the hypural plate in Scombrini and Scomberomorini (Collette and Chao 1975 pp 75, Collette, Reeb and Block 2001 pp 5). Some discussion in Johnson 1984 about whether this is a suitable character due to the relative size of the hypural notch. This has been kept in for now, but may need reassessing.

62. Fusion of upper and lower hypural plates. Not fused (0); fused (I). (Collette et al 1984 [34], Johnson 1986 [39])

63. Fusion of parahypural to hypural plate. Separate (0); fused (1). (Collette et al 1984 [36])

64. Number of autogenous haemal spines. Two (0); one (1). (Collette et al 1984 [37])

65. Tips of neural and haemal spines of preural vertebra 4. Tips not flattened (0), tip of one flattened (1), tips of both flattened (2). (Collette et al 1984 [38])

66. Procurrent spur: well developed with foreshortened preceding ray (0), absent (1), reduced, preceding ray not foreshortened (2). (modified from Johnson 1986 [15])

    Johnson (1986) notes that a reduced spur occurs in some gempylines, and for that reason I have added a character to account for this, should this analysis ever be used amongst a wider subset of Pelagiaria.

Ontogenetic Characters

67. Dorsal fin developmental sequence. Second dorsal develops before first dorsal (1); first dorsal develops before second dorsal (0). (Collette et al 1984 [4])

68. Shape of premaxilla in larvae. Not beak-like (0); beak-Like (1). (Collette et al 1984 [5], Johnson 1986 [41])

69. Pelvic fins: do not increase in size (0), large in juveniles, and reduce in size in adults (1). (Collette, Reeb and Block 2001)

Other

70. Corselet (A densely scaled area in certain tuna-like fishes usually behind the pectoral fins). Absent (0); present (1). (Collette et al 1984 [22])

71. Subcutaneous vascular system. Absent (0): present (1). (Collette et al 1984 [23])

    Collette and Chao 1975 (p. 75) indicate that Sardini lack a specialised subcutaneous vascular system seen in Thunnini. Other taxa are coded from Collette et al 1984.

72. Thick crescent of adipose tissue along posterior margin of eye. Absent (0), Present (1). (Johnson 1986 [5])

73. Countercurrent heat exchanger system of retia mirabilia: Absent (0), Present, central and lateral heat exchangers (1), Present, lateral heat exchange only (2). (Collette, Reeb and Block 2001)

    Thunnini are united in the presence of a countercurrent heat exchanger system of retia mirabilia in the circulatory system (Collette, Reeb and Block 2001 p.12), allowing tunas to maintain body tissue temperatures warmer than the surrounding water. Auxis, Euthynnus, Katsuwonus, Thunnus albacares, Thunnus atlanticus *and* Thunnus tonggol *have central as well as lateral heat exchangers while* Thunnus obesus, Thunnus maccoyii, Thunnus thynnus, Thunnus alalunga *and* Thunnus orientalis *do not, but have a well-developed lateral heat exchange (Carey et al. 1971; Graham 1973, 1975; Collette, Reeb and Block 2001 p.12).*

74. Cycloid scales: Present (0), Absent (1). (Collette, Reeb and Block 2001)

75. Brain heater derived from lateral extraocular muscle: Absent (0), Present (1). (Collette, Reeb and Block 2001)

76. Swimbladder: Absent (0); Present (1).

Coded from Collette, Reeb and Block (2001)

77. Anterior projections of swim bladder: does not extend into back of skull (0), extend into the back of skull (1). (Collette, Reeb and Block 2001)

    Collette, Reeb and Block (2001), large anterior projection of swim bladder of Gasterochisma *into the posterior of the skull.*

78. Thick layer of fat under scales: Absent (0); Present (1). (Collette, Reeb and Block 2001) *Collette, Reeb and Block (2001) report "a thick layer of fat is visible under the scales" of* Gasterochisma.

79. Additional lateral line: Absent (0); Present (1). (Collette, Reeb and Block 2001) Grammatorcynus *differs from* Scomberomorus *in having two lateral lines.*

B.5 Removed characters

1. Angle of lateral and medial arms of fourth epibranchial. More acute (0); less acute (1). (Collette and Russo 1984 [47])

   This character has been removed as it does not refer to a specific angle and is therefore difficult to assess

2. Deleted Johnson characters 46-49 as they refer solely to Xiphioids, and are invariate in scombrids.

B.6 Character Matrix

	1-10										11-20										21-30										31-40									
Scombrolabrax_heterolepis	0	0	0	0	0	0	0	3	0	1	2	0	0	0	1	0	0	2	0	1	2	0	0	0	0	1	0	0	0	0	0	?	0	0	1	0	0
Pomatomus_saltatrix	0	0	0	0	0	0	0	3	0	1	2	0	0	0	1	0	0	0	2	0	1	2	0	0	1	0	0	0	0	1	1	0	?	0	0	0	0	0
Gasterochisma_melampus	0	0	0	0	0	0	0	1	0	0	1	2	0	0	1	0	1	1	2	1	2	2	0	0	0	1	0	0	0	0	0	?	0	0	0	0	?	1
Scomber_scombrus	2	1	1	1	2	0	0	1	1	0	1	1	0	1	0	1	0	2	1	1	?	1	0	1	1	0	0	0	0	0	2	1	2	?	0	0	1	1	1
Scomber_japonicus	2	1	1	1	2	0	0	1	1	0	1	2	0	1	1	0	1	0	2	1	1	1	1	0	1	1	0	0	0	0	2	1	2	?	0	0	1	1	1
Scomber_australasicus	2	1	1	1	2	0	0	1	1	0	1	2	0	1	1	0	1	0	2	1	1	?	1	0	0	1	1	0	0	0	0	2	1	2	?	0	0	1	1	1
Rastrelliger_kanagurta	2	1	1	1	2	0	0	1	2	2	0	2	2	0	1	1	0	1	0	2	1	1	?	1	0	0	1	0	0	0	0	2	0	2	?	0	0	1	1	1
Scomberomorus_regalis	1	1	1	1	1	0	0	1	3	0	0	1	0	0	1	0	1	2	0	1	1	2	0	0	1	0	1	0	0	0	1	2	1	2	?	1	1	1	1	1
Scomberomorus_niphonius	1	1	1	1	1	0	0	1	3	0	0	1	0	0	1	0	1	2	1	1	1	2	0	0	1	0	1	0	0	0	1	2	1	2	?	1	1	1	1	1
Scomberomorus_maculatus	1	1	1	1	1	0	0	1	3	0	0	1	0	0	1	0	1	2	0	1	1	2	0	0	1	0	1	0	0	0	1	2	1	2	?	1	1	1	1	1
Acanthocybium_solandri	1	1	1	1	1	0	0	1	?	0	0	1	0	0	1	0	1	2	3	1	2	2	0	1	1	0	1	0	0	0	0	2	1	1	?	1	1	1	0	1
*Grammatorcynus_*	1	1	1	1	1	?	1	0	1	?	0	0	0	0	1	0	1	1	2	1	0	0	0	0	1	0	0	0	0	0	1	2	1	1	?	0	0	1	1	1
Orcynopsis_unicolor	1	1	1	1	1	2	0	1	1	0	0	0	2	0	0	1	0	1	1	2	1	1	1	0	0	1	0	0	0	0	1	2	1	1	?	0	0	1	1	1
Cybiosarda_elegans	1	1	1	1	1	2	0	1	1	0	0	0	2	0	0	1	0	1	1	2	1	1	1	0	0	1	0	0	0	0	1	2	1	1	?	0	0	1	1	1
Sarda_sarda	1	1	1	1	1	0	0	1	1	0	0	0	2	0	0	1	0	1	1	2	1	1	1	0	0	1	0	0	0	0	1	2	1	1	?	0	0	1	1	1
Gymnosarda_unicolor	1	1	1	1	1	2	0	1	1	0	0	0	2	0	0	1	0	1	1	2	1	2	0	0	0	1	0	0	0	0	1	2	0	1	?	0	0	1	1	1
Allothunnus_fallai	1	1	1	1	1	0	0	0	1	1	0	2	0	0	1	0	1	1	2	1	1	0	0	0	1	0	0	0	0	1	1	2	0	1	?	0	0	1	1	1
Auxis_thazard	1	1	1	1	1	0	0	0	1	1	1	0	2	0	0	1	0	1	1	2	1	?	?	0	0	1	0	0	0	0	1	2	1	1	?	0	0	1	1	1
Auxis_rochei	1	1	1	1	1	0	0	0	1	1	1	0	2	0	0	1	0	1	1	2	1	?	?	0	0	1	0	0	0	0	1	1	2	1	?	0	0	1	1	1
Euthynnus_affinis	1	1	1	1	1	0	0	0	1	1	1	0	2	0	0	1	0	1	1	2	1	?	?	0	0	1	0	0	0	1	1	2	1	1	?	0	0	1	1	1
Katsuwonus_pelamis	1	1	1	1	1	0	0	0	1	1	1	0	2	0	0	1	0	1	1	2	1	?	?	0	0	1	0	0	0	1	1	2	1	1	?	0	0	1	1	1
Thunnus_tonggol	1	1	1	1	1	0	0	1	1	1	1	0	2	0	0	1	0	1	1	2	1	?	?	0	0	1	1	0	0	0	1	2	1	1	?	0	0	1	1	1
Thunnus_orientalis	1	1	1	1	1	0	0	1	1	1	1	0	2	0	0	0	1	0	1	1	2	1	2	1	0	0	1	0	0	0	1	1	1	1	?	0	0	1	1	1
†*Landanichthys_lusitanicus*	?	?	?	?	?	?	?	?	?	?	?	?	?	0	0	?	0	1	2	?	?	?	1/2	0	0	1	?	0	?	?	?	?	?	0	?	?	?	?	1	?	?
†*Eocoelopoma_portentosum*	?	?	?	?	?	?	?	?	?	?	?	?	?	0	0	?	0	1	2	?	?	?	1	0	0	1	0	?	?	?	?	?	?	?	?	?	?	?	?	?	?
†*Eocoelopoma_curvatum*	?	?	?	?	?	?	?	?	?	?	?	?	?	?	?	?	0	1	2	?	?	?	?	0	0	1	0	?	?	?	?	?	?	?	?	?	?	?	?	?	?

| | | |

B.7 Phylogenetic Analysis

Phylogenetic analysis was undertaken on a morphology only and a combined (molecular and morphological) dataset.

Additionally, the relationships among Scombridae are sensitive to the placement of †*Landanichthys*in the analysis, but are relatively stable when only extant taxa are included. In the PAUP analysis the relationships within Scombrini are unstable, and 10 trees are obtained from this analysis.

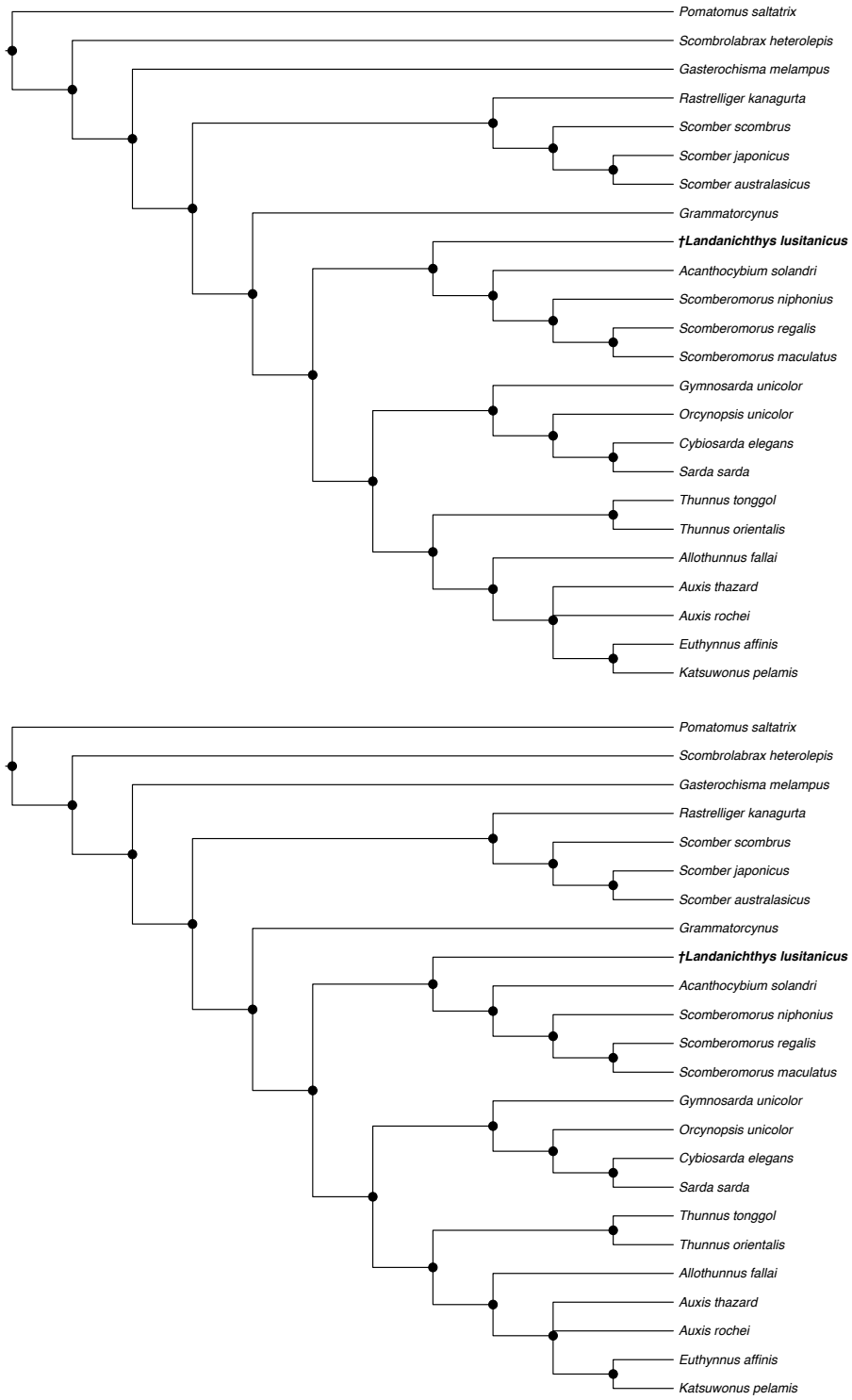


Figure B.10: Two possible placements of †*Landanichthys*; top, with Scomberomorini, bottom, with Thunnini. Remaining uncertainty is in the resolution of extant taxa.



Figure B.11: Trees obtained from Bayesian analysis of the Morphology only dataset in MrBayes. Top, maximum clade credibility tree, bottom, majority-rule consensus tree. Circles at nodes indicate Bayesian posterior probabilities above 0.5.

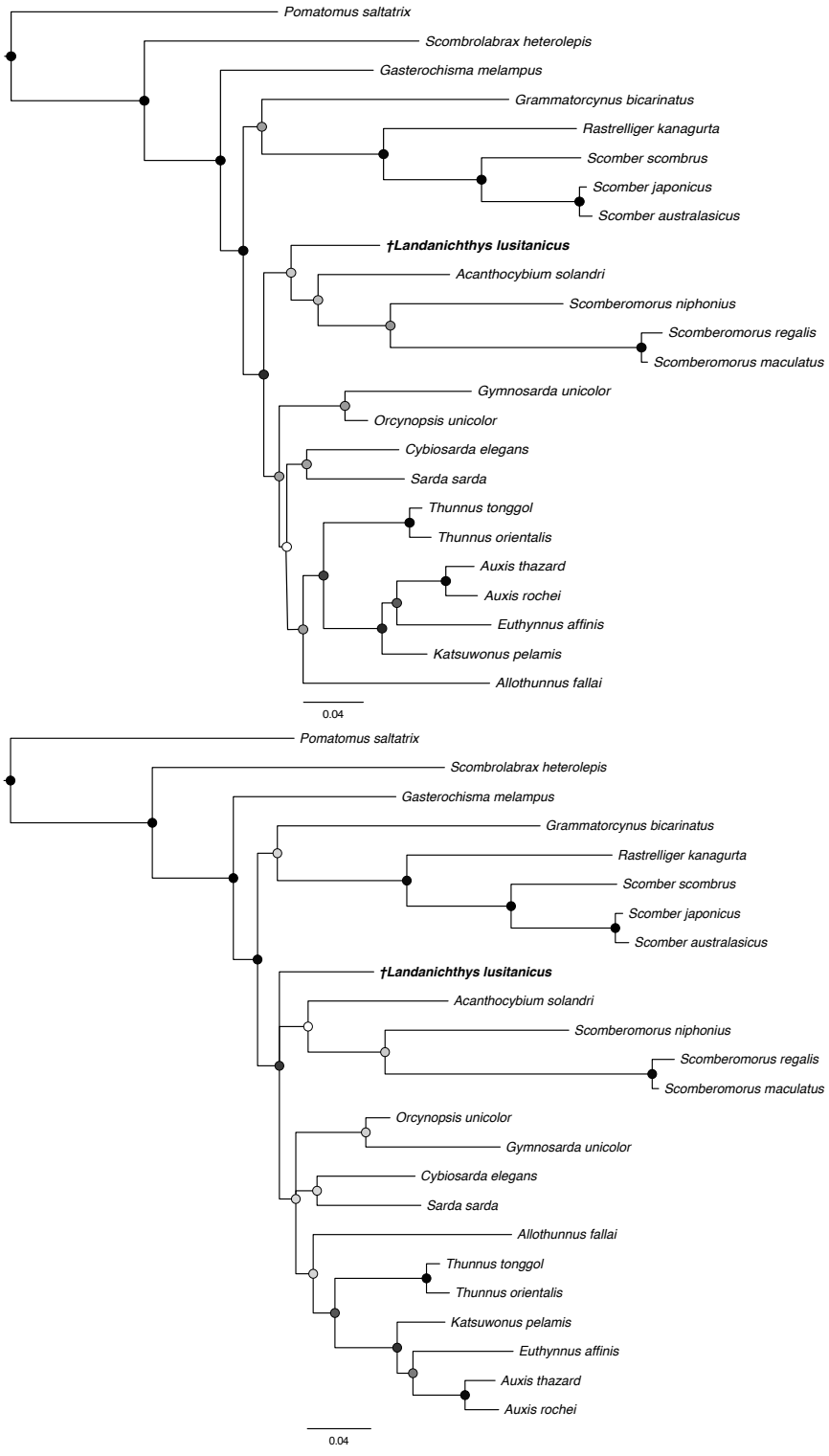


Figure B.12: Trees obtained from Bayesian analysis of the combined (molecular and morphological) dataset in MrBayes. Top, maximum clade credibility tree, bottom, majority-rule consensus tree. Circles at nodes indicate Bayesian posterior probabilities above 0.5.

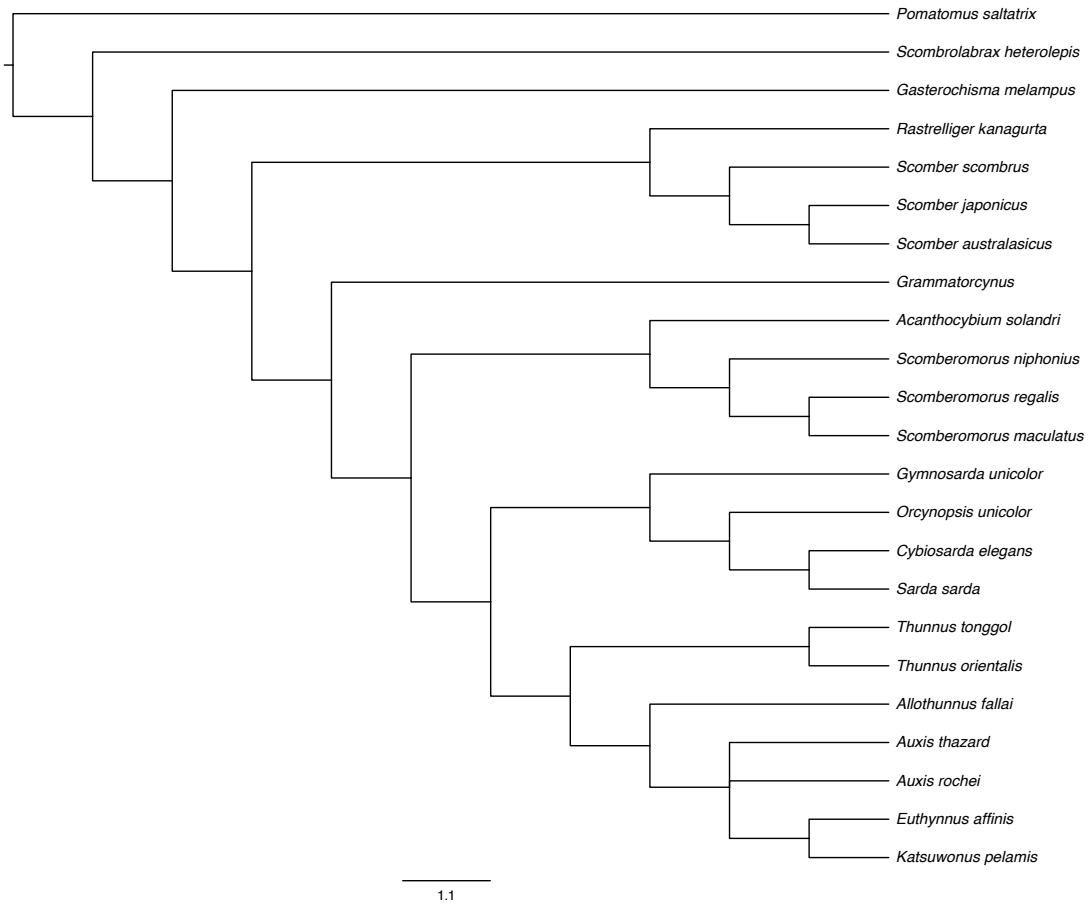


Figure B.13: Parsimony analysis of the morphology only dataset with only extant taxa included. 10 trees are obtained from PAUP, shown here is Tree 8.

B.8 Optimisation Tree

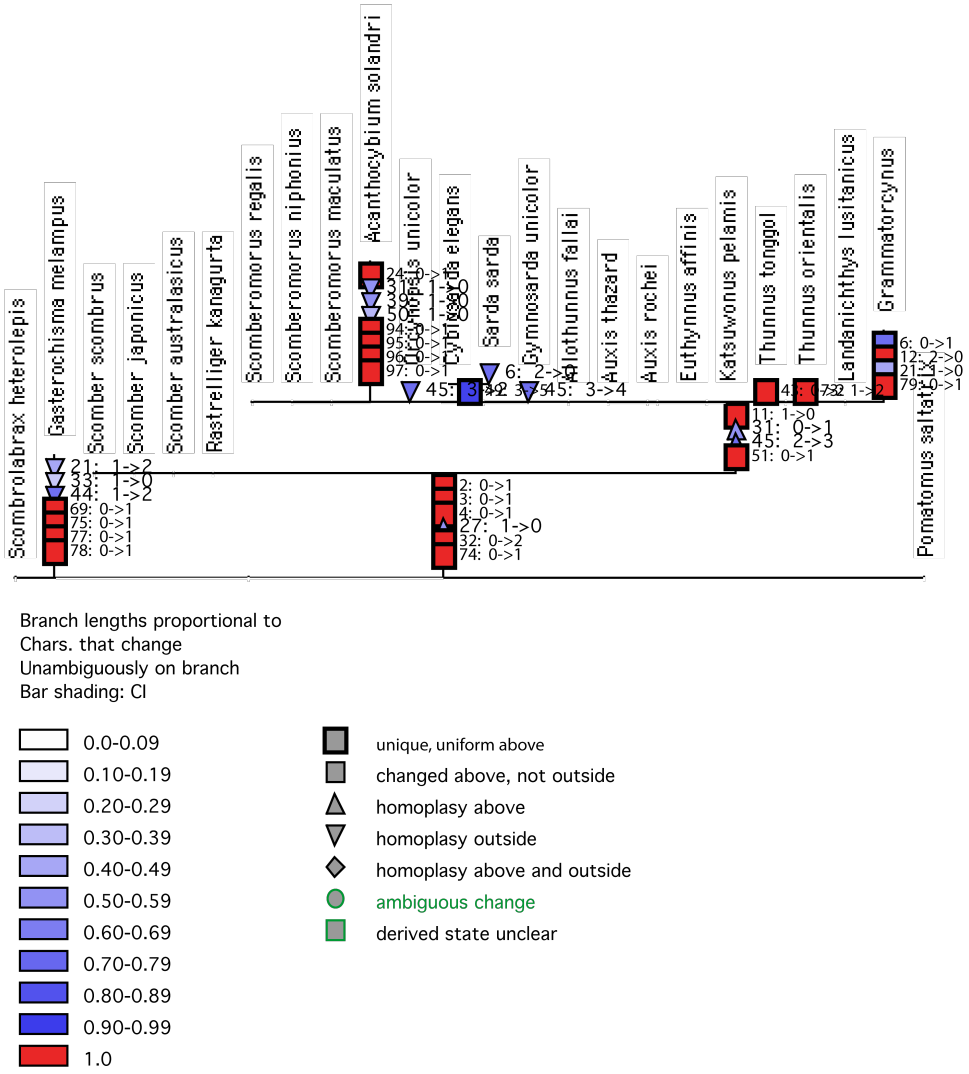


Figure B.14: Scombrid optimisations from morphological parsimony analysis. This png file is output from MacClade. A key is included.

Appendix C

Supplementary Information associated with Chapter 5 'Patterns of phenotypic evolution in Pelagiaria' - Scan Parameters for extant specimens used in this study

The scan parameters for all extant specimens used in this thesis are included in the table below. W indicates a scan of the whole specimen, H indicates a scan of only the head.

Specimen	**Sample Scanned**		**Voxel Size (mm)**	**Filter**	**(mm)**	**kV**	**mA**
Acanthocybium solandri	FMNH 44400	H	0.020	Copper	0.25	132	155
Aphanopus carbo	BMNH 2006.6.27.1	H	0.072	Copper	0.25	175	175
Ariomma bondi	UMMZ 228950	W	0.054	Copper	0.1	95	225
		H	0.025	Copper	0.1	95	220
Ariomma indica	UMMZ 219645	W	0.084	Copper	0.25	160	200
		H	0.033	Copper	0.1	100	250
Ariomma melanum	MCZ 168623_6	H	0.041	Copper	0.1	90	91
Arripis trutta	UMMZ 209265	H	0.039	Copper	0.1	105	255
Auxis rochei	UMMZ 250172	H	0.059	Copper	0.1	100	255
Auxis thazard	UMMZ 238740	W	0.122	Copper	0.25	160	200
		H	0.043	Copper	0.1	100	250
Benthodesmus simonyi	BMNH 1972.1.10.64	H	0.042	Copper	0.1	175	175
Benthodesmus taenius	FMNH 88043	W	0.107	Copper	0.25	160	120
		H	0.052	Copper	0.25	175	225
Brama caribbea	FMNH 48931	W	0.122	Copper	0.25	160	200
		H	0.041	None		70	140
Brama dussumieri	UMMZ 234770	W	0.063	Copper	0.1	150	215
		H	0.035	Copper	0.1	95	220
Brama japonica	UMMZ 191017	H	0.057	None		75	155
Caristius macropus	FMNH 76316	W	0.094	Copper	0.25	175	255
		H	0.084	None		75	155
Chiasmodon niger	UMMZ 228958	W	0.041	None		70	140
		H	0.022	None		70	130

Specimen	Sample Scanned		Voxel Size (mm)	Filter	(mm)	kV	mA
Cubiceps baxteri	BMNH 1997.9.17.27	H	0.023	Copper	0.1	180	180
		H	0.043	Copper	0.1	90	250
Cubiceps gracilis	UMMZ 228951	H	0.035	Copper	0.1	95	220
Cubiceps whiteleggi	BMNH 1986.10.6:37-40	H	0.021	Copper	0.1	95	190
Diplospinus multistriatus	LACM 45473	H	0.026			81	117
Dysalotus oligoscolus	BMNH 2002.3.2.86	H	0.039	Copper	0.1	140	200
Dysalotus alticocki	BMNH 1930.1.12.1063	H	0.021	None	None	75	170
Eumegistus illustris	LACM 38573	H	0.020			106	107
Euthynnus affinis	UMMZ 223134	H	0.044	Copper	0.1	105	255
Gasterochisma melampus	BMNH 1868.6.22.2_?	H	0.018	Copper	0.1	195	157
Gempylus serpens	FMNH 71423	W	0.064	Copper	0.25	175	225
		W	0.039	None		75	160
Gymnosarda unicolor	FMNH 89962	W	0.091	Copper	0.5	190	240
		H	0.050	Copper	0.1	100	240
Hyperoglyphe japonica	UMMZ 233106	H	0.102	Copper	0.75	125	328
Icosteus aenigmaticus	UMMZ 147495	H	0.120	Copper	0.5	100	220
	UMMZ 190048	W	0.122	None		70	140
		H	0.045	None		70	130
Kali macrodon	BMNH 1996.2.14.15	H	0.021	Copper	0.1	85	170
Kali macrura	BMNH 1988.2.25.7-8	H	0.018	None		75	180
Kali normani	FMNH 88149	W	0.084	None		75	155
		H	0.027	None		70	130
Katsuwonus pelamis	FMNH 41899	H	0.086	Copper	0.25	160	200

Specimen	**Sample Scanned**		**Voxel Size (mm)**	**Filter**	**(mm)**	**kV**	**mA**
Lepidocybium flavobrunneum	LACM 36320	H	0.020	Copper	0.25	132	155
Lepidopus altifrons	FMNH 64192	W	0.093	Copper	0.25	165	235
		H	0.044	Copper	0.25	165	235
Lepidopus caudatus	BMNH 1928.6.27.22	H	0.051	Copper	0.1	190	180
Lepturacanthus savala	UMMZ 219522	H	0.052	Copper	0.1	105	255
Neoepinnula americana	FMNH 65717	W	0.091	Copper	0.5	190	240
		H	0.047	Copper	0.1	90	250
Nesiarchus nasutus	FMNH 71422	W	0.094	Copper	0.25	175	255
		H	0.053	Copper	0.1	100	250
Pampus argenteus	UMMZ 225567	H	0.084	Copper	0.25	160	200
Pampus chinensis	UMMZ 225238	W	0.084	Copper	0.25	160	200
Paradiplospinus antarcticus	LACM 10908_5	H	0.032			110	140
Paradiplospinus gracilius	BMNH 2009.5.18.143	H	0.028	Copper	0.1	190	175
Peprilus alepidotus	UMMZ 199053	W	0.063	Copper	0.1	150	215
Peprilus burti	UMMZ 249257	W	0.084	Copper	0.25	160	200
		H	0.025	Copper	0.1	95	220
Peprilus simillimus	UMMZ 93979	W	0.063	Copper	0.1	150	215
		H	0.035	Copper	0.1	95	220
Peprilus triacanthus	UMMZ 244723	W	0.054	Copper	0.1	95	225
		H	0.025	Copper	0.1	95	220
Pomatomus saltatrix	UMMZ 111069	W	0.106	Copper	0.25	160	200
		H	0.042	Copper	0.1	100	255
Promethichthys prometheus	UMMZ 250143	H	0.076	Copper	0.1	105	255
Psenes arafurensis	BMNH 1997.9.17.10	H	0.027	Copper	0.1	180	180

Specimen	**Sample Scanned**		**Voxel Size (mm)**	**Filter**	**(mm)**	**kV**	**mA**
Psenes cyanophrys	UMMZ 86219	W	0.106	Copper	0.25	160	200
		H	0.044	Copper	0.1	100	250
Psenopsis anomala	UMMZ 182977	W	0.106	Copper	0.25	160	200
		H	0.044	Copper	0.1	100	250
Pseudoscopelus altipinnis	2004.8.17.39	H	0.022	Copper	0.1	190	180
Psuedoscopelus scutatus	FMNH 88160	W	0.041	None		70	140
		H	0.022	None		70	130
Psuedoscopelus astronesthidens	MCZ 1614171	H	0.041			90	91
Psuedoscopelus piebartus	MCZ 164590	H	0.041			90	91
Pterycombus brama	BMNH 1979.3.21.393	H	0.077	Copper	0.1	180	150
		H	0.070	Copper	0.1	145	190
Pterycombus petersii	BMNH 1969.7.14.3	H	0.018	Copper	0.1	185	175
		H	0.015	None		65	170
Rastrelliger kanagurta	UMMZ 226911	W	0.084	Copper	0.25	160	200
		H	0.033	Copper	0.1	100	250
Rexea prometheoides	FMNH 120779	W	0.094	Copper	0.25	175	255
		H	0.042	Copper	0.1	100	250
Rexea solandri	UMMZ 216751	H	0.062	Copper	0.1	105	255
Ruvettus pretiosus	BMNH 1938.6.23	H	0.061	Copper	0.1	190	180
	UMMZ 86218	W	0.044	Copper	0.1	100	250
Sarda sarda	UMMZ 145849	W	0.106	Copper	0.25	160	200
Schedophilus medusophagus	BMNH 1972.2.22.101	H	0.039	Copper	0.1	180	175
Scomber australiasicus	UMMZ 250152	W	0.084	Copper	0.25	160	200
		H	0.033	Copper	0.1	100	250

Specimen	**Sample Scanned**		**Voxel Size (mm)**	**Filter**	**(mm)**	**kV**	**mA**
Scomber japonicus	UMMZ 250083	W	0.121	Copper	0.25	160	200
		H	0.043	Copper	0.1	100	255
Scomber scombrus	UMMZ 214543	W	0.121	Copper	0.25	160	200
		H	0.043	Copper	0.1	100	255
Scomberomorus maculatus	UMMZ 199143	W	0.121	Copper	0.25	160	200
		H	0.044	Copper	0.1	105	255
Scomberomorus niphonius	UMMZ 167374	W	0.106	Copper	0.25	160	200
		H	0.043	Copper	0.1	100	255
Scomberomorus regalis	UMMZ 143137	W	0.121	Copper	0.25	160	200
		H	0.042	Copper	0.1	100	255
Scombrolabrax heterolepis	FMNH 65350	W	0.047	Copper	0.1	90	250
		H	0.093	Copper	0.5	190	240
Taractes asper	BMNH 1953.10.28.2	H	0.054	Copper	0.1	140	200
Taractes rubescens	MCZ 148060-5	H	0.182			100	170
Taractichthys steindachneri	FMNH 63863	H	0.028	Copper	0.25	180	160
Tentoriceps cristatus	BMNH 1974.3.5.1-3	H	0.040	Copper	0.1	180	195
	BMNH 1987.1.23:28	H	0.041	Copper	0.1	100	200
Tetragonurus atlanticus	FMNH 88285	W	0.064	Copper	0.25	175	225
		H	0.057	None		75	155
Thunnus orientalis	FMNH 58745	W	0.091	Copper	0.5	190	240
		H	0.041	Copper	0.1	100	250
Thunnus tonggol	UMMZ 225078	H	0.051	Copper	0.1	100	255
Thyrsitoides marleyi	BMNH 1986.9.8.147	H	0.066	Copper	0.1	185	180
Trichiurus lepturus	UMMZ 219710	H	0.052	Copper	0.25	175	225

Appendix D

Supplementary Information associated with Chapter 5 'Patterns of phenotypic evolution in Pelagiaria'

D.1 Landmarks

D.1.1 Midline

SOC_a - Placed at the anteriormost midline point of the supraoccipital crest where it meets the bdorsal surface of the neurocranium

SOC_pd - Placed at the posterio-dorsal most point of the supraoccipital crest

SOC_pv - Placed at the posterio-ventral point of the supraoccipital crest where it sutures with the exoccipitals

neurocranium_anterior_midline - Placed at the anterior midline tip of the neurocranium.

neurocranium_dorsoposterior_midline - Placed at the posterior midline tip of the neurocranium, where the neurocranium meets V1.

occipital_condyle_centre - Placed in the centre of the occipital condyle.

U_a - Placed at the anteroventral midline tip of the urohyal.

D.1.2 Left and Right

Left and Right landmarks are placed under the same scheme and indicated by _L and _R respectively.

AQJ - Placed on the ventral tip of the quadrate's articular process where it articulates with the angular.

COR - Placed at the posterodorsal tip of the articular, where it comes to a point.

HM_ad - Placed at the anterodorsal tip of the hyomandibular head where it articulates anteriorly with the neurocranium.

HM_OP - Placed centrally in the the articular facet between the hyomandibular and operculum.

MAND_a - Placed on the anterior point of the dentary.

MAND_p - Placed at the posterior point of the lower jaw, on the angular, behind the articulation with the quadrate.

MX_a - Placed on the anterior point of the maxilla.

MX_p - Placed at the posterior point of the maxilla.

NA_NEU - Placed on the anterior tip of the nasal tube.

OP_IOP - Placed at the ventral point of the operculum where it articulates with the interoperculum.

OP_p - Placed at the ventral point of the operculum where it articulates with the interoperculum.

OP_pd - Placed at the ventral point of the operculum where it articulates with the interoperculum.

ORB_a - Placed on the anterior surface of the sclerotic ossicle where it sits next to the posterior surface of the lateral ethmoid.

ORB_d - Placed on the ventral surface of the sphenotic at the peak of the orbit.

ORB_p - Placed on the posterior surface of the sclerotic ossicle.

ORB_v - Placed on the dorsal surface of the lateral ridge of the endopterygoid.

PMX_ant - Placed on the anterior tip of the premaxilla.

PMX_ap - Placed on the posterodorsal tip of the premaxillary process.

PMX_p - Placed on the posterior tip of the premaxilla.

POP_d - Placed on the dorsal tip of the preoperculum

POP_pv - placed on the posteroventral corner of the POP.

POP_v - Placed on the anteroventral tip of the POP.

S_PT - Placed at the anterior tip of the post-temporal where it sutures to the neurocranium.

D.2 Additional fossil specimens

†*Duplexdens macropomus* OUMNH P272 a cranium from the Eocene (Ypresian, 52-49 Ma) London Clay Formation, UK; †*Tamesichthys decipiens* NMHUK PV OR 41319 a cranium from the Eocene (Ypresian, 52-49 Ma) London Clay Formation, UK; †*Micrornatus hopwoodi* NHMUK PV OR 36136 a cranium from the

Eocene (Ypresian, 52-49 Ma) London Clay Formation, UK; †*Eocoelopoma curvatum* NHMUK PV OR 44877a, P623a, P9455; crania from the Eocene (Ypresian, 52-49 Ma) London Clay Formation, UK; †*Woodwardella patellifrons* NHMUK PV P26903 a cranium from the Eocene (Ypresian, 52-49 Ma) London Clay Formation, UK.

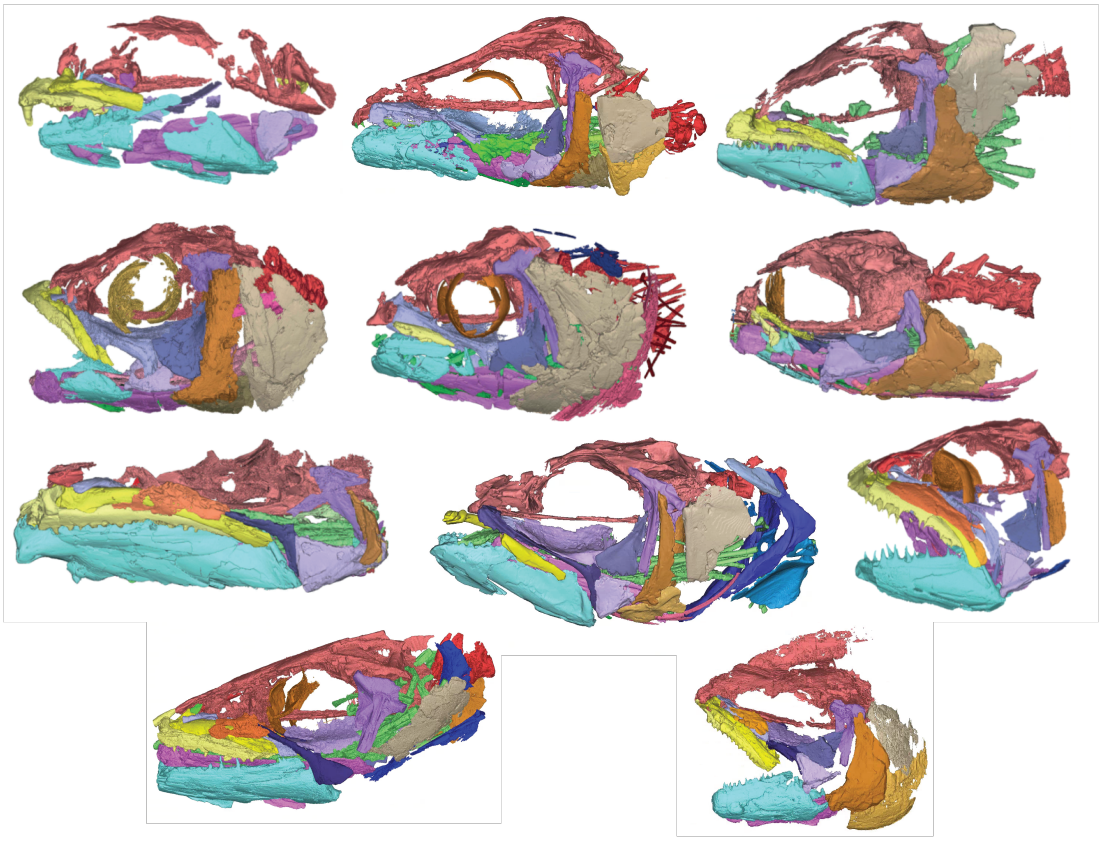


Figure D.1: μCT scanned fossil specimens considered in this study in left lateral view.

D.3 Fossil placement argumentation

†*Bramoides brieni* Age Constraint: 49-52 Ma (London Clay, Friedman et al., 2016).

Phylogenetic constraint: Sister to *Gasterochisma melampus* based on *pers. obvs.* Both †*Bramoides* and *Gasterochisma* bear a large supraoccipital crest, with an anteriorly placed suture with the frontals. The jaw joint is placed relatively anteriorly, unlike in bramids. Additionally a large lacrimal is present in †*Bramoides*, lacking in bramids.

†*Eocoelopoma curvatum* Age Constraint: 49-52 Ma (London Clay, Friedman et al., 2016)

Phylogenetic constraint: As sister to any of *Gymnosarda unicolor, Thunnus orientalis, Thunnus tonggol, Euthynnus affinis, Katsuwonus pelamis, Auxis rochei, Auxis thazard* or the clades therein. Monsch and Bannikov (2012) suggest that †*Eocoelopoma* seems to possess a combination of characters that would place them "between more primitive scombrids and the Sardini + Thunnini clade".

†*Progempylus edwardsii* Age Constraint: 49-52 Ma (London Clay, Friedman et al., 2016)

Phylogenetic constraint: As sister to *Ruvettus pretiosus, Nesiarchus nasutus* based on argumentation put forward in Chapter 3.

†*Wetherellus cristates* Age Constraint: 49-52 Ma (London Clay, Friedman et al., 2016)

Phylogenetic constraint: As sister to any of *Gasterochisma melampus, Rastrelliger kanagurta, Scomber scombrus, Scomber australiasicus, Scomber japonicus, Scomberomorus maculatus, Scomberomorus regalis, Scomberomorus niphonius, Acanthocybium solandri, Gymnosarda unicolor, Thunnus orientalis, Thunnus tonggol, Euthynnus affinis, Katsuwonus pelamis, Auxis rochei, Auxis thazard* or the clades therein. The affinities of †*Wetherellus cristates* are relatively uncertain and the phylogenetic constraint is relatively open to reflect this.

D.4 A sample UCE Tree from Friedman et al. (Submitted)

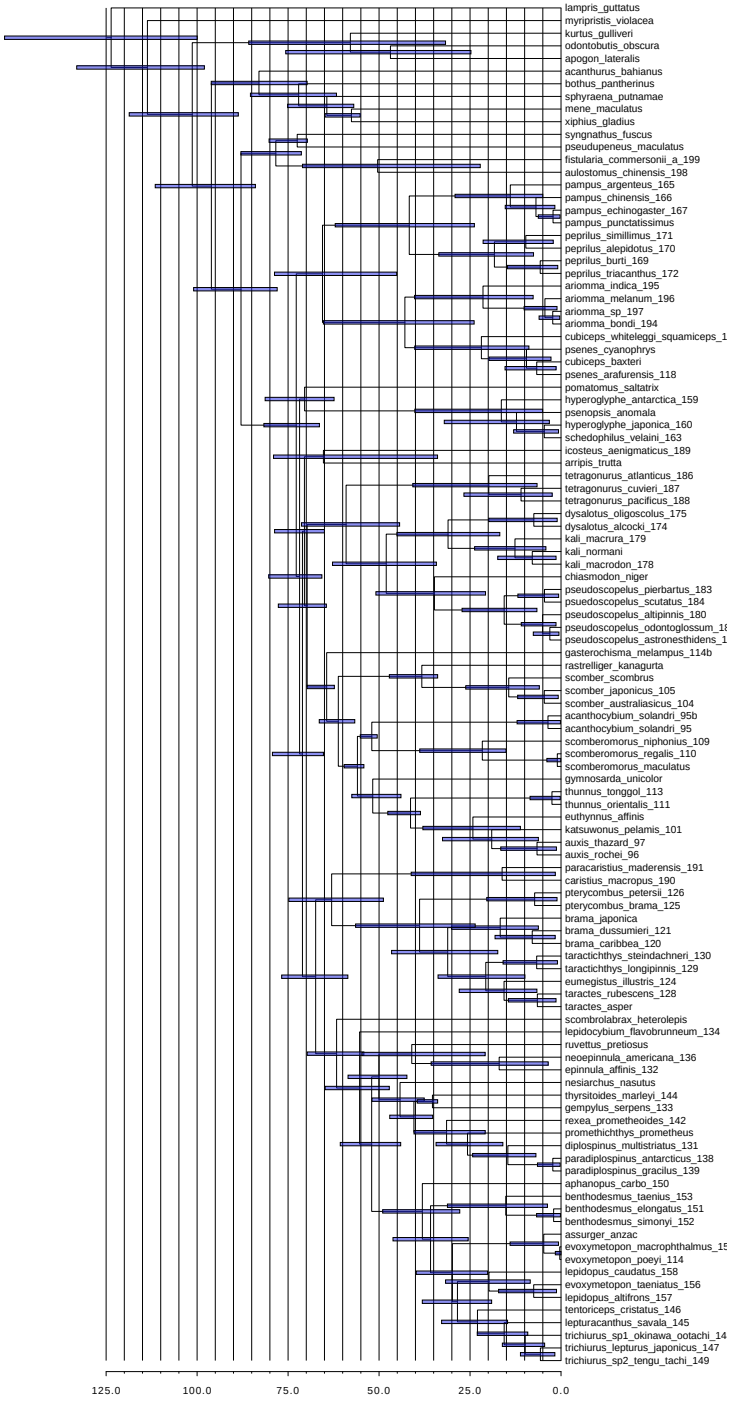


Figure D.2: Time calibrated UCE tree from Friedman et al. (Submitted) as an illustration of the relationships recovered in that analysis.

Appendix E

Supplementary Information associated with Chapter 5 - Parameters obtained in mvMORPH models

This appendix contains the parameters obtained for the mvMORPH models in Chapter 5.

Table E.1: Parameter values reported as the median value for all 100 trees in the extant only dataset. The age estimate for the SHIFT model is reported as a mean value.

		BM Model					**EB Model**					**SHIFT Model**				
		PC1	PC2	PC3	PC4	PC5	PC1	PC2	PC3	PC4	PC5	PC1	PC2	PC3	PC4	PC5
α	PC1	NA	NA	NA	NA	NA	NA	NA	NA	NA	NA	0.136	0.007	0.001	-0.053	0.006
	PC2	NA	NA	NA	NA	NA	NA	NA	NA	NA	NA	0.007	0.015	-0.007	-0.003	0.004
	PC3	NA	NA	NA	NA	NA	NA	NA	NA	NA	NA	0.001	-0.007	0.151	-0.041	-0.025
	PC4	NA	NA	NA	NA	NA	NA	NA	NA	NA	NA	-0.053	-0.003	-0.041	0.361	-0.043
	PC5	NA	NA	NA	NA	NA	NA	NA	NA	NA	NA	0.006	0.004	-0.025	-0.043	0.041
σ	PC1	0.00045	0.00005	0.00014	-0.00029	$-3x10^5$	0.00046	0.00004	0.00014	-0.00031	$-3x10^5$	0.00143	0.00012	0.00023	-0.00077	$-3x10^5$
	PC2	0.00005	0.00018	-0.00003	-0.00002	$1x10^5$	0.00004	0.00018	-0.00003	-0.00002	$1x10^5$	0.00012	0.00028	-0.00011	-0.00005	$4x10^5$
	PC3	0.00014	-0.00003	0.00028	-0.00025	$-1x10^5$	0.00014	-0.00003	0.00029	-0.00027	$-1x10^5$	0.00023	-0.00011	0.00074	-0.00063	$-4x10^5$
	PC4	-0.00029	-0.00002	-0.00025	0.00044	$2x10^5$	-0.00031	-0.00002	-0.00027	0.00045	$2x10^5$	-0.00077	-0.00005	-0.00063	0.00133	$1x10^5$
	PC5	-0.00003	0.00001	-0.00001	0.00002	$6x10^5$	-0.00003	0.00001	-0.00001	0.00002	$6x10^5$	-0.00003	0.00004	-0.00004	0.00001	$7x10^5$
θ_0		0.05	0.001	-0.011	0.001	0.001	0.05	0.001	-0.011	0.001	0.001	0.073	0.001	-0.011	0.001	0.000
β		NA					0					NA				
Age		NA					NA					47.5				

Table E.2: Parameter values reported as the median value for all 100 trees in the combined dataset. The age estimate for the SHIFT model is reported as a mean value.

		BM Model					**EB Model**					**SHIFT Model**				
		PC1	PC2	PC3	PC4	PC5	PC1	PC2	PC3	PC4	PC5	PC1	PC2	PC3	PC4	PC5
α	PC1	NA	NA	NA	NA	NA	NA	NA	NA	NA	NA	0.129	0.003	0.007	-0.075	0.001
	PC2	NA	NA	NA	NA	NA	NA	NA	NA	NA	NA	0.003	0.016	-0.008	-0.001	0.003
	PC3	NA	NA	NA	NA	NA	NA	NA	NA	NA	NA	0.007	-0.008	0.164	-0.078	-0.015
	PC4	NA	NA	NA	NA	NA	NA	NA	NA	NA	NA	-0.075	-0.001	-0.078	0.293	-0.035
	PC5	NA	NA	NA	NA	NA	NA	NA	NA	NA	NA	0.001	0.003	-0.015	-0.035	0.05
σ	PC1	0.00043	0.00004	0.00013	-0.00027	-0.00002	0.00048	0.00004	0.00015	-0.00031	-0.00003	0.00117	0.00008	0.00025	-0.00076	-0.00004
	PC2	0.00004	0.00018	-0.00001	-0.00004	0	0.00004	0.00019	-0.00001	-0.00004	0	0.00008	0.00027	-0.00005	-0.00009	0.00002
	PC3	0.00013	-0.00001	0.00032	-0.00029	0	0.00015	-0.00001	0.00035	-0.00032	-0.00001	0.00025	-0.00005	0.00094	-0.00087	0
	PC4	-0.00027	-0.00004	-0.00029	0.00046	0.00002	-0.00031	-0.00004	-0.00032	0.00051	0.00002	-0.00076	-0.00009	-0.00087	0.00142	0
	PC5	-0.00002	0	0	0.00002	0.00008	-0.00003	0	-0.00001	0.00002	0.00008	-0.00004	0.00002	0	0	0.00015
θ_0		0.049	0.005	0.027	-0.031	-0.005	0.049	0.005	0.026	-0.031	-0.005	0.068	0.006	-0.001	-0.014	-0.007
β		NA					0					NA				
Age		NA					NA					49.6				

Appendix F

Supplementary Information associated with Chapter 5 - Code for Evolutionary Analysis

This appendix contains the source code required for Chapter 5 including all of the dependent functions.

```
#### 3D Pelagia Data ####

#install.packages('abind')
#install.packages("geomorph")
#install.packages("Morpho")
#install.packages("surface")
#install.packages("phangorn")
#install.packages("ggplot2")
#install.packages("ggfortify")
#install.packages("FactoMineR")
#install.packages("Hmisc")
#install.packages ("phytools")
```

```
13 #install.packages("gtools")
14 #install.packages("mvMORPH")
15 library(gtools)
16 library(abind)
17 library(geomorph)
18 #library(Morpho)
19 library (ape)
20 library (phytools)
21 library (surface)
22 library (phangorn)
23 library (ggplot2)
24 library (ggfortify)
25 library (FactoMineR)
26 library(Hmisc)
27 library(mvMORPH)
28 library(paleotree)
29 library(spptest)
30 library(geiger)
31 library(furrr)
32 library(dplyr)
33 library(mvMORPH)
34
35
36
37 #NEED to use CORRECTED source code from https://github.com/mwpennell/
       geiger-v2/blob/master/R/disparity.R
38 source("https://raw.githubusercontent.com/mwpennell/geiger-v2/master/
       R/disparity.R")
39
```

```
#Modified dtt function to call modified MDI function and allow user to change y-axis
source("https://raw.githubusercontent.com/djmurrell/DTT-Envelope-code/master/dtt1.R")

#Modified code for two sided MDI test. Note this is the CORRECTED version of the MDI test in geiger
source("https://raw.githubusercontent.com/djmurrell/DTT-Envelope-code/master/getMDI1.R")

#This function takes a dtt produced object and runs it through the rank envelope test
source("https://raw.githubusercontent.com/djmurrell/DTT-Envelope-code/master/rank_dtt.R")
```

./Appendices/RCode/00_startup.R

```
# 01_functions.R

# Author: Kara Feilich
# Date modified: 08 June 2018
# This script contains custom functions used for running the analysis.

#' Replaces the Epinnula species, and drops non-matching tips from a tree
#'
#' clean.tree() cleans the names in order to match a single Pelagia tree with
#' the aspect.ratios data set
#' @param tree A phylo object
```

```
12 #' @param traits The dataframe of a single continuous trait variable
13 #'
14 #' @returns a cleaned phylo object
15 clean.tree <- function(tree, traits) {
16   cleaned.tree <- tree
17   # checks data in tree, traits
18   matches <- geiger::name.check (cleaned.tree, traits)
19     # drops non-matching taxa
20   cleaned.tree <- ape::drop.tip (cleaned.tree, c(matches$tree_not_
       data))
21   return(cleaned.tree)
22 }
23
24
25 #' calls clean.tree() on list of trees
26 #'
27 #' clean.trees() is a wrapper to call clean.tree on a list of phylo
     objects,
28 #' and returns a list of outputs.
29 #' @param trees A list of phylo objects, in this case, the posterior
     trees
30 #' @param traits The dataframe of a single continuous trait variable
31 #'
32 #' @return A list of cleaned phylo objects
33 clean.trees <- function(trees, traits) {
34   cleaned.trees <- sapply(X = trees, FUN = clean.tree, traits,
       simplify = FALSE)
35   return(cleaned.trees)
36 }
37
```

```
#' Returns a p value from the output of a rank envelope test
#'
#' getPvalue() returns the p-value from the output of the rank
    envelope test
#' from Murrell 2018
#'
#' @param rank.env.output An object of class "envelope_test"
#' @return a number (the p value)
getPvalue <- function(rank.env.output){
  p.value <- rank.env.output$p
  return(p.value)
}

#' Returns p-value interval bounds from the output of a rank envelope
     test
#'
#' getPinterval() returns the p-value interval from the output of the
     rank
#' envelope test from Murrell 2018
#'
#' @param rank.env.output An object of class "envelope_test"
#' @return a dataframe with upper and lower bounds for the p value
getPinterval <-function(rank.env.output){
  p.int <- rank.env.output$p_interval
  p.int.df <- data.frame("Lower" = p.int[1], "Upper" = p.int[2])
  return(p.int.df)
}


```

```
64 #' For a paired tree and rank envelope output, this function returns whether the
65 #' datum at each relative time point is lower (=1) than the rank envelope, or
66 #' whether it isn't (=0)
67 #' @param tree A phylo object
68 #' @param rank.env.output  An object of class "envelope_test"
69 #'
70 #' @return A dataframe showing whether each time point is lower than envelope
71 checkIsLower <- function(tree, rank.env.output){
72   # First, put together all of the relevant variables in a data.frame for ease
73   # of analysis
74   time.env.output <- data.frame("relative.time" = rank.env.output$r,
75                                 "data.curve" = rank.env.output$data_curve,
76                                 "lower" = rank.env.output$lower,
77                                 "upper" = rank.env.output$upper)
78   # Calculate the height of the tree (root age)
79   tree.height <- max(phytools::nodeHeights(tree))
80   # Calculate the actual time from each relative time
81   time.env.output$actual.time <- (1-time.env.output$r) * tree.height
82   # Initialize each check of whether the data are lower than the envelope
83   # with 0 -- indicating that the data are not lower than the envelope
84   time.env.output$is.it.lower <- 0
85   # For the timepoints that actually ARE lower, make is.it.lower = 1
86   time.env.output$is.it.lower[which(
```

```
87      time.env.output$data.curve < time.env.output$lower)] <-1
88    # Outputs the whole dataframe
89    time.env.output$row.index <- as.numeric(seq(1:nrow(time.env.output)
          ))
90    return(time.env.output)
91  }
92
93  #' For the output of checkIsLower, return runs of 2 or more is.it.
        lower == 1
94  #'
95  #' This function shows runs of 2 or more timepoints that were lower
        than the
96  #' rank envelope.
97  #' @param is.it.lower.result A dataframe output by checkIsLower()
98  #'
99  #' @return A dataframe with run start and end points for sig. lower
        runs
100 findLowerRuns <- function(is.it.lower.result){
101   is.lower.runs <- with(rle(is.it.lower.result$is.it.lower), {
102     ok <- values == 1 & lengths > 2
103     ends <- cumsum(lengths)
104     starts <- ends - lengths + 1
105     data.frame(starts, ends)[ok, ]
106   })
107   is.lower.runs$starts <- is.it.lower.result[is.lower.runs$starts, "
          actual.time"]
108   is.lower.runs$ends <- is.it.lower.result[is.lower.runs$ends, "
          actual.time"]
109   return(is.lower.runs)
110 }
```

```
111
112
113 #' Returns a MDI statistic p-value from the output of dtt1().
114 #'
115 #' getMDIPvalue() returns the p-value from the output of the rank
        envelope test
116 #' from Murrell 2018
117 #'
118 #' @param dtt1.output An object of class "envelope_test"
119 #' @return a number (the p value)
120 getMDIPvalue <- function(dtt1.output){
121   p.value <- dtt1.output$MDIpVal
122   return(p.value)
123 }
124
125
126 #' Returns the value of the MDI statistic from the output of dtt1().
127 #'
128 #' getMDI() returns the p-value from the output of the rank envelope
        test
129 #' from Murrell 2018
130 #'
131 #' @param dtt1.output An object of class "envelope_test"
132 #' @return a number (the MDI statistic)
133 getMDI <- function(dtt1.output){
134   mdi <- dtt1.output$MDI
135   return(mdi)
136 }
```

./Appendices/RCode/01_functions.R

```
#Authors: Jonathan Harrison, Hermione Beckett
#Last edited June 2018

### Script contains modified bind.tip, bind.tree, locate.fossil and
    fossil.ML functions to deal with errors in fossil placement.

bind.tip.JH <- function (tree, tip.label, edge.length = NULL, where =
    NULL,
          position = 0, interactive = FALSE, ...)
{
  if (!inherits(tree, "phylo"))
    stop("tree should be an object of class \"phylo\".")
  use.edge.length <- if (is.null(tree$edge.length))
    FALSE
  else TRUE
  if (use.edge.length == FALSE)
    tree <- compute.brlen(tree)
  if (interactive == TRUE) {
    plotTree(tree, ...)
    cat(paste("Click where you would like to bind the tip \"",
              tip.label, "\"\n", sep = ""))
    flush.console()
    obj <- get.treepos(message = FALSE)
    where <- obj$where
    position <- obj$pos
  }
  else if (is.null(where))
    where <- length(tree$tip.label) + 1
  if (where <= length(tree$tip.label) && position == 0) {
    pp <- 1e-12
```

```
29      if (tree$edge.length[which(tree$edge[, 2] == where)] <=
30          1e-12) {
31        tree$edge.length[which(tree$edge[, 2] == where)] <- 2e-12
32        ff <- TRUE
33      }
34      else ff <- FALSE
35    }
36    else pp <- position
37    if (is.null(edge.length) && is.ultrametric(tree)) {
38      H <- nodeHeights(tree)
39      if (where == (length(tree$tip.label) + 1))
40        edge.length <- max(H)
41      else edge.length <- max(H) - H[tree$edge[, 2] == where,
42                                     2] + position
43    }
44    tip <- list(edge = matrix(c(2, 1), 1, 2), tip.label = tip.label,
45                edge.length = edge.length, Nnode = 1)
46    class(tip) <- "phylo"
47    obj <- bind.tree.JH(tree, tip, where = where, position = pp)
48    if (where <= length(tree$tip.label) && position == 0) {
49      nn <- obj$edge[which(obj$edge[, 2] == which(obj$tip.label ==
50                                                  tip$tip.label)), 1]
51      obj$edge.length[which(obj$edge[, 2] == nn)] <- obj$edge.length[
          which(obj$edge[,2] == nn)] + 1e-12
52      obj$edge.length[which(obj$edge[, 2] == which(obj$tip.label == tip
          $tip.label))] <- 0
53      obj$edge.length[which(obj$edge[, 2] == which(obj$tip.label ==
          tree$tip.label[where]))] <- 0
54    }
55    root.time <- if (!is.null(obj$root.time))
```

```
    obj$root.time
  else NULL
  obj <- untangle(obj, "read.tree")
  if (!is.null(root.time))
    obj$root.time <- root.time
  if (interactive)
    plotTree(obj, ...)
  if (!use.edge.length)
    obj$edge.length <- NULL
  obj
}

bind.tree.JH <- function (x, y, where = "root", position = 0,
    interactive = FALSE)
{
  nx <- length(x$tip.label)
  mx <- x$Nnode
  ROOTx <- nx + 1L
  ny <- length(y$tip.label)
  my <- y$Nnode
  if (interactive) {
    lastPP <- get("last_plot.phylo", envir = .PlotPhyloEnv)
    if (lastPP$type != "phylogram" || lastPP$direction !=
        "rightwards")
      stop("you must plot tree 'x' as a 'rightward phylogram'")
    cat("Click where you want to graft tree 'y'...\n")
    xy <- locator(1)
    d <- abs(xy$y - lastPP$yy)
    d[lastPP$xx - xy$x < 0] <- Inf
    where <- which.min(d)
```

```
85      position <- lastPP$xx[where] - xy$x
86      if (position < 0)
87        position <- 0
88      cat("The following parameters are used:\n")
89      cat("  where =", where, " position =", position, "\n")
90    }
91    else {
92      if (where == 0 || where == "root")
93        where <- ROOTx
94      if (position < 0)
95        position <- 0
96      if (where > nx + mx)
97        stop("argument 'where' out of range for tree 'x'")
98    }
99    switch(is.null(x$edge.length) + is.null(y$edge.length) +
100             1L, wbl <- TRUE, {
101               x$edge.length <- y$edge.length <- NULL
102               wbl <- FALSE
103               warning("one tree has no branch lengths, they have been
                      ignored")
104             }, wbl <- FALSE)
105   yHasNoRootEdge <- is.null(y$root.edge)
106   xHasNoRootEdge <- is.null(x$root.edge)
107   if (where == ROOTx)
108     case <- 1
109   else {
110     i <- which(x$edge[, 2] == where)
111     case <- if (where <= nx)
112       2
113     else 3
```

```
114   }
115   if (position && wbl) {
116     if (case == 1) {
117       if (xHasNoRootEdge)
118         stop("tree 'x' has no root edge")
119       if (position > x$root.edge)
120         stop("'position' is larger than x's root edge")
121     }
122     else {
123       if (x$edge.length[i] < position)
124         position = x$edge.length[i] #edited to try to fix weird
              behaviour
125       #         stop("'position' is larger than the branch length")
126     }
127   }
128   if (case == 2 && ny == 1 && !position) {
129     x$tip.label[x$edge[i, 2]] <- y$tip.label
130     if (wbl)
131       x$edge.length[i] <- x$edge.length[i] + y$edge.length
132     return(x)
133   }
134   x <- reorder(x)
135   y <- reorder(y)
136   nodes <- x$edge > nx
137   x$edge[nodes] <- -(x$edge[nodes] - nx)
138   nodes <- y$edge > ny
139   y$edge[nodes] <- -(y$edge[nodes] - ny + mx)
140   ROOT <- -1L
141   next.node <- -(mx + my) - 1L
142   new.nx <- if (where <= nx && !position)
```

```
143     nx - 1L
144   else nx
145   y$edge[!nodes] <- y$edge[!nodes] + new.nx
146   if (!yHasNoRootEdge) {
147     y$edge <- rbind(c(0, y$edge[1]), y$edge)
148     next.node <- next.node - 1L
149     if (wbl)
150       y$edge.length <- c(y$root.edge, y$edge.length)
151   }
152   switch(case, {
153     if (position) {
154       x$root.edge <- x$root.edge - position
155       x$edge <- rbind(c(next.node, x$edge[1]), x$edge)
156       ROOT <- next.node
157       if (wbl) x$edge.length <- c(position, x$edge.length)
158     }
159     if (yHasNoRootEdge) {
160       j <- which(y$edge[, 1] == y$edge[1])
161       y$edge[j, 1] <- ROOT
162     } else y$edge[1] <- ROOT
163     x$edge <- rbind(x$edge, y$edge)
164     if (wbl) x$edge.length <- c(x$edge.length, y$edge.length)
165   }, {
166     if (position) {
167       x$edge[i, 2] <- next.node
168       x$edge <- rbind(x$edge[1:i, ], c(next.node, where),
169                       x$edge[-(1:i), ])
170       if (wbl) {
171         x$edge.length[i] <- x$edge.length[i] - position
172         x$edge.length <- c(x$edge.length[1:i], position,
```

```
                                x$edge.length[-(1:i)])
    }
    i <- i + 1L
    if (yHasNoRootEdge) {
      j <- which(y$edge[, 1] == y$edge[1])
      y$edge[j, 1] <- x$edge[i, 1]
    } else y$edge[1] <- x$edge[i, 1]
  } else {
    if (yHasNoRootEdge) x$edge[i, 2] <- y$edge[1] else {
      if (wbl) y$edge.length[1] <- y$edge.length[1] +
          x$edge.length[i]
      y$edge[1] <- x$edge[i, 1]
      x$edge <- x$edge[-i, ]
      if (wbl) x$edge.length <- x$edge.length[-i]
      i <- i - 1L
    }
    x$tip.label <- x$tip.label[-where]
    ii <- which(x$edge[, 2] > where & x$edge[, 2] <=
                  nx)
    x$edge[ii, 2] <- x$edge[ii, 2] - 1L
  }
  x$edge <- rbind(x$edge[1:i, ], y$edge, x$edge[-(1:i),
                                                ])
  if (wbl) x$edge.length <- c(x$edge.length[1:i], y$edge.length,
                              x$edge.length[-(1:i)])
}, {
  if (position) {
    if (yHasNoRootEdge) {
      j <- which(y$edge[, 1] == y$edge[1])
      y$edge[j, 1] <- next.node
```

```
203       } else y$edge[1] <- next.node
204       x$edge <- rbind(x$edge[1:i, ], c(next.node, x$edge[i,2]), x$
              edge[-(1:i), ])
205       x$edge[i, 2] <- next.node
206       if (wbl) {
207         x$edge.length[i] <- x$edge.length[i] - position
208         x$edge.length <- c(x$edge.length[1:i], position,
209                            x$edge.length[-(1:i)])
210       }
211       i <- i + 1L
212     } else {
213       if (yHasNoRootEdge) {
214         j <- which(y$edge[, 1] == y$edge[1])
215         y$edge[j, 1] <- x$edge[i, 2]
216       } else y$edge[1] <- x$edge[i, 2]
217     }
218     x$edge <- rbind(x$edge[1:i, ], y$edge, x$edge[-(1:i),])
219     if (wbl) x$edge.length <- c(x$edge.length[1:i], y$edge.length,
220                                 x$edge.length[-(1:i)])
221   })
222   x$tip.label <- c(x$tip.label, y$tip.label)
223   if (is.null(x$node.label)) {
224     if (!is.null(y$node.label))
225       x$node.label <- c(rep(NA, mx), y$node.label)
226   }
227   else {
228     x$node.label <- if (is.null(y$node.label))
229       c(x$node.label, rep(NA, my))
230     else c(x$node.label, y$node.label)
231   }
```

```
232   n <- length(x$tip.label)
233   x$Nnode <- dim(x$edge)[1] + 1L - n
234   if (!is.null(x$node.label))
235     x$node.label <- x$node.label[sort(-unique(x$edge[, 1]))]
236   newNb <- integer(x$Nnode)
237   newNb[-ROOT] <- n + 1L
238   sndcol <- x$edge[, 2] < 0
239   x$edge[sndcol, 2] <- newNb[-x$edge[sndcol, 2]] <- n + 2:x$Nnode
240   x$edge[, 1] <- newNb[-x$edge[, 1]]
241   if (!is.null(x$node.label))
242     x$node.label <- x$node.label[order(newNb[newNb > 0])]
243   x
244 }
245
246 locate.fossil.JH <- function (tree, X, ...)
247 {
248   if (!inherits(tree, "phylo"))
249     stop("tree should be object of class \"phylo\".")
250   if (hasArg(plot))
251     plot <- list(...)$plot
252   else plot <- TRUE
253   if (hasArg(quiet))
254     quiet <- list(...)$quiet
255   else quiet <- FALSE
256   if (hasArg(rotate))
257     rotate <- list(...)$rotate
258   else rotate <- TRUE
259   if (hasArg(edge.constraint))
260     edge.constraint <- list(...)$edge.constraint
261   else edge.constraint <- tree$edge[, 2]
```

```
262   if (hasArg(time.constraint))
263     time.constraint <- list(...)$time.constraint
264   else time.constraint <- c(0, max(nodeHeights(tree)))
265   if (any(time.constraint < 0))
266     time.constraint <- max(nodeHeights(tree)) + time.constraint
267   if (length(time.constraint) == 1)
268     time.constraint <- rep(time.constraint, 2)
269   if (!is.matrix(X))
270     X <- as.matrix(X)
271   tip <- setdiff(rownames(X), tree$tip.label)
272   fossilML.JH(tree, X, quiet, tip, edge.constraint, time.constraint,
273               plot, search, rotate)
274 }
275
276
277 fossilML.JH<-function(tree,X,quiet,tip,edge.constraint,time.
      constraint,plot,search,rotate){
278   if(!quiet) cat(paste("Optimizing the phylogenetic position of ",tip
        ," using ML. Please wait....\n",sep=""))
279   if(ncol(X)>1&&rotate){
280     pca<-phyl.pca(tree,X[tree$tip.label,])
281     obj<-phyl.vcv(X[tree$tip.label,],vcv(tree),1)
282     X<-(X-matrix(rep(obj$a[,1],nrow(X)),nrow(X),ncol(X),byrow=TRUE))%
          *%pca$Evec
283   }
284   lik.tree<-function(par,tip,tree,edge,height,XX,rotate,time.
        constraint){
285     tip.depth<-par[1]
286     tip.height<-par[2]
287     if(tip.height>(tip.depth+1e-6)){
```

```
288         ii<-which(tree$edge[,2]==edge)
289         tree<-bind.tip.JH(tree,tip,where=edge,position=min(height[2]-
                tip.depth,tree$edge.length[ii]),
290                           edge.length=tip.height-tip.depth)
291         if(!rotate) XX<-phyl.pca(tree,XX[tree$tip.label,])$S
292         obj<-phyl.vcv(as.matrix(XX[tree$tip.label,]),vcv(tree),1)
293         ll<-vector()
294         for(i in 1:ncol(XX))
295           ll[i]<-sum(mnormt::dmnorm(XX[tree$tip.label,i],mean=rep(obj$a
                [i,1],nrow(XX)),obj$C*obj$R[i,i],log=TRUE))
296         if(plot){
297           plotTree(tree,mar=c(2.1,0.1,3.1,0.1),ftype="i",fsize=0.8)
298           obj<-lapply(time.constraint,function(x,tree) lines(rep(x,2),
                c(0,Ntip(tree)+1),col="red",lty="dashed"),tree=tree)
299           title(paste("log(L) = ",signif(sum(ll),6),sep=""))
300           axis(1)
301         }
302         logL<-sum(ll)
303       } else logL<--.Machine$double.xmax/1e100
304       logL
305     }
306     ee<-intersect(tree$edge[,2],edge.constraint)
307     H<-nodeHeights(tree)
308     hh<-unique(c(tree$edge[H[,1]<=time.constraint[2],2],tree$edge[H
          [,2]<=time.constraint[2],2]))
309     #check whether time constraint and edge constraint are consistent
310     while (length(intersect(ee,hh))==0){
311       print('relaxing the time constraint')
```

```
312     time.constraint = c(max(0,time.constraint[1]-(mean(time.
            constraint)-time.constraint[1])),min(max(nodeHeights(tree)),
            time.constraint[2]+(mean(time.constraint)-time.constraint[1]))
            )
313     hh<-unique(c(tree$edge[H[,1]<=time.constraint[2],2],tree$edge[H
            [,2]<=time.constraint[2],2]))
314     print(paste('updated intersection: ', intersect(ee,hh), sep=""))
315   }
316   ee<-intersect(ee,hh)
317   fit<-vector(mode="list",length=length(ee))
318   for(i in 1:length(ee)){
319     ii<-which(tree$edge[,2]==ee[i])
320     lower<-c(H[ii,1],time.constraint[1])
321     upper<-c(H[ii,2],time.constraint[2])
322     par<-c(mean(lower),mean(upper))
323     fit[[i]]<-optim(par,lik.tree,tip=tip,tree=tree,edge=ee[i],height=
            H[ii,],XX=X,rotate=rotate,
324                     time.constraint=time.constraint,
325                     method="L-BFGS-B",lower=lower,upper=upper,control
                            =list(fnscale=-1))
326   }
327   logL<-sapply(fit,function(x) x$value)
328   ii<-which(logL==max(logL))
329   if(length(ii)==1){
330     fit<-fit[[ii]]
331     edge<-ee[ii]
332     mltree<-bind.tip.JH(tree,tip,where=edge,
333                         position=H[which(tree$edge[,2]==edge),2]-fit$par
                                [1],
334                         edge.length=fit$par[2]-fit$par[1])
```

```
335     mltree$logL<-fit$value
336   } else {
337     fit<-fit[ii]
338     mltree<-vector(mode="list",length=length(ii))
339     for(i in 1:length(ii)){
340       edge<-ee[ii[i]]
341       mltree[[i]]<-bind.tip.JH(tree,tip,where=edge,
342                     position=H[which(tree$edge[,2]==edge),2]-fit[[i]]$
                          par[1],
343                     edge.length=fit[[i]]$par[2]-fit[[i]]$par[1])
344       mltree[[i]]$logL<-fit[[i]]$value
345     }
346     class(mltree)<-"multiPhylo"
347   }
348   if(!quiet) cat("Done.\n")
349   if(plot){
350     if(class(mltree)=="phylo"){
351       plotTree(mltree,mar=c(2.1,0.1,3.1,0.1),ftype="i",fsize=0.8)
352       obj<-lapply(time.constraint,function(x,tree) lines(rep(x,2), c
            (0,Ntip(tree)+1),col="red",lty="dashed"),tree=tree)
353       title(paste("Optimized position of taxon \"",tip,"\"",sep=""))
354       axis(1)
355     } else {
356       par(mfrow=c(1,length(mltree)))
357       for(i in 1:length(mltree)){
358         plotTree(mltree[[i]],mar=c(2.1,0.1,0.1,0.1),ftype="i",fsize
              =0.8)
359         obj<-lapply(time.constraint,function(x,tree) lines(rep(x,2),
              c(0,Ntip(tree)+1),col="red",lty="dashed"),tree=tree)
360         axis(1)
```

```
        }
      }
    }
    mltree
}
```

./Appendices/RCode/01b_functions_JH.R

```
#Authors: Hermione Beckett
#Last edited: 07/08/2018

#folder.path <-"/Users/admin/Dropbox/3D Landmarking/Mimi Pelagia Landmarking/"
#setwd(folder.path)

source("00_startup.R")
source("01_functions.R")

#Import landmarks using folder paths, having landmarks saved in Avizo pack and go format.
species <- list.files( folder.path ) #creates an object with a list of the folders in the folder path
paths <- list.files( folder.path , full.names = T ) #creates an object with a list of the folders in the folder path with the full name of the folder path


landmark.paths <- c() #creates an empty object which the following for loops fill

```

```
17 #for all of the folders in the folder path cycles through each folder
       if there is more than one thing in the folder (failsafe) and
     outputs each subfolder with ending -files
18
19 for( i in 1:length( paths ) ) {
20   paths.temp <- list.files( paths[ i ] , full.names = T )
21   if( length( paths.temp ) > 1 ) { landmark.paths[ i ] <- paths.temp[
         grepl( "-files" , paths.temp ) ] }
22 }
23
24 species <- species[ ! is.na( landmark.paths ) ] #is.na selects
     anything that is NA, ! reverses the operation. Reallocates species
      to delete any NA values
25 paths <- paths[ ! is.na( landmark.paths ) ]
26 landmark.paths <- landmark.paths[ ! is.na( landmark.paths ) ]
27
28 landmarks.data <- list() #creates an empty list
29
30 #takes all of files in those folders, only keeping the ones that dont
       have .ply, .grayScale etc in name
31
32
33 for( i in 1:length( landmark.paths ) ) {
34   lm.files.temp <- list.files( landmark.paths[ i ] )
35   lm.paths.temp <- list.files( landmark.paths[ i ] , full.names = T )
36   lm.files.temp <- lm.files.temp[! grepl( ".ply" , lm.paths.temp ) &
       ! grepl( "grayScale" , lm.paths.temp ) & ! grepl( "temperature.
       icol" , lm.paths.temp ) & ! grepl( "physics.icol" , lm.paths.
       temp ) & ! grepl("volrenGreen.col", lm.paths.temp)]
```

```
37  lm.paths.temp <- lm.paths.temp[! grepl( ".ply" , lm.paths.temp ) &
        ! grepl( "grayScale" , lm.paths.temp ) & ! grepl( "temperature.
        icol" , lm.paths.temp ) & ! grepl( "physics.icol" , lm.paths.
        temp ) & ! grepl("volrenGreen.col", lm.paths.temp)]
38
39  species.landmarks.temp <- list() #creates an object, then populates
        with the landmark data
40  for( j in 1:length( lm.files.temp ) ) {
41    lm.lines.temp <- readLines( lm.paths.temp[ j ] ) #reads the lines
          into that object
42    lm.lines.temp <- lm.lines.temp[ ( which( grepl( "Data section" ,
        lm.lines.temp ) ) + 2 ):( length( lm.lines.temp ) - 1 ) ] #
        takes the line(s) that are between Data section and one from
        the end
43
44    lm.lines.temp <- as.numeric( strsplit( lm.lines.temp , " " )[[ 1
        ]] ) #turns into a number and splits the string based on a
        space
45    species.landmarks.temp[[ j ]] <- lm.lines.temp # stores in a
        renamed object looping through each folder
46    names( species.landmarks.temp )[ j ] <- lm.files.temp[ j ] #names
          the previous object based on the file names
47  }
48  landmarks.data[[ i ]] <- do.call( rbind , species.landmarks.temp )
      #binds all individual landmarks into a single matrix
49  colnames( landmarks.data[[ i ]] ) <- c( "x" , "y" , "z") #renames
        columns x y z
50  names( landmarks.data )[ i ] <- species[ i ] # associates each set
        of landmarks with their species name.
51 }
```

```
52
53
54 for( i in 1:length( landmarks.data ) ) {
55   if( i == 1 ) { rowNames <- rownames( landmarks.data[[ i ]] ) }
56   if( i > 1 ) { rowNames <- cbind( rowNames , rownames( landmarks.
       data[[ i ]] ) ) }
57 }
58
59 midline <- as.vector(row.names((landmarks.data[[1]][-grep("L$|R$",
     rownames(landmarks.data[[1]])), ])))
60 left <- as.vector(row.names((landmarks.data[[1]][grepl("L$", rownames
     (landmarks.data[[1]])), ])))
61 right <- as.vector(row.names((landmarks.data[[1]][grepl("R$",
     rownames(landmarks.data[[1]])), ])))
62
63 landmark.names<-rownames(landmarks.data[[1]])
64
65
66
67
68
69 source("OSymm.R")
70 lm.data<-landmarks.data
71
72 #### RUN OSYMM TO MIRROR REMAINING LANDMARKS
     ##############################################################
73
74 # create new object to receive reflected landmarks
75 OSymm.output <- vector("list",length(lm.data)); names(OSymm.output)
     <- names(lm.data)
```

```
76
77 #run OSymm (NOTE: THIS STEP REORDERS THE LANDMARKS!!)
78 for (i in 1:length(lm.data)) {
79
80   OSymm.output[[i]] <- OSymm(X=lm.data[[i]], midline=midline, right=
       right, left=left)
81
82 }
83
84
85 # copy mirrored, symmetrical landmarks into new object
86 rec.orig.lm <- list(); rec.ref.lm <- list(); symmconf.lm <- list()
87
88 for (i in 1:length(lm.data)) {rec.orig.lm[[i]] <- OSymm.output[[i]]$
    rec.orig} # original landmark configuration
89 for (i in 1:length(lm.data)) {rec.ref.lm[[i]] <- OSymm.output[[i]]$
    rec.ref} # reflected configuration, not symmetrised
90 for (i in 1:length(lm.data)) {symmconf.lm[[i]] <- OSymm.output[[i]]$
    symmconf} # symmetrical consensus configuration
91
92 # change landmark names because the default output is wrong
93 for (i in 1:length(lm.data)) {rownames(rec.ref.lm[[i]]) <- rownames(
    OSymm.output[[i]]$symmconf)}
94
95 # reorder reflected landmarks to match lm.data ordering
96 for (i in 1:length(rec.orig.lm)) {rec.orig.lm[[i]] <- rec.orig.lm[[i
    ]][rownames(lm.data[[1]]), ]}
97 for (i in 1:length(rec.ref.lm)) {rec.ref.lm[[i]] <- rec.ref.lm[[i]][
    rownames(lm.data[[1]]), ]}
```

```
98 for (i in 1:length(symmconf.lm)) {symmconf.lm[[i]] <- symmconf.lm[[i
       ]][rownames(lm.data[[1]]), ]}
99
100 # Change NaNs to NAs
101 symmconf.lm <- rapply(symmconf.lm, f=function(x) ifelse(is.nan(x),NA,
       x), how="replace")
102 names(symmconf.lm) <- names(lm.data) # note: this may mess up the
       script?
103 for (i in 1:length(symmconf.lm)) {colnames(symmconf.lm[[i]]) <- NULL}
        #might be useful when using $rec.ref
104
105 # select landmark configuration to be used for further analyses
106 rr.lm <- symmconf.lm
107
108 # print percentage of data present to console
109 cat("Percent of landmarks present after mirroring: ")
110 lm.completeness.after.mirroring <- numeric(length(names(lm.data)));
       names(lm.completeness.after.mirroring) <- names(lm.data)
111 for (i in 1:length(lm.data)) {lm.completeness.after.mirroring[i] <-
       round(100*(1-sum(!complete.cases(rr.lm[[i]]))/length(landmark.
       names)))}
112 as.matrix(sort(lm.completeness.after.mirroring))
113
114
115 landmarks.data.sym<-abind(rr.lm, along=3)
116
117
118
119
120 landmarks.data<-landmarks.data.sym
```

```
121 #Create a 3D array which contains the landmark data
122 landmarks.data <- abind(landmarks.data,along=3)
123
124
125
126
127
128
129
130 #PCA/RELATIVE WARP ANALYSIS
131
132 #To drop (using -) any landmarks you dont want (shows the dimensions
        of the object, rows, columns, dimensions)
133 landmarks.data <- landmarks.data[-c(54:57),,] #in this case getting
        rid of the last 4 landmarks; upper_jaw_anterior and upper_jaw_
        posterior on both sides
134
135
136
137 #Estimate the position of missing landmarks using a regression method
        (other option is TPS)
138 landmarks.data.est <- estimate.missing(A = landmarks.data, method = "
        Reg")
139
140 #Warp the dataset to account for size differences
141 #Procrustes alignment
142 pelagia.3D.proc <- gpagen(landmarks.data.est, Proj = TRUE, ProcD =
        TRUE, curves = NULL, surfaces = NULL)
143
```

```
144 #plot the specimens to see how they fall and to see if any are
        largely out
145 plotAllSpecimens(pelagia.3D.proc$coords, links=NULL)
146
147 #A vector of names from the above list
148 pelagia.3D.names <- names(pelagia.3D.proc)
149
150 #Perform PCA
151 pelagia.3D.PCA <- plotTangentSpace(pelagia.3D.proc$coords) #, axis1 =
        1, axis2 = 2, warpgrids = FALSE, mesh = NULL, label = pelagia.3D.
        names, groups= NULL, verbose = FALSE)
152
153
154 #Save the raw PCA data before pruning for the extant tree so that
        this data can be pulled into _Placing_fossils to create the
        combined dataset
155 save(pelagia.3D.PCA, file="PelagiaPCArawAug7.Rda")
156
157
158
159 #Check deformation/visualise deformation
160 plotOutliers(pelagia.3D.proc$coords) #looks for outliers using
        procrustes distnace from Mean (outliers show red)
161
162 #make a scree plot to see where most of the variance is acccounted
        for
163 par(mfrow=c(1,1))
164 variance <- pelagia.3D.PCA$sdev^2/sum(pelagia.3D.PCA$sdev^2)
165 summary(pelagia.3D.PCA) # summarise the variance accounted for
```

```
166 plot(variance,type="points") # plots a scree plot with points to see
        where it levels off
167
168
169
170 #####Read in TREE #####
171
172 pelagia.trees <- read.nexus("Posterior_100_pruned.nex")
173
174 #####Clean the PCA data #####
175
176 #Check that everything matches up on the tree and PCA
177 pelagia.3D.pcscores <- pelagia.3D.PCA$pc.scores #takes out the PC
        data from
178
179 row.names(pelagia.3D.pcscores)<-gsub(" ","_",row.names(pelagia.3D.
        pcscores))
180
181 #Save the raw PC score data before pruning for the extant tree so
        that this data can be pulled into _Placing_fossils to create the
        combined dataset
182 save(pelagia.3D.pcscores, file="PelagiaPCArawAug7.Rda")
183
184
185 pelagia.tree1<-pelagia.trees[[1]]
186 species_in_tree_logical <- rownames(pelagia.3D.pcscores) %in% pelagia
        .tree1$tip.label
187 pelagia.3D.pcscores<-pelagia.3D.pcscores[species_in_tree_logical,]
188
```

```
traits1<-pelagia.3D.pcscores[, c(1:5)] #pull out PCs 1:x the PC data,
    i.e. x number of PCs
traits<- as.data.frame(traits1) #turn the PC traits into a dataframe


#### Prune TREE ####

#Prune trees to match extant dataset
pruned.trees<-clean.trees(pelagia.trees,traits)


#### Save data to pull in to other analyses ###

save(traits, pruned.trees, file="PelagiadataAug7.rda")
```

./Appendices/RCode/02_Processing_data.R

```
#Authors: Hermione Beckett
#Last edited: 07/08/2018

###02b_Phylomorphospace###

load("PelagiadataAug7.rda")

#create a matrix with family info so that can colour things in for
   plotting
family.info<-matrix(c(row.names(traits),rep.int(NA,nrow(traits))),
                    nrow = length(row.names(traits)), ncol = 2)
colnames( family.info ) <- c( "Species" , "Family" ) #renames columns

family.info[c(2,9:10,29:32,63,67:68),2]=c('Trichiuridae')
```

```
family.info[c(17, 22,33:34,36:37,41,51:52),2]=c('Gempylidae')
family.info[c(6),2]=c('Arripidae')
family.info[c(3:5),2]=c('Ariommatidae')
family.info[c(1, 7:8,20,21,23,28,50,53:58,65:66),2]=c('Scombridae')
family.info[c(11:12,19,49,60:62),2]=c('Bramidae')
family.info[c(13),2]=c('Caristiidae')
family.info[c(14,18,26:27,45:48),2]=c('Chiasmodontidae')
family.info[c(24,44),2]=c('Centrolophidae')
family.info[c(25),2]=c('Icosteidae')
family.info[c(35,38:39),2]=c('Stromateidae')
family.info[c(40),2]=c('Pomatomidae')
family.info[c(15:16,42:43),2]=c('Nomeidae')
family.info[c(24,44),2]=c('Centrolophidae')
family.info[c(59),2]=c('Scombrolabracidae')
family.info[c(64),2]=c('Tetragonuridae')

family.info<-as.data.frame(family.info) #turns matrix into more
    useable dataframe

##Colour the nodes based on family groupings and create a
    phylomorphospace for PC1 v PC2
pdf("Phylomorphospace3DAug7namesTree2.pdf")
family.colours<-c("blue","chartreuse","darkgoldenrod1","cyan","
    darkolivegreen1","darkorchid1",
                  "darkorange","deeppink","firebrick1","green","
                      lightpink","peru","magenta",
                  "violet","yellow")
palette(family.colours)
tip.cols<-family.info$Family
names(tip.cols)<-pruned.trees[[2]]$tip.label
```

```
cols<-c(tip.cols[pruned.trees[[2]]$tip.label],rep("black",pruned.trees[[2]]$Nnode))
names(cols)<-1:(length(pruned.trees[[2]]$tip)+pruned.trees[[2]]$Nnode)
phylomorphospace(pruned.trees[[2]],traits[,1:2],control=list(col.node=cols), label="radial")
#tip.cols<-setNames(palette()[1:length(family.info$Family)],family.info)
legend("topright", "(x,y)", sort(unique(family.info$Family), decreasing=FALSE), pch=20, cex=0.6, horiz=F, ncol = 2, bty="n", col=family.colours)
dev.off()
```

./Appendices/RCode/03_Phylomorphospace.R

```
##### Processing fossil data #####
#Authors: Hermione Beckett, Jonathan Harrison
#Last edited: 07/08/2018

 folder.path <-"/Users/admin/Dropbox/3D Landmarking/Mimi Pelagia Landmarking/"
setwd(folder.path)

load(file="PelagiadataAug7.rda")
load(file="PelagiaPCArawAug7.rda")
source("01b_functions_JH.R")

ntraits <- 5
traits <- traits[,1:ntraits]

```

```
#rownames(pelagia.3D.pcscores)<-gsub("\\(","",rownames(pelagia.3D.
    pcscores))
#rownames(pelagia.3D.pcscores)<-gsub("\\)","",rownames(pelagia.3D.
    pcscores))
#traits <- gsub("\\(","",rownames(traits_f_e))
############## Placing FOSSILS into tree ###################


#### Fossil placement ####s

fossil.info<-read.csv(paste('fossils_to_place3D.csv',sep=''),
    stringsAsFactors = FALSE, na.strings=(""))
fossil.info<-fossil.info[-c(2,4,5,7,9),]
rownames(fossil.info)<-c(1:4)

fossils.names <- intersect(rownames(pelagia.3D.pcscores), fossil.info
    $Fossil.taxon)
fossils<-pelagia.3D.pcscores[rownames(pelagia.3D.pcscores) %in%
    fossils.names,1:ntraits]
#fossils<-fossils[c(1,3,6,8),]
#creates an object traits_f_e that is the combination of extant and
    fossil data
traits_f_e<-pelagia.3D.pcscores[rownames(pelagia.3D.pcscores) %in% c(
    rownames(traits),rownames(fossils)),1:ntraits]

save(traits_f_e, file="FossiltraitsAug7.Rda")

place_individual_fossils <- function(single.tree) {
  #place individual fossils in the tree
  ##################
```

```
#par(mfrow=c(1,1))
tipdata<-c()
for( i in c(1:4)){
  temptraits <- rbind(traits, fossils[i,,drop=FALSE])
  if(is.na(fossil.info$mrca.2[i])){
    tipdata[[i]]<-locate.fossil.JH(single.tree, temptraits,
                                   time.constraint=c(fossil.info$Max.
                                       age[i],fossil.info$Min.age[i]),
                                   edge.constraint=c(which(single.tree
                                       $tip.label==fossil.info$mrca.1[i
                                       ])), plot=FALSE)
  } else {
    if(is.na(fossil.info$mrca.3[i])) {
      tipdata[[i]]<-locate.fossil.JH(single.tree, temptraits,
                    time.constraint=c(fossil.info$Max.age[i],fossil.
                        info$Min.age[i]),
                    edge.constraint=c(getMRCA(single.tree, c(fossil.
                        info$mrca.1[i],fossil.info$mrca.2[i]))), plot=
                        FALSE)
    } else {
      tipdata[[i]]<-locate.fossil.JH(single.tree, temptraits,
                    time.constraint=c(fossil.info$Max.age[i],fossil.
                        info$Min.age[i]),
                    edge.constraint=c(getDescendants(single.tree,
                    getMRCA(single.tree, c(fossil.info$mrca.1[i],
                        fossil.info$mrca.2[i])),
                    curr=NULL)), plot=FALSE)
    }
  }
}
```

```
60
61   #when given multiple trees, take just the first
62   for (j in seq_len(nrow(fossils))) {
63     if (!(class(tipdata[[j]])=="phylo")){
64       tipdata[[j]] = tipdata[[j]][[1]]
65     }
66   }
67   return(tipdata)
68 }
69
70
71   bind_successive_trees <- function(single.tree, single.tipdata){
72   ##Bind each tip successively into the tree
73   fossil.tree <- single.tipdata[[1]]
74   for (i in 2:nrow(fossils)) {
75     taxon.name <- fossil.info$Fossil.taxon[i] #takes tip name
76     fos.tree <- single.tipdata[[i]] #takes first fossil tree
77     tip <- which(fos.tree$tip.label==taxon.name) #which tip is the
         fossil at
78     foss.edge <- which(fos.tree$edge[,2]==tip) #which edge is the
         fossil on
79     foss.edge.length <- fos.tree$edge.length[foss.edge] #what is the
         edge length of the fossil branch
80     ancestor.node <- fos.tree$edge[foss.edge,1] #at which node is the
          fossil in the placed tree
81     sisters <- which(fos.tree$edge[,1]==ancestor.node)#what are the
         sister taxa of the fossil taa
82     other <- sisters[which(sisters!=foss.edge)] #remove the fossil
         tip from this list
```

```
83      other.length <- fos.tree$edge.length[other] #find out the length
            of the edge lenth above the point at which the fossil subtends
             the branch
84      other.tax <- fos.tree$tip.label[getDescendants(fos.tree,fos.tree$
            edge[other,2])] #what are the names of sisters
85    #if more than one taxon, need to get MRCA
86      if(length(other.tax)==1) {
87       other.node <- which(fossil.tree$tip.label==other.tax)
88      } else {
89       other.node <- getMRCA(fossil.tree,other.tax[!is.na(other.tax)])
90      }
91      #if there is a polytomy need to just take one length as it will
            go below that node
92      if (length(other.length)>1){other.length <- other.length[1]}
93      if (any(other.length > fossil.tree$edge.length[fossil.tree$edge[,
             2] ==
94                                                  other.node])){
95       #deal with this case to prevent failure
96       other.length = fossil.tree$edge.length[fossil.tree$edge[, 2] ==
97                                                other.node]
98      }
99
100     fossil.tree<-bindPaleoTip(fossil.tree, taxon.name, nodeAttach =
            other.node,
101                               edgeLength = foss.edge.length,
102                               positionBelow = other.length,
103                               noNegativeEdgeLength = TRUE)
104   }
105   return(fossil.tree)
106   }
```

```
107
108 placed.trees <- purrr::map(pruned.trees, place_individual_fossils)
109 fossil.trees <- purrr::map2(pruned.trees, placed.trees, bind_
        successive_trees)
110 save(fossil.trees, file='fossil_trees_aug7.rda')
111
112 par(mfrow=c(1,1))
113 #plot the fossil tree.
114 plot(fossil.trees[[64]], cex=0.5)
```

./Appendices/RCode/04_Placing_fossils.R

```
1 ####DTT Analysis extant
2 #Authors: Hermione Beckett, Kara Fielich
3 #Last edited: 07/08/2018
4
5 #source("02_Processing_data.R")
6
7 folder.path <-"/Users/admin/Dropbox/3D Landmarking/Mimi Pelagia
        Landmarking/"
8 setwd(folder.path)
9
10 source("00_startup.R")
11 source("01_functions.R")
12
13 #pull in the data from 02_Processing_data.R
14 load(file="PelagiadataAug7.rda")
15
16 #source("multiDTT.R")
17
```

```
#This runs the DTT1 analysis from Murrell 2018 across all trees with nsim>2500 to avoid errors in rank env testing.
#If you want to run with data simulated using simulate use multiDTT, but DTT1 should be calculating multivariate data
results.for.all.trees <- purrr::map(pruned.trees, function(x)
  dtt1(x, traits, plot=FALSE, nsim = 2500, calculateMDIp=TRUE))


save(results.for.all.trees, file="DTTresultsAug7.rda")

load("DTTresultsAug7.rda")

# Pull the values of the MDI statistic into a vector
mdi.values <- purrr::map_dbl(results.for.all.trees, getMDI)

# Pull the p-values associated with the MDI statistic into a vector
mdi.p.values <- purrr::map_dbl(results.for.all.trees, getMDIPvalue)

# Bind the MDI values and the p-values into a dataframe
mdi.output <- data.frame("MDI" = mdi.values, "MDI.pval" = mdi.p.values)


# Calculate rank envelopes for each set of dtt results ##########################


# This iterates the rank envelope function over the list of dtt results (the
```

```
42 # output from the previous function call), and returns the rank
       envelope result
43 # as a list of each individual set of results
44 rank.envelope.results <- purrr::map(results.for.all.trees, rank_env_
       dtt, Plot = F, test = "less")
45
46 # Find significant times
       ##########################################################
47
48 # Call checkIsLower on all tree-rankenv pairs. purrr::map2 iterates
       the function
49 # (checkIsLower), over each x, y pair of (cleaned.trees, rank.
       envelope.results)
50 is.it.lower.results <- purrr::map2(pruned.trees, rank.envelope.
       results,
51                                    checkIsLower)
52
53 lower.runs<-lapply(is.it.lower.results, function(x) findLowerRuns(x))
54
55 lower.runs <- purrr::map(is.it.lower.results, findLowerRuns)
56
57
58 # To get the index of the tree in cleaned.trees that produced each
       output, we
59 # need to name the elements of 'is.it.lower.results'
60 names(is.it.lower.results) <- as.numeric(seq(1:length(is.it.lower.
       results)))
61
62 # merge all relative time points from all trees into one giant
       dataframe
```

```
63 all.timepoints <- purrr::map_dfr(is.it.lower.results, rbind, .id = '
       tree.index')
64
65
66 # Summarize significant time points by tree for each million years
       ##############
67
68 # First, we need maximum root age of all of the trees
69 unnamed.trees <- pruned.trees  # Need to clear off the names or
       result is wonky
70 names(unnamed.trees) <- NULL
71 root.ages <- purrr::map_dbl(unnamed.trees,
72                             function(x) max(phytools::nodeHeights(x))
                                )
73 maximum.root.age <- max(root.ages)
74
75 # Then, we need sensible bins (every million years)
76 all.timepoints$time.bins <- cut(all.timepoints$actual.time,
77                                 breaks = c(0, seq(1,maximum.root.age
                                    +1)),
78                                 labels=FALSE)
79
80 # NOTE: bin labels mean that the time point was in the interval
81 # (1-binlabel, bin label)
82
83 # Then, aggregate the significantly lower points by tree and by bin
84 agg.timepts <- aggregate(x= list(is.lower = all.timepoints$is.it.
       lower),
85                          by = list(Tree = all.timepoints$tree.index,
```

```
                                        Bin = all.timepoints$time.bins),
                                          FUN = sum)

# Set it so multiple points from the same tree in the same bin only
    count as 1
agg.timepts$is.lower[which(agg.timepts$is.lower > 0)] <- 1
# Get dataframe of only significant points
lower.timepts <- agg.timepts[which(agg.timepts$is.lower == 1),]
# Aggregate by bin
lower.bins <- aggregate(x=list(NumTrees = lower.timepts$is.lower),
                        by = list(Bin = lower.timepts$Bin), FUN = sum
                            )


dtt.results.all<-results.for.all.trees

# This is a custom ggplot theme to get rid of the ugly backgrounds
    and gridlines
theme_custom <- function() {
  theme_bw(base_size = 12, base_family = "") %+replace%
    theme(panel.grid.major = element_blank(),
          panel.grid.minor = element_blank())
}

# Plot all of the significantly lower points from rank envelope
    ##################
##This produces the proportion of posterior trees plot which shows
    where the deviations occur through time
timepoints.plot <- ggplot(data = lower.bins,
```

```
109                                 aes(x = Bin, y = NumTrees/length(pruned.
                                        trees))) +
110   geom_col(position=position_nudge(x=0.5), fill = "black") +  # Nudge
          b/c of bin bounds
111   scale_y_continuous(expand = c(0, 0), limits = c(0, 1.0)) +
112   labs(x='Millions of years ago (binned)', y='Proportion of Posterior
          Trees') +
113   scale_x_reverse()+
114   geom_vline(xintercept = 66, colour = 'grey75', linetype = "dashed")
          +
115   theme_custom()
116
117 timepoints.plot
118
119
120 # Make rank envelope p-value range histograms
      ####################################
121
122 # Pulls all p-values from list of rank-envelope results into a vector
      (type double)
123 p.values <- purrr::map_dbl(rank.envelope.results, getPvalue)
124
125 # Pulls all p-value intervals from list of rank envelope results into
      a dataframe
126 # with columns of Lower (bound) and Upper (bound)
127 p.intervals <- purrr::map_df(rank.envelope.results, getPinterval)
128 p.intervals$y.position <- as.numeric(row.names(p.intervals))  #
      Needed for plotting
129
130 # Plot p-value histogram
```

```
p.val.hist<- ggplot(data=as.data.frame(p.values), aes(p.values)) +
  geom_histogram(fill="red", binwidth=0.001, aes(y=..count../sum(..
      count..)), alpha=0.4) +
  labs(x = "Rank Envelope p-values", y = "Proportion of trees") +
  theme_custom()
p.val.hist

# Plot p-value ranges
p.int.plot <- ggplot(data = p.intervals, aes(x = Lower, y = y.
    position,
                                             xend = Upper, yend=y.
                                                 position)) +
  geom_segment() +
  labs(title="Extant") +
  theme(plot.title = element_text(face="bold", hjust=0.5, size=12))
p.int.plot ##


# Plot MDI statistic histogram
    ##################################################
mdi.val.hist <- ggplot(data=mdi.output, aes(MDI)) +
  geom_histogram(fill="black", binwidth = 0.005, aes(y=..ndensity..))
      +
  scale_y_continuous(expand = c(0,0), limits = c(0,1.0)) +
  labs(x = "MDI values", y = "Proportion of Trees") +
  theme_custom()
mdi.val.hist

# Plot MDI p-values histogram
    ##################################################
```

```
mdi.p.hist <- ggplot(data=mdi.output, aes(MDI.pval)) +
  geom_histogram(fill="black", binwidth = 0.001, aes(y=..ndensity..))
      +
  scale_y_continuous(expand = c(0,0), limits = c(0,1.0)) +
  labs(x = "MDI p-values", y = "Proportion of Trees") +
  theme_custom()
mdi.p.hist
```

./Appendices/RCode/05_DTT.R

```
### Fossil DTT ###
#Authors: Hermione Beckett, Kara Fielich
#Last edited: 07/08/2018

source('C:/Users/admin/Dropbox/3D Landmarking/Mimi Pelagia
    Landmarking/BranchingTimesFossil.R')
source('C:/Users/admin/Dropbox/3D Landmarking/Mimi Pelagia
    Landmarking/fossilDTT.R')

folder.path <-"/Users/admin/Dropbox/3D Landmarking/Mimi Pelagia
    Landmarking/"
setwd(folder.path)

#source("02_Processing_data.R")


source("00_startup.R")
source("01_functions.R")

#pull in the data from _Processing_fossil_data.R
load('fossil_trees_Aug7.rda')
```

```
19 load("FossiltraitsAug7.Rda")
20
21 #source("multiDTT.R")
22
23 #This runs the fossil DTT analysis from Murrell 2018 across all trees
       with nsim>2500 to avoid errors in rank env testing.
24 #If you want to run with data simulated using simulate use multiDTT,
     but DTT1 should be calculating multivariate data
25 results.for.fos.trees <- purrr::map(fossil.trees, function(x)
26   fossilDTT(x, traits_f_e, plot=FALSE, nsim = 2500, calculateMDIp=
       TRUE))
27
28
29
30 save(results.for.fos.trees, file="DTTfosresults_Aug7.rda")
31
32 load("DTTfosresults_Aug7.rda")
33
34 # Pull the values of the MDI statistic into a vector
35 mdi.values.fos <- purrr::map_dbl(results.for.fos.trees, getMDI)
36
37 # Pull the p-values associated with the MDI statistic into a vector
38 mdi.p.values.fos <- purrr::map_dbl(results.for.fos.trees,
     getMDIPvalue)
39
40 # Bind the MDI values and the p-values into a dataframe
41 mdi.output.fos <- data.frame("MDI" = mdi.values.fos, "MDI.pval" = mdi
     .p.values.fos)
42
43
```

```
44 # Calculate rank envelopes for each set of dtt results
   ############################
45
46
47 # This iterates the rank envelope function over the list of dtt
   results (the
48 # output from the previous function call), and returns the rank
   envelope result
49 # as a list of each individual set of results
50 rank.envelope.results.fos <- purrr::map(results.for.fos.trees, rank_
   env_dtt, Plot = F, test = "less")
51
52 # Find significant times
   ##############################################################
53
54 # Call checkIsLower on all tree-rankenv pairs. purrr::map2 iterates
   the function
55 # (checkIsLower), over each x, y pair of (cleaned.trees, rank.
   envelope.results)
56 is.it.lower.results.fos <- purrr::map2(fossil.trees, rank.envelope.
   results.fos,
57                                        checkIsLower)
58
59 lower.runs.fos <- purrr::map(is.it.lower.results.fos, findLowerRuns)
60
61
62 # To get the index of the tree in cleaned.trees that produced each
   output, we
63 # need to name the elements of 'is.it.lower.results'
```

```
64 names(is.it.lower.results.fos) <- as.numeric(seq(1:length(is.it.lower
       .results.fos)))
65
66 # merge all relative time points from all trees into one giant
       dataframe
67 all.timepoints.fos <- purrr::map_dfr(is.it.lower.results.fos, rbind,
       .id = 'tree.index')
68
69
70 # Summarize significant time points by tree for each million years
       ##############
71
72 # First, we need maximum root age of all of the trees
73 unnamed.trees <- fossil.trees  # Need to clear off the names or
       result is wonky
74 names(unnamed.trees) <- NULL
75 root.ages.fos <- purrr::map_dbl(unnamed.trees,
76                                 function(x) max(phytools::nodeHeights(x))
                                    )
77 maximum.root.age.fos <- max(root.ages)
78
79 # Then, we need sensible bins (every million years)
80 all.timepoints.fos$time.bins <- cut(all.timepoints.fos$actual.time,
81                                     breaks = c(0, seq(1,maximum.root.age
                                        +1)),
82                                     labels=FALSE)
83
84 # NOTE: bin labels mean that the time point was in the interval
85 # (1-binlabel, bin label)
86
```

```
87 # Then, aggregate the significantly lower points by tree and by bin
88 agg.timepts.fos <- aggregate(x= list(is.lower = all.timepoints.fos$is
       .it.lower),
89                              by = list(Tree = all.timepoints.fos$tree.
                                   index,
90                                        Bin = all.timepoints.fos$time.bins
                                       ), FUN = sum)
91
92 # Set it so multiple points from the same tree in the same bin only
       count as 1
93 agg.timepts.fos$is.lower[which(agg.timepts.fos$is.lower > 0)] <- 1
94 # Get dataframe of only significant points
95 lower.timepts.fos <- agg.timepts.fos[which(agg.timepts.fos$is.lower
       == 1),]
96 # Aggregate by bin
97 lower.bins.fos <- aggregate(x=list(NumTrees = lower.timepts.fos$is.
       lower),
98                             by = list(Bin = lower.timepts.fos$Bin), FUN =
                                  sum)
99
100
101 dtt.results.fos<-results.for.fos.trees
102
103 # This is a custom ggplot theme to get rid of the ugly backgrounds
       and gridlines
104 theme_custom <- function() {
105   theme_bw(base_size = 12, base_family = "") %+replace%
106     theme(panel.grid.major = element_blank(),
107           panel.grid.minor = element_blank())
108 }
```

```
109
110 # Plot all of the significantly lower points from rank envelope
    ##################
111 ##This produces the proportion of posterior trees plot which shows
    where the deviations occur through time
112 timepoints.plot.fos <- ggplot(data = lower.bins,
113                               aes(x = Bin, y = NumTrees/length(fossil.
                                      trees))) +
114   geom_col(position=position_nudge(x=0.5), fill = "black") +  # Nudge
        b/c of bin bounds
115   scale_y_continuous(expand = c(0, 0), limits = c(0, 1.0)) +
116   labs(x='Millions of years ago (binned)', y='Proportion of Posterior
        Trees') +
117   scale_x_reverse()+
118   geom_vline(xintercept = 66, colour = 'grey75', linetype = "dashed")
        +
119   theme_custom()
120
121 timepoints.plot.fos
122
123 # Make rank envelope p-value range histograms
    ######################################
124
125 # Pulls all p-values from list of rank-envelope results into a vector
      (type double)
126 p.values.fos <- purrr::map_dbl(rank.envelope.results.fos, getPvalue)
127
128 # Pulls all p-value intervals from list of rank envelope results into
      a dataframe
129 # with columns of Lower (bound) and Upper (bound)
```

```
130 p.intervals.fos <- purrr::map_df(rank.envelope.results.fos,
        getPinterval)
131 p.intervals.fos$y.position <- as.numeric(row.names(p.intervals.fos))
        # Needed for plotting
132
133 # Plot p-value histogram
134 p.val.hist.fos <- ggplot(data=as.data.frame(p.values.fos), aes(p.
        values.fos)) +
135   geom_histogram(fill="blue",binwidth=0.001, aes(y=..count../sum(..
          count..)), alpha=0.4) +
136   labs(x = "Rank Envelope p-values", y = "Proportion of trees") +
137   theme_custom()
138 p.val.hist.fos
139
140 # Plot p-value ranges - DTT outputs a range of pvalues rather than a
        single p value for each tree, therefore need to see range
141 p.int.plot.fos <- ggplot(data = p.intervals.fos, aes(x = Lower, y = y
        .position,
142                                                      xend = Upper, yend=y.
                                                           position)) +
143   geom_segment() +
144   labs(title="Combined") +
145   theme(plot.title = element_text(face="bold", hjust=0.5, size=12),
146         axis.title.y=element_blank())
147 p.int.plot.fos
148
149
150 # Plot MDI statistic histogram
      ##################################################
151 mdi.val.hist.fos <- ggplot(data=mdi.output.fos, aes(MDI)) +
```

```
152   geom_histogram(fill="black", binwidth = 0.005, aes(y=..ndensity..))
          +
153   scale_y_continuous(expand = c(0,0), limits = c(0,1.0)) +
154   labs(x = "MDI values", y = "Proportion of Trees") +
155   theme_custom()
156 mdi.val.hist.fos
157
158 # Plot MDI p-values histogram
      ##########################################################
159 mdi.p.hist.fos <- ggplot(data=mdi.output.fos, aes(MDI.pval)) +
160   geom_histogram(fill="black", binwidth = 0.001, aes(y=..ndensity..))
          +
161   scale_y_continuous(expand = c(0,0), limits = c(0,1.0)) +
162   labs(x = "MDI p-values", y = "Proportion of Trees") +
163   theme_custom()
164 mdi.p.hist.fos
```

./Appendices/RCode/05b_DTT_foss.R

```
1 ###DTT Figure Plotting
2
3 #Authors: Hermione Beckett, Jonathan Harrison
4 #Last edited: 07/08/2018
5
6 folder.path <-"/Users/admin/Dropbox/3D Landmarking/Mimi Pelagia
      Landmarking/"
7 setwd(folder.path)
8
9 load("DTTresultsAug7.rda")
10 load("DTTfosresults_Aug7.rda")
11
```

```
12 theme_custom <- function() {
13   theme_bw(base_size = 12, base_family = "")  %+replace%
14     theme(panel.grid.major = element_blank(),
15           panel.grid.minor = element_blank())
16 }
17
18 library(ggplot2)
19 library(dplyr)
20
21 ###Facetwrapped p-interval plot
22 p.intervals.full <- full_join(mutate(p.intervals,source_of_data="
     Extant"),
23                               mutate(p.intervals.fos,source_of_data="
                                    Fossil"))
24 p.intervals.comb <- ggplot(data = p.intervals.full, aes(x = Lower, y
     = y.position,
25                                xend = Upper, yend=y.position)) +
26   labs(x="p-Interval",y="Tree Number",title="A") +
27   geom_segment() +
28   facet_wrap(~source_of_data)
29 p.intervals.comb
30
31 # ###Combined rank envelope p-value plots
32 combined.p.values<-data.frame(p.values=c(p.values,p.values.fos),
     source_of_data=c(rep('Extant',100),rep('Fossil',100)))
33
34 p.values.RE <- ggplot(data=combined.p.values, aes(p.values, fill=
     source_of_data)) +
```

```
35    geom_histogram(binwidth=0.001, data=subset(combined.p.values,source
          _of_data=='Extant'), aes(y=..count../sum(..count..)), alpha=0.4)
          +
36    geom_histogram(binwidth=0.001, data=subset(combined.p.values,source
          _of_data=='Fossil'), aes(y=..count../sum(..count..)), alpha=0.4)
          +
37    labs(x = "Rank Envelope p-values", y = "Proportion of trees",title=
          "B") +
38    theme_bw() +
39    theme(legend.title=element_blank(),legend.position = c(0.85,0.8))
40
41  p.values.RE
42
43
44  ###Combined timepoints rank envelope plot
45  combined.lower.bins<- full_join(mutate(lower.bins,source_of_data="
        Extant"),
46                                  mutate(lower.bins.fos,source_of_data="
                                        Fossil"))
47  timepoints.plot.comb <- ggplot() +
48    geom_col(data = combined.lower.bins,
49             aes(x = Bin, y = NumTrees/length(fossil.trees), fill=
                 source_of_data),
50             position=position_nudge(x=0.5), alpha=0.4) + # Nudge b/c
                 of bin bounds
51    scale_y_continuous(expand = c(0, 0), limits = c(0, 1.0)) +
52    labs(x='Millions of years ago (binned)', y='Proportion of Posterior
          Trees',title='C') +
53    scale_x_reverse(breaks=seq(from=0,to=100,by=10), limits = c(NA,0))
        +
```

```
  geom_vline(xintercept = 66, colour = 'grey75', linetype = "dashed")
      +
  theme_custom() +
  theme(legend.title=element_blank(),legend.position = c(0.9,0.8))
timepoints.plot.comb




library(patchwork) # see https://github.com/thomasp85/patchwork for
    details

DTT.plot={p.intervals.comb + p.values.RE} / timepoints.plot.comb
DTT.plot


ggsave('DTTresults.pdf', width=180, height=140, units="mm", dpi=600)
```

./Appendices/RCode/05c_DTTFigPlotting.R

```

###### Author: Hermione Beckett, Jonathan Harrison #######
#Last edited: 2018-07-21

source("00_startup.R")
source("01_functions.R")

#last edited JH 2018-07-18
######## MV MORPH ######

load(file="PelagiadataAug7.rda")
```

```
12 #subset the traits
13 ntraits <- 5
14 traits <- traits[,seq_len(ntraits)]
15 ntrees <- 100
16
17 #This function fits each of BM, EB and SHIFT models to the inputted
       data
18 #NB. tip.label of trees and traits must be in the same order
19 run_mvmorph <- function(single.tree,id){
20   print(id)
21   BM.model<-mvBM(single.tree, traits, error = NULL)
22   EB.model<-tryCatch(mvEB(single.tree, traits, error=NULL, method="
         rpf", diagnostic=F, echo=F),
23                      error=function(cond){
24                        return(mvEB(single.tree, traits, error=NULL,
                               method="pseudoinverse", diagnostic=F, echo=
                               F))})
25   #Fit a BM followed by a shift to OU at an age which is optemised
26   fit_SHIFT_at_given_age <- function(shift_age){
27     BM.ER.model_op<-mvSHIFT(single.tree, traits, model="BMOU",method=
           "rpf", param=list(age=inv.logit(shift_age,min=0,max=max(
           nodeHeights(single.tree)))))
28     return(BM.ER.model_op$LogLik)}
29   z = optim(1,fit_SHIFT_at_given_age,control=list(maxit=10))
30
31   age_estimate = inv.logit(z$par,min=0,max=max(nodeHeights(single.
         tree)))
32   SHIFT.model<-mvSHIFT(single.tree, traits, model="BMOU",method="rpf"
         , param=list(age=age_estimate))
33
```

```
34    mv_morph_res <- list(BM.model=BM.model,EB.model=EB.model,SHIFT.
          model=SHIFT.model,age_estimate=age_estimate)
35    #This outputs a single .rda object for each tree, in case of errors
          in the code, so it is clear where in the set of trees the error
          is occuring.
36    save(mv_morph_res, file=paste("mvmorph_results_Aug7",id,".rda",sep=
          ""))
37    return(mv_morph_res)
38  }
39  #run mvmorph analysis on for each tree from the list of trees from
      the posterior
40  mv_morph_all_results <- purrr::map2(pruned.trees, seq_len(100), run_
      mvmorph)
41
42  #load morph results if above code has errored and want to load from
      rda objects.
43  #mv_morph_all_results <- list()
44  #for (i in 1:100){
45  #  load(paste("mvmorph_results_as_we_go",i,".rda",sep=""))
46  #  mv_morph_all_results[[i]] = mv_morph_res
47  #}
48
49  #Save these results for plotting.
50  save(mv_morph_all_results, file="mvMorphExtant_Aug7.rda")
```

./Appendices/RCode/06a_mvmorph.R

```
1  ###mvMorph Fossil
2  #Authors: Hermione Beckett
3  #Last edited: 07/08/2018
4  source("00_startup.R")
```

```
5
6  folder.path <-"/Users/admin/Dropbox/3D Landmarking/Mimi Pelagia
       Landmarking/"
7  setwd(folder.path)
8
9  ######## MV MORPH ######
10 load('fossil_trees_Aug7.rda')
11 load("FossiltraitsAug7.Rda")
12 ntrees <- 100
13 #This function fits each of BM, EB and SHIFT models to the inputted
       data
14 #NB. tip.label of trees and traits must be in the same order, when
       fossils are inserted they are not.
15 run_mvmorph <- function(single.tree,id){
16   print(id)
17   traits_reordered <- traits_f_e[single.tree$tip.label,]
18   BM.model<-mvBM(single.tree, traits_reordered, error = NULL)
19   EB.model<-tryCatch(mvEB(single.tree, traits_reordered, error=NULL,
         method="rpf", diagnostic=F, echo=F),
20                      error=function(cond){
21                        return(mvEB(single.tree, traits_reordered,
                              error=NULL, method="pseudoinverse",
                              diagnostic=F, echo=F))})
22   #Fit a BM followed by a shift to OU at an age which is optemised
23   fit_SHIFT_at_given_age <- function(shift_age){
24     BM.ER.model_op<-mvSHIFT(single.tree, traits_reordered, model="
           BMOU",method="rpf",
25                             param=list(age=inv.logit(shift_age,min=0,
                                   max=max(nodeHeights(single.tree)))))
26     return(BM.ER.model_op$LogLik)}
```

```
27    z = optim(1, fit_SHIFT_at_given_age, control=list(maxit=10))
28
29    age_estimate = inv.logit(z$par, min=0, max=max(nodeHeights(single.
          tree)))
30    SHIFT.model<-mvSHIFT(single.tree, traits_reordered, model="BMOU",
          method="rpf", param=list(age=age_estimate))
31
32    mv_morph_res <- list(BM.model=BM.model, EB.model=EB.model, SHIFT.
          model=SHIFT.model, age_estimate=age_estimate)
33    save(mv_morph_res, file=paste("mvmorph_fos_results_reordered_Aug7",
          id, ".rda", sep=""))
34    print(id)
35    return(mv_morph_res)
36  }
37  #run mvmorph analysis on for each tree from the list of trees from
        the posterior
38  mv_morph_fossil_results <- purrr::map2(fossil.trees, seq_len(ntrees),
        run_mvmorph)
39
40  #load morph results if above code has errored and want to load from
        rda objects.
41  #mv_morph_fossil_results <- list()
42  #for (i in 1:100){
43  #  load(paste("mvmorph_results_as_we_go",i,".rda",sep=""))
44  #  mv_morph_fossil_results[[i]] = mv_morph_res
45  #}
46
47  #Save these results for plotting.
```

```
save(mv_morph_fossil_results, file="mvMorphFoss_Aug7.rda")
```

./Appendices/RCode/06b_fossilmvMorph.R

```
###mvMORPH figure plotting

#### Authors: Hermione Beckett, Jonathan Harrison ####
#### Last edited: 2018-07-21 ####

##### Plotting figures #####

load("mvMorphExtant_Aug7.rda")
load("mvMorphFoss_Aug7.rda")

library(dplyr)
theme_custom <- function() {
  theme_bw(base_size = 12, base_family = "") %+replace%
    theme(panel.grid.major = element_blank(),
          panel.grid.minor = element_blank())
}

library(ggplot2)

#### mvMORPH AICs ####

#AICs <- c(BM.model$AIC,EB.model$AIC,OU.model$AIC,BM.ER.BMOU$AIC)
#barplot(akaike.weights.extant$weights, ylim=c(0:1), ylab="Akaike
    weights", names.arg=c("Brownian Motion","Early Burst","OU model","
    Shift model"))

```

```
25 BM.AICcs <- purrr::map_dbl(mv_morph_all_results, function(x) x$BM.
       model$AICc)
26 EB.AICcs <- purrr::map_dbl(mv_morph_all_results, function(x) x$EB.
       model$AICc)
27 SHIFT.AICcs <- purrr::map_dbl(mv_morph_all_results, function(x) x$
       SHIFT.model$AICc)
28
29 BM.AICcs.fos <- purrr::map_dbl(mv_morph_fossil_results, function(x) x
       $BM.model$AICc)
30 EB.AICcs.fos <- purrr::map_dbl(mv_morph_fossil_results, function(x) x
       $EB.model$AICc)
31 SHIFT.AICcs.fos <- purrr::map_dbl(mv_morph_fossil_results, function(x
       ) x$SHIFT.model$AICc)
32
33 age_estimates <- purrr::map_dbl(mv_morph_all_results, function(x) x$
       age_estimate)
34 age_estimates_fos <- purrr::map_dbl(mv_morph_fossil_results, function
       (x) x$age_estimate)
35
36
37 #pytting AIC results into data frames so it can be shown via ggplot
38 AICs_df <- data.frame(BM=BM.AICcs, EB=EB.AICcs, SHIFT=SHIFT.AICcs)
39 AICs_df_tidied <- tidyr::gather(AICs_df,"Method","AICc",1:3)
40 AICs_df_temp <- t(purrr::pmap_dfc(AICs_df, ~data.frame(weights = qpcR
       ::akaike.weights(c(..1, ..2, ..3))$weights)))
41 colnames(AICs_df_temp) <- c("BM","EB","SHIFT")
42 AICs_df_akaike_weights <- tidyr::gather(as.data.frame(cbind(AICs_df_
       temp,seq_len(100))),"Method","weight",1:3)
43 #Average Akaike Weight
44 Av.extant<-apply(AICs_df_temp,2,mean)
```

```
45
46 AICs_df.fos <- data.frame(BM=BM.AICs.fos, EB=EB.AICs.fos, SHIFT=SHIFT
       .AICs.fos)
47 AICs_df_tidied.fos <- tidyr::gather(AICs_df.fos,"Method","AICc",1:3)
48 AICs_df_temp.fos <- t(purrr::pmap_dfc(AICs_df.fos, ~data.frame(
       weights = qpcR::akaike.weights(c(..1, ..2, ..3))$weights)))
49 colnames(AICs_df_temp.fos) <- c("BM","EB","SHIFT")
50 AICs_df_akaike_weights.fos <- tidyr::gather(as.data.frame(cbind(AICs_
       df_temp.fos,seq_len(100))),"Method","weight",1:3)
51 Av.fossil<-apply(AICs_df_temp.fos,2,mean)
52
53 AICs.comb <- rbind(AICs_df_tidied,AICs_df_tidied.fos)
54 Data.source=c(rep('Extant',300),rep('Fossil',300))
55 AICs.comb <- cbind(AICs.comb,Data.source)
56
57 #Violin plot for both datasets
58 comb.violin.plot <- ggplot(data=AICs.comb, aes(color=Data.source,
       fill=Data.source)) +
59   geom_violin(data=subset(AICs.comb, Data.source=='Extant'), aes(x=
         Method, y=AICc, fill=Data.source, alpha=0.4)) +
60   geom_violin(data=subset(AICs.comb, Data.source=='Fossil'), aes(x=
         Method, y=AICc, fill=Data.source, alpha=0.4)) +
61   labs(x="Model") +
62   theme_custom()
63 comb.violin.plot
64
65 #Create a histogram of the SHIFT ages
66 combined_age_estimates <- data.frame(age_estimates=c(age_estimates,
       age_estimates_fos),
```

```
67                                          source_of_data=c(rep('Extant'
                                                ,100),rep('Fossil',100)))
68
69 combined.age.est.hist <- ggplot(data=combined_age_estimates, aes(age_
       estimates, fill=source_of_data)) +
70   geom_histogram(binwidth=1, data=subset(combined_age_estimates,
         source_of_data=='Extant'), aes(y=..count..), alpha=0.4) +
71   geom_histogram(binwidth=1, data=subset(combined_age_estimates,
         source_of_data=='Fossil'), aes(y=..count..), alpha=0.4) +
72   labs(x = "Age Estimate", y = "Number of trees") +
73   theme_bw() +
74   scale_x_reverse(breaks=c(70,60,50,40,30,20,10)) +
75   theme(legend.title=element_blank())
76 combined.age.est.hist
77
78 #Density Plot of the age estimates
79 # combined.age.est.density <- ggplot(data=combined_age_estimates, aes
       (age_estimates, color=source_of_data, fill=source_of_data)) +
80 #   geom_density(alpha=0.4) +
81 #   labs(x = "Age Estimate", y = "Proportion of trees") +
82 #   theme_bw()+
83 #   scale_x_reverse(breaks=c(70,60,50,40,30,20,10)) +
84 #   theme_bw() +
85 #   theme(legend.title=element_blank())
86 # combined.age.est.density
87
88 #Plot the relative Akaike weights
89 extant.stacked.hist <- ggplot(AICs_df_akaike_weights, aes(x=V4, y=
       weight, fill=factor(Method))) +
90   geom_bar(stat="identity") +
```

```
91    theme_bw() +
92    labs(x="Tree id", y= "Akiake weight") +
93    theme(legend.title=element_blank()) +
94    scale_fill_manual(values=c("#feb24c","#af8dc3","#7fbf7b")) +
95    scale_x_continuous(breaks=seq(from=0,to=100,by=5))
96  extant.stacked.hist
97
98  fos.stacked.hist <- ggplot(AICs_df_akaike_weights.fos, aes(x=V4, y=
        weight, fill=factor(Method))) +
99    geom_bar(stat="identity") +
100   theme_bw() +
101   labs(x="Tree id", y= "Akiake weight") +
102   theme(legend.title=element_blank()) +
103   scale_fill_manual(values=c("#feb24c","#af8dc3","#7fbf7b"))+
104   scale_x_continuous(breaks=seq(from=0,to=100,by=5))
105 fos.stacked.hist
106
107 ###Facetwrapped Akaike weights plot
108 combAweights <- full_join(mutate(AICs_df_akaike_weights,source_of_
        data="Extant"),
109                                 mutate(AICs_df_akaike_weights.fos,
                                      source_of_data="Fossil"))
110 combAWeights.plot <- ggplot(combAweights, aes(x=V4, y=weight, fill=
        factor(Method))) +
111                               geom_bar(stat="identity") +
112                               theme_bw() +
113                               labs(x="Tree ID", y= "Akiake Weight") +
114                               theme(legend.title=element_blank()) +
115                               scale_fill_manual(values=c("#feb24c","#
                                      af8dc3","#7fbf7b"))+
```

```
                                scale_x_continuous(breaks=seq(from=0,to
                                    =100,by=5)) +
  facet_wrap(~source_of_data, ncol=1,nrow=2)
combAWeights.plot

# install.packages("devtools")
#devtools::install_github("thomasp85/patchwork")
library(patchwork) # see https://github.com/thomasp85/patchwork for
    details
mvResultsPlot = {comb.violin.plot + theme(legend.position = 'None') +
     combined.age.est.hist} -
  combAWeights.plot +
  plot_layout(ncol = 1)
mvResultsPlot

p4 = {comb.violin.plot + theme(legend.position = 'None') + combined.
    age.est.hist} -
  extant.stacked.hist + theme(legend.position = 'None') + fos.stacked
      .hist +
  plot_layout(ncol = 1)
p4
ggsave('mvResultsnolab.pdf')
```

./Appendices/RCode/07_FigurePlotting.R

```
######## Parametric Bootstrapping ########
# last edit 2018-08-30
# run this with command line arguments to run bootstrap on single
    tree from the posterior of trees
# arguments needed: id of tree in posterior (integer 1 to 100), nsim
    number of simulations from BM model (integer),
```

```
# run_on_fossils either 0 or 1 indicating whether to use extant data
    or combined with fossils (logical)
############################
#set up
library(mvMORPH)
set.seed(123) #set seed for reproducibility
args = commandArgs(trailingOnly=TRUE) #can run with command line
    inputs
id = as.numeric(args[1])
nsim = as.numeric(args[2])
run_on_fossils = as.numeric(args[3]) #third input argument tells us
    whether to run on fossil data or not
if (is.na(run_on_fossils)) run_on_fossils = as.logical(args[3])

if (run_on_fossils){
  load(file = "mvMorphFoss_aug.rda")
  load(file="fossil_trees_aug.rda")
  load('Fossiltraits.Rda')
  mv_morph_results = mv_morph_fossil_results #rename things so can
      work the same for fossil and extant
  trees.list = fossil.trees
  traits = traits_f_e #note renaming this also so be careful if
      running other things in same environment
}  else  {
  load(file="Pelagiadata.rda")
  load(file="mvMorphExtant.rda")
  mv_morph_results = mv_morph_all_results
  trees.list = pruned.trees
}
############################
```

```
30
31 #subset the traits
32 ntraits <- 5
33 ntrees <- 100
34 traits <- traits[,seq_len(ntraits)]
35 SHIFT.AICs <- purrr::map_dbl(mv_morph_results, function(x) x$SHIFT.
       model$AIC)
36 age_estimates <- purrr::map_dbl(mv_morph_results, function(x) x$age_
       estimate)
37
38 sim.data <- purrr::map2(mv_morph_results[1:ntrees], trees.list[1:
       ntrees], function(x,y) simulate(x[[1]], tree=y, nsim=nsim)) #[[1]]
        extracts out the BM model
39
40 bootstrap_wrapper <- function(single.tree,single.sim.data,age_
       estimate){
41   #do parametric bootstrapping on this simulated object
42   bootstrap <- purrr::map(single.sim.data, function(x) tryCatch(mvBM(
         single.tree, x, method='rpf', echo=F, diagnostic = F), error=
         function(err) NA))
43   bootstrapSHIFT <- purrr::map(single.sim.data, function(x) tryCatch(
         mvSHIFT(single.tree, x, model="BMOU", method='rpf', param=list(
         age=age_estimate), echo=F, diagnostic = F), error=function(err)
         NA))
44   return(list(bootstrapBM=bootstrap, bootstrapSHIFT=bootstrapSHIFT))
45 }
46 #run for a single tree (tree id)
47 single.result <- bootstrap_wrapper(single.tree=trees.list[[id]],
       single.sim.data=sim.data[[id]],age_estimate=age_estimates[[id]])
```

```
save(sim.data,single.result,file=paste("parameteric_bootstrap",ifelse
    (run_on_fossils,'_foss',''),id,".rda",sep=""))
print('done')
```

./Appendices/RCode/08a_bootstrapping_single_trees.R

```
######## Parametric Bootstrapping ########
# last edit 2018-08-30
# loads in bootstrapping results and generates plot
##########################
library(mvMORPH)

gather_results_and_ggplot <- function(run_on_fossils=FALSE, tree_ids
    = seq_len(100)){
#bring together results from several trees and plot the distribution
    of del-AIC values for each
library(ggplot2)
library(dplyr)
  if (run_on_fossils){
    load('mvMorphFoss_aug.rda')
    mv_morph_results = mv_morph_fossil_results
  } else {
    load(file="mvMorphExtant.rda")
    mv_morph_results = mv_morph_all_results
  }
full_df <- data.frame(aics=numeric(), id=numeric(), obs=numeric())
for (i in tree_ids){
  print(i)
  if (run_on_fossils){
    load(paste("parameteric_bootstrap_foss",i,".rda",sep=""))
  } else {
```

```
    load(paste("parameteric_bootstrap",i,".rda",sep=""))
  }
  log.dist.BM <- sapply(single.result$bootstrapBM, function(x)
      tryCatch(AIC(x),error=function(err) NA))    #if has NA previously
      , return NA for AIC
  log.dist.SHIFT <- sapply(single.result$bootstrapSHIFT, function(x)
      tryCatch(AIC(x),error=function(err) NA))
  observed_del_AIC <- mv_morph_results[[i]]$SHIFT.model$AIC - mv_
      morph_results[[i]]$BM.model$AIC
  single_df <- data.frame(aics=log.dist.SHIFT-log.dist.BM, id=rep(i,
      length(single.result[[1]])), obs=rep(observed_del_AIC,length(
      single.result[[1]])))
  full_df <- full_join(full_df,single_df)
}
# add bounds for the aic values to compare to true data
full_df <- full_df %>%
  group_by(id) %>%
  summarise(lb=quantile(aics,0.025,na.rm=TRUE), ub=quantile(aics
      ,0.975,na.rm=TRUE)) %>%
  ungroup() %>%
  full_join(full_df) %>%
   mutate(outside = (obs<lb) | (obs>ub))
g <- ggplot(full_df, aes(aics)) +
  geom_histogram(fill="black", binwidth = 2, aes(y = ..ndensity..)) +
  labs(x = "Delta AIC values", y = "Proportion of trees") +
  theme_bw()
g
ggsave('hist.png')
h <- ggplot(full_df, aes(aics)) +
```

```
46    geom_density(kernel = "gaussian", aes(group = factor(id)), colour =
          alpha("grey", 0.7)) +
47    geom_density(kernel = "gaussian", aes(group = factor(id), colour =
          outside), data = full_df %>% filter(!outside)) +
48    geom_vline(aes(xintercept = obs, colour=outside), linetype=5) +
49    labs(x = latex2exp::TeX(paste('$\\','Delta','$',' AIC values',sep='
          ')), y="Density") +
50    scale_color_discrete(name="Empirical Data Outside") +
51    theme_bw()
52  h
53  save.name = ifelse(run_on_fossils,'another_hist_foss.png','another_
      hist.png')
54  ggsave(save.name)
55  return(h)
56  }
57
58  ntrees=100
59  #check which rda files exist corresponding to which trees have been
      processed
60  processed_tree_ids = seq_len(ntrees)[file.exists(paste('./parameteric
      _bootstrap',1:ntrees,'.rda',sep=""))]
61  gather_results_and_ggplot(run_on_fossils = FALSE, processed_tree_ids)
62
63  processed_tree_ids = seq_len(ntrees)[file.exists(paste('./parameteric
      _bootstrap_foss',1:ntrees,'.rda',sep=""))]
64  gather_results_and_ggplot(run_on_fossils = TRUE, processed_tree_ids)
```

./Appendices/RCode/08b_plot_bootstrapping.R

Appendix G

Applying the SHIFT model to the 'classical' mammal radiation

To investigate evolutionary patterns across groups, I applied the models developed using mvSHIFT for Pelagiaria to the mammal dataset of Slater (2013).

The .nex file and .tre file were taken from the Supplementary Information of Slater (2013) and run through the BM and SHIFT models in R under the same parameters as Pelagiaria. Brownian motion was found to be slightly favoured over all analyses, see Fig G.2.

```
setwd("/Users/admin/Dropbox/3D Landmarking/Mimi Pelagia Landmarking/")


##Process data##
mammal.tree<-read.tree("mammal.nex")

Eutheria<-extract.clade(mammal.tree, 223)
Placentals<-extract.clade(mammal.tree, 222)
```

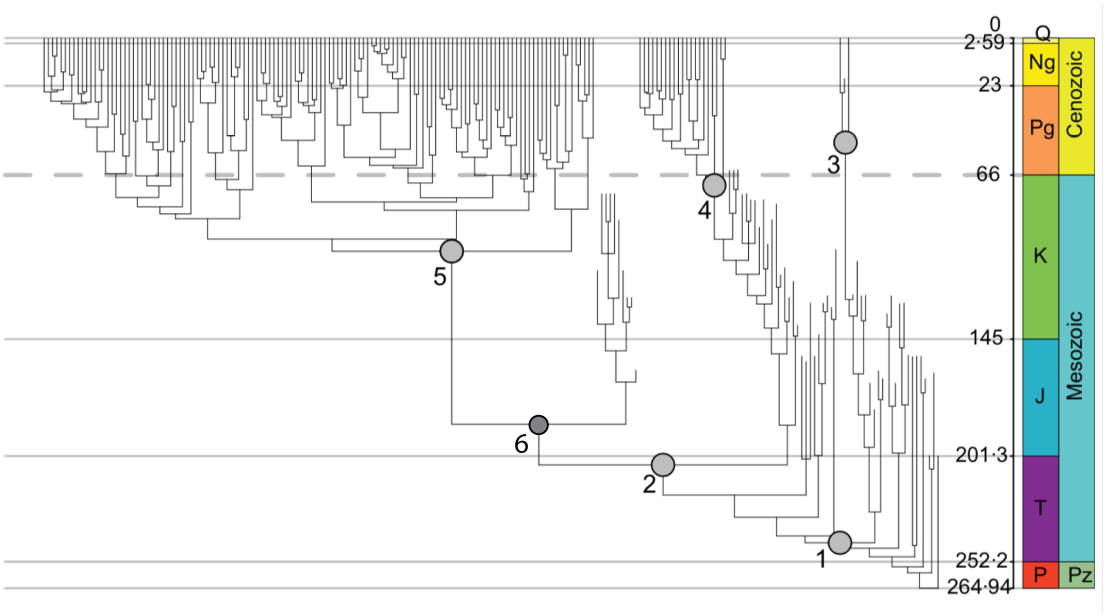


Figure G.1: The tree from Slater (2013) used for this analysis. Three datasets were run, the whole tree, eutherians (node 6) and placentals (node 5).

```
9
10 mammal_data<-read.csv("mammal_mass.csv")
11
12
13 rownames(mammal_data)<-mammal_data$Taxon
14 mammal_data<-mammal_data[2:3]
15
16
17 mammal_data_Epruned<-mammal_data[Eutheria$tip.label,]
18 mammal_bodymass_E<-mammal_data_Epruned[1]
19 mammal_SEM_E<-mammal_data_Epruned[2]
20
21
22
23 ### Carry out on Eutheria in dataset ###
```

```
24
25 BM.mammals<-mvMORPH::mvBM(Eutheria, mammal_bodymass_E)
26
27 fit_SHIFT_at_given_age <- function(shift_age){
28   BM.ER.mammal<-mvMORPH::mvSHIFT(Eutheria, mammal_bodymass_E, model="
         BMOU",method="sparse",
29                                  param=list(age=inv.logit(shift_age,min=0,max=
                                        max(nodeHeights(Eutheria)))))
30   return(BM.ER.mammal$LogLik)
31 }
32 zm = optim(1,fit_SHIFT_at_given_age,control=list(maxit=10))
33
34 age_estimate_mammals_E = inv.logit(zm$par,min=0,max=max(nodeHeights(
       Eutheria)))
35
36 mammal_shift<-mvMORPH::mvSHIFT(Eutheria, mammal_bodymass_E, model="
       BMOU",method="rpf", param=list(age=age_estimate_mammals_E))
37
38
39
40 ### Carry out different models on only the Placentals in the dataset
       ###
41
42 mammal_data_Ppruned<-mammal_data[Placentals$tip.label,]
43 mammal_bodymass_P<-mammal_data_Ppruned[1]
44 BM.mammals.P<-mvMORPH::mvBM(Placentals, mammal_bodymass_P)
45
46 fit_SHIFT_at_given_age <- function(shift_age){
47   BM.ER.mammal<-mvMORPH::mvSHIFT(Placentals, mammal_bodymass_P, model
         ="BMOU",method="sparse",
```

```
48                                  param=list(age=inv.logit(shift_age,min=0,max=
                                        max(nodeHeights(Placentals)))))
49    return(BM.ER.mammal$LogLik)
50  }
51  zm = optim(1,fit_SHIFT_at_given_age,control=list(maxit=10))
52
53  age_estimate_mammals_P = inv.logit(zm$par,min=0,max=max(nodeHeights(
        Placentals)))
54
55  mammal_shift_P<-mvMORPH::mvSHIFT(Placentals, mammal_bodymass_P, model
        ="BMOU",method="rpf", param=list(age=age_estimate_mammals_P))
56
57
58
59  ### Carry out different models on the whole dataset ###
60
61  mammal_data_whole<-mammal_data[mammal.tree$tip.label,]
62  mammal_bodymass_w<-mammal_data_whole[1]
63  BM.mammals.w<-mvMORPH::mvBM(mammal.tree, mammal_bodymass_w)
64  EB.mammals<-mvMORPH::mvEB(mammal.tree, mammal_bodymass_w, error=NULL,
        method="rpf", diagnostic=TRUE, echo=TRUE)
65  OU.mammals<-mvMORPH::mvOU(mammal.tree, mammal_bodymass_w, error =
        NULL)
66
67
68  fit_SHIFT_at_given_age <- function(shift_age){
69    BM.ER.mammal<-mvMORPH::mvSHIFT(mammal.tree, mammal_bodymass_w,
          model="BMOU",method="sparse",
70                                  param=list(age=inv.logit(shift_age,min=0,max=
                                        max(nodeHeights(mammal.tree)))))
```

```
71    return(BM.ER.mammal$LogLik)
72  }
73  zm = optim(1,fit_SHIFT_at_given_age,control=list(maxit=50))
74
75  age_estimate_mammals_w = inv.logit(zm$par,min=0,max=max(nodeHeights(
        mammal.tree)))
76
77  mammal_shift_w<-mvMORPH::mvSHIFT(mammal.tree, mammal_bodymass_w,
        model="BMOU",method="sparse", param=list(age=age_estimate_mammals_
        w))
78
79
80
81  #summarise data with Akaike Weights
82
83
84  par(mfrow=c(1,3))
85
86  AICs.Eutheria <- c(BM.mammals$AIC,mammal_shift$AIC)
87  akaike.weights.E<-qpcR::akaike.weights(AICs.Eutheria)
88  barplot(akaike.weights.E$weights, ylim=c(0:1), ylab="Akaike weights",
        names.arg=c("Brownian Motion", "Shift model"), main="Placentals
        only")
89
90  AICs.Placentals <- c(BM.mammals.P$AIC,mammal_shift_P$AIC)
91  akaike.weights.Placentals<-qpcR::akaike.weights(AICs.Placentals)
92  barplot(akaike.weights.Placentals$weights, ylim=c(0:1), ylab="Akaike
        weights", names.arg=c("Brownian Motion", "Shift model"), main="
        Eutheria")
93
```

```
94 AICs.whole <- c(BM.mammals.w$AIC,mammal_shift_w$AIC)
95 akaike.weights.Whole<-qpcR::akaike.weights(AICs.whole)
96 barplot(akaike.weights.Whole$weights, ylim=c(0:1), ylab="Akaike
       weights", names.arg=c("Brownian Motion","Shift model"), main="
       Whole Dataset")
```

./Appendices/SlaterMammal/MammalScript.R

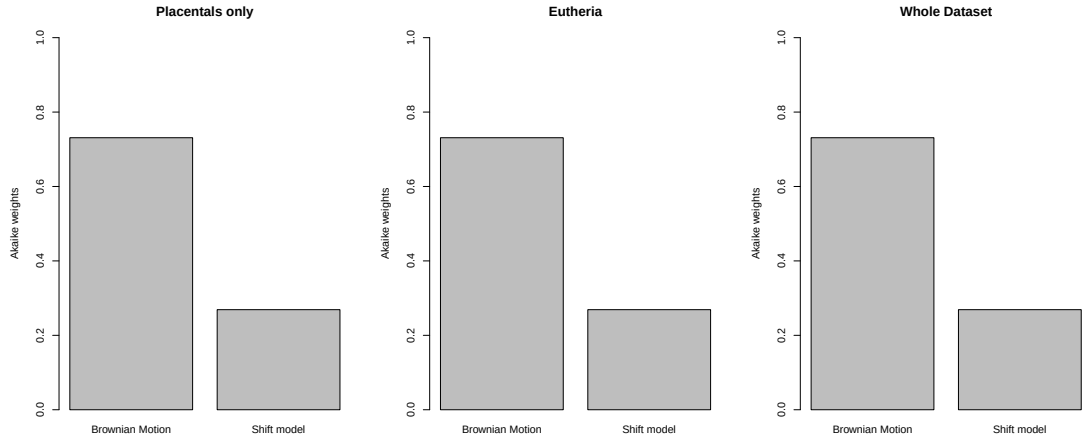


Figure G.2: Akaike weights for the three subsets of data within the mammal body mass data taken from Slater (2013).